UNIVERSIDAD COMPLUTENSE DE MADRID

FACULTAD DE CIENCIAS FÍSICAS

Departamento de Física Teórica I

TESIS DOCTORAL

Quantum detectors and vacuum correlations in space and time: theoretical results and simulation proposals

Detectores cuánticos y correlaciones de vacío en espacio y tiempo: resultados teóricos y propuestas de simulación

MEMORIA PARA OPTAR AL GRADO DE DOCTOR

PRESENTADA POR

Marco del Rey Zapatero

Director

Juan León García

Madrid, 2014

DEPARTAMENTO DE FÍSICA TEÓRICA I
UNIVERSIDAD COMPLUTENSE DE MADRID

DOCTORAL THESIS

Quantum Detectors and Vacuum Correlations in Space and Time: Theoretical Results and Simulation Proposals.

Author:
Marco DEL REY ZAPATERO

Supervisor:
Dr. Juan LEÓN GARCÍA

INSTITUTO DE FÍSICA FUNDAMENTAL
CONSEJO SUPERIOR DE INVESTIGACIONES CIENTÍFICAS

DEPARTAMENTO DE FÍSICA TEÓRICA I
UNIVERSIDAD COMPLUTENSE DE MADRID

TESIS DOCTORAL

Detectores Cuánticos y Correlaciones de Vacío en Espacio y Tiempo: Resultados teóricos y propuestas de simulación.

Autor:
Marco DEL REY ZAPATERO

Director:
Dr. Juan LEÓN GARCÍA

INSTITUTO DE FÍSICA FUNDAMENTAL
CONSEJO SUPERIOR DE INVESTIGACIONES CIENTÍFICAS

Acknowledgements

All this happened, more or less.

Y de un modo u otro, a lo largo del camino, la tesis se acabó por concluir.

Han sido años de tiza, charlas y pizarras. De nuevos amigos, de aventuras cómo no, de viajes. Han sido años de transformación, con mezcla de ilusiones y frustraciones, caminando en un ciclo que espero haya sido de espiral y que me haya llevado a mejores síntesis de mí mismo. Lo cierto es que ahora, mientras salgo de la crisálida y me pongo a hacer repaso, al menos no puedo negar haber vivido este tiempo con intensidad, críticamente que diría Per Bak, aunque quizá no siempre autoorganizado, oscilante entre los periodos de serenidad y los de profunda agitación, siempre al borde de la avalancha... cerca de ese lugar entre el orden y el caos en el que algunos, con gusto, vivimos nuestras vidas.

Llegado el final de esta tesis y el umbral de una inflexión, siempre le queda a uno la incertidumbre de lo que está por venir. Al menos en esta ocasión ese futuro incierto viene acompañado de la seguridad de haber alcanzado algo. Por eso es inevitable pararse a pensar un momento en todos aquellos que han estado ahí, a los que me han ayudado a llegar hasta aquí, recordar a toda esa gente a la que de un modo u otro deseo, o mejor dicho necesito, dar las gracias.

Los que me conocen bien saben de mi tendencia a evitar cumplidos. Quizá por huir de la hipocresía, o al menos eso me gusta pensar, navego a veces al borde de la incorrección. Pero tampoco debería extrañar a nadie que aquí agradezca. Aun así quiero dejar claro que estas palabras de afecto son sinceras, que van más allá del compromiso y la corrección política. De verdad.

Porque es lógico y merecido, me gustaría en primer lugar agraceder a Juan León, mi supervisor durante estos años, su apoyo científico, su dedicación como tutor, su insistencia en el rigor del cálculo y su paciencia ilimitada con su estudiante más rebelde. Hasta tendría sentido disculparme por haber sido tan díscolo, de no ser porque reconozco que ha sido parte importante de nuestra relación, de nuestra amistosa guerra director-doctorando en la que hemos aprendido a entendernos, en la que ya no hacen falta las palabras para

comunicarnos. Pese a algunos momentos de mayor distancia, no sólo he aprendido de Juan mucha, mucha física, he aprendido también la importancia de darle a los demás lo mejor de uno mismo. Juan ha sabido soportar mis aventuras de insurrecto inexperto y ha encontrado siempre, de algún modo, la manera de apoyarme, darme la libertad de seguir mi propio camino y reírse de nuestras diferencias.

En términos científicos y personales no sólo pienso en Juan, sino también en mi amigo Eduardo Martín-Martínez, junto al que que ha sido y será un placer siempre trabajar y disfrutar de una buena *ale*. Para él mi más honda admiración por su entusiasmo, por su capacidad y su energía, misterios de la naturaleza tan profundos como los que explora en Ontario, allá en los confines del mundo helado. Nuestras aventuras en Londres y Madrid con multimillonarios visionarios que no exploran postulados anteriores, pero los corrigen, pasarán a la historia, como pasó el elemento "c" que no era la velocidad de la luz, pero lo fue luego.

Borja Peropadre también compartió aquel delirio. Estos años de tesis no habrían sido lo mismo de no haber estado junto a semejante sujeto pared con pared. A él también le debo las gracias por soportarme con tanto estilo, por nuestras batallas dialécticas y tantas charlas más allá del bien y del mal... por rellenar de humor los momentos difíciles y por ser con su tolerancia de amigo el mejor de mis críticos.

No me olvido de Carlos Sabín, malabarista de palabras, cuyas personalidades múltiples incluyen un físico, un poeta y un poco de todos nosotros cuando nos imita en los ratos libres; ni tampoco de Emilio Alba, que con su humor costumbrista y su memoria prodigiosa ha hecho de cada día en el CSIC un día mejor en la constante batalla contra lo cotidiano. Me alegro de que el futuro nos haya deparado nuevos proyectos juntos en el sector de la venta de sueños.

Juanjo García Ripoll ha sido también un gran apoyo. Desde aquella colaboración inicial en la que investigamos los vericuetos de la causalidad, siempre se ha mostrado dispuesto a resolver cualquier duda con la que le haya asaltado. También lo han sido todos los otros quinfogeros, los que llegaron y los que se fueron, los que se quedaron... en especial Andrea Cadarso porque salvó Malta del hundimiento, pero también Alejandro, Diego, Matías, Andreas, Jordi, Johannes, Guillermo, Benjamín, Miguel, Mónica, Xabi, Jordi y Lucas. Hans Westman merece un trato especial, porque a parte de ser el sueco más dicharachero y estar como un auténtico cencerro, ha sido un colega extraordinario en la salud y en la enfermedad. A Luis Garay me gustaría agradecerle su integridad y que sea un ejemplo vivo de que hacemos esto porque nos gusta, aunque en parte esa pasión fuera la responsable de que al final no llegara a tomar nunca su examen de Relatividad General. Merece también

unas palabras Diego Porras, por su estilo natural al moverse por los vericuetos de la física, haciendo parecer que la cosa más complicada es simple, como hizo con aquellas simulaciones en iones atrapados que inventamos.

En mis aventuras por el mundo ha sido también placer conocer a Ivette Fuentes, intrépida aventurera científica en los confines de la relatividad y la cuántica, a Andrzej Dragan, artista, cineasta y creo que físico. También a muchos otros personajes que han amenizado congresos y veladas varias con conversaciones apasionantes, entre ellos a Antony R. Lee, Nick Menicucci y Nico Friis. De mi estancia en Ulm guardaré siempre un recuerdo fantástico de Martin Plenio y Susana Huelga, de mi vecino Javi Almeida y de todos los otros miembros del grupo en especial de Ramil, Mischa y Felipe. Berlín, the best place to be, fue también un tiempo fantástico que debo agradecer a Jens Eisert, para el que sólo tengo buenas palabras, y en el que tuve ocasión de chocarme con Mathis Friesdorf, cocinero de estupendos risottos y productor de código perfecto, guía moral para pobres almas como la mía, y con Arnau Riera, con el que ya había compartido momentos intensos en el pasado, y al que la vida me llevó a reencontrar, como por casualidad, en aquella pequeña pero acogedora oficina de Dahlem.

Todos los mencionados hasta ahora han compartido conmigo momentos directamente relacionados con esta aventura doctoral, pero no son los únicos que la han hecho posible. De hecho, nada de esto hubiera sucedido si cuando volví de Holanda cinco años atrás, no hubiera encontrado en Madrid un hogar tan agradable como el que compartí en Tirso de Molina con Blanca, Héctor y Amandine. Entonces fuimos felices. A veces, en los momentos oscuros, vuelvo ahí con la memoria y sonrío.

Al poco de aquello, por casualidades del destino y una beca, yo y mis bártulos acabamos en la Residencia de Estudiantes en la que he vivido la mayor parte de estos años de tesis. Del tiempo que pasé allí atesoro nuevos amigos. Gracias Sofía por redescubrirme mi ciudad, la poesía y aquel jazz en la 424; Carlos, por tu verbo veloz que amenaba las comidas y tus balas de goma siempre rebotadoras y bien dirigidos, Roberto, por el ojo maléfico y las historias absurdas que nos contaste y las que nos contarás y por tu amor incondicional a las ponchongas, universalmente compartido; Pedro, por tu presencia eterna entre esos muros. A mi bloodbro Andrés y a mis compañeros de generación... Pepa, Esther, Antonio, Andrea, Irene, Óscar, Javi, Jose, Ángel, Julia, os tengo siempre presentes. Gracias a Ángela, porque con ella me convertí en quien soy y la llevaré siempre conmigo, y desde luego a mis amigos del *Chami* a quienes conocí hace ya diez años y a los que difícilmente unas breves palabras pueden agradecer el estar siempre ahí. A Angy y Dani, por su ayuda a coger ritmo en la escritura. También gracias a Esther, mi querida Rizos, por el apoyo que me dio durante el

principio tesis y porque con ella me sentí seguro por primera vez en mucho tiempo.

A toda mi familia le tengo que agradecer que hayan sido siempre tan cariñosos conmigo, sobre todo a mis abuelos que ya no están, y a José Luis que pese a ser mi tío se siente sobre todo amigo.

Y a mis padres, a los sí que debo todo. No sabiendo dónde empezar ni terminar serán sólo estas palabras. Gracias Javier por enseñarme el mundo desde tus ojos más que curiosos, por permitirme hacer mía la inquietud tuya... por contaminarme con tu deseo de saber y adornar mi infancia con esa ingeniería de salón en la que construíamos máquinas con las que volaba mi imaginación. Gracias Lola por tu cariño eterno, por tu fortaleza, por transmitirme esa conciencia hippie que ya de niño veía emanar desde el sol amarillo que brillaba en el centro de tu jersey rosa. A los dos, por apoyarme, por haber sabido protegerme, por enseñarme a disfrutar de esta vida.

Y por último, gracias Francesca, por enseñarme tantas cosas, por hacerme pensar en lo importante, por creer en mí más que yo mismo y haber estado ahí con tu buen humor y tu cariño en tantas tantas ocasiones.

Madrid, 14 de octubre de 2014.

Contents

List of Figures

List of Abbreviations

AC	Alternating Current,
AQFT	Algebraic Quantum Field Theory,
ARDA	Advanced Research and Development Activity,
DC	Direct Current,
JC	Jeynes-Cummings Model,
JJ	Josephson Junction,
LOCC	Local Operations and Classical Communication,
POVM	Positive Operator Valued Measures,
RWA	Rotating Wave Approximation,
SQUID	Superconducting QUantum Interference Device,
QFT	Quantum Field Theory,
QM	Quantum Mechanics,
RQI	Relativistic Quantum Information,
UDW	Unruh-DeWitt Detector,

List of Symbols

$\otimes_S$	Symmetrized tensor product,
C	Capacitance,
$\mathfrak{F}$	Fock space,
$\mathfrak{F}^G$	Global Fock space,
$\mathfrak{F}^L$	Local Fock space,
$\mathfrak{H}$	Hilbert Space, single-particle sector,
H	Hamiltonian,
$\mathcal{H}$	Hamiltonian density,
$\mathcal{L}$	Lagrangian,
L	Inductance,
R	Resistance,
$\mathfrak{S}$	Solution space of KG equation

Published articles derived from this thesis

The research included in this thesis has given rise to the following articles:

- **What does it mean for half of an empty cavity to be full?** [1]
  Eric Brown, Marco del Rey, Hans Westman and Juan León.
  arXiv:1409.4203.

- **Local quanta, unitary inequivalence, and vacuum entanglement**. [2]
  Matías R. Vázquez, Marco del Rey, Hans Westman and Juan León.
  Annals of Physics 351(0), 112 – 137, 2014.

- **Wavepacket detection with the Unruh-DeWitt model**. [3]
  Eduardo Martín-Martínez, Miguel Montero and Marco del Rey.
  Phys. Rev. D 87, 064038 (2013)

- **Non-monotonic entanglement of physical EM field states in non-inertial frames**. [4]
  Miguel Montero, Marco del Rey and Eduardo Martín-Martínez.
  Phys. Rev. A 86, 012304 (2012)

- **Extracting past-future vacuum correlations using circuit QED.** [5]
  Carlos Sabín, Borja Peropadre, Marco del Rey and Eduardo Martín-Martínez.
  Phys. Rev. Lett. 109 033602 (2012)

- **Simulating accelerated atoms coupled to a quantum field.** [6]
  Marco del Rey, Diego Porras and Eduardo Martín-Martínez.
  Phys. Rev. A 85, 022511 (2012)

- **Short-time quantum detection: probing quantum fluctuations.** [7]
  Marco del Rey, Carlos Sabín and Juan León.
  Phys. Rev. A 85, 045802 (2012)

- **The Fermi problem with artificial atoms in circuit QED.** [8]
  Carlos Sabín, Marco del Rey, Juan José Garcá-Ripoll and Juan León.
  Phys. Rev. Lett. 107, 150402 (2011)

Also, during the development of this thesis two more works have been published by its author

- **Emergence of coherence and the dynamics of quantum phase transitions**. [9]
  S. Braun, M. Friesdorf, S. S. Hodgman, M. Schreiber, J. P. Ronzheimer, A. Riera, M. del Rey, I. Bloch, J. Eisert and U. Schneider.
  arXiv:1403.7199.

- **Exploiting structured environments for efficient energy transfer: The phonon antenna mechanism**. [10]
  M. del Rey, A. W. Chin, S. F. Huelga and M. B. Plenio.
  J. Phys. Chem. Lett., 4, 903 - 907 (2013)

Conferences and Research Visits

During these thesis years, I have been glad to present my work in the following conferences:

- FUNDAMENTAL PROBLEMS IN QUANTUM PHYSICS,
  Weizmann Institute, Rehovot, Israel. - Mar 23rd to Mar 27th 2014
  Poster: *Local quanta, unitary inequivalence and Vacuum entanglement.*

- QUANTUM INFORMATION WORKSHOP,
  Centro de Ciencias de Benasque Pedro Pascual, Benasque, Spain. - Jun 30th to Jul 7th 2013
  Seminar: *Quantum Biology - Effect of structured environments in efficient energy transfer.*

- QUO VADIS, QUANTUM PHYSICS?,
  Centro de Ciencias de Benasque Pedro Pascual, Natal, Brazil. - Feb 18th to Mar 1st 2013
  Talk: *The phonon antenna mechanism.*

- HIGHLIGHTS OF QUANTUM OPTICS - 500. WILHELM UND ELSE HERAEUS SEMINAR,
  Physikzentrum Bad Honnef, Germany - May 6th to May 11th 2012
  Poster: *Simulating accelerated atoms.*

- QUANTUM MALTA 2012: FUNDAMENTAL PROBLEMS IN QUANTUM PHYSICS ,
  University of Malta, La Valetta - Apr 24th to Apr 27th 2012
  Poster: *Extraction of vacuum entanglement with superconducting circuits*

- INTRODUCTION TO CIRCUIT AND CAVITY QED (CCQED),
  École de Physique des Houches, Les Houches, France - Feb 26th to Mar 2nd 2012
  Poster: *Quantum detection at short times.*

- RELATIVITY MEETS ENTANGLEMENT AND HIGH ENERGY ,
  Imperial College, London. - Sep 13th to Sep 15th 2011
  Talk: *Accelerated Quantum Emitters.*

- RQI - (N) WORKSHOP ,
  Campus CSIC Serrano, Madrid - Sep 05th to Sep 07th 2011
  Talk: *Short-time Quantum Detection*

- SUSSP67 SUMMERSCHOOL,
  University of Strathclyde, Glasgow, UK - Jul 28th to Aug 10th 2011
  Poster and talk: *The Fermi Problem with Artificial Atoms in Circuit QED*

- QUANTUM SIMULATIONS WORKSHOP,
  Centro de Ciencias de Benasque Pedro Pascual, Benasque, Spain. - Feb 28th to Mar 05th 2011
  Poster: *Causality in Quantum Field Theory: The Fermi Problem with Quantum Circuits*

I was also granted the opportunity to spend a few months in the following groups:

- DAHLEM CENTER FOR COMPLEX QUANTUM SYSTEMS,
  Place: Freie Universität Berlin, Germany
  Host: Dr. Jens Eisert
  Period: 20th August to 18th December 2012

- INSTITUTE OF THEORETICAL PHYSICS,
  Place:University of Ulm, Germany
  Host: Dr. Martin Plenio
  Period: 25th September to 23rd December 2011

Resumen

Esta tesis se centra en el estudio de las correlaciones de vacío en el espacio y el tiempo y en el uso de distintas técnicas para explorarlas: modelos de detección, desde un punto de vista teórico, y simulaciones cuánticas, desde una perspectiva más práctica. A lo largo de esta exploración hemos encontrado resultados que podemos situar en tres categorías, que se corresponden a su vez con las tres partes en que la tesis está dividida. En la primera parte hemos estudiado *modelos de detección cuántica*, y más en concreto, modelos de detectores para el análisis de estados realistas, localizados. También en esta parte hemos propuesto una simulación en laboratorio del comportamiento teórico de uno de estos modelos, el detector Unruh-DeWitt (UDW), en el caso de ser acelerado en presencia de un campo monomodo. En la segunda parte de la tesis nos hemos centrado en el estudio de detectores en el régimen más allá de la aproximación de onda rotante, descubriendo la aparición de comportamientos muy interesantes, a priori no esperados. En la tercera y última parte de la tesis, estudiamos las correlaciones de vacío, comenzando por una propuesta experimental para extraer un cierto tipo de ellas y concentrándonos a continuación en la interesante cuestión de la localización de estados, desarrollando un formalismo de cuantización local en el que se busca llegar al concepto de "partícula perfectamente localizada" de forma constructiva, y analizar su problemática. Finalmente, apoyándonos en los resultados y la comprensión alcanzada a lo largo de la tesis, estudiamos cómo estás partículas locales pueden ser liberadas al desplegar rápidamente un espejo en el medio de una cavidad, y proponemos una vía experimental para observar este nuevo efecto, de tipo Casimir-dinámico.

Este resumen pretende motivar el interés en estos aspectos, inscribirlos en un marco más amplio y finalmente descender al detalle para pormenorizar en los resultados alcanzados y su relevancia.

La computación cuántica: Un nuevo paradigma

La teoría de la información clásica fue uno de los pilares más importantes en el desarrollo de las tecnologías de la información y la telecomunicación de hoy día. Sus méritos son innu-

merables: la caracterización de los canales de comunicaciones, el descubrimiento de límites fundamentales para la capacidad de canal, la comprensión rigurosa de la compresión, la codificación y la interacción entre señal y ruido son ejemplos simples que han extendido los horizontes del procesado de la información mucho más lejos de lo que podríamos haber imaginado hace tan sólo unas décadas.

Entre sus hallazgos más importantes, destaca el teorema de Shannon-Hartley, un resultado que limita la tasa máxima a la que se puede transmitir información sobre un canal (la capacidad de canal C) cuando se dispone de un ancho de banda limitado B y existe una cierta relación señal a ruido (S/N:

$$C = B \log_2 \left(1 + \frac{S}{N}\right). \tag{0.0.1}$$

Las tecnologías de la comunicación de hoy día operan al borde de ese límite y de hecho, para potencias de transmisión constantes, las mejoras en la velocidad de datos provienen directamente del uso de mayor ancho de banda (como ocurre en el caso de las redes 3G) [1].

En el caso de los ordenadores, la velocidad de procesado de la información no está limitada (por ahora) por las velocidades de transmisión de datos entre registros. El número de operaciones por unidad de tiempo que un ordenador puede efectuar depende más bien de su potencia de cálculo, que crece con la complejidad del procesador y con la velocidad de conmutación de sus transistores. Incrementar el número de transistores mientras se mantiene el tamaño del ordenador implica miniaturizar el sistema. Afortunadamente, al reducir el tamaño de los componentes también se consigue incrementar la velocidad de conmutación. De hecho, hoy en día en 2014, las dimensiones de los transistores de los ordenadores personales (supercomputadores) son en torno a 45nm (22nm), frente a los 250nm del año 1997.

Pero la miniaturización presenta ciertos problemas. Hasta el año 2005 la "ley" de Moore, que afirma que la potencia de cómputo se duplica cada 2 años, se apoyaba en el "scaling" de Dennard: el calor liberado por unidad de área funcionando a la máxima frecuencia disponible se mantenía constante (tanto el voltaje como la corriente escalaban inversamente al tamaño). En 2005, sin embargo, el "scaling" de Dennard dejó de verificarse. Con la disminución del tamaño aumentan las fugas de corriente y con ellas la potencia térmica liberada. La industria informática sólo ha podido contener esta "barrera térmica" limitando la velo-

[1] Lo cierto es que el límite de Shannon se verifica para canales punto a punto. Las nuevas tecnologías presentes en los terminales 4G y 5G pueden ir aún más allá combinando enlaces multipunto a multipunto con ayuda de varias antenas, cada uno de los múltiples canales operando no obstante al borde del límite de Shannon.

cidad de reloj de los procesadores [2]. EDesde el 2005, los incrementos en el rendimiento de los ordenadores se han debido fundamentalmente a los aumentos en la complejidad de los sistemas. Aprovechando que la densidad de transistores ha seguido incrementándose se han diseñado arquitecturas capaces de llevar a cabo procesado en paralelo, "multithread", sobre múltiples núcleos, "multicore". Sin embargo, este incremento en la complejidad conlleva en general un aumento en la información necesaria para dirigir y enrutar los cálculos y muchos científicos argumentan que la ganancia conseguida es muy inferior a la que se conseguía con la regla Dennard [11], anticipando así el fin de la "ley" de Moore.

Por otro lado, la existencia de otros límites más fundamentales también lleva a esa conclusión. De un lado está la barrera de Landauer, que remite al hecho de que por cada bit de información borrado se disipa al menos una cantidad de energía $kT \ln 2$ [12]. La miniaturización supone una reducción en la energía disipada por operación elemental, y nos estamos acercando peligrosamente a ese límite. Si todo siguiera al ritmo actual, se llegaría a esa barrera aproximadamente en 2034 [13]. Sólo un cambio en el paradigma de computación hacia un modelo reversible podría evitarlo.

De otro lado, está el límite de Margolus y Levitin. En sus artículos de 1998 y 2009 [14,15] demostraron que para conmutar entre estados ortogonales, un sistema cuántico de energía media E requiere un tiempo de al menos $\Delta t = \pi\hbar/2E$. Basados en esto, la estimación es que ese límite se alcanzaría en 75 u 80 años [15].

Con esto en mente a nadie sorprenderá que las compañías de superconductores estén dedicando esfuerzos económicos enormes en tratar de superar los paradigmas actuales. Nuevas arquitecturas y nuevos modelos de computación como la computación cuántica se preven muy importantes desde el punto de vista práctica en el futuro cercano de la informática.

Esta es una de las motivaciones fundamentales para trabajar en información cuántica. La información cuántica da sustento teórico a la computación cuántica. En esta tesis llevamos a cabo varios estudios usando sus herramientas. En algunos de ellos observamos fenómenos límite que podrían darse regularmente si ciertas plataformas experimentales se convirtieran en la implementación final de los ordenadores cuánticos, pero en realidad nuestro énfasis está puesto en otra dirección. La teoría de la información cuántica tiene mucho más que ofrecer a parte de la mejora de nuestra tecnología informática, de hecho es una puerta a comprender mejor ciertas cuestiones fundamentales. Con ayuda de la teoría de campos y de conceptos más cercanos al mundo relativista, nosotros nos hemos concentrado más bien en el estudio de las correlaciones existentes el vacío, cómo sondearlas y cómo extraerlas con

[2] Es por eso que los chips todavía funcionan a 3 GHz, prácticamente la misma frecuencia que hace 10 años.

propósitos prácticos. A lo largo de esta tarea nos hemos acercado al estudio de la causalidad, la teoría de la detección, escenarios relativistas y fundamentos de física cuántica. Todos estos campos están muy interconectados y en todo ellos juega un papel fundamental uno de los fenómenos más interesantes de la física cuántica: el entrelazamiento.

Un potente concepto

El entrelazamiento es sin duda uno de los conceptos más importantes de la teoría cuántica de la información, si no de toda la mecánica cuántica. La historia del entrelazamiento, o más bien la historia de su descubrimiento y estudio, remonta a las primeras décadas del siglo veinte, en particular a un artículo de Albert Einstein, Boris Podolsky y Nathan Rosen [16], en el que describían un experimento teórico con la intención de demostrar la incompletitud de la mecánica cuántica. El experimento, resumido por Leo Rosenfeld, es como sigue:

Supongamos dos partículas (A y B) con momentos opuestos que interaccionan entre sí en un punto conocido. Si un observador externo tiene acceso a una de las partículas lejos de la región de interacción y mide su momento, entonces por las condiciones del experimento debe poder deducir el de la otra partícula. Si por contra, decide medir la posición, debe poder saber instantáneamente dónde está la otra partícula. Es una deducción lógica pero.. ¿no es muy paradójico? ¿Cómo puede ser que el estado de la segunda partícula se vea influenciado por la medida hecha sobre la primera, después de que toda interacción haya cesado?

La idea que rondaba a Einstein es que, si la teoría cuántica fuera *completa*, según el argumento EPR se podrían asignar valores reales a la posición o al momento de la segunda partícula sin haberla medido, de modo que valores para ambos observables debían existir simultáneamente en B, violando el principio de incertidumbre. Era un argumento sutil, pero por supuesto tenía suposiciones implícitas. En particular Einstein estaba descartando la posibilidad de que el estado en B se viera instantáneamente afectado por la medición en A. En las discusiones a las que llevó este artículo, Einstein reconoció que ésta era la esencia de su argumento, e incómodo con la situación describió este fenómeno como "spukhafte Fernwirkung" o "espeluznante acción a distancia".

Erwin Schrödinger fue el primero que analizó el problema utilizando la palabra entrelazamiento (*entanglement* en inglés, *Verschränkung* en alemán), en una carta a Einstein:

Cuando dos sistemas (...) entran en interacción física temporal debido a la existencia fuerzas entre ellos, y después de un tiempo de influencia mutua se separan, no pueden ser descritos como previamente, otorgándoles una representación propia a cada uno. Diría que éste no un fenómeno más, sino quizá el más característico de los fenomenos de la mecánica cuántica, el que da lugar a la

auténtica divergencia frente a la línea de pensamiento clásica. Por medio de esa interacción las dos funciones de onda se han entrelazado.

El entrelazamiento es sin duda algo peculiar. No puede ser producido interaccionando con una de las partes localmente, a menos que exista una interacción entre ambas o que se disponga de un recurso entrelazado compartido. En esos casos caso el entrelazamiento se podrá destilar, redistribuir o intercambiar de un sistema a otro [17–19]. Pero todo ello son descubrimientos recientes.

El entrelazamiento fue debatido y no del todo bien comprendido hasta 1964. Fue entonces cuando John S. Bell, en un artículo histórico [20], publicó su famoso teorema en que definió lo que era una teoría realista en términos de variables ocultas e introdujo un nuevo experimento basado en el EPR que incluía medidas de espín. Formuló una desigualdad basada en las estadísticas se se obtendrían en la repetición del experimento que sería satisfecha por cualquier teoría de variables ocultas y violada para la teoría cuántica en ciertos estados de naturaleza entrelazada. Por primera vez se demostraba que ninguna teoría local realista podría reproducir todas las predicciones de la mecánica cuántica.

Se hicieron muchos esfuerzos para probar el resultado de Bell [21–23], en acuerdo con la mecánica cuántica, pero los más famosos fueron los llevados a cabo por Alain Aspect y su equipo [24–26] donde se obtuvieron violaciones máximas de la desigualdad. Aunque los experimentos tenían ciertas lagunas, los llamados *loopholes*, deficiencias que no se han llegado a superar (al menos no todas a la vez) en ningún experimento hasta la fecha, el carácter no local de la naturaleza es a día de hoy plenamente aceptado, y el artículo EPR es uno de los más citados de toda la historia de la ciencia.

El entrelazamiento es ya un concepto familiar para cualquier persona versada en la teoría cuántica, pero además tiene importantes implicaciones y es fundamental en el estudio de un gran número de procesos cuánticos. Por ejemplo, la detección. Supongamos que en laboratorio contamos con un átomo S originalmente excitado y un detector cuántico D. Si dejamos que el sistema evolucione, lo lógico sería esperar que terminase en una superposición de la forma:

$$\Psi = \alpha \left| S_{\mathrm{e}} D_{\text{no click}} \right\rangle + \beta \left| S_{\mathrm{g}} D_{\text{no click}} \right\rangle + \gamma \left| S_{\mathrm{e}} D_{click} \right\rangle \tag{0.0.2}$$

Este estado está entrelazado. El primer término representa el caso en que el átomo S no ha emitido ningún fotón, el segundo, aquel en el que el átomo ha emitido un fotón pero el fotón no ha llegado o no ha sido detectado, y el tercero, el caso de detección exitosa de la emisión atómica. Si, a través de una medida local, descubrimos que el detector ha hecho click, el estado total del sistema colapsará y podremos estar seguros de que el átomo ha

emitido un fotón. ¿Seguros? Digamos que hemos descrito el caso ideal. Un detector realista no sería 100 % eficiente y podría registrar partículas aún no habiendo ninguna (conteos oscuros o *dark counts*).

En esta tesis hemos dedicado un esfuerzo considerable a entender bien los procesos de detección desde las últimas consecuencias de la mecánica cuántica. Como mostraremos más adelante, el análisis aquí presentado asume una aproximación que se mostrará válida sólo en regímenes de tiempos cortos y pequeños acoplos. La historia al completo, como veremos en detalle, es bastante más complicada a la aquí presentada.

Otro aspecto interesante relacionado con estas cuestiones fundamentales de la información cuántica, en el que también nos hemos centrado, es la cuestión de la causalidad. Como expondremos más adelante, la mecánica cuántica es una teoría "non-signalling" [27, 28], es decir, las estadísticas obtenidas a través de las medidas de una parte A deben ser completamente independientes de lo que haga otra parte B si A y B están espacialmente separados. Por esta razón, la mecánica cuántica no permite transmisión de información más rápida que la luz [29]. Las correlaciones cuánticas tienen que estar asistidas con operaciones locales y comunicación clásica para cualquier proceso de transferencia de información, como en el caso de la teleportación cuántica [30].

Pese a que la causalidad en el sentido relativista está garantizada por estas razones, un experimento mental ha tenido a la comunidad en jaque prácticamente desde los años 30. En aquel entonces, en un largo artículo donde presentaba una primera formulación de la electrodinámica cuántica, Fermi propuso una situación sencilla, con dos átomos, para estudiar el comportamiento causal en la excitación de uno de ellos debida a la desexcitación del otro. Con su fuerte intuición conceptual Fermi se las arregló para conseguir una demostración que mantuvo a todo el mundo satisfecho durante décadas. Sin embargo, un error detectado en su argumento [31] (una aproximación válida tan sólo a tiempos largos) abrió un debate [32, 33] que ha continuado prácticamente hasta hoy [34–36].

En esta tesis hemos dedicado un capítulo entero al problema de Fermi. Lo diseccionamos en detalle en el caso de 1 dimensión, ofrecemos una prueba no perturbativa de la causalidad y explicamos el origen de los conflictos que parecen existir. Más aún, proponemos un experimento que modela la situación original usando qubits superconductores que emulan átomos artificiales, contectados a través de una línea de transmisión. Esperamos que un estudio experimental sobre el fenómeno ponga fin a esta controversia de décadas.

Este problema despertó mi interés en el mundo de las simulaciones cuánticas. Habiendo orientado mi investigación principalmente hacia los aspectos teóricos de los procesos de detección, las simulaciones cuánticas eran una posibilidad de explorar las consecuencias ex-

perimentales y comprobar el impacto de los interesantes fenómenos físicos que estábamos estudiando en condiciones realistas. Así fue como, inspirados por el problema de Fermi y nuestros estudios sobre detección y con esta idea en mente, escribimos tres artículos más donde propusimos experimentos para simular átomos acelerados, extracción del entrelazamiento del vacío y procesos rápidos de detección [5–7]. A cada uno de ellos le dedicamos un capítulo de esta tesis.

Entrelazamiento del vacío e información cuántica relativista

La teoría de la Información cuántica suele operar en escenarios no relativistas con un número finito de grados de libertad. Pese a ello, el entrelazamiento acepta extensiones al dominio de la teoría cuántica de campos [37–39].

Desde ese punto de vista se puede comprobar que el propio vacío cuántico está entrelazado, como demuestra el teorema de Reeh-Schlieder [40]. Este hecho, descubierto hace ya 50 años, se consideraba un resultado puramente formal hasta que fue estudiado desde un punto de vista más aplicado en [41]. Desde entonces, esta propiedad tan inquietante del vacío, ha atraído mucha atención como posible nuevo recurso para tareas de procesado de información cuántica [42–45].

Como se ve en [41], el entrelazamiento contenido en el vacío de un campo puede ser transferido a un par de detectores de dos niveles separados espacialmente que interaccionan con el campo . Desafortunadamente, este resultado teórico es muy difícil de demostrar experimentalmente, incluso en el contexto de una simulación de iones atrapados [42].

En los últimos años muchos estudios han considerado la posibilidad práctica de extraer correlaciones del vacío [46–50]. En esta tesis, nosotros hacemos nuestra contribución particular. Discutiremos una propuesta experimental con circuitos superconductores y mostraremos cómo un tipo particular de correlaciones, a las que nos referimos como pasado-futuro, pueden ser en principio extraídas con éxito.

A través de esta línea de estudio, me familiaricé con ciertos aspectos del problema de entrelazamiento del vacío, que puede ser considerado como un asunto bastante fundamental. En particular, el estudio del entrelazamiento entre regiones separadas lleva implícito el uso de observables locales, intrínsecamente distintos de los observables globales. De hecho, no existen operadores número locales que predigan cero partículas en el estado de vacío [51,52]. La razón de ello es relativamente simple. Si el vacío es un estado puro entrelazado, el estado reducido sobre cualquier región compacta del espacio deberá ser necesariamente una mezcla.

También el teorema de Malament theorem [53] argumenta la imposibilidad de existencia para los estados perfectamente localizados de una sola partícula. Este tipo de interesantes cuestiones teóricas se estudian fundamentalmente desde el punto de vista de la notablemente abstracta Teoría Cuántica de Campos Algebraica. Nosotros hemos querido acercarnos a ellas de una manera más práctica, más constructiva y más física si cabe. Más concretamente, trabajando con un campo escalar en una cavidad hemos diseñado un procedimiento de cuantización local con el que explorar este tipo de teoremas.

Lo cierto es que la naturaleza entrelazada del vacío cuántico está estrechamente relacionada con otros efectos interesantes como el efecto Unruh [54], por el que un observador uniformemente acelerado detecta un baño térmico de partículas donde uno inercial experimenta el vacío, y la radiación de Hawking [55] emitida por agujeros negros. Estos fenómenos se suelen ver como efectos geométricos relacionados con la existencia de un horizonte y el entrelazamiento existente entre los modos del campo a uno y otro lado. Lo discutiremos más en detalle en el capítulo 2. El efecto Casimir Dinámico es otro fenómeno de este estilo, en el que las partículas se procuden debido al movimiento oscilatorio de un horizonte (un espejo por ejemplo). Aunque ni la radiación de Hawking ni el efecto Unruh hayan sido observados directamente hasta la fecha, el efecto Casimir Dinámico ha sido recientemente comprobado en laboratorio [56–59].

Al final de la tesis, como resultado de nuestro análisis sobre el entrelazamiento del vacío y nuestra cuantización local, hemos ideado un experimento mental donde al desplegar rápidamente un espejo en el centro de una cavidad se genera un fenómeno de producción de partículas de este estilo. También estudiamos la posibilidad de comprobarlo en el laboratorio.

El estudio de este tipo de fenómenos combina a menudo conceptos de Información Cuántica, Relatividad General y Teoría de Campos en Espacio-Tiempos curvos, que se han constituido en intereses de un nuevo campo interdisciplinar dentro de la Física con el nombre de Información Cuántica Relativista.

Este campo arrancó en los años 90 cuando nadie prestaba atención a cómo la información podía verse afectada bajo la influencia del movimiento de los sistemas en el espacio-tiempo y cómo podría depender del punto de vista del observador o de cómo hubiera sido codificada en primer lugar (diferentes grados de libertad pueden ser afectados de forma diferente por el movimiento). La razón de ello es obvia: la información cuántica opera en general en escenarios no relativistas. El primero en trabajar en estos aspectos fue Czachor en 1997 [60], demostrando que la violación de las desigualdades de Bell por un par de partículas separadas dependería de sus velocidades. Desde entonces, una increíble cantidad

de esfuerzo, creatividad, tiempo y trabajo ha sido dedicado al estudio de las correlaciones cuánticas en escenarios no inerciales, el núcleo de la información cuántica relativista. Dentro de ese marco se han estudiado temas que van desde el estudio de la invariancia Lorentz del entrelazamiento bajo determinados supuestos [61–65] o los efectos del movimiento no uniforme [66, 67], hasta casos más centrados en la física de agujeros negros y la cosmología [68–72].

Y por supuesto entre estos temas, muchos otros, como los que ocupan a esta tesis: el estudio del entrelazamiento en estados locales y globales, modelos de detección y la naturaleza profunda del entrelazamiento en el vacío, incluyendo fenómenos de creación de partículas como los mencionados.

En esta tesis, mucho del trabajo puede ser comprendido en este marco. En los primeros estudios de Información Cuántica Relativista, a la hora de estudiar el entrelazamiento visto por distintos observadores se trabajaba con modos globales, una aproximación interesante, sobre todo desde el punto de vista académico, pero poco práctica ya que ningún observador realista puede tener acceso a ellos. Últimamente sin embargo, esta cuestión ha sido tratada en escenarios más realistas, con paquetes de onda [3, 4] o considerando cavidades como en [73–75].

En esta tesis hemos tratado de contribuir a la superación de esos primeros trabajos. En los primeros capítulos, tras la introducción, nos dedicamos a estudiar modelos de detección. Derivamos en concreto el modelo de Unruh-DeWitt de primeros principios y sugerimos modificaciones que faciliten el estudio teórico de paquetes de onda localizados, más realistas. De igual modo, usando un modelo particular basado en medida proyectiva enfrentamos también el análisis de estados de campo localizados de dos fotones entrelazados.

En este punto deberían quedar claras las motivaciones de esta tesis. Hemos tratado de enfocar el estudio de las correlaciones del vacío estudiando en primer lugar qué es lo que miden los detectores. Con las herramientas de la información cuántica y la teoría de campos hemos presentado resultados sobre estados localizados y explorado el concepto de partícula a través de simulaciones. Hemos profundizado en los problemas de la localización perfecta, la naturaleza entrelazada del vacío y como estas cuestiones se relacionan entre sí, dando lugar a fenómenos como el que describimos al final de esta tesis.

Estructura

La tesis comienza con una introducción (**Preliminares**) dividida en tres capítulos:

- **Capítulo 1** Información Cuántica.

- **Capítulo 2** Teoría Cuántica de Campos.
- **Capítulo 3** Plataformas Experimentales para la Simulación Cuántica.

Con este material, se pretender fijar una notación y proveer al lector con las herramientas y conceptos más importantes en la investigación llevada a cabo en esta tesis. No es una introducción exhaustiva, pero cubre una gran variedad de temas. El núcleo de la tesis, desarrollado tras estos preliminares, se divide en tres partes, cada una de ellas a su vez, dividida en varios capítulos.

- **Parte I** Dedicada al estudio teórico de modelos de detección.
  - **Capítulo 4** Este capítulo acerca al lector a los modelos de detección. Se resumen algunos resultados previos y se describen brevemente los modelos de Unruh-DeWitt y el detector proyectivo con los que se trabaja a continuación.
  - **Capítulo 5** Aquí consideramos el modelo Unruh DeWitt y sus propiedades de localización. Mostramos que las modificaciones simples del mismo que incorporan perfiles espaciales presentan problemas al tratar ciertos estados interesantes de los campos. Deducimos que en el caso de la detección de paquetes de onda el perfil espacial considerado debe verificar ciertas propiedades. Hemos estudiado el origen de este perfil para el caso de un detector atómico derivando la interacción Unruh-DeWitt de primeros principios y relacionando el modelo de perfil suavizado con la forma usual $\boldsymbol{p}\cdot\boldsymbol{A}$ de la interacción QED acoplando átomos y campos electromagnéticos. Exponemos un modo de conectar la forma del perfil con la función electrónica de los orbitales relevantes del átomo. Mostramos también que si queremos que el detector sirva para detectar radiación resonante, esa información debe estar presente en el perfil. Finalmente sugerimos un método para introducirla y explicamos cómo calcular la probabilidad de detección para el caso de un detector acelerado.
  - **Capítulo 6** En este capítulo empleamos un modelo proyectivo de detector para analizar el entrelazamiento de sistemas entrelazados de fotones individuales desde un punto de vista no inercial. Como caso particular analizamos el comportamiento de entrelazamiento de un estado de dos fotones entralazados y mostramos cómo los efectos cuánticos de la aceleración relativista pueden amplificar el entrelazamiento y no sólo destruirlo. Así mismo hemos analizado el caso de detectores con detección de banda estrecha en frecuencia y estudiado el coste computacional de considerar detectores de banda ancha.

  - **Capítulo 7** Presentamos aquí un método para simular un conjunto de detectores Unruh-DeWitt acelerados acoplados a un modo único del campo con dos plataformas: iones atrapados por un lado y circuitos superconductores por otro. La idea está basada en inducir "sidebands" dependientes del tiempo en los acoplos átomo-campo. Mostramos cómo nuestra idea puede ser extendida a experimentos con varios iones que podrían simular resultados no.-simulables en computadores clásicos como trayectorias no-inerciales arbitrarias o muchos detectores acoplados al mismo campo. Terminamos efectuando una conexión nueva entre la física de los procesos fuera del equilibrio y los efectos cuánticos debidos a la aceleración.

- **Parte II** Esta parte se centra en el comportamiento de detectores más allá de la aproximación de la onda rotante. La parte termina respondiendo una pregunta interesante... ¿qué significado debemos atribuir al click de un detector?

  - **Capítulo 8** Contrariamente a la creencia generalizada, bajo la aproximación de onda rotante pueden aparecer fenómenos no causales. Sólo cuando se considera el Hamiltoniano al completo emerge la causalidad. Comenzamos esta parte con una breve digresión sobre el concepto de causalidad en filosofía y en física e introduciendo lo que sigue.
  - **Capítulo 9** Discutimos aquí el problema de Fermi: un ejemplo paradigmático donde presentamos un marco teórico bajo el que entender con claridad los misterios de la causalidad. Ofrecemos una prueba de causalidad no perturbativa en una dimensión y discutimos un experimento donde verificar cuantitativamente las predicciones del análisis cuántico. Hemos considerado para ello un sistema de dos qubits superconductores acoplados a una linea de transmisión. Con un procedimiento novedoso basado en la activación del acoplo ultrafuerte usando procesos de Landau Zener podemos conectar y desconectar los qubits de la línea de forma efectiva y llevar a cabo mediciones independientes.
  - **Capítulo 10** Inspirados por nuestros estudios previos hemos centrado el análisis de este capítulo en el comportamiento de detectores en tiempos cortos. En estos regímenes la aproximación de onda rotante debe ser descartada. Mostramos que para parámetros típicos en circuitos superconductores, y en tiempos pequeños, la información aportada por el click de un detector respecto a la posible desexcitación de una fuente originalmente excitada es mínima debido a las excitaciones del detector. Sólo tras un cierto tiempo podemos comenzar a

confiar en el estado del detector como indicativo de la desexcitación de la fuente. Nuestros resultados se aplican a otras plataformas y detectores cuánticos, pero es el campo de los circuitos superconductores donde estos fenómenos pueden afectar a la interpretación de posibles resultados experimentales.

- **Parte III** Esta última parte se dedica al estudio de correlaciones de vacío y la localización de estados en Teoría Cuántica de campos.

  - **Capítulo 11** En este capítulo introductorio discutimos en detalle la conexión entre localización y entrelazamiento de vacío. Motivamos nuestro trabajo con un repaso histórico sobre el progreso en la cuestión y describimos algunos de los problemas más relevantes en lo que se refiere a la construcción de estados de partícula localizados. Discutimos también cómo el formalismo que será desarrollado en los siguientes capítulos puede iluminar la cuestión de los fenómenos de producción de partículas por emergencia de horizontes, en este caso de una barrera física. Discutimos también el concepto de entrelazamiento de género espacio y de género tiempo y, como introducción de lo que sigue, discutimos las posibilidades de extracción de entrelazamiento del vacío.
  - **Capítulo 12** Dado que muchas propuestas de extracción de entrelazamiento del vacío hasta la fecha resultan bastante impracticables sugerimos aquí un experimento dentro de las posibilidades de la tecnología actual. Caracterizamos por completo, cualitativa y cuantitativamente el tipo de correlaciones que pueden ser transferidas a un par de qubits P y F, que interaccionan con el campo exclusivamente en el pasado y en el futuro respectivamente, aun cuando los qubits en ningún momento coexisten. Discutimos las posibilidades de uso de esa extracción y el potencial de nuestro esquema para funcionar como una memoria cuántica.
  - **Capítulo 13** En este capítulo desarrollamos nuestro formalismo de cuantización local. Interesados sobre la imposibilidad teórica de construir estados de una partícula perfectamente localizados en teoría cuántica de campos decidimos explorar cómo surgirían los problemas al intentar una construcción concreta. Hemos identificado el principal problema en el requerimiento de que el espacio de Hilbert de una sola partícula se construya con modos de frecuencia positiva. En concreto los paquetes de onda construidos de ese modo no pueden ser localizados en una región espacial finita, incluso en intervalos de tiempo infinitesimales. Al basar nuestra cuantización en modos localizados de norma positiva, podemos

dar cuenta de estados de una partícula. Llevamos a cabo esta cuantización en una cavidad. Al calcular los coeficientes de Bogoliubov que relacionan las cuantizaciones local y global demostramos que ambas son *unitariamente no-equivalentes*. Pese a ello, mostramos que los creadores y destructores locales están bien definidos por sus acciones en el espacio de Fock global $\mathfrak{F}^G$ y lo mismo ocurre con el operador número local, concluyendo con un buen set de herramientas listas para analizar y caracterizar propiedades locales de estados de ese espacio. Específicamente analizamos las propiedades del vacío global $|0_G\rangle \in \mathfrak{F}^G$ en términos de los operadores números locales y demostramos, como era de esperar, la existencia de entrelazamiento entre las secciones izquierda y derecha de la cavidad.

– **Capítulo 14** Hemos dejado para el último capítulo un resultado que relaciona muchos de los conceptos discutidos en esta tesis. Usando nuestro formalismo local describimos la situación de una cavidad en la que desplegamos un espejo dividiéndola rápidamenteen dos partes iguales. Explicamos cómo en ese caso tiene lugar un fenómeno de producción de partículas. Damos una respuesta a la pregunta "¿Qué quiere decir que la mitad de una cavidad vacía esté llena?". Comprobamos que las partículas producidas son matemáticamente equivalentes a las excitaciones locales del vacío descritas en nuestro formalismo y verificamos que las partículas producidas están entrelazadas entre sí. De hecho vamos más allá y estudiamos el caso en el que dos espejos, en lugar de solo uno, se despliegan a una cierta distancia. Dado que en esa situació, las partículas producidas en la región más a la izquierda y más a la derecha surgen entrelazadas, podemos concluir que este entrelazamiento no es producido por la introducción de los espejos, sino que estaba presente previamente en el vacío. A lo largo de este capítulo usamos la teoría de estados gaussianos para derivar los estadios reducidos y las correlaciones del estado de vacío en distintas regiones de la cavidad.

En una última sección de conclusiones volvemos a resumir los resultados de esta tesis.

Preface

A new paradigm for computation

Classical Information Theory has been one of the most important pillars in the development of current information and communication technologies. Originally developed by Harry Nyquist, Claude Shannon, Norbert Wiener among others in the 40's and 50's, it became the foundational theory of information processing. In its core is the concept of information entropy, which defines the information content of a certain message produced by a source by relating it to the unpredictability of the message. [3]

The merits of Classical Information Theory are countless: the mathematical characterization of communication channels, the discovery of fundamental limits for channel capacity, the rigorous understanding of compression, coding and the interplay between signal and noise are just examples that have expanded the horizons of information processing much further than we could have imagined just a few decades ago. [4]

Among the most important of these findings, the Shannon-Hartley theorem is a limiting result that sets the maximum rate at which information can be transmitted (capacity C) over a communications channel of a certain bandwidth B for a certain S/N ratio

$$C = B \log_2 \left(1 + \frac{S}{N}\right). \tag{0.0.4}$$

Current communication technologies are incredibly close to it. Given usually a limited transmission power, as it is the case with mobile phones, most of the improvements we experience in transfer speeds come directly from the use of bigger and bigger bandwidths

[3] The entropy of a certain source X that emits messages $\{x_i\}$ with probability p_i can be calculated as:

$$H(X) = -\sum_i p_i \log p_i \tag{0.0.3}$$

.

[4] For more details in Classical Information Theory we refer the interested reader to [76]. In the main body of this thesis we will just concentrate on its Quantum counterpart.

for information transfer (e.g. 3G as compared to 2G mobile networks) [5].

For the computing case, the information processing rate limit is not so highly dependent on the (in principle) limited transmission speeds from register to register. The number of operations per time unit that a computer is able to perform depends rather on its processing capabilities, which grow with the processor's complexity (transistor density), and on the switching speed of those transistors. Increasing the number of transistors while maintaining the computer size involves miniaturization. Coincidentally, increasing the switching speed can be also attained through reducing component size. As in a simple RC circuit, the logical gate switching time happens to be proportional to the RC time constant of a circuit [77]. Modeling all resistances and capacitances that constitute a logical semiconductor gate and their dependences with size, it can be found that this RC delay is at first order proportional to the length scale [78,79], which has provided much of the performance gains in the past. Transistor dimensions in personal computers (supercomputers) are now in 2014 around 45nm (22nm), while the dimensions in 1997 were around 250nm.

Miniaturization did not come without problems. Until 2005, the conspicuous Moore's law, which states that computer power doubles every 24 months, relied heavily on what is known as Dennard scaling: as transistors got smaller, speeds (clock rates) could get higher, as the heat released per area unit stayed constant (both voltage and current scaled downward with length). In 2005, however, Dennard scaling broke down. At small sizes, current leakage poses big challenges, and causes the chip to heat up creating the threat of thermal runaway. The computer processor industry could not get rid of that extra amount of heat (*the power wall*) and the solution was to relinquish any further increase in the clock rates.[6] Since then, improvements in performance have been achieved by working on the complexity side: the increased number of transistor density has allowed to allocate more processors in the same area, capable of carrying on parallel operations, in a multi-core framework. This evolution has been simultaneous to a change in the software design paradigm, where multithread code has helped to divide and distribute tasks into the different cores improving complexity but at the expense of introducing a considerable amount of overhead data. In that sense, many scientists argue that further gains to be obtained through multi-threading are actually much lower than those that could be achieved had Dennard scaling continued, foreseeing the end of Moore's law. [11]

As Seth Lloyd points out *"Moore's law is a law not of nature, but of human ingenuity. Com-*

[5] It must be taken into account that Shannon's limit is for a point to point channel. New technologies like 4G and 5G mobile telecommunications technologies make use of the possibility of establishing multipoint to multipoint links creating many channels for a single transmission and therefore challenging that very limit

[6] That is the reason why our computers still run at 3 GHz, not much faster than 10 years ago.

puters have gotten two times faster every eighteen months [7] *because every eighteen months engineers have figured out how to halve the size of the wires and logic gates from which they are constructed."* [80] In other words, Moore's law acts as a reference, a target, and in doing so becomes a self-fulfilling prophecy, but as happened with Malthus' law of exponential growth, we can be certain that it will eventually break down. Exponential growth laws are usually really difficult to maintain. Also Moore's was never a law in any scientific sense , but rather a rule of thumb (but of course "Moore's Rule" sounds much less impressive to say)

In this particular case, there are also different physical limits that will also make its maintenance if not difficult, impossible.

First of all, given that most current computational technologies are based in irreversible computing, there is the Landauer barrier. It accounts to the fact that every bit of information deleted requires the dissipation of at least $kT \ln 2$ of energy [12]. Miniaturization is progressively reducing the energy dissipation per computational step, and it is progressively approaching that barrier. If the current pace is maintained it will be hit around 2034. Either we have switched to a reversible paradigm by then or there would be no way to scale down the heat released. [13].

Besides that, we can consider other limitations. In a result that relates closely to the Heisenberg Uncertainty relation for time and energy, Margolus and Levitin [14] showed that a quantum system with average energy E takes at least at time $\Delta t = \pi\hbar/2E$ to evolve to an orthogonal state. This implies that the computation speed of a computer is fundamentally limited by the energy available to it for information processing. Using that simple idea, Seth Lloyd, in a pretty original work [81], studied how fast the ultimate laptop [8] could perform. Extrapolating Moore's law to the future, Lloyd estimated a 250 years time to reach that totally idealized limit.

In a more realistic approach to that of Lloyd, Levitin and Toffoli [15], based on a new better bound for the rate of quantum dynamics have estimated the time to hit that quantum limit within 75 to 80 years time.

With all that in mind, no doubt current semiconductor companies are studying new technologies that challenge the current computational paradigm. The current scenario is

[7] In origin, most people interpreted Moore's Law as referring to the number of transistors on a 1 inch (2.5 cm) diameter of silicon doubling every x months. Some people say it takes 18 months, others say 24. Some have interpreted the law to be rather about the doubling of processing power. Most of those rules, when interpreted adequately, happen to be rather accurate to date, as does Seth's version.

[8] That would be a laptop of 1 kg of mass and 1 L of volume, which is roughly the size of a conventional laptop computer, operating at the limits of speed and memory space allowed by physics, where all its energy could be put to use to perform universal quantum logic operations.

not a reason for dismay. More on the contrary, existing possibilities may take the future of computing to a new level. More and more attention is being paid to alternative models of computation like Quantum, Reversible and Molecular Computing.

In this thesis we would be conducting studies using Quantum Information (QI) tools. Quantum Information is the basic theory behind Quantum Computing. The motivation to work along those lines should be clear by now, but still, Quantum Information has still much more to offer than just improvement of current computer technology. Actually, this thesis deals mostly with other aspects of it, less related to Computing and more connected to Causality, Detection Theory, Relativistic scenarios, Quantum Field Theory (QFT), and Foundations of Quantum Physics. All these fields have links to one other and in all of them plays a role one of most interesting phenomena of Quantum Physics: entanglement.

A powerful concept

Entanglement is one of the main concepts of Quantum Information. The history of Entanglement, or rather the history of its discovery and study, goes back to the first decades of the twentieth century, in particular to a paper by Albert Einstein, Boris Podolsky and Nathan Rosen [16], which described what later came to be known as the EPR paradox.

Einstein never really liked Quantum Mechanics (QM). He was especially against the Copenhagen Interpretation, that thought of the wave function in quantum theory as just a tool to calculate the probability for the outcomes of measurements. Einstein was at unease by the theory being silent about what was true in the absence of observation. He wanted laws to say how things were, independently of how one looks, and that theory was not Quantum Mechanics, so he set on a quest to prove its flaws, in particular its not-realistic aspects [82].

In May 1935, in collaboration with two postdoctoral researchers at the Institute of Advanced Study, Boris Podolsky and Nathan Rosen, Einstein co-authored a paper (the EPR paper, by the names of the authors) in which they proposed a thought experiment trying to make obvious this incompleteness of QM. As Leo Rosenfeld summarized it, the argument goes as follows:

Suppose two particles, A and B, are set in motion towards each other with the same, very large, momentum, and that they interact with each other for a very short time when they pass at known positions. Consider now an observer who gets hold of one of the particles, far away from the region of interaction, and measures its momentum; then, from the conditions of the experiment, he will obviously be able to deduce the momentum of the other particle. If, however, he chooses to measure

the position of the first particle, he will be able to tell where the other particle is. This is a perfectly correct and straightforward deduction from the principles of quantum mechanics; but is it not very paradoxical? How can the final state of the second particle be influenced by a measurement performed on the first, after all physical interaction has ceased between them?

The main idea was that, if QM were complete, one could in principle attach real values to both position or momentum of the second particle without having measured it, actually "without in any way disturbing it", so values for both observables should exist simultaneously, which was incompatible with quantum mechanics. It was a very subtle argument, but of course it had some implicit assumptions.

What Einstein was discarding was the possibility that the state in B could be instantaneously affected by the measurement carried on in A. Bohr's reply to the EPR paper made obvious to Einstein that any valid claims against his reasoning were incorporating this nonlocal nature of QM. He himself had also expressed similar concerns about the collapse of the wave function in the Solvay Conference of 1927 [83]. Years later, Einstein, still not comfortable with this fact, which seemed to challenge his own relativity theory, in a famous letter to Max Born, called it " spukhafte Fernwirkung", "spooky action at distance", a sentence that went down in history.

Erwin Schrödinger, who at the time was also contrary to the Copenhagen Interpretation and hoped for a return to deterministic physics, was really interested in the EPR experiment. Inspired by it, within a few months after the publication of the EPR paper, he wrote a couple of articles [84, 85] discussing the issues raised by the EPR, and discussing along other problems with QM, among which would be his cat paradox. In all of these papers, he used the word "entanglement" for the first time, *verschränkung* [9] referring to that mysterious Quantum Mechanical feature, noticing that a multipartite system might not be described as just a sum of its parts [10]

Entanglement is definitely peculiar, it cannot be produced locally: a system of two parts with no access to any entangled shared resource and which may communicate only through classical channels cannot become entangled by performing local quantum operations separately on each subsystem. When entanglement already exists, it may be redistributed, dis-

[9] Actually he had used the word before, in a letter to Einstein. In his own words: *When two systems, of which we know the states by their respective representatives, enter into temporary physical interaction due to known forces between them, and when after a time of mutual influence the systems separate again, then they can no longer be described in the same way as before, viz. by endowing each of them with a representative of its own. I would not call that one but rather the characteristic trait of quantum mechanics, the one that enforces its entire departure from classical lines of thought. By the interaction the two representatives (or ψ-functions) have become* ***entangled***.

[10] Or more accurately, might not be factored out into the states of its constituents.

tilled, swapped or delivered [17–19] from one subsystem to another. But those features are recent findings.

Entanglement has been considered to be a key piece in Quantum Mechanics ever since the EPR paper, if not the "key piece". Many scientists, however, were dissatisfied with it, because it seemed to violate the limit of transmission of information set implicitly as the speed of light by the theory of relativity. We will discuss this in much more detail in chapter 8, but for the moment, let us say that the measurement of one of the two particles in an EPR experiment does not involve faster-than-light classical bodies or any sort of radiation signal so, in principle, the displayed non-locality does not have to be at odds with special relativity.

Anyhow, if truth be told, the whole entanglement concept was debated and highly challenged until 1964. That year, in a groundbreaking paper [20], John S. Bell disclosed his theorem putting all these concepts on much firmer ground. He defined accurately what a local hidden-variable theory was mathematically and used a version of the EPR experiment proposed by David Bohm, which included spin-correlation measurements, to introduce a new thought experiment. He formulated a simple inequality based on the experiment statistics that would be satisfied by any physics following a hidden variable theory and showed that using certain QM entangled states, the inequality was violated. This result, known as *Bell's theorem* makes obvious that no hidden local-variable theory would ever reproduce all the predictions of QM.

Within the next years after that, many efforts were put trying to make Bell's result testable. In 1972 the first experimental test [21] came to light and was in agreement with QM. In the coming years new inequalities as the CHSH and the CH74 were derived [86, 87] and more experiments were carried on by Clauser, and Fry and Thompson [22, 23], in agreement with QM predictions. The most conclusive and famous experiments where however those carried on by Alain Aspect and his team [24–26] where they obtained maximum violations of Bell's inequalities.

Those experiments and the ones coming after them had certain loopholes. Under the idea that maybe nature conspires against the experimenter (metaphorically of course), it is possible that the experimental results match the predictions of quantum mechanics just because nature finds its way through minor errors and deficiencies in the setups. To date, no test has simultaneously closed all the loopholes. It is also true that no one, among the ones carried on accurately, has ever found any result that could challenge the QM predictions.

The non-local character of quantum mechanics is nowadays fully accepted, and the EPR paper, the first one noticing it, remains one of the most cited papers of Science, accumulating

so far more than 12500 citations, according to Google Scholar.

Again, entanglement is not just a theoretical concept. It is basic in the Quantum Computation paradigm [88]. Based on Quantum Entanglement, many algorithms have been developed for Quantum Computers that can produce solutions for some NP problems [11] in polynomial time. Shor's algorithm for factorization would allow us to decipher top secure current transmissions in matter of seconds had we a Quantum Computer available. Alternatives for traditional cryptography have been proposed and even built: Quantum Information has been used to develop commercial Quantum Key Distribution systems, unbreakable 100 % secure cyphering systems that could even detect eavesdropping [12]. Quantum Machines performing Quantum Algorithms on systems up to 512 superconducting qubits are being developed by US company D-wave and there is evidence that they might solve instances of the NP Travelling Salesman problem in polynomial time. It is highly impressive, indeed, what has been achieved over the last 30 years of Quantum Information research. Who can know what will come next?

Let us come back to Entanglement. Entanglement is everywhere, has important consequences and it is basic when it comes to describing certain Quantum Phenomena. Detection for example, is one of those process where entanglement plays an important role. Imagine that we have in the same isolated laboratory an originally excited atom S, which acts as a quantum source, and a quantum detector, D. If we let the system evolve, in principle, we would assume that it ends up in a quantum superposition:

$$\Psi = \alpha \left| S_{\text{excited}} D_{\text{no click}} \right\rangle + \beta \left| S_{\text{decayed}} D_{\text{no click}} \right\rangle + \gamma \left| S_{\text{decayed}} D_{click} \right\rangle \tag{0.0.5}$$

This state is entangled. The first term represents the case where the source has not decayed, the second, that of the source having decayed but the photon emitted having missed the detector, and the third, the case of a successful detection of the decay event. If, through a local measurement, we find out that the detector has clicked, the whole state collapses and we can be sure that the source has decayed. If we were to consider a realistic detector there would be other cases, as it would not be 100 % efficient and it could also register *dark counts*. The case here described should at least be a good portrait of the ideal detection process. But this turns out to not be the case.

In this thesis we have devoted much work in trying to understand the detection process according to the ultimate predictions of Quantum Mechanics. As we will show later, the

[11] Roughly and rather unprecisely, a P problem is a decision problem that can be solved on a deterministic Turing machine in an amount of time that is polynomial in the size of the input. Analogously, an NP problem is a decision problem for which a solution can be verified in polynomial time given the right information.

[12] Vadim Makarov (The Quantum Hacker), might think otherwise... [89, 90]

analysis that we have sketched above assumes an approximation that would prove only valid for long times and small coupling regimes. The whole picture, as will be shown, is much more complex.

Other issue, related to QI, where we have put our focus in this thesis, is that of causality. As we will discuss later in more extent, Quantum Mechanics is a non-signaling theory [27, 28], i.e. the statistics of any measurements performed by a certain party A are completely independent of the measurements carried on by the other party B if A and B are space-like separated. For that reason, QM does not allow for faster-than-light information transfer: quantum correlations must be assisted with local operations and classical communication (LOCC) in order to transmit information [29]. Quantum Teleportation is a paradigmatic example of this [30].

Even if Relativistic Causality is granted through those considerations, a particular thought experiment has kept the community particularly busy since the 1930's. At that time, in a long paper where he presented a first formulation of Quantum Electrodynamics [8], Fermi proposed a simple situation, with just two atoms, to study the causal behavior in the excitation of one of them. With his strong conceptual intuition, he managed to obtain a proof for it and for years everybody was satisfied. However, a flaw detected in his argument [31] (an approximation only valid for long times) opened a can of worms that was source of debate for many years [32, 33] . It was not until very recently that the picture of the whole situation became clearer [34, 35].

In this thesis we have devoted a full chapter to the study of the Fermi problem. There we dissect the whole problem for the 1D case, provide a non-perturbative proof of causality and explain in detail what the origin of all discrepancies is. Furthermore, we also propose a setup that models the Fermi problem using superconducting qubits coupled to a transmission line, and that would allow a detailed study of the issue from the experimental point of view that could put an end to an eight-decade old controversy.

This very problem started my interest to work on Quantum Simulations. Having focused my research mainly in theoretical aspects of detection, Quantum Simulations were a genuine possibility to explore the experimental consequences, and check the impact of the interesting physical phenomena we were studying in real setups. Inspired by the Fermi problem and our studies on detection, with this Quantum Simulation mindset, we wrote three articles making experimental proposals dealing with accelerated atoms, vacuum entanglement extraction and short-time detectors [5–7].

Vacuum Entanglement and Relativistic Quantum Information

Although QI has always been mostly studied in non-relativistic settings with a finite number of degrees of freedom, most of its concepts can be formulated in abstract algebraic terms engulfing both non-relativistic QM and QFT [37–39], extending therefore the notion of entanglement in a natural way to domains with infinitely many degrees of freedom.

Entanglement is ubiquitous. Most quantum states are entangled [91], and most of them are even too entangled to be useful for computational purposes [92, 93]. When looked from the algebraic perspective, also the vacuum is entangled, as shown by the Reeh-Schlieder theorem [40]. Moreover, it violates Bell's inequalities maximally, without setting up a source [94, 95].

This fact, discovered long ago, was considered a mere formal result until it was addressed from a more applied perspective in [41]. Since then, this intriguing property has attracted a great deal of attention as a possible new resource for Quantum Information tasks [42–45].

As shown in [41], the entanglement contained in the vacuum of a scalar field can be transferred to a pair of two-level space-like separated detectors interacting with the field at the same time. Unfortunately, this theoretical result seems to be very difficult to translate into an experiment, even in the context of a trapped-ion simulation [42].

In the last years many studies have considered the possibilities for practical extraction of vacuum correlations [46–50]. In this thesis, we will discuss a particular experimental setup where we propose to use superconducting circuits and show how a particular kind of correlations, that we call past-future, can be extracted from the vacuum in a feasible way.

Through this line of study, I became acquainted with some aspects of the whole vacuum entanglement situation, which could be considered to be rather fundamental. In particular, the study of entanglement between space-like separated regions involves the use of local observables, which are intrinsically distinct from the global ones [13]. As a matter of fact, there are no non-trivial positive local operators with zero vacuum expectation value. In particular, as shown by Redhead [51, 52], no candidate for a local particle number operator can have zero expectation value in the vacuum state. Also Malament theorem [53] addresses the impossibility of having local one-particle states by showing that no local particle projector exists whose eigenstates would correspond to a particle definitely being in the subregion of space or not. These aspects and many others which we will explore in more detail later have been studied from the perspective of the notoriously abstract Algebraic Quantum

[13] One immediate consequence of vacuum entanglement is that, the vacuum being a entangled pure state, its reduction to any local region in space must necessarily be mixed and thus excited

Field Theory (AQFT). In this thesis we have aimed to illuminate these intriguing results and insights of AQFT by providing a concrete and simple construction using language and methods familiar to physicists. Specifically, by working with a scalar field in a cavity we have envisioned a local quantization, in contrast to the global standard one, and with the help of it explored the aforementioned ideas.

The entangled nature of the quantum vacuum is very much related to other interesting effects like the Unruh [54] and Hawking [55] effects. These phenomena are usually viewed as geometric effects related to the existence of a horizon. We will go through more detail later in the chapter 2, but it might be worth mentioning here that from the point of view of Quantum Field Theory, their origin can be explained in terms of a decomposition into this-side-of-the-horizon modes and the-other-side-of-the-horizon modes. Let us explain it further. If we can fully decompose the vacuum of a Quantum field in modes that fall into a horizon (or are causally disconnected to our observer trajectory) and modes that do not (or are causally connected to our observer), we will for most cases obtain an expression where the vacuum state is described explicitly in terms of entangled modes. By then tracing away the modes that cannot be accessed by our observer, we might end up with a remaining thermal-like state.

In the case of flat Minkowski space time and a decomposition into modes accelerating towards or away from a certain horizon, this is exactly what happens and the picture would correspond to the Unruh effect: an observer with uniform acceleration a in the flat quantum vacuum perceives a thermal bath of particles of temperature $T_{\text{Unruh}} = \hbar a/2\pi c k_{\text{B}}$. Analogously, an observer positioned at a fixed proper distance from a black-hole horizon has uniform acceleration (the closer to the horizon the larger the acceleration), and therefore will see a thermal bath. This acceleration, if red shifted to an infinite distance from the black hole, becomes the black hole's "surface gravity", $\kappa = c^2/2R_{\text{BH}}$. Then, by making use of the equivalence-principle, we can replace the a by κ in the Unruh temperature to obtain the Hawking temperature: $T_{\text{Hawking}} = T_{\text{Unruh}}|_{a=\kappa} = \hbar c/4\pi R_{\text{BH}}$ [96, 97]. The Dynamical Casimir Effect (DCE) is susceptible to a similar analysis [98]. There the situation is not stationary, but in any case particles are produced due to the oscillatory movement of a horizon (a mirror boundary). Although neither the Hawking radiation or the Unruh effects have been simulated yet, their cousin, the DCE, has been successfully observed in a few experiments to date [56–59].

Thinking about vacuum entanglement and our local formalism, our ideas led naturally to explore a dynamical-Casimir-like effect where a cavity in the vacuum state is divided into two parts by slamming a mirror in the middle. Our mathematical toolbox can be directly

applied to this problem where local virtual quanta get transformed into local measurable particles. Moreover, we show mathematically how the entanglement existent between the particles being produced corresponds exactly to previously existing vacuum entanglement and we further suggest possible experimental settings where to see this.

This sort of phenomena whose study combines more often than not concepts of Quantum Information, Gravity, Relativistic Mechanics and Quantum Field Theory in Curved spacetimes, are engulfed in the interests of a relatively new interdisciplinary field within physics, known under the name of Relativistic Quantum Information (RQI).

At the end of the last century a seemingly unrelated development of Quantum Information theory helped to resolve some of the long-standing conceptual problems within quantum mechanics. The scientific and technological breakthroughs followed a realization that information is physical, so its acquisition and processing are ultimately subjected to the laws of physics. Also in the recent years also, a trend can be observed, with many scientists exploring the possibilities of setting information as a more fundamental concept in the understanding of our universe, e.g. by deriving quantum theory from a set of information processing principles [99], or studying how gravity could be an emergent force consequence of the "information associated with the positions of material bodies" [100] (also known as entropic gravity), or even exploring the possibility of time being an emergent phenomenon based on entanglement [101–103].

Although those are rather exotic possibilities, it should be clear by now that the study of information in all kind of contexts is highly motivated. Until the end of the 1990's however, nobody paid attention to the study of how information is affected under the influence of movement through spacetime, how it might depend on the point of view of the observer or how the final state of that information depends on the way it was encoded in the first place (different inner degrees of freedom of a system are disturbed in different ways). For standard Quantum Information any relativistic effect was negligible. The first one to work on this kind of topic was Czachor in 1997 [60], who found that the violation of Bell's inequalities by a pair of separated massive particles depended on their velocities. Since then, an incredible amount of work, creativity, time and effort has been devoted to the study of quantum correlations in non-inertial settings, which constitutes RQI basic focus. Given the vast collection of papers, we will mention just a few references that might inspire the reader.

A few years after Czachor's seminal paper, a review by Peres and Terno [104] pointed out that a reassessment of several quantum information concepts was needed and pointed out some research directions to follow. At the beginning, a central theme emerged in the

first RQI papers: the study of entanglement dependence on the inertial observers reference frames and, in particular, the effects of motion in both spin and momentum entanglement [61–65]. The conclusion was that although spin entanglement or momentum entanglement were not observer independent, when you consider both together, entanglement could be seen to be Lorentz invariant. However, the possibilities of gathering experimental evidence on this fact have been rather limited, given the dependence of measurement of spin and momentum, [105]. As a matter of fact, the discussion about the definition of a relativistic spin operator started back then and has not ended yet [106–108].

In parallel, people started to look into the study of the effects of non-uniform motion [66, 67]. In that respect, the famous paper by I. Fuentes, *Alice falls into a black hole*, [68] started a series of works on the effects of spacetime curvature that have continued as of today [69,70], and inspired other studies in black-hole physics and cosmology [71,72].

The effects of acceleration on entanglement involve in general the degradation of it for both fermionic and bosonic cases (although with remarkable differences), and in different scenarios (cavities and free-space, local and global modes) [66, 109–111], but surprisingly enough, and for some situations, acceleration might have an amplification of entanglement as a consequence [4,112,113]. We will discuss this later in chapter 6. The trade-off between particle and antiparticle modes for non-inertial frames, has also been considered [114,115].

The article production rate in RQI has boomed in the last 10 years. Nowadays it extends its arms to ideas that go from the extended study of observer dependence of entanglement (the curious reader might find a recent review of those in [116]) to the study of the information loss paradox [117,118]. And of course, in between those, many others: the study of entanglement behavior for local and global states, detector models, entanglement dependence for inertial and non-inertial observers, non-uniform accelerations and curved space-times, the profound nature of Vacuum Entanglement, particle creation phenomena, signatures of Cosmological phenomena and many more.

Although its motivation was mostly theoretical at the beginning, it has progressively moved towards interesting experimental scenarios as current technologies and, in particular, Quantum Information technologies, have stepped into realms where relativist effects could be of interest, like satellite quantum communications [119,120] Also, the improvement of Quantum technologies has given rise to a broad range of platforms to engineer quantum systems, like ion traps or superconducting circuits, where to experiment and verify predictions of RQI, produce analog computations of certain problems, simulate relativistic settings and reproduce thought experiments [6,8,121–123].

In this thesis much of our work can be understood under that framework. In particular

we have proposed the simulation of two thought experiments [7, 8] and the study of the emission features of atoms accelerated in a quantum field [6].

Also among the RQI lines of study are particle creation phenomena such as the Unruh-Hawking radiation, the Unruh effect, or the Dynamical Casimir effect, mentioned earlier. After the corresponding seminal works, many studies have focused on the use of Quantum Information tools to better describe such phenomena, focusing on how to probe them using detectors. [124–127].

For most of those studies, and for those that study entanglement observer dependence, the study of quantum detectors in spacetime has been paramount. The analyses carried on in RQI usually involve studying the detection of particles using simple phenomenological detector models such as the Unruh-DeWitt model. Actually, much of the work in the RQI field has involved their study [75, 127, 128, 128–137] and corrections to former assumptions in the detection process, like the single mode approximation [138].

Until very recently, many RQI studies, in order to study entanglement behavior as seen by different observers, considered these particular detector models while working with entangled states of quantum-field global modes. It was mainly a theoretical approach, as global modes can never be probed by any realistic observer. Lately, however, this issue has been addressed by working in more realistic settings, either studying more physical states, like wavepackets [3, 4] or considering cavities as in [73–75].

In this thesis we have contributed our bit to this area. We have studied how the Unruh-DeWitt model can be derived from first-principles and, introducing some modifications to it, considered the case of detecting localized wavepackets. We have also considered a particular projection-based detector model introduced in [139] as a practical method to study field entanglement for localized two single-photon bipartite electromagnetic field states.

Finally we would like to mention the interesting work being done in the emerging field of Relativistic Quantum Metrology where the tools of relativistic quantum information harness quantum optics technology and merge with it in synergically in the quest to design new better detectors, thermometers, accelerometers, seismometers and even gravitational wave detectors [140–147]

By now, it should be clear what are the main motivations of this thesis. Mainly we have tried to contribute to the study of what a particle is and what is it that is measured by a detector. With the tools of Quantum Information, Relativistic Information and Quantum Field Theory we will present ways for detector models to be modified and better adjust to physical relevant phenomena. We will use them to study more localized states, atypical in the literature, and explore the concept of particle through simulations, like checking their

propagation in ideal setups (Fermi problem) or the excitations of detectors in extraordinary regimes (ultrastrong, extremely short-times). Furthermore, we will see some of the problems intrinsic to the idea of local particles, the entangled nature of the vacuum and how these two concepts relate to one another. We will describe vacuum entanglement using Rindler quanta but also from the point of view of spacelike and timelike separated detectors and, at the end of the thesis, we will finally to bring some ideas together by building a local particle description. We will show that, although purely virtual, this description has an exact correspondence to a particle production phenomenon that could, in principle, be observed in the lab.

Structure of the thesis

This thesis starts with an introductory section (**Preliminaries**) divided in three chapters:

- **Chapter 1** Quantum Information.
- **Chapter 2** Quantum Field Theory.
- **Chapter 3** Quantum Simulation Platforms.

With this review material, we aim to fix notation while providing the reader with the most important tools and concepts used in the research program of this thesis. It is not exhaustive in its contents, but covers a large background of topics.

The research core of the thesis, detailed from here on, is divided in three parts, each of them, in turn, divided in several chapters.

- **Part I** The first part is devoted to a couple of theoretical studies about quantum detection. There we study two detectors, the Unruh-DeWitt (UdW) model and a projective detector. For the first one we obtain a derivation from first principles and suggest convenient modifications for the study of wavepackets. For the second, we use it to study entanglement behavior of certain EM quantum states. We do so as part of a larger effort to move away from the use of typical global-mode cases and to extend the use of these theoretical models to more realistic cases like electromagnetic field states or wavepackets. We finalize the part with a more practical work, where we make a concrete proposal for simulating an accelerated UDW detector in the lab.
  - **Chapter 4** This chapter is an introduction to detector models. We will cover briefly some results of entanglement degradation and amplification under non-inertial settings and discuss the peculiarities of the detectors later studied.

- **Chapter 5** Here we consider the UdW model and its localization properties. We show how natural extensions of it, incorporating spatial profiles, meet a series of problems in their spectral response, especially when dealing with certain interesting physical states of the fields. Additionally we provide a derivation of the smeared UdW interaction from QED first principles.
- **Chapter 6** In this chapter we analyse the quantum effects of acceleration on realistic spatially-localized EM field states entangled in the polarization degree of freedom. We do so by using a particular projective detector model. In line with previous results [113] we find that quantum entanglement might build up as the acceleration increases for a certain regime, in contrast to the extended belief that the Unruh effect can only destroy entanglement.
- **Chapter 7** Here we present a study to simulate accelerated UdW detectors in the lab, by showing an analogy with static quantum emitters. Harnessing this connection we propose two setups, one using trapped ions and another with superconducting circuits, where we show how to model some relativistic quantum scenarios that are beyond current computational power. Furthermore we show a simple connection with non-equilibrium physics to make calculations with relativistic atoms.

- **Part II** In this part we study some phenomena that concern the behavior of detectors beyond rotating wave. Contrary to former standard belief, when the interaction Hamiltonian is simplified through a rotating wave approximation, acausal behavior might appear. Only when one considers the full Hamiltonian does causality emerge. Now, we start this part with a brief discussion on the causality concept and an introduction to what comes next. We proceed to discuss the Fermi Problem, a paradigmatic case where we can fully understand these mysteries, and finally we head on to consider another interesting question that relates to regimes beyond rotating wave... if a detector can self-excite, how reliable is the information we get from a click as what regards to the de-excitation of a certain source?

  - **Chapter 8** We devote this chapter to a general discussion about causality in physics and a brief explanation and motivation to the problems and scenarios that we would like to simulate in the lab and that would be described in the next chapters.
  - **Chapter 9** This is a full dissection of the Fermi problem. We disentangle previous misconceptions and give a general framework to understand causality

issues in quantum theories. We produce a non-perturbative proof for causality in 1D and discuss an experiment to verify the causal behavior, and to allow for a quantitative verification of the quantum mechanical predictions.

  - **Chapter 10** Inspired by our studies of the Fermi problem, we discuss here a thought experiment about quantum detection at short-times. We quantify the details of a detection process and verify that the information collected by a detector from a source is minimum for short-times and increases as time evolves.

- **Part III** We have devoted the final part of the thesis to the study of vacuum correlations and localizability of states in Quantum Field Theory. In an introductory chapter we present some algebraic quantum field theory concepts and discuss how the localization conundrum has been explored in the past. We put vacuum entanglement under the light of the Reeh-Schlieder theorem and discuss the recently phrased concept of timelike entanglement. After this introduction, a new chapter contains an experimental proposal for the extraction of past-future vacuum correlations in a circuit QED setup. Later we describe a local formalism, developed by us in order to see how the problems of localizability would appear while defining local particles constructively. We also discuss how vacuum entanglement can be understood within this construction. In spite of the expected problems we come up with a consistent mathematical apparatus that, in the final chapter, relates this virtual perspective to an interesting particle production phenomenon.

  - **Chapter 11** In this chapter we discuss in detail the connection between vacuum entanglement and localization. We motivate our work by making a short historical review of the subject and presenting some of the relevant issues when it comes to building localized particle states. We also discuss how the formalism to be developed in the next chapters can help to further illuminate the question of particle production in the appearance of physical boundaries, e.g. a mirror. We discuss what is meant when people talk about time-like entanglement vs. space-like entanglement of the vacuum and, as an introduction to what comes next, we present the state-of-the-art regarding vacuum entanglement extraction.
  - **Chapter 12** Given that previous proposals to extract time-like correlations in the vacuum where experimentally unfeasible, we suggest here an experiment using circuit QED, where past-future correlations can be extracted. We characterize fully, both quantitative and qualitatively, the kinds of correlations extracted and show how to perform quantum teleportation in time with our proposal, and

how this can be seen as an exotic quantum memory that stores a quantum bit of information in the vacuum.

- **Chapter 13** Here is where we present our mathematical toolbox to analyze and characterize local features of free quantum fields. By using two different quantization procedures we show how to analyze, on a sound mathematical footing, the local particle content within a certain region of a box. We show explicitly another way of seeing the existence of entanglement between left and right regions of the box. Moreover, we relate abstract concepts such as Unitary Inequivalence to our particular constructive approach in order to give a better grasp of their implications. In the process we define a local vacuum, with interesting features, and a set of local operators which act naturally on the standard Fock space.
- **Chapter 14** As the cherry on the top of the cake, we have left for the very last a most interesting chapter that brings together many of the concepts discussed in this thesis. Using our local formalism we describe here the situation of a box where a mirror is slammed down, dividing it into two equal parts. We describe the process of particle production under this light and verify that the burst of particles produced can be exactly expressed in terms of the original content of entangled virtual local particles. We end up discussing what the experimental prospects are when it comes to probing this scenario in the lab.

We end up with a conclusion section where we summarize all the results here exposed.

Preliminaries

Background and Tools of *Quantum Information*, *Quantum Field Theory* and *Quantum Optics*

CHAPTER 1

Quantum Information

This chapter aims to be a short introduction, mostly notational, to some basic notions on entanglement and separability for pure and mixed states. We will also discuss briefly how entanglement measures can help us to calculate the amount of entanglement in bipartite systems. We will regrettably leave aside some other fundamental concepts, e.g. entanglement witnesses, protocols, positive maps, majorization, etc., as they are not used directly in this work. Entanglement is a very wide topic, still a very active field of research, and its developments so broad and extensive that any brief introduction is doomed to be merely a shadow of the field's vastness. The interested reader may find more information about the topic in the following reviews [148–150], which have inspired the present section.

In the preface we described entanglement as a distinctive characteristic of quantum mechanics. It is surely not the only one. Quantum systems exhibit several non-classical features like state superposition, interference or tunneling. These are all phenomena that can be observed in individual systems, composed of just one particle. Entanglement however, manifests itself in composite arrangements, where different subsystems (or independent degrees of freedom [1]) can be identified . In classical physics, the correlations between different subsystems can be explained in terms of classical probabilities, but this turns out not to be the case for all quantum systems. The states that present that peculiar sort of correlations are called entangled.

Along this chapter we focus on bipartite systems[2], associated to a finite dimensional Hilbert space $\mathcal{H}_{AB}$ that is the tensor product of the associated Hilbert spaces of the two subsystems $\mathcal{H}_{AB} = \mathcal{H}_A \otimes \mathcal{H}_B$, with dimension $d_S = \dim(\mathcal{H}_{AB}) = d_A d_B$, being $d_A = \dim(\mathcal{H}_A)$ and $d_B = \dim(\mathcal{H}_B)$. For most cases we will work with states of two qubits: $d_A = d_B = 2$.

[1] We say this to make it clear that entanglement can manifest itself also in a single particle, if we consider as subsystems its independent degrees of freedom, e.g. momentum and spin.

[2] Most of the ideas presented here, however, can be generalized to multipartite systems.

We will discuss separately the cases of pure and mixed states.

1.1 Pure states

Let us consider a pure state of the form:

$$|\Psi_S\rangle = |\psi_1\rangle \otimes |\psi_2\rangle \tag{1.1.1}$$

If we perform for example a projective measurement on the subsystem A, say by considering an operator $O \otimes \mathbb{1}$, the final state of subsystem A will end being an eigenstate of the first subsystem A, say $|o\rangle$ and the state of the subsystem B will remain unchanged: $|\Psi\rangle_{AB} = |o\rangle \otimes |\psi_B\rangle$ and all future local measurements on B would be independent of that any measurements carried on at A. This is what is called a separable state. Notwithstanding, these states are not the general case. The general bipartite state takes the form:

$$|\Psi\rangle_{AB} = \sum_{ij} c_{ij} \, |\psi_i\rangle_A \otimes |\psi_j\rangle_B \,, \tag{1.1.2}$$

where $\{|\psi_i\rangle_A\}$ and $\{|\psi_i\rangle_B\}$ constitute bases for the subspaces A and B respectively, and the coefficients c_{ij} verify $\sum_{ij} |c_{ij}|^2 = 1$. The indexes i, j run up to the corresponding subspaces dimensions d_A and d_B.

There is always however a more "economical" expansion in which only one index is needed, the *Schmidt decomposition*. Let us formulate here the following theorem.

Theorem 1.1 (Schmidt decomposition) *For every pure bipartite state $|\Psi\rangle_{AB}$ there exist orthonormal sets $\{|\phi_i\rangle_A\} \subseteq \mathcal{H}_A$ and $\{|\varphi_i\rangle_B\} \subseteq \mathcal{H}_B$ such that,*

$$|\Psi\rangle_{AB} = \sum_{i=1}^{n} \lambda_i \, |\phi_i\rangle_A \otimes |\varphi_i\rangle_B \,,$$

where $1 \leq n \leq \min(d_A, d_B)$ and the Schmidt coefficients λ_i are all real, non-negative $\lambda_i \geq 0$ and satisfy $\sum_{i=1}^{n} \lambda_i^2 = 1$

The minimum possible value for n, n_{min}, is called the *Schmidt rank* of the state for that partition AB. States of Schmidt rank $n_{\text{min}} = 1$ are called *separable*, and have the form of Eq. (1.1.1). Any other state with $n_{min} > 1$ is called *entangled*. In particular, those states with $n_{\text{min}} = min(d_1, d_2)$ are called *maximally entangled states*. A paradigmatic example of maximally entangled states in a two-qubit case are the Bell states, $\{|\Psi^+\rangle, |\Psi^-\rangle, |\Phi^+\rangle, |\Phi^+\rangle\}$. For example, $|\Psi^-\rangle = \frac{1}{\sqrt{2}}(|\downarrow\uparrow\rangle - |\uparrow\downarrow\rangle)$.

An easier definition of separable and entangled states can be given simply as:

Definition 1.1 (Separable pure state) *A pure state $|\Psi\rangle_{AB} \in \mathcal{H}_{AB}$ is said to be separable with respect to the partition $\mathcal{H} = \mathcal{H}_A \otimes \mathcal{H}_B$ iff it can be written as a tensor product of individual subspace states, i.e. if there are states $|\psi\rangle \in \mathcal{H}_A$ and $|\psi\rangle_B \in \mathcal{H}_B$ such that :*

$$|\Psi\rangle_{AB} = |\psi\rangle_A \otimes |\psi\rangle_B .$$

Definition 1.2 (Entangled pure state) *A pure state $|\Psi\rangle_{AB} \in \mathcal{H}_{AB}$ is said to be entangled with respect to the partition $\mathcal{H}_{AB} = \mathcal{H}_A \otimes \mathcal{H}_B$ iff it is not separable with respect to that partition, i.e. iff for all states $|\psi\rangle \in \mathcal{H}_A$ and $|\psi\rangle_B \in \mathcal{H}_B$ we have :*

$$|\Psi\rangle_{AB} \neq |\psi\rangle_A \otimes |\psi\rangle_B .$$

1.2 Mixed states

While considering statistical mixtures of bipartite states, it may seem natural to demand for a global mixed state, ρ_{AB} to be separable, that it should accept a decomposition as the product of the corresponding mixed sub-states $\rho_{AB} = \rho_A \otimes \rho_B$ with $\rho_A = \mathrm{Tr}_B\{\rho_{AB}\}$, and $\rho_B = \mathrm{Tr}_A\{\rho_{AB}\}$. This view is, however, too restrictive. Of course that would be a separable state, but so should be any convex mixture of that kind of mixed states.

With that caveat in mind we can make the following definition:

Definition 1.3 (Separable mixed state) *A mixed state $\rho_{AB} : \mathcal{H}_{AB} \to \mathcal{H}_{AB}$ is said to be separable with respect to the partition $\mathcal{H}_{AB} = \mathcal{H}_A \otimes \mathcal{H}_B$ iff it can be written as a convex combination of tensor products of mixed states of the individual subsystems as:*

$$\rho_{AB} = \sum_i p_i \rho_i^{(A)} \otimes \rho_i^{(B)} \tag{1.2.1}$$

with $p_i \geq 0$ and $\sum_{i=1}^{n} p_i = 1$

We must point out to the reader that the existence of a separable state does not mean the absence of correlations. As a matter of fact, for the general case of a separable mixed state there will be local observables O_A, O_B leading to correlated measurement results, i.e.

$$\mathrm{Tr}\{\rho_{AB}(O_A \otimes O_B)\} \neq \mathrm{Tr}\{\rho_{AB}(O_A \otimes \mathbb{1})\}\mathrm{Tr}\{\rho_{AB}(\mathbb{1} \otimes O_B)\} = \mathrm{Tr}_A\{\rho_A O_A\}\mathrm{Tr}_B\{\rho_B O_B\}^{3} \tag{1.2.2}$$

The definition of entangled mixed states follows directly:

[3] Part or all of those correlations might be explainable classically. The part that cannot be classified as "classical" is called *Quantum discord*. It has been proposed as a measure for the most general kind of Quantum

Definition 1.4 (Entangled mixed state) *A mixed state $\rho_{AB} : \mathcal{H}_{AB} \to \mathcal{H}_{AB}$ is said to be entangled with respect to the partition $\mathcal{H}_{AB} = \mathcal{H}_A \otimes \mathcal{H}_B$ iff it is not separable, i.e. iff there are no local states $\rho_i^{(A)}$, $\rho_i^{(B)}$, and non-negative weights p_i such that ρ_{AB} can be written as a convex mixture:*

$$\nexists\, \rho_i^{(A)}, \rho_i^{(B)}, p_i \geq 0, \text{ with } \sum_i p_i = 1 \text{ such that } \rho_{AB} = \sum_i p_i \rho_i^{(A)} \otimes \rho_i^{(B)} \tag{1.2.3}$$

1.3 Von-Neumann entropy

The entropy of information as defined in Classical Information Theory has a natural extension to Quantum Mechanics. There it represented the uncertainty associated with the next message emitted by a source, or the next outcome of a random experiment. We can translate this to the uncertainty we have for a mixed state $\rho = \sum_i p_i |\psi_i\rangle\langle\psi_i|$ to be in one of its constituent pure states $|\psi_i\rangle$. If we know that our system is in a certain pure state, then the entropy should be zero. This is exactly what happens with the Von-Neumann entropy:

Definition 1.5 (Von-Neumann entropy) *The Von-Neumann entropy $S(\rho)$ of a certain density matrix ρ with a decomposition $\rho = \sum_i p_i |\psi_i\rangle\langle\psi_i|$ in pure states is given by:*

$$S(\rho) = -\sum_i p_i \log p_i = -\mathrm{Tr}(\rho \log \rho) \tag{1.3.1}$$

where *log* is usually taken to be the binary logarithm.

The connection of this concept with entanglement will be unveiled soon, when we consider entanglement measures.

1.4 Entanglement detection

Given the importance of entanglement in Quantum Computing, it would be incredibly useful to have a test that could check whether or not a given state is entangled. The search of that kind of tests is a very active research area and has produced many necessary and sufficient criteria for entanglement (check [149] for references). A different approach to it is given by Entanglement Witness and Positive Maps [149, 153].

Notwithstanding, these are all partial solutions as there is not yet a universal, both necessary and sufficient test. However, if we restrict ourselves to the case of Hilbert spaces of

Correlations [151, 152]. We will omit a more precise definition here, but let us say that it is non-negative and mention that *separable pure states* have zero discord, *entangled states* (pure or mixed) have non-zero discord and *certain separable mixed states* (which are therefore not entangled) have non-zero discord.

2×2 or 2×3 dimensions, there exists such a criterion. We think it is worth presenting it here:

Definition 1.6 (Peres-Horodecki Criterion, PPT Criterion [4] [154, 155]) *Let us consider a state ρ acting on $\mathcal{H}_{AB} = \mathcal{H}_A \otimes \mathcal{H}_B$ with $d_A d_B \leq 6$*

$$\rho = \sum_{ijkl} \rho_{kl}^{ij} |i\rangle\langle j| \otimes |k\rangle\langle l| \tag{1.4.1}$$

Its partial transpose (with respect to B) is given by:

$$\rho^{T_B} := (\mathbb{1}_A \otimes T_B)(\rho) = \sum_{ijkl} \rho_{kl}^{ij} |i\rangle\langle j| \otimes (|k\rangle\langle l|)^T = \sum_{ijkl} \rho_{kl}^{ij} |i\rangle\langle j| \otimes |l\rangle\langle k| \tag{1.4.2}$$

Then, the criterion states that iff ρ is separable all ρ^{T_B} eigenvalues are non-negative. The criterion also verifies when considering ρ^{T_A} instead. For other dimensions of the subsystems the positivity of the partial transpose is not sufficient but it is still necessary for a state to be separable.

1.5 Quantum steering

The most interesting aspect of entanglement is probably the "spooky action at distance", how a measurement performed in a part of the system can modify (or rather, collapse) the state of the other part. This notion, called by Schrödinger "quantum steering", can be simply put as follows: if A (Alice) and B (Bob) share a certain bipartite state, what kind of states can Alice prepare for Bob, considering she acts just locally?[5]. The Quantum Steering theorem might shed some light on it. Although we will omit its proof here, a very simple one can be found in [156]:

Theorem 1.2 (Quantum steering [85, 157]) *Let Alice and Bob share a pure bipartite state $|\Psi\rangle_{AB}$ on $\mathcal{H}_{AB} = \mathcal{H}_A \otimes \mathcal{H}_B$, with Bob's local density matrix being $\rho_B = \mathrm{Tr}_A\{|\Psi\rangle_{AB}\langle\Psi|_{AB}\}$. Then there exist a POVM on Alice side where she can produce the ensemble $\{p_i^B, \sigma_i^B\}$ iff there is a convex decomposition of ρ_B in that particular ensemble, i.e. iff $\rho_B = \sum_i p_i^B \sigma_i^B$.*

The theorem is casted in a peculiar language that would benefit from some clarifications. The whole question of Quantum Steering is extremely subtle. First, as a straightforward consequence of the rules of quantum measurement theory, it is impossible for Alice, no matter what operations she performs, to locally modify the density matrix of Bob's subsystem ρ_B (if she could, there would be signaling), so, in what sense are saying that Alice can prepare

[5] If the reader hints here a rather strong connection between Quantum Steering and Teleportation, he is right. Quantum Teleportation can be naturally and easily understood in those terms [156]

certain states? It is all a matter of information. When dealing when mixed states we are talking about ensembles, an statistical description of the states we deal with. If Bob were to do tomography on his final state, repeating the experiment many times for many copies of that shared entangled state $|\Psi\rangle_{AB}$, he would obtain a density matrix ρ_B no matter what Alice has done. However, if he were to do tomography with only those states that Alice told him he should look (for which she would have performed the appropriate POVM and obtained the result corresponding to the final $\{\sigma_k^B\}$ then Bob would observe a density matrix σ_k^B.

Alice can change Bob state, but only through post-selection. Unless Bob does know the result of Alice measurement, he will not update his description of the system to a new density matrix within the ensemble, because the state that Alice prepares is a different one every time. Alice, on her side, cannot choose which one she prepares. Her preparation, as happens with all quantum mechanical measurements, even if it may follow an accurate recipe, it is like cooking a mysterious cake whose final flavor can only be discovered at the moment you taste it.

1.6 Entanglement measures

When it comes to saying which one of two states is more entangled, the qualitative distinction between entangled and separable states that we have hitherto discussed proves to be insufficient. In order to come up with a quantitative description we will consider some properties of entangled states and how they can be affected by certain operations.

While talking about entanglement, we have left it clear that it was an intrinsically quantum feature related to the quantum correlations that occur in many-party quantum states. In order to define quantum correlations, it is easy to think about them as those that are not classical, and then we must try to define what classical means. In Quantum Information, and for operational purposes, we can define classical correlations as those that can be build up while performing *local operations and classical communication* (LOCC) between parties. The idea is that both parties can make operations on their systems and then tell the other what results they have obtained through a classical communication channel. LOCC operations can create correlations but those should remain classical, and in that sense, they should not increase entanglement. A natural requirement for any entanglement measure is therefore that it should not increase under LOCC. That leads to define the concept of entanglement monotone [158]:

Definition 1.7 (Entanglement monotone (I)) *An entanglement monotone $E(\rho)$ is a mapping*

from density matrices into real numbers that does not increase, on average, under LOCC [6]

Given a function $E(\rho)$ that satisfies this monotonicity axiom, E must be *minimal* and *constant* on separable states, because any separable state can be obtained by LOCC from any other state [158]. Therefore it is customary to set that value to zero and introduce, without loss of generality, this other definition.

Definition 1.8 (Entanglement monotone (II)) *A mapping from density matrices into real positive numbers $E : \rho \to \mathbb{R}^+$ is an entanglement monotone iff:*

- $E(\rho_{sep}) = 0$ *for all separable states* ρ_{sep}.
- E *does not increase, on average, under LOCC.*

In addition to those, it is common in the literature to require more conditions in order to define an entanglement measure. The choosing for these criteria is often source of debate [149], so we will stick to the ones here presented and will not make any distinction between monotone and measure. However, it can be worth to present some:

- *Normalization* The idea is to set the entanglement value for a state made of qubit maximally-entangled states (Ψ_2^+) in terms of how many other qubits can be teleported using it as a resource. With this convention,

$$E[(\Psi_2^+)^{\otimes n}] = n$$

- *Assymptotic Continuity* For every two states ρ_n, σ_n acting on a Hilbert space $\mathcal{H}_n$ of dimension n one must have:

$$\|\rho_n - \sigma_n\|_1 \to 0 \Rightarrow |E(\rho_n) - E(\sigma_n)|/\log n \to 0$$

- *Weak Additivity* For every state ρ we must have $E(\rho \otimes \rho) = 2E(\rho)$

Other examples of properties often considered are full additivity[7] , convexity [8], faithfulness [9] or monogamy [10].

[6] With this we mean that, if we consider stochastic LOCCs, the estimated value of E does not increase, i.e.

$$E(\rho) \geq p_i E(\rho_i) \tag{1.6.1}$$

, where ρ_i are the possible outputs, each with probability p_i, of the LOCC.

[7] For every two states ρ and σ, $E(\rho \otimes \sigma) = E(\rho) + E(\sigma)$

[8] A monotones is convex iff $E(\sum_i p_i \rho_i) \leq p_i \sum_i E(\rho_i)$, with $\sum p_i = 1, p_i \geq 0$

[9] A monotone is faithful iff for every ρ_{ent} entangled, $E(\rho_{\text{ent}}) > 0$

[10] A monotone is monogamous iff for every $E(\rho_{A\tilde{A}B}) \geq E(\rho_{AB}) + E(\rho_{\tilde{A}B})$

If we limit ourselves to the study of just pure states, a natural measure of entanglement is the Von-Neumann entropy of the reduced state for any of the two subsystems, also called *entropy of entanglement*.

Definition 1.9 (Entropy of Entanglement) *The entropy of entanglement $\mathcal{E}_S$ of a pure state ρ_{AB} is given by:*

$$\mathcal{E}_S(\rho_{AB}) = S(\rho_A) = S(\rho_B),\ \textit{with}\ \rho_A = \mathrm{Tr}_B\rho_{AB},\ \ \rho_B = \mathrm{Tr}_A\rho_{AB} \tag{1.6.2}$$

, with S being the Von-Neumann entropy as defined in Eq. (1.5))

This entropy is a measure of the mixedness of one of the system parts after we have trace the other. Its use as a measure of the matches perfectly with the simple intuition that the more a system is entangled, the more mixed one part will look like after we have disentangled it.

The *entropy of entanglement* accepts many extensions to mixed states, some of them faithful [11], like the *relative entropy of entanglement* .

Definition 1.10 (Relative entropy of entanglement [159]) *The relative entropy of entanglement $\mathcal{E}_R$ of a state ρ is given by:*

$$\mathcal{E}_R(\rho_{AB}) = \min_{\sigma_{sep}} S(\rho\|\sigma_{sep}) \tag{1.6.3}$$

Where the minimization is taken over all separable states σ_{sep} and $S(\rho\|\sigma) = S(\rho) - \mathrm{Tr}(\rho\log\sigma)$

It reduces to the entropy of entanglement for pure states and it is a faithful monotone, convex, normalized, asymptotically continuous and faithful, but not weakly additive. It has many applications in quantum entanglement theory, especially in quantum hypothesis testing [160], but its calculation implies a complex minimization process and there are other faithful measures that can be calculated in a much simpler way. *Concurrence* and *negativity* are examples of those, which will be used in this thesis. Neither of them, however, reduces to the entropy of Entanglement in the case of pure states.

Concurrence

Concurrence is the most usual measure of entanglement for non-pure two-qubit states. It is defined as follows:

[11] Faithfulness makes it easy to probe for entanglement as $E(\sigma = 0)$ means automatically that σ is separable.

Definition 1.11 (Concurrence [161]) *The concurrence $\mathcal{C}$ of a state of two qubits ρ acting on $\mathcal{H}_{AB} = \mathcal{H}_A \otimes \mathcal{H}_B$ is given by:*

$$\mathcal{C}(\rho) = \max\{0, \lambda_1 - \lambda_2 - \lambda_3 - \lambda_4\} \tag{1.6.4}$$

and the $\{\lambda_i\}$ are the eigenvalues, in decreasing order, of the Hermitian matrix $R = \sqrt{\sqrt{\rho}\tilde{\rho}\sqrt{\rho}}$. Alternatively, the λ_i are also the square roots of the eigenvalues of the non-Hermitian matrix $\rho\tilde{\rho}$. The matrix $\tilde{\rho}$ represents the spin-flipped state:

$$\tilde{\rho} = (\sigma_y \otimes \sigma_y)\rho^*(\sigma_y \otimes \sigma_y) \tag{1.6.5}$$

where the complex conjugate[12] is taken in the standard basis, which for a pair of spin-1/2 particles is $\{|\uparrow\uparrow\rangle, |\uparrow\downarrow\rangle, |\downarrow\uparrow\rangle, |\downarrow\downarrow\rangle\}$

Generalizations of concurrence in arbitrary dimensions exist only for pure states. Luckily enough, we will restrict ourselves to its use in two-qubit states.

Negativity

Based on the PPT criterion presented in Sec. 1.6, the *negativity* quantifies how much a given state fails to be positive after its partial transposition. It is simply calculated as the absolute sum of the negative eigenvalues for the partial transpose.

Definition 1.12 (Negativity [162]) *The negativity $\mathcal{N}$ of a bipartite state ρ acting on $\mathcal{H}_{AB} = \mathcal{H}_A \otimes \mathcal{H}_B$ is given by:*

$$\mathcal{N}(\rho) = \sum_i \frac{|\lambda_i| - \lambda_i}{2} \tag{1.6.6}$$

where the $\{\lambda_i\}$ are the eigenvalues of the partial transpose of the state, ρ^{T_B} (or ρ^{T_A}).

The negativity is a convex monotone and it can be evaluated easily for pure and non-pure states in arbitrary dimensions. It is only faithful, however, for the 2 x 2 (two qubits) and 2 x 3 (a qubit and a qutrit) dimensions (the only cases where the PPT criterion is a sufficient and necessary condition for separability).

[12] Unlike the Hermitian conjugate, the complex conjugate of a density operator depends on the basis in which it is expressed

CHAPTER 2

Quantum Fields

Most of the research of this thesis is carried on within the framework of Quantum Field Theory. Here we would like to go through some basic notions about quantum fields, quantization in curved spacetimes and discuss some of particle production phenomena such as the Unruh effect. In order to simplify the discussion, and given that in this thesis we do not deal with fermions, we would restrict ourselves to the bosonic cases.

Also it is worth to say that Quantum Field Theory is an extremely broad topic and we are studying it only laterally, in what it relates to our Relativistic Quantum Information studies.

A very interesting concept that has played a major role in the understanding, interpretation and development of Quantum Theory has been that of particle. In the early days of quantum mechanics, single particles were the fundamental objects under study. At the end of the day the Schrödinger equation was a single particle equation and the wavefunction represented originally the quantum properties of such an object. It was when QM and Special Relativity came together into Quantum Field Theory that the focus on the single particle drifted towards quantum fields, where those particles where envisaged as basic elementary excitations. On top of a quantum background field, particles could be created or annihilated, they could interact and even produce other particles of different nature. And in the beginning such an understanding of the particle idea became satisfactory to a great extent. The later success of QFT predicting experimental results in particle accelerators, the electroweak unification, the development of Quantum Chromodynamics and the discovery of the Higgs boson have strengthened that feeling. However, the concept of particle has several problems when one looks at it from a fundamental point of view. First, a particle is not a well localized object. Our naïve picture of particles being thought as minute compact objects propagating at subluminical speeds is far from what the theory boilds down to. We

will discuss this issue in detail later in part III of this thesis. Secondly, particles are typically understood as rather free objets, but actually this free picture is in conflict with the existence of interactions. As Rudolf Haag proved in 1955, the interaction particle representation is unitarily inequivalent to the free particle representation, being this last one basic in the definition of the asymptotic states used to represent particles in the study of typical experiments. We will give some thought to these unitary inequivalence issues also in chapter 13. Thirdly, the concept of particle is ambiguous in curved spacetimes. There is no preferred natural choice for the spacetime coordinates and, classically, all the possible choices have an equal standing, even if they might lead to different unitarily inequivalent representations and therefore not just different, but rather incompatible particle definitions. This is known as the "multiple choice" problem.

Actually, the whole problem of defining particles in general spacetimes is a bit tricky. For a general trajectory where no conserved quantities can be assumed to exist, there is no way to consistently choose a definition for a particle that does not change in time. For that matter we need to restrict ourselves to the study of observers whose particle definitions do not change in time. The concept of Killing fields is key there. A Killing field is basically an isometry of the metric tensor, which we can make use of to define a Hamiltonian and an evolution parameter to properly define particles in the usual way.

We will first try to show how this procedure works for the paradigmatic case of the free scalar bosonic field in a flat spacetime, and perform its quantization in Rindler coordinates, but first we will show the quantization in the Minkowski coordinates. We will then proceed to show how Bogoliubov transformations can help us to relate solutions of different quantizations of the same field. We will discuss unitarily inequivalence between representations and finally we will show an easy derivation of the Unruh effect through the identification of inertial and accelerated observers to the Minkowski and Rindler quantizations. We will try to be rather concise. For a more extended exposition of these topics we suggest the reader to check [163–166].

2.1 Quantization schemes

2.1.1 Klein Gordon field in flat spacetime: Minkowski quantization

Originally thought as the relativistic version for the Schrödinger equation, the Klein Gordon (KG) equation when reinterpreted as a field equation in Minkowski coordinates with $c = 1, \hbar = 1$ reads:

$$(\Box - m^2)\Phi = (-\partial_t^2 + \partial_x^2 - m^2)\Phi = 0 \tag{2.1.1}$$

Where the flat space metric has been taken as $\eta^{\mu\nu} = \text{diag}(-,+,+,+)$. We will use this convention all throughout the thesis.

The first step is to identify the KG scalar product (emerging from the conserved current density), defined for any two modes ϕ_i, ϕ_j of the vector space of solutions $\mathfrak{S}$:

$$(\phi_i, \phi_j) = \mathrm{i}\int_\Sigma \mathrm{d}\mathbf{x}\, \phi_i^* \overset{\leftrightarrow}{\partial}_t \phi_j = \mathrm{i}\int_\Sigma \mathrm{d}\mathbf{x}\, (\phi_i^* \partial_t \phi_j - \phi_j \partial_t \phi_i^*)\,, \tag{2.1.2}$$

Where Σ is a Cauchy spacelike hypersurface that for convenience we have taken to be $t = 0$. Note that this inner product is not positive definite, so $\mathcal{S}$ does not form a Hilbert space. Only by restricting the solution space to some choice of a positive frequency sector does the KG pseudo inner product become positive definite. Of course, as is well known ,such a restriction is not robust as any interaction will quickly bring us outside any positive frequency subspace of the vector space of solutions of the Klein-Gordon equation.

The following relations are satisfied for the KG inner product:

$$(\phi, \varphi)^* = (\varphi, \phi), \qquad (\phi, \varphi) = -(\phi^*, \varphi^*) \tag{2.1.3}$$

It will be useful to introduce a Dirac notation to denote the vectors and dual vectors on $\mathfrak{S}$ and $\mathfrak{S}^*$. First we make the identification $\Phi(x,t) \sim |\Phi) \in \mathfrak{S}$. In order to determine the form of the corresponding bra vector $(\Phi| \in \mathfrak{S}^*$ we make use of the fact that the sesqui-linear pseudo Klein-Gordon inner product $(\cdot|\cdot) \to \mathbb{C}$ defines a map between the vector space of solutions $\mathfrak{S}$ and its conjugate dual space $\mathcal{S}^*$. The pseudo metric on the vector space of solutions is $g = \mathrm{i}\overset{\leftrightarrow}{\partial}_t \delta(\mathbf{x} - \mathbf{x}')$. Thus we identify the bra vector as $(\Phi|\cdot)$ or written in ordinary notation

$$(\Phi| = \int_\Sigma \mathrm{d}\mathbf{x}' \Phi^*(\mathbf{x}', t)\mathrm{i}\overset{\leftrightarrow}{\partial}_t \delta(\mathbf{x} - \mathbf{x}') = \mathrm{i}\Phi^*(\mathbf{x}, t)\overset{\leftrightarrow}{\partial}_t \tag{2.1.4}$$

In typical treatments the basis of plane wave solutions is used:

$$u_{\mathbf{k}}(\mathbf{x}, t) = \frac{1}{\sqrt{2\omega_{\mathbf{k}}(2\pi)^3}} \mathrm{e}^{i(\mathbf{k}\mathbf{x} - \omega_{\mathbf{k}} t)}, \tag{2.1.5}$$

with $\omega_{\mathbf{k}}^2 = \mathbf{k}\cdot\mathbf{k} + m^2$. These modes satisfy the orthogonality conditions:

$$(u_{\mathbf{p}}|u_{\mathbf{q}}) = \delta_{\mathbf{p}-\mathbf{q}}, \qquad (u_{\mathbf{p}}^*|u_{\mathbf{q}}^*) = -\delta_{\mathbf{p}-\mathbf{q}}, \qquad (u_{\mathbf{p}}^*|u_{\mathbf{q}}) = 0, \tag{2.1.6}$$

where the δs represent Dirac delta functions: $\delta_{\mathbf{p}} = \delta(\mathbf{p}) = \delta(p_x)\delta(p_y)\delta(p_z)$.

In order to construct a Hilbert space for the theory, we need to separate the positive and negative norm modes, which, as we can see, correspond exactly to the positive and negative frequency plane wave modes, as $K = \partial_t$ is a Killing vector in the Minkowski space which correspond to inertial observers. Precisely in the plane wave solution basis we have:

$$\partial_t u_{\mathbf{k}}(\mathbf{x}, t) = -\mathrm{i}\omega_{\mathbf{k}} u_{\mathbf{k}}(\mathbf{x}, t), \tag{2.1.7}$$

$$\partial_t u^*_{\mathbf{k}}(\mathbf{x}, t) = \mathrm{i}\omega_{\mathbf{k}} u_{\mathbf{k}}(\mathbf{x}, t). \tag{2.1.8}$$

Rigorously, the splitting of the Hilbert space should be made explicit through the introduction of a *complex structure* [165]. In our notation it takes the form:

$$\mathcal{J} = \mathrm{i}\left(\int_{\mathbf{k}} \mathrm{d}_{\mathbf{k}} |u_{\mathbf{k}})(u_{\mathbf{k}}| + |u^*_{\mathbf{k}})(u^*_{\mathbf{k}}|\right) \tag{2.1.9}$$

We also have the following decomposition of the identity in $\mathfrak{S}$:

$$\mathbb{1} = \int_{\mathbf{k}} \mathbf{dk} |u_{\mathbf{k}})(u_{\mathbf{k}}| - |u^*_{\mathbf{k}})(u^*_{\mathbf{k}}| \tag{2.1.10}$$

We can therefore decompose any mode into its positive and negative frequency components:

$$\Phi = \int_{\mathbf{k}} \mathbf{dk}[a^M_{\mathbf{k}} u_{\mathbf{k}} + a^{M^*}_{\mathbf{k}} u^*_{\mathbf{k}}], \qquad \Phi(\mathbf{x}, t) = \int_{\mathbf{k}} \mathbf{dk}\, [a^M_{\mathbf{k}} u_{\mathbf{k}}(\mathbf{x}, t) + a^{M^*}_{\mathbf{k}} u^*_{\mathbf{k}}(\mathbf{x}, t)] \tag{2.1.11}$$

With $a^M_{\mathbf{k}} = (u_{\mathbf{k}}|\Psi),\ a^{M^*}_{\mathbf{k}} = -(u^*_{\mathbf{k}}|\Psi)$.

Now we can proceed to quantize the field, promoting the field to a quantum field operator and introducing the canonical commutation relations:

$$\left[\hat{\Phi}(\mathbf{x}, t), \hat{\Pi}(\mathbf{x}', t)\right] = \mathrm{i}\delta(\mathbf{x} - \mathbf{x}'), \qquad \left[\hat{\Phi}(\mathbf{x}, t), \hat{\Phi}(\mathbf{x}', t)\right] = 0, \qquad \left[\hat{\Pi}(\mathbf{x}, t), \hat{\Pi}(\mathbf{x}', t)\right] = 0 \tag{2.1.12}$$

Where $\Pi(\mathbf{x}, t) = \partial_t \Phi(\mathbf{x}, t)$ is the associated canonical momentum. These relations have the consequence of promoting the functions $a^M_{\mathbf{k}}, a^{M^*}_{\mathbf{k}}$ to operators $\hat{a}^M_{\mathbf{k}}, \hat{a}^{M\dagger}_{\mathbf{k}}$ verifying:

$$[\hat{a}^M_{\mathbf{p}}, \hat{a}^{M\dagger}_{\mathbf{q}}] = \delta_{\mathbf{p}-\mathbf{q}}, \qquad [\hat{a}^M_{\mathbf{p}}, \hat{a}^M_{\mathbf{q}}] = [\hat{a}^{M\dagger}_{\mathbf{p}}, \hat{a}^{M\dagger}_{\mathbf{q}}] = 0 \tag{2.1.13}$$

From now on we will abuse the notation and drop the hats while referring to these operators.

Now we can go and construct the Hilbert space of states which will be the Fock space $\mathfrak{F}^M$ associated to the set of creation and annihilation operators. In contradistinction to $\mathfrak{S}$, the Fock space $\mathfrak{F}^M$ is a Hilbert space, i.e. a vector space equipped with a positive definite inner product. We denote members of this Fock space $|\psi\rangle \in \mathfrak{F}$ to distinguish them from the members of the vector space of solutions $|\psi) \in \mathfrak{S}$ which do not form a Hilbert space.

As usual, we will define the vacuum state $|0\rangle_M$ to be the state annihilated by all operators $a^M_{\mathbf{k}}$. It is normalized, ${}_M\langle 0|0\rangle_M = 1$, and interpreted as the state with no particles:

$$a^M_{\mathbf{k}}|0\rangle = 0 \; \forall \; \mathbf{k} \in \mathbb{R}^3. \tag{2.1.14}$$

We can proceed and define the general one-particle state as:

$$|\psi\rangle_1 = \int_{\mathbf{k}} \mathrm{d}\mathbf{k} \; \zeta_{\mathbf{k}} a^{M\dagger}_{\mathbf{k}}|0\rangle_M, \qquad \text{with} \int_{\mathbf{k}} \mathrm{d}\mathbf{k}|\zeta_{\mathbf{k}}|^2 = 1 \tag{2.1.15}$$

The set of all possible one-particle states constitutes a Hilbert space, $\mathfrak{H}$, that we will refer to as the *single-particle sector*. We can continue and construct the *two particle sector* by making the tensor product of $\mathfrak{H}$ with itself and then symmetrizing it to account for the bosonic nature of the field $(\mathfrak{H} \otimes_S \mathfrak{H})$. In this way we can combine all particle sectors to create the full bosonic Fock space $\mathfrak{F}^M$ is, as spanned by this basis, i.e.

$$\mathfrak{F}^M(\mathfrak{H}) = \bigoplus_{n=0}^{\infty} \bigotimes_S^n \mathfrak{H} = \mathbb{C} \oplus \mathfrak{H} \oplus (\mathfrak{H} \otimes_S \mathfrak{H}) \oplus \dots. \tag{2.1.16}$$

For each mode we have a natural basis obtained by repeated application of the creation operators on the vacuum state:

$$|n_{\mathbf{k}}\rangle_M = \frac{(a^{M\dagger}_{\mathbf{k}})^n}{\sqrt{n!}}|0\rangle_M, \tag{2.1.17}$$

Also, any vector $|\psi\rangle$ belonging to the Fock space is required to contain a "finite number of particles", $\int_{\mathbf{k}} \mathrm{d}\mathbf{k}\langle\psi|a^{M\dagger}_{\mathbf{k}}a^M_{\mathbf{k}}|\psi\rangle < \infty$

2.1.2 Rindler quantization

Even in the simplest case of a flat spacetime, different observers can see essential differences when checking the same state. The Minkowski quantization, represented by the Killing field ∂_t, describes the point of view of an inertial observer (Alice) and is based on the typical Minkowski coordinates $(t, \mathbf{x}) = (t, x, y, z)$. As opposed to it, the Rindler quantization, represented by the other timelike Killing field of the Minkowski metric (the Lorentz generator

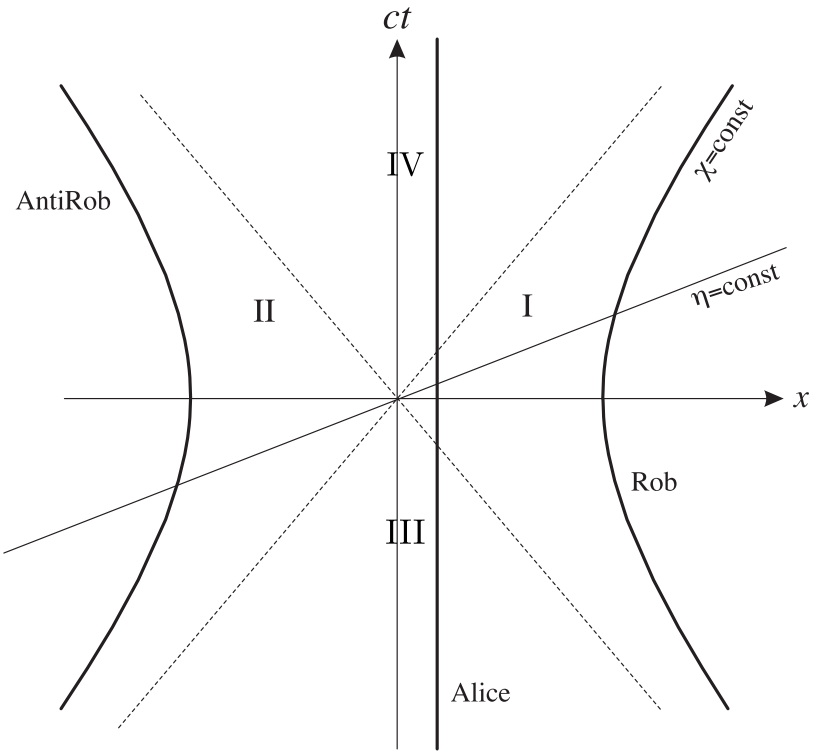

Figure 2.1: Spacetime diagram showing the division of a flat spacetime in Rindler regions.

$x\partial_t + t\partial_x$) describes how uniformly accelerated observers would perceive a quantum field around them. In order to describe this situation we recur to the Rindler coordinates $(\eta, \boldsymbol{\chi})$, where y and z are unchanged, $\boldsymbol{\chi} = (\chi, y, z)$ [167] :

$$t = \chi \sinh(\eta) \tag{2.1.18}$$

$$x = \chi \cosh(\eta) \tag{2.1.19}$$

We remind the reader that we are using the convention $c = 1, \hbar = 1$ all along this chapter. As in the previous section, we will work considering the full three dimensional space. The 1 dimensional case is simpler and can be derived in an analogous way.

With these coordinates we only cover a part of the spacetime that we will refer to as the right Rindler wedge or region I ($x < |t|$). We can analogously define another set of coordinates

$$t = -\chi \sinh(\eta) \tag{2.1.20}$$

$$x = -\chi \cosh(\eta) \tag{2.1.21}$$

with the same coordinate range $\chi > 0$, $\eta \in \mathbb{R}$. They describe a different kind of observer (AntiRob), covering the left Rindler wedge or region II ($x < -|t|$) (check Fig. 2.1). Observers in region I are causally disconnected from observers in region II, so a particle emitted in one wedge will never be detected in the other wedge. As a consequence of that, no transmission of information is possible between the two. Regions I and II only contain part of the total spacetime, however we will see later that this should be enough for the present purposes. Later in this thesis, in chapter 12, we will discuss how regions III (past) and IV (future) can also be taken into account to study the concept of timelike entanglement.

In order to get a feeling about the Rindler space coordinates let us simplify this and work in the 1+1 case. The spacetime metric for both regiones reads:

$$\mathrm{d}s^2 = -\mathrm{d}t^2 + \mathrm{d}x^2 = -\chi^2 \mathrm{d}\eta^2 + \mathrm{d}\chi^2 \tag{2.1.22}$$

For an observer who follows a worldline of constant χ we obtain that the proper time is:

$$\mathrm{d}\tau^2 = -\mathrm{d}s^2 = \chi^2 \mathrm{d}\eta^2 \tag{2.1.23}$$

So we can identify $\eta = \tau/\chi$, which could lead to a different Rindler parametrisation in terms of the proper time along those trajectories. For the region I, that would be:

$$\begin{aligned} t &= \chi \sinh(\tau/\chi) \\ x &= \chi \cosh(\tau/\chi) \end{aligned} \tag{2.1.24}$$

Fixing χ and using thes eequations we can check that, seen by an inertial observer, a Rindler trajectory follows a hyperbolic line $x^2 - t^2 = \chi$ asymptotically approaching the cone $x = |t|$.

Why do we say that these lines represent constantly accelerated observers? If using (2.1.24) we just calculate the first components of the 4-acceleration $\boldsymbol{\alpha}$ we obtain:

$$\alpha^0 = \frac{\mathrm{d}^2 t}{\mathrm{d}\tau^2} = \frac{1}{\chi} \sinh(\tau/\chi) \tag{2.1.25}$$

$$\alpha^1 = \frac{\mathrm{d}^2 x}{\mathrm{d}\tau^2} = \frac{1}{\chi} \cosh(\tau/\chi) \tag{2.1.26}$$

And to obtain the proper acceleration we must just calculate its norm, i.e. $\alpha = \sqrt{-|\alpha^0|^2 + |\alpha^1|^2} = 1/\chi$.

So we have shown that these coordinates, $\chi > 0$, $\eta \in \mathbb{R}$, for a chosen fixed value of $\chi > 0$ represent in the inertial frame the hyperbolic trayectory of an observer (Rob, in the region

I) moving with constant acceleration $\mathbf{n}_\chi/\chi$, which precisely at $t = 0$ passes through $x = \chi$. Rob's proper time is given by $\mathrm{d}\tau = \chi \mathrm{d}\eta$

The Klein Gordon equation in Rindler coordinates reads:

$$-\partial_\eta^2\phi + (\chi\partial_\chi)^2\phi + \chi^2(\partial_y^2\phi + \partial_z^2\phi) - \chi^2 m^2\phi = 0 \tag{2.1.27}$$

And the KG inner product in Rindler coordinates is:

$$(\phi_i^R, \phi_j^R) = \mathrm{i}\int_\Sigma \mathrm{d}\boldsymbol{\chi}\frac{\phi_i^{R*}\partial_\eta\phi_j^R - \phi_j^{R*}\partial_\eta\phi_i^R}{\chi}, \tag{2.1.28}$$

where Σ is here the spacelike hypersurface $\eta = 0$.

For quantization purposes, we will recur to modes which solve this equation $u_{\mathbf{k}}(\eta, \boldsymbol{\chi})$, are orthogonal in the KG product, as in Eq. (2.1.6), and are associated with the corresponding future-directed Killing vector field (which in region I takes the form $\partial_\eta = x\partial_t + t\partial_x$, whereas in region II is -∂_η). This last fact is what allow us to classify them into positive and negative Rindler frequency modes, or positive and negative norm for that matter. These are the positive modes for the right wedge (r):

$$u^R_{r,\Omega,\mathbf{k}_\perp} = \sqrt{\frac{\sinh(\pi\Omega)}{4\pi^2}}K_{\mathrm{i}\Omega}(\chi m)\mathrm{e}^{-\mathrm{i}\Omega\eta + \mathrm{i}\mathbf{k}_\perp\cdot\mathbf{y}_\perp} \tag{2.1.29}$$

where $K_{\mathrm{i}\Omega}$ is a modified Bessel function of the second kind, $\Omega \in (0, \infty)$, $\mathbf{k}_\perp = (k_y, k_z)$ and $\mathbf{y}_\perp = (y, z)$. The negative modes are just the conjugates of these. We can expand any field in the right wedge (r) using these modes:

$$\Phi = \int_{\Omega,\mathbf{k}_\perp} \mathrm{d}\Omega\mathrm{d}\mathbf{k}_\perp[a^R_{r,\Omega,\mathbf{k}_\perp}u^R_{r,\Omega,\mathbf{k}_\perp} + a^{R*}_{r,\Omega,\mathbf{k}_\perp}u^{R*}_{r,\Omega,\mathbf{k}_\perp}], \tag{2.1.30}$$

Analogously we could obtain modes for region II (l). Even doing this, we would not cover the whole spacetime. However, the modes (2.1.29) and the corresponding modes in the left wedge happen to be enough, as they can be extended analytically to cover regions III(p) and IV (f) [54, 168, 169]. Given that, the field can be fully expanded in the whole spacetime as:

$$\Phi = \int_{\Omega,\mathbf{k}_\perp} \mathrm{d}\Omega\mathrm{d}\mathbf{k}_\perp \sum_{\epsilon=l,r}[a^R_{\epsilon,\Omega,\mathbf{k}_\perp}u^R_{\epsilon,\Omega,\mathbf{k}_\perp} + \mathrm{H.c.}], \tag{2.1.31}$$

The quantization procedure goes as usual. As regions I and II are disconnected we may treat them independently. We will identify the modes $u^R_{\epsilon,\Omega,\mathbf{k}_\perp}$ with the single-particle Hilbert space $\mathfrak{H}_\epsilon$. Imposing the canonical conmmutation relations we obtain for the creation and annihilation operators:

$$[a^R_{\epsilon,\Omega,\mathbf{p}_\perp}, a^{R\dagger}_{\epsilon',\Omega',\mathbf{q}'_\perp}] = \delta_{\epsilon,\epsilon'}\delta_{\mathbf{p}_\perp-\mathbf{q}_\perp}\delta(\Omega-\Omega'), \qquad [a^R_{\epsilon,\Omega,\mathbf{p}_\perp}, a^R_{\epsilon',\Omega',\mathbf{q}'_\perp}] = [a^{R\dagger}_{\epsilon,\Omega,\mathbf{p}_\perp}, a^{R\dagger}_{\epsilon',\Omega',\mathbf{q}'_\perp}] = 0 \tag{2.1.32}$$

The Rindler vacuum $|0\rangle_R = |0\rangle_l \otimes |0\rangle_r$ is defined as:

$$a^R_{\epsilon,\Omega,\mathbf{k}_\perp}|0\rangle_R = 0 \; \forall \; \epsilon, \Omega, \mathbf{k}_\perp \tag{2.1.33}$$

2.2 Bogoliubov transformations

It is interesting to be able to transform a field state description between different basis, from its Minkowski form to its Rindler form, as that relates to how different observers, inertial and accelerated, may describe the same field. In fact, it is using this formalism of converting from one basis to another that we can study the entanglement shared by two parties when one or both are accelerated.

A Bogoliubov transformation is basically a change of basis between quantizations based on different choices of modes. To this end, let $\{f_i, f_i^*\}$ and $\{\tilde{f}_i, \tilde{f}_i^*\}$ be two complete sets of orthonormal modes in the sense of the KG inner product, see Eq. (2.1.6). Then we can expand the quantum field in two distinct ways:

$$\phi(x,t) = \sum_i f_i(x,t)a_l + f_i^*(x,t)a_i^\dagger = \sum_i \tilde{f}_i(x,t)\tilde{a}_i + \tilde{f}_i^*(x,t)\tilde{a}_i^\dagger. \tag{2.2.1}$$

Using the orthogonality relations we can immediately read off the relations

$$\tilde{a}_i = \sum_n (\tilde{f}_i|f_j)a_j + (\tilde{f}_i|f_j^*)a_j^\dagger, \tag{2.2.2}$$

$$\tilde{a}_i^\dagger = \sum_j (f_j|\tilde{f}_i)a_j^\dagger + (f_j^*|\tilde{f}_i)a_j. \tag{2.2.3}$$

The complex coefficients $(\tilde{f}_i|f_j)$, $(\tilde{f}_i|f_j^*)$, $(f_j|\tilde{f}_i)$, and $(f_j^*|\tilde{f}_i)$ are the *Bogoliubov coefficients*[1]. In the literature they are commonly denoted by α and β (and their complex conjugates), defined by

$$\alpha_{ij} \equiv (f_j|\tilde{f}_i), \qquad \beta_{ij} \equiv -(f_j^*|\tilde{f}_i). \tag{2.2.4}$$

Given that the Bogoliubov transformation must leave the canonical commutation relations invariant, the coeffients must satisfy:

[1] More formally speaking, a Bogoliubov transformation is a transformation that preserves the symplectic structure in the case of classical fields, or the canonical commutation relations in a QFT.

$$\sum_l \left(\alpha_{lj}\alpha^*_{li} - \beta_{li}\beta^*_{lj}\right) = \delta_{ij} \tag{2.2.5}$$

$$\sum_l \left(\alpha_{li}\beta^*_{lj} - \beta^*_{li}\alpha_{lj}\right) = 0. \tag{2.2.6}$$

which can be verified easily using the orthogonality relations for the modes :

$$\begin{aligned}\sum_l \left(\alpha_{lj}\alpha^*_{li} - \beta_{li}\beta^*_{lj}\right) &= \sum_l [(f_j|\tilde{f}_l)(f_i|\tilde{f}_l)^* - (f_i^*|\tilde{f}_l)(f_j^*|\tilde{f}_l)^*] = \\ &= \sum_l [(f_j|\tilde{f}_l)(\tilde{f}_l|f_i) - (f_j|\tilde{f}_l^*)(\tilde{f}_l^*|f_i)] = (f_j|f_i) = \delta_{ij} \end{aligned} \tag{2.2.7}$$

$$\begin{aligned}\sum_l \left(\alpha_{li}\beta^*_{lj} - \beta^*_{li}\alpha_{lj}\right) &= \sum_l [(f_i|\tilde{f}_l)(f_j^*|\tilde{f}_l)^* - (f_i^*|\tilde{f}_l)^*(f_j|\tilde{f}_l)] = \\ &= \sum_l [(f_i|\tilde{f}_l)(\tilde{f}_l|f_j^*) - (f_i|\tilde{f}_l^*)(\tilde{f}_l^*|f_j^*)] = (f_i|f_j^*) = 0 \end{aligned} \tag{2.2.8}$$

Now, let us focus the discussion on the Minkowski and Rindler cases. We have two different quantizations of the real Klein Gordon field, one based on the use of Minkowski coordinates, and the other based on the Rindler coordinates. For simplicity we will work just in 1+1 dimensions, which basically means changing the normalization factors and dropping the y and z coordinates and the corresponding momenta.

The field can be expanded using both bases:

$$\Phi(x,t) = \int_k \mathrm{d}k\ [a_k^M u_k(x,t) + a_k^{M\dagger} u_k^*(x,t)], \tag{2.2.9}$$

$$\Phi(\chi,\eta) = \int_\Omega \mathrm{d}\Omega \sum_{\epsilon=l,r} [a^R_{\epsilon\Omega} u^R_{\epsilon\Omega} + a^{R\dagger}_{\epsilon\Omega} u^{R*}_{\epsilon\Omega}], \tag{2.2.10}$$

Both expressions must be equal so, using the scalar product, we can obtain a relation between the different creation and annihilation operators:

$$a^R_{\epsilon\Omega} = \int_k \mathrm{d}k\ a_k^M (u^R_{\epsilon\Omega}|u_k) + a_k^{M\dagger}(u^R_{\epsilon\Omega}|u_k^*) = \sum_k \alpha^{\epsilon *}_{k\Omega} a_k - \beta^{\epsilon *}_{k\Omega} a_k^\dagger, \tag{2.2.11}$$

$$a_k^M = \int_\Omega \mathrm{d}\Omega\ a^R_{\epsilon\Omega}(u_k|u^R_{\epsilon\Omega}) + a^{R\dagger}_{\epsilon\Omega}(u_k|u^{R*}_{\epsilon\Omega}) = \sum_\Omega \alpha^\epsilon_{k\Omega} a^R_{\epsilon\Omega} + \beta^\epsilon{}_{k\Omega} a^{R\dagger}_{\epsilon\Omega}, \tag{2.2.12}$$

The exact values of the Bogoliubov coefficients $\alpha^\epsilon_{k\Omega}$, $\beta^\epsilon_{k\Omega}$ for the 3+1 case can be found for example in [170], their equivalents in 1+1 dimensions are computed in [171]

2.3 A sufficient condition for unitary inequivalence

We say that two Fock representations are unitarily equivalent if there exists a unitary map $\mathfrak{B} : \mathfrak{F} \to \tilde{\mathfrak{F}}$ that relates the Fock spaces associated with the representations, $\mathfrak{F}$ and $\tilde{\mathfrak{F}}$. Necessary and sufficient conditions for two Fock representations to be unitarily equivalent are given in [165].

For simplicity, and given that we will be more concerned with unitary inequivalence, we will present here only the following condition.

> **Sufficient condition for unitary inequivalence:** Two Fock representations of the CCR are unitarily inequivalent if the vacuum state of one representation has infinitely many particles in terms of the number operator of the other representation, i.e.
>
> $$\sum_m \langle\tilde{0}|N_m|\tilde{0}\rangle = \sum_m \langle 0|\tilde{N}_m|0\rangle = \sum_{mn} |(\tilde{f}_m|f_n^*)|^2 = \sum_{mn} |(\beta_{mn})|^2 = \infty, \tag{2.3.1}$$
>
> where $a_m|0\rangle = \tilde{a}_m|\tilde{0}\rangle = 0\ \forall m \in \mathbb{N}^+$, $N_m \equiv a_m^\dagger a_m$, and $\tilde{N}_m \equiv \tilde{a}_m^\dagger \tilde{a}_m$.

Well-known cases of unitarily inequivalent representations can be found in [169, 172–174]. In particular, Rindler and Minkowski quantizations are unitarily inequivalent:

$$\int_k \int_\Omega \mathrm{d}k\ \mathrm{d}\Omega |\beta^\epsilon_{k\Omega}|^2 = \infty. \tag{2.3.2}$$

2.4 The Unruh effect

The Fulling-Davies-Unruh effect [54, 172, 175] is the prediction that an accelerated observer would see a thermal bath of particles where an inertial observer sees none. More precisely, let us consider an inertial observer who sees the "natural" vacuum (Minkowski), i.e. the state of no particles in a flat spacetime. According to the Unruh effect, another observer in a uniformly accelerated frame with acceleration a would observe a thermal distribution

Neither the Unruh radiation nor the Hawking radiation have been directly observed, although some experiments have verified the existence of closely related similar phenomena like the Dynamical Casimir Effect [58]. We could say their experimental proof is still a somehow open question, although they are not disputed theoretically. As a matter or fact it is partially the intention of this thesis to explore ways of getting close to a feasible experimental proposal where the Unruh effect or other similar phenomena can be observed.

For a detailed treatment of the Unruh effect we refer the reader to [54, 163, 168, 169, 176]. Here we would present a rather simple derivation, omitting the discussion of some subtleties that we will however mention, but anyhow interesting in the context of Relativistic Quantum Information.

Making use of Eq. 2.2.11, the correct expressions for the Bogoliubov coefficients and a proper ansatz, an expresion for the Minkowski vacuum $|0\rangle_M = \otimes_k |0_k\rangle_M$ can be obtained in terms of the Rindler modes [169]:

$$|0_k\rangle_M = \sqrt{1 - \mathrm{e}^{-2\pi\Omega_k}} \sum_{n=0}^{\infty} \mathrm{e}^{-n\pi\Omega_k} |n_k\rangle_l^R \otimes |n_k\rangle_r^R \tag{2.4.1}$$

Which means that the Minkowski vacuum can be expressed as a decomposition into left and right Rindler particle states. Actually as we will briefly check now, the Minkowski vacuum is spatially entangled in terms of the disconnected observers from regions I and II. Considering that Rob has no access to AntiRob's modes, to analyse what he would experience in presence of the Minkoswki vacuum we should trace out region II (the left wedge - l) :

$$\rho_k^{|0\rangle_M} = \mathrm{Tr}_l |0_k\rangle_M = (1 - \mathrm{e}^{-2\pi\Omega_k}) \sum_{n=0} \mathrm{e}^{-2n\pi\Omega_k} |n_k\rangle_r^R \langle n_k|_r^R. \tag{2.4.2}$$

which is a mixed state and actually a thermal state whose temperature we can find as: $E_m/k_B T = 2\pi\Omega_m$ To obtain the relation between E and Ω we only have to consider Eq. (2.1.23) $\eta = \tau/\chi = \alpha\tau$. Given that, the Rindler observer will observe a proper energy of Ω , but rather $E = \Omega/\chi = \Omega\alpha$. Hence we have:

$$T_{\text{Unruh}} = \frac{E}{2\pi k_B \Omega} = \frac{\alpha}{2\pi k_B} \tag{2.4.3}$$

In the SI, $T_{\text{Unruh}} = \hbar a/2\pi c k_B$.

A different way to obtain this is directly from Eq. 2.2.11 imposing $a_k^M |0\rangle_M = 0$ and using the fact that $\beta_\Omega^\epsilon = -\mathrm{e}^{-\pi\Omega}\alpha_\Omega^\epsilon$:

$$(a_{\epsilon\Omega}^R - \mathrm{e}^{-\pi\Omega} a_{\epsilon\Omega}^{R\dagger}) |0\rangle_M = 0 \tag{2.4.4}$$

and so,

$$\langle 0| a_{\epsilon\Omega}^R a_{\epsilon\Omega}^{\dagger R} |0\rangle_M = (e^{2\pi\Omega} - 1)^{-1} \tag{2.4.5}$$

formula from which again we obtain the correct temperature.

The attentive reader may be bewildered by the fact that, while here we have described how a Rindler observer sees a thermal bath of particles in the Minkowski vacuum, in the

previous section we mentioned that Rindler and Minkowski quantizations were unitarily inequivalent. That should mean that the Minkowski vacuum, when seen from the point of view of a Rindler observer, has an infinite amount of particles, in clear contradiction with a thermal spectrum.

Indeed, our derivation here was rather formal, as so is the expression of the Rindler vacuum in terms of Minkowski states. Dealing with inequivalent representations it is not rigurous to decompose one state on one representation into states of the other. As a matter of fact, we just obtained the factor that makes the distribution thermal, but the total summation leads to an infinity. We will not get into details, but let us just say that it is the fact that the observer is accelerating for all time what makes the total particle count infinite. Instead of considering that quantity, it would be more interesting to study the flux of particles that acumulate in a mode per unit time, or rather the amount of particles one would observe when accelerating for just a certain period of time. In order to do so one can work with localized modes instead of the standard non-square integrable modes, and then one of the two summations can be omitted as it relates precisely to the sum for all possible mode locations. The interested reader can check such a wavepacket derivation in [163, 177] where the issue is clearly addressed. The possibility also exists to prove the Unruh effect without recurring to the Rindler quantization, analysing the problem from a purely inertial perspective as in [164, 169, 176, 178]. In any case, although mathematically problematic and not rigurously justified, the use of unitarily inequivalent representations to derive physical results is quite regular and most times successful.

As an example of this we have Haag's theorem [179] from Algebraic Quantum Field Theory, which proves the unitarily inequivalence between the free and the interaction picture quantizations in particle physics. While the theorem challenges the mathematical grounds for the calculation of the scattering terms, the predictive power of the theory is undisputed and as far as concrete computations go and succeed, nobody would question its accuracy and modern particle physics is definitely good science. Haag's theorem simply tells us that we do not know exactly why the computational tools of perturbative particle physics work so well.

As a matter of fact, even the existence of profound mathematical differences between quantizations could still allow for the same physical predictions and in that sense they could still be equivalent. However, the question remains open, as for the case of different unitarily inequivalent representations some observables might behave quite differently [180]. The situation gets more complicated in curved spacetimes, where it not always clear what representation should be preferable.

In any case, at the end of this thesis, in chapter 13 we will discuss again the issue of unitary inequivalence.

CHAPTER 3

Quantum Simulation Platforms

In this thesis we have tried to avoid limiting our study of quantum phenomena to their theoretical aspects. On part I we focus on theoretical detector models, but we study their behavior when dealing with realistic physical states. The situation becomes more interesting in part II, where we have striven to link any theoretical analysis with a possible experiment, as in our scrutiny of the Fermi problem, the short-time detection scenarios and the study of accelerated emitters in Chapters 9, 10, 7. This connection between theory and experiment reaches its highest expression in the final part of the thesis, which starts with a proposal for vacuum correlation extraction in superconducting circuits (chapter 12) and then continues with a purely theoretical analysis of a cavity in local terms, carried on in Chapter 13. An analysis that is the foundation for a very interesting connection, described in Chapter 14, which links the *local virtual particles* in the vacuum to the *real particles* created by the introduction of a physical barrier, a mirror in our case, opening a way for probing a new dynamical-Casimir-like effect.

3.1 Quantum Simulations

One of Feynman's most famous quotes, taken from the final words of his 1981 lecture 'Simulating physics with computers' [181], is a customary opening for any reference to the world of Quantum simulations:

Nature isn't classical, dammit, and if you want to make a simulation of nature, you'd better make it quantum mechanical, and by golly it's a wonderful problem, because it doesn't look so easy.

In that lecture Feynman discussed the difficulties that a standard computer would face when simulating quantum mechanical experiments of increasing size. At one point of the

talk, he discussed the possibility of building a Quantum Computer, and in particular talked about a "suitable class of quantum machines (that) could imitate any quantum system, including the physical world", wondering whether it would be possible "to work out the classes of different kinds of quantum mechanical systems which are really inter-simulatable" in a similar way of what has been done in classical computing. This problem has not been easy to solve. As a matter of fact, it is still open.

But incredible progress has been made since then. Quantum simulators are not a fantasy anymore, but a reality. Thanks to the tremendous advances in measuring and manipulating individual quantum systems, many experiments have already proved the principle by simulating particular problems in quantum mechanical analog systems such as optical lattices of neutral atoms, trapped ions, photonic systems or superconducting circuits.

In this thesis, we will expose several Quantum Mechanical theoretical problems, and propose ways to model them in different experimental setups. In that sense, some of our results can be circumscribed into this thriving field of Quantum Simulations. Sometimes we have just aimed to reproduce an effect in a similar context as the theoretical one in order to observe it, to look for interesting aspects thereof and to verify the physics behind it as we understand it. Some other times, however, we have dealt with a concept that was really hard to realize experimentally in a direct way, e.g. relativistically accelerated atoms, and still we have looked for indirect ways to reproduce its physics using alternative setups where the variables of interest have been mapped, by resorting to mathematical analogies between different-system behaviors, to some experimental measurements, in such a way that makes possible to interpret the results under a different light.

In that sense, we can make a distinction of two kinds of works in this thesis that could be classified as quantum simulations: those that consist of experiments testing the physics of certain problems through a direct interpretation of the experiment variables, by profiting from the high degree of control and parameter tuning allowed by modern experimental platforms, and those others where the variables of the problem are mapped into experimental variables that would evolve under a particular Hamiltonian, but still stay related by some function to the original ones [1].

From our point of view, experiments of the first kind are not just simulations, but rather direct observations of the effects reproduced. For example, the recent experiments probing

[1] In the more general framework of quantum simulations, the classification is more along the lines of differentiating *digital* and *analog* quantum simulations, depending on whether the experimental system is evolved through the sequential application of gate actions in an approximate way (simulating the problem Hamiltonian effectively) or engineered so that the Hamiltonian of the simulator matches exactly that of the problem. In our case we are always presenting analog simulation cases.

the Dynamical Casimir effect [56,57,59] are the first experimental evidences of the real effect, and not just a simulation of it based on analogous behavior of other systems. The second kind of experiments, on the contrary, are not exactly evidences of the existence of a certain effect, but rather the verification that, if the experiment is successful in showing the expected behavior, the effect can be understood as a consequence of the mathematical description we have for it. In that case, whether that description is accurate for the original case has not been proven, so we cannot say that the effect has been observed, but rather *simulated*.

We hope that this small digression has not taken the reader away from the main topic: the possibility of reproducing quantum mechanical problems through the use of different quantum experimental platforms. Platforms where their quantum constituents can be controlled in such a way that the interactions can be tuned precisely and the Hamiltonian of the system engineered to match the solution of an ideal theoretical scenario. Certainly, our motivation to see a problem simulated in the lab can be very diverse. We might do it because we have no means of simulating it in our classical computer due to its size or maybe we are just working on basic instances of a more difficult problem in order to verify that we are properly modeling it before scaling up. There is also the chance that we just do it for the sake of it, because we find it worth it to observe or confirm a peculiar prediction in the lab.

In order to understand how a particular simulation works, it is key to have a rather accurate knowledge of the experimental platform in question. For that matter, we would like here to present a brief introduction to the two platforms for which we have proposed experiments in this thesis: trapped ions and superconducting quantum circuits.

A broader perspective on the topic of Quantum Simulation and the possible physical alternatives available is amply discussed in the reviews of [182, 183] and the collection of articles in [184].

3.2 Trapped Ions: A Quantum Toolbox

One of the most successful experimental platforms for quantum information science have been strings of trapped ions confined in radiofrequency traps. The trap sits in an ultrahigh vacuum, and the ions are cooled simultaneously to both their internal and motional ground states. Those conditions define one of the cleanest playgrounds available for manipulating quantum systems, measurements are highly accurate and coherence times are really high, well above 10 seconds, higher in two orders of magnitude than basic gate operations. There, although alternatives exist, a qubit is usually encoded in each ion, as a hyperfine or Zeeman

ground states[2] and they are manipulated and their interactions controlled through pulses of laser and microwave radiation, exploiting both the internal energy levels and the vibrational degrees of freedom within the trap. The evolution of the system can be carefully controlled and finally the qubit states detected via fluorescence measurement. Some of the most impressive feats in the field of quantum control and quantum information processing have been achieved in this platform, as recognized by the Nobel Prize in Physics 2012 to David Wineland (shared with Serge Haroche). Already back in 2004, the ARDA report [185] pointed to the ion trapped platform to be at the forefront among those competing in the race for Quantum Computation, at least in terms of achievement of the DiVincenzo's criteria [186] for a scalable Quantum Computer architecture.

The list of merits for the ion trapped systems is so long it will take us pages to enumerate them, so we will just mention a few milestones. Already the first theoretical proposal for a physical implementation of quantum processing tasks by Cirac and Zoller [187] was in trapped ions, bringing a lot of attention to a platform that was already quite promising. In the same year, the first implementation of a quantum gate was realized by Wineland and his team [188]. Soon many more proposals and implementations followed. In these last 20 years, among those accomplishments we can remark the first demonstration of deterministic quantum teleportation between atoms [189, 190], the entangling of up to eight atoms in a controlled manner, therefore creating the first quantum byte (qubyte), and later the creation of 14-qubit entangled states [191,192], the first observation of entanglement between a single trapped atom an a single photon [193] or several Quantum Simulations [194], among which we can highlight that of free relativistic particles obeying the Dirac equation [195,196], where for the first time the interesting Zitterbewegung [3] was seen - although *simulated*. Finally we should also note the progress achieved in quantum clocks, see for example [197].

This is just a small set of accomplishments among the many, but they hint already at the high possibilities of the platform.

3.2.1 Traps

One of key elements of a trapped ion experiment is the trap itself. Having charged particles the most easy way to confine them is by using electrical or electromagnetic forces, however, given that the trapping cannot be stable by just using electrostatic fields (Earnshaw theorem [198]), a combination of both magnetic and electrical forces must be used, or a time dependent electric field. The last one is the case of the Paul trap [199], used in most trapped

[2] Also as combinations of a ground state and an excited metastable electronic state.

[3] A theoretical rapid quivering motion of a free Dirac particle along its trajectory.

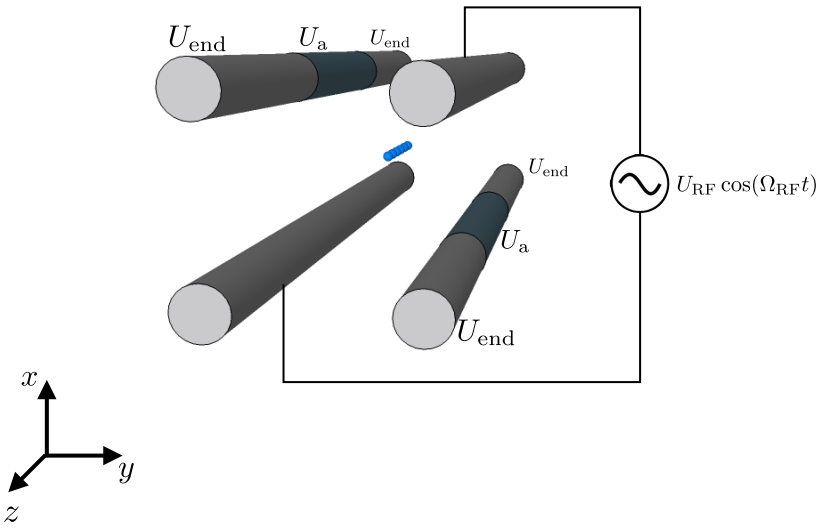

Figure 3.1: Linear Paul trap scheme. An alternating voltage applied to opposing electrodes confines the ions in the transverse plane. U_{a} and the confining endcap voltage U_{end} are DC voltages applied to the other two electrodes.

ions setups today.

We will consider here The Paul trap, or rather the linear Paul trap based on the same principles. It consists of four electrodes in a quadrupole configuration. In the trap axis the confinement is provided by a static field through the DC voltage U_{end}. Trapping in the transverse plane is achieved by applying an oscillating voltage to two opposing electrodes which generates an alternating saddle potential. By averaging over the transverse micromotion of the ions at the RF frequency, an effective harmonic potential is obtained:

$$U(x,y,z) = \frac{1}{2}m(\omega_x^2 x^2 + \omega_y^2 y^2 + \omega_z^2 z^2) \tag{3.2.1}$$

with the secular frequencies ω (with values much smaller than Ω_{RF}) are determined by the geometry, the voltages applied and the charge and mass of the ions. For a detailed derivation using the Mathieu equations we refer the reader to [200].

Typical trap sizes are at the mm scale in the transverse plane and at the $mm - cm$ scale for axial length, with voltages of 100-500 V and RF fields of a few 10's of MHz leading to an axial $\omega_t = \omega_z$ in the low MHz range and transverse frequencies $\omega_x, \omega_y \sim 10\omega_z$. For these typical values the ions are strongly confined in the radial direction. They arrange as a linear chain along the trap axis as transverse movement is negligible when the system has been properly cooled. The distance between the ions is determined by the equilibrium of the axial confinement potential and the Coulomb repulsion.

We should finally point out although typical linear ion traps are still widely used, they are progressively giving way to integrated microfabricated traps, mostly based on the same principles [201].

3.2.2 The physics of trapped ions - Available degrees of freedom

For most quantum experiments with trapped ions the available degrees of freedom are the internal state of the ions and the external - axis motion - vibrational modes. In Quantum information processing experiments, the qubit (which abstractly can be seen as a two-level atom) is typically internally encoded. An appropriate ion species should have a rather simple level structure in order to realize a close two-level system without too many lasers, also the levels must be rather stable from spontaneous decay to avoid decoherence and they should allow for easy state detection. This conditions basically rule out everything but simple atomic ions with just one outer electron, such as the alkaline elements Be^+, Mg^+, Ca^+ and Ba^+, and some transition metals, e.g. Cd^+, Yb^+ or Hg^+.

For some of those cases the qubit is encoded into two levels with a forbidden direct optical transition between them (*optical qubit*), for others it is encoded into the hyperfine structure (*hyperfine qubit*). For the former case, the manipulation of the states is carried on using two lasers far detuned from an intermediate level, with a frequency difference equal to the hyperfine energy distance between the states of interest, in a process called *Raman resonance*. In any case, the lasers used to control the state of individual qubits light only the ion in question, and not the whole chain. Keeping all this in mind, we can just assume that our ion internal states, $|g\rangle$ and $|e\rangle$, behave according to an internal Hamiltonian given by:

$$H_{atom} = \frac{\hbar\omega_{eg}}{2}\sigma^z \tag{3.2.2}$$

where in this matrix notion we are using the basis $\{|g\rangle,\ |e\rangle\}$ and $\omega_{eg} = \omega_e - \omega_g$ is much bigger than the vibrational ω_z. For that reason we can make use of the Born-Oppenheimer approximation and treat internal and vibrational degrees of freedom independently.

As what regards to the vibrational degrees of freedom, for the typical values considered in the previous section and cold enough temperatures, the transverse terms can be discarded (strong confinement) and the Hamiltonian giving the motion of N ions in a linear trap can be simplified as:

$$H = \sum_{i=1}^{N}\left(\frac{p_i^2}{2m} + \frac{m\omega_z^2 z_i^2}{2}\right) + \sum_{i=1}^{N-1}\sum_{j>i}\frac{q^2}{4\pi\epsilon_0|z_j - z_i|} \tag{3.2.3}$$

For this Hamiltonian we have N axial normal modes. For our purposes here, it will suffice to consider just the lowest mode, the center of mass mode (CoM), where the ions

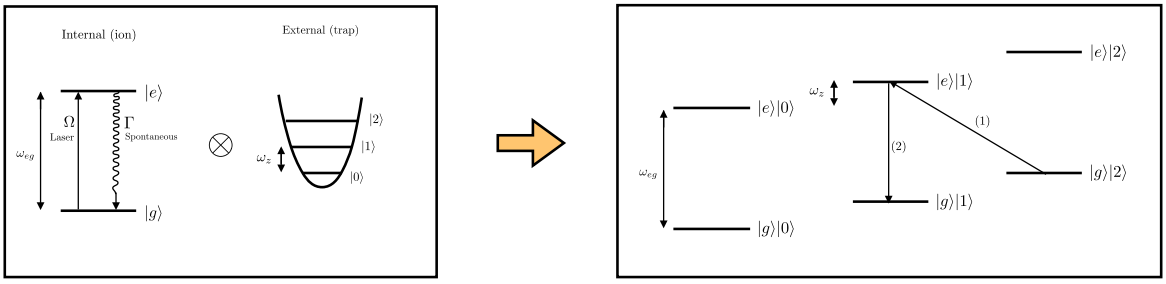

Figure 3.2: Internal and external level scheme for a single trapped ion. The external modes refer to the CoM mode. The numbers in parenthesis on the right identify sideband cooling transitions.

move together at the trap frequency ω_z as a rigid body. The next lowest mode would be the breathing mode (Br) at frequency $\sqrt{3}\omega_z$ where the ions on different sides of the center move with opposite phases.

States relevant to Quantum simulations and Quantum processing purposes can therefore be characterized as $|i_1, ..., i_N\rangle\,|n_{\text{CoM}}\rangle\,|n_{\text{Br}}\rangle$ where $i_1, ..., i_N$ refer to the internal state of each ion (generic superpositions of $|g\rangle$ and $|e\rangle$ states) and $|n\rangle\,|n_{Br}\rangle$ to the vibrational state of the whole chain (see Fig. 3.2). For our purposes and from here on we will consider the center of mass (CoM) mode to be the only relevant one, so we will just consider states of the type $|i_1, ..., i_N\rangle\,|n\rangle$.

3.2.3 Ion-Laser interaction

Most control operations on the ions are carried on by beaming lasers upon them. Resonant interaction with lasers is used in all stages of ion trap quantum processes. Ion cooling, quantum gates and unitaries, tuning of the couplings, state preparation and measurement and Hamiltonian engineering are all operations performed through an appropriate combination of laser pulses acting on different ions or the whole chain.

Let us consider a propagating wave [4] produced by a laser of frequency ω_L acting along the trap axis [5]. Considering just the ion j being beamed on, the interaction Hamiltonian in the Schrödinger picture is:

$$H_{\text{int}} = \hbar\frac{\Omega}{2}\left(\mathrm{e}^{\mathrm{i}(k_L z_j - \omega_L t - \phi)} + \mathrm{e}^{-\mathrm{i}(k_L z_j - \omega_L t - \phi)}\right)(\sigma_j^+ + \sigma_j^-), \tag{3.2.4}$$

where Ω is defined as:

[4] A standing wave situation, created by opposing laser beams, is highly analogous and at the end of the derivation involves a Rabi frequency two times bigger than in 3.2.5

[5] To address ions individually a slantwise beam can be used. For that case one must use instead of $k_L = 2\pi/\lambda_{\text{L}}$, the new wavenumber $k_L = 2\pi\cos(\phi)/\lambda_{\text{L}}$.

$$\Omega = \frac{eE_0}{\hbar}\langle e|\boldsymbol{\epsilon}\cdot\boldsymbol{\mu}|g\rangle \tag{3.2.5}$$

with E_0 being the field amplitude; $\boldsymbol{\epsilon}$ the field polarization and $\boldsymbol{\mu}$ the ion's dipolar operator for the $e-g$ transition. For levels coupled via a Raman transitions (assisted by two lasers) we should use the effective associated couplings instead (check [202] for details).

The z_j are the operators corresponding to the ion displacements, relative to the equilibrium positions along the chain. We express those displacements in terms of phonon operators,

$$z_j = \sum_n \mathcal{M}_{j,n}\Delta_{z_n}(a_n + a_n^\dagger), \tag{3.2.6}$$

where $\mathcal{M}_{j,n}$ are phonon wavefunctions for the vibrational mode n, and $\Delta_{z_n} = \sqrt{\frac{\hbar}{2m\omega_n}}$. Considering just the CoM mode, $z_j = \mathcal{M}_j\Delta_z(a+a^\dagger)$, and $\mathcal{M}_j = 1/\sqrt{N}$, N being the total number of ions in the chain.

In the interaction picture, rotating with the laser frequency ω_L and taking a RWA we can simplify 3.2.4:

$$H^I = \hbar\frac{\Omega}{2}\left(\mathrm{e}^{\mathrm{i}(k_L z_j-\phi)}\sigma_j^+ + \mathrm{e}^{-\mathrm{i}(k_L z_j-\phi)}\sigma_j^-\right), \tag{3.2.7}$$

Now, let us consider the Lamb-Dicke parameter, which relates the optical wavelength of the laser beaming the ion with the extension of the ion's wavefunction:

$$\eta = \frac{2\pi\Delta_z}{\lambda_\mathrm{L}} = k_L\Delta_z, \text{ with } \Delta_z = \sqrt{\frac{\hbar}{2m\omega_t}} \tag{3.2.8}$$

When $\eta \ll 1$ the ion's motion is confined to a region much smaller than the laser wavelength. That is typically the case, e.g. for $^{40}Ca^+$ linear traps $\eta \sim 0.01$. On top of that the system usually operates under the so-called Lamb-Dicke regime, which amounts to having $\eta\langle\Psi|(a+a^\dagger)|\Psi\rangle = \frac{\eta}{\sqrt{N}}\sqrt{(2n+1)} \ll 1$, and allows us to expand the exponential in the interaction Hamiltonian.

$$\mathrm{e}^{\mathrm{i}k_L z_j} = \mathrm{e}^{\mathrm{i}\frac{\eta}{\sqrt{N}}(a+a^\dagger)} = 1 + \mathrm{i}\frac{\eta}{\sqrt{N}}(a+a^\dagger) + \mathcal{O}(\eta^2) \tag{3.2.9}$$

And so we obtain:

$$H^I = \hbar\frac{\Omega}{2}\left\{\left[1+\mathrm{i}\frac{\eta}{\sqrt{N}}(a+a^\dagger)\right]\mathrm{e}^{\phi}\sigma_j^- + \left[1-\mathrm{i}\frac{\eta}{\sqrt{N}}(a+a^\dagger)\right]e^{-\phi}\sigma_j^+\right\}, \tag{3.2.10}$$

Now, for particular values of the laser frequency ω_L the Hamiltonian can be further simplified by discarding the corresponding off-resonant terms:

- **Carrier resonance:** If $\omega_L - \omega_{eg} \ll \omega_t$, transitions with changes in the n number are suppressed .

$$H^I_{\text{carrier}} = \hbar\frac{\Omega}{2}\left(\mathrm{e}^{\mathrm{i}\phi}\sigma_j^- + e^{-\mathrm{i}\phi}\sigma_j^+\right), \tag{3.2.11}$$

- **Red sideband:** If $\omega_L = \omega_a - \omega_t$ (red detuned), the only relevant transitions are those that *reduce* n while absorbing a photon (and their conjugates).

$$H^I_{\text{red}} = -\mathrm{i}\frac{\hbar\Omega}{2}\frac{\eta}{\sqrt{N}}\left(a\mathrm{e}^{-\mathrm{i}\phi}\sigma_j^+ - a^\dagger\mathrm{e}^{\mathrm{i}\phi}\sigma_j^-\right), \tag{3.2.12}$$

- **Blue sideband:** If $\omega_L = \omega_a + \omega_t$ (blue detuned), the only relevant transitions are those that *increase* n while absorbing a photon (and their conjugates).

$$H^I_{\text{blue}} = \mathrm{i}\frac{\hbar\Omega}{2}\frac{\eta}{\sqrt{N}}\left(a\mathrm{e}^{\mathrm{i}\phi}\sigma_j^- - a^\dagger\mathrm{e}^{-\mathrm{i}\phi}\sigma_j^+\right), \tag{3.2.13}$$

These different Hamiltonians allow us to implement several operations by just beaming the appropriate ion. Quantum gate operations can be made through smart combinations of laser pulse of definite duration. Single qubit gates, for example, can be obtained by adjusting the laser to match the carrier resonance. Two qubit gates, such as the CNOT gate proposed by [187], can be implemented using the motional state of the chain as a bus to transfer correlations, through a combination of laser pulses of different frequencies. As a matter of fact, the possibility of building those gates just shows that the laser actions previously mentioned constitute a universal set of quantum operations. To better see how they operate, we will express the action of the laser pulses for a time interval t in terms of matrix operators:

- **Carrier resonance:** In the basis $\{|g,n\rangle, |e,n\rangle\}$ such an action leads to the operator:

$$R_c(\theta,\phi) = \mathrm{e}^{-\frac{\mathrm{i}H_c^I t}{\hbar}} = \begin{pmatrix} \cos(\theta/2) & -\mathrm{i}\mathrm{e}^{-\mathrm{i}\phi}\sin(\theta/2) \\ -\mathrm{i}\mathrm{e}^{\mathrm{i}\phi}\sin(\theta/2) & \cos(\theta/2) \end{pmatrix} \tag{3.2.14}$$

  where $\theta = \Omega_R t = \Omega t$. The continuous action of this operator produces oscillatory transitions between $|e,n\rangle$ and $|g,n\rangle$ with Rabi frequency $\Omega_R = \Omega$.

- **Red sideband:** In the basis $\{|g,n\rangle, |e,n-1\rangle\}$:

$$R_r(\theta,\phi) = \mathrm{e}^{-\frac{\mathrm{i}H_r^I t}{\hbar}} = \begin{pmatrix} \cos(\theta/2) & \mathrm{e}^{-\mathrm{i}\phi}\sin(\theta/2) \\ -\mathrm{e}^{\mathrm{i}\phi}\sin(\theta/2) & \cos(\theta/2) \end{pmatrix} \tag{3.2.15}$$

  and here $\theta = \Omega_R t = \frac{\eta\sqrt{n}}{\sqrt{N}}\Omega t$. This action induces oscillatory transitions between the levels $|g,n\rangle$ and $|e,n-1\rangle$ with Rabi frequency $\Omega_R = \frac{\eta\sqrt{n}}{\sqrt{N}}\Omega$.

- **Blue sideband:** In the basis $\{|g,n\rangle, |e,n+1\rangle\}$, $R_b(\theta,\phi)$ looks exactly as $R_r(\theta,\phi)$:

$$R_b(\theta,\phi) = \mathrm{e}^{-\frac{\mathrm{i}H_b^I t}{\hbar}} = \begin{pmatrix} \cos(\theta/2) & \mathrm{e}^{-\mathrm{i}\phi}\sin(\theta/2) \\ -\mathrm{e}^{\mathrm{i}\phi}\sin(\theta/2) & \cos(\theta/2) \end{pmatrix} \tag{3.2.16}$$

  but here $\theta = \Omega_R t = \frac{\eta\sqrt{n+1}}{\sqrt{N}}\Omega t$. For this case, the oscillation occurs between levels $|g,n\rangle$ and $|e,n+1\rangle$ with $\Omega_R = \frac{\eta\sqrt{n+1}}{\sqrt{N}}\Omega$.

3.2.4 State preparation

There are several procedures to prepare states depending on the species used and using intelligent mechanisms based on the final desired state. However, a standard procedure involves a cooling stage that takes the ion chain the ground level $|g_1,\cdots,g_N,0\rangle$ and then acting with beam laser pulses of precise duration and phase to excite the adequate transitions.

The control of a two level system requires the implementation of two types of rotations: transversal (σ_x,σ_y) and longitudinal (σ_z) .The first ones change the amount of population between the two states, the second modify the relative phase between them.

In the trapped-ion case, the transversal rotations can be easily controlled by adjusting the duration of the pulse through the θ variable and the ϕ phase as can be easily checked in the previous section. In particular π-pulses for the θ phase involve a full flip between the states in consideration (which vary depending on whether the laser is tuned to resonance, red detuned or blue detuned). $\pi/2$-pulses, on the contrary, create a balanced superposition. By acting with lasers upon different ions entangled states can be created.

Longitudinal rotations σ_z can be implemented just using the free qubit precession or, if there is a need to perform them faster, by decomposing them into σ_x and σ_y rotations since $\sigma_z = -\mathrm{i}[\sigma_x,\sigma_y])/2$, but there are other methods that would depend of course on the atom species used and on the particular experimental setup. Among them we can highlight the use of a far detuned laser beam that would shift differently the energies of both levels through an AC-Stark shift .

We will not deal here with more details, as it would lead us far apart from our merely introductory purposes.

3.2.5 Cooling

There are several cooling schemes available to take the ion chain progressively to its ground state including laser cooling, resistive cooling, collisional cooling and sympathetic cooling. We will briefly discuss the laser cooling processes, which for ion traps usually involve Doppler and sideband cooling [203].

Doppler cooling

The Doppler cooling process is based on a photon-ion scattering process. The ions are beamed with a red detuned laser ($\omega_{\text{red}} = \omega - \Delta$) from a certain dipole transition (ω). The optimal cooling requires $\Delta \simeq \Gamma/2$. The ions moving towards the incoming light with kinetic energy (K) would see a tuned laser and would absorb the photon ending up with a total energy $K + \hbar\omega_{\text{red}}$ but with less momentum. Eventually they would emit the photon spontaneously but in a random direction, and when this is averaged over many absorption-emission processes it amounts to a net average loss of momentum equivalent to the initial ($\hbar\omega_{\text{red}}/c$). This standard discussion conceals the fact that reducing the expected value for the momentum to zero does not mean reducing the energy (for which the average of the square velocity is the meaningful quantity). A proper semi-classical treatment that considers the adequate absorption and emission profiles and the random-walk that the ions experience due to the constant absorption and emission processes can be seen in [204], where net cooling is actually derived. For a full quantum-mechanical treatment check [205]. The cooling can be maintained while the kinetic energy of the ions is above the line-width Γ of the transition. At that point the net cooling balance stops, the Doppler temperature limit being $T_{\text{Doppler}} = \frac{\hbar\Gamma}{2k_B}$.

Considering trap frequencies in the MHz range, the residual excitation at the Doppler limit is $\langle n \rangle \sim 10$. For higher frequencies it can reach $\langle n \rangle \sim 1$.

Sideband cooling

Doppler cooling takes the ion chain into the Lamb-Dicke regime $\eta\sqrt{(2n+1)} \ll 1$, but the motional state is still excited. The ion chain can be cooled down to it using sideband cooling.

Here we will explain the process for the case of a single ion in a chain. The typical level structure of a single ion can be seen in Fig. 3.2. A laser is then tuned to a transition leading to an excited internal state in a lower motional excitation.

The process (1) in Fig. 3.2 corresponds to a forbidden dipole transition or is carried on using an auxilary third level through a Raman resonance. Also, given that we are in the Lamb-Dicke regime, the spontaneous emission is bound to occur following (2) and not through some other channel that changes the motional state,

3.2.6 State reading

Again, there are several possibilities for reading the state of the system. Usually one is only interested in the internal state of the ions, so we will only discuss this possibility. The simplest case there is where the ion is beamed with light resonant to a strong dipole trans-

ition between one of the two qubit states (let us assume it to be $|g\rangle$ to a third state $|p\rangle$ which decays rapidly, as compared to the $e-g$ transition. While the beam is acting upon it, the ion will absorb and re-emit photons only it is in $|g\rangle$ but if it is in the excited state, $|e\rangle$, the laser will not induce any transition. The detection of the scattered fluorescence photons is therefore a projective measurement that shows the ion to be in its internal ground state $|g\rangle$. The advantage of the procedure is that it can be used simultaneously in several ions of the chain. Of course, in order to obtain the average populations of the different levels, the quantum simulation or computation has to be repeated from the beginning, and the final measurement carried on a sufficiently big number of times. Moreover, if coherences have to be measured, one will have to use more complicated procedures. A very simple one would be just to keep measuring populations but after performing specific local unitaries on the ion.

3.2.7 Simulations

The possibilities of this Quantum toolbox in terms of simulations are vast.

For digital quantum simulations, we must mention here that having a universal set of quantum operations, as presented in Section 3.2.3, we should in principle be capable of efficiently [6] simulating any local quantum system [206] by approximating its evolution with a stroboscopic sequence of quantum gates (Trotter decomposition). Of course the times of operation and the limited size of controllable chains put a limit to that, but some successful simulations of small spin chains have already been successful [207].

For the case of analog simulations, the possibilities are so many and so different that it impossible to present here even a short collection of them that is in anyway representative. We will just give here a few hints on how to simulate a Hamiltonian that will concern us in the future (Chapter 7)

The Hamiltonian in question is:

$$H_{\mathrm{I}}=\sum_{j} g_j \sigma_j^{+} e^{i\Omega_j \tau}\left(a_m e^{-i\Phi_m(\tau)}+a_m^{\dagger} e^{i\Phi_m(\tau)}\right)+H.c., \tag{3.2.17}$$

where τ represents a certain time parameter, and $\Phi_m(\tau)$ can be seen as a time dependent phase that relates to the coupling of an accelerated atom (with acceleration a) to a certain Minkowski mode k_m of a quantum field.

$$\Phi_m(\tau)=-k_m\xi e^{-a\tau/c}=-\frac{k_m c^2}{a}e^{-a\tau/c} \tag{3.2.18}$$

[6] i.e. if the system size grows linearly so will the size of our simulator (trap)

Now let us consider a single ion trapped, beamed by two lasers coupling its internal levels $|g\rangle$ and $|e\rangle$ by means of a Raman transition, with corresponding amplitudes $\Omega_{\mathrm{L},j}$ (depending on the laser intensities), and two frequencies $\omega_{\mathrm{L}_{1,2}}$, (see [202] for details), the interaction in the Schrödinger picture as in 3.2.4 should be:

$$H_{\mathrm{L}}(\tau) = \sum_{j,\nu=1,2} \frac{\Omega_{\mathrm{L},j}}{2} \sigma_j^+ e^{ik_{\mathrm{L}} z_j} e^{-i\omega_{\mathrm{L}_\nu}\tau - i\phi_\nu(\tau)} + \mathrm{H.c.}. \tag{3.2.19}$$

The small differences with 3.2.4, come from the fact that we are not using just one laser, but rather exciting a Raman transition with two lasers of different frequencies. In the Lamb-Dicke regime, under some working assumptions and with an adequate choice of the laser phases $\phi_1(\tau), \phi_2(\tau)$ we will be able to cast this last equation into 3.2.18. At this point this should not be such a big surprise to the reader. We will describe this to the last detail when we discuss the whole problem in chapter 7.

3.2.8 Final remarks

In all the sections covered up so far, the expert reader may have found that our descriptions account for the most basic of the many possible scenarios. We acknowledge that. In fact, there are many subtleties in all of the aspects here presented, and this rather simple presentation omits the discussion of many interesting cases, but still, with the didactic purposes of this section in mind, we hope to have conveyed if not all at least some of the most important ideas of the subject.

3.3 Superconducting circuits: Another Quantum toolbox

Along this thesis, most of the proposals for simulations that we will present are based on the use of superconducting circuits as experimental platform.

Superconducting circuits have emerged in the last years as one of the most promising platforms to implement the Quantum Computer after successfully replicating many of the most interesting Cavity QED and ion trapped experiments to date. Its main advantage is of course its inherent scalability. Making use of the existing litography techniques for chip fabrication, once made one qubit, it is easy to replicate it and fabricate many more on the same chip. The challenges do however exist and they amount to limiting all the noise sources as the chip scales up, and to be able to provide reliable, controlable and switchable coupling between the distant qubits.

We will try to discuss here briefly the theory behind circuit quantization and discuss circuits and means to couple them as well as the typical qubit readout. For a more rigor-

ous description of these and other models and situations we refer the reader to [208–211], sources that we have used as constant reference along this section.

3.3.1 Superconducting Quantum Circuits

Superconductivity was first discovered experimentally in 1911, but it was not until 1957 however that Bardeen, Cooper and Schrieffer (BCS [212]) came up with a genuine quantum theory that properly explained the phenomenon at the microscopic level. One of the most fundamental concepts of the theory is that of the Cooper pair, a composite boson made of two electrons, that as such, tend to condense into the same ground state under a certain critical temperature T_c. Materials like Niobium and Aluminum, that are commonly used for constructing this kind of circuits show that behavior. In the superconducting phase, the conductor's state can be described as a macroscopic wavefunction $\Psi(\boldsymbol{r},t) = \sqrt{n(\boldsymbol{r},t)}\mathrm{e}^{\mathrm{i}\theta(\boldsymbol{r},t)}$, where n is the density of Cooper pairs and θ represents the phase of the condensate.

The quantum study of circuits started long ago, when it became clear that quantum effects in circuits where observable. However, it was shown in the 80s [213] that a full microscopic theory is not necessary to study circuits quantum mechanically. As a matter of fact, the study of macroscopic degrees of freedom related to standard electrical variables is sufficient for most purposes and therefore the knowledge of many subtleties of superconductivity is in this context not revelant.

The theory of Quantum Networks, developed by Yurke and Denker in the early 80s [213] and more recently analyzed further by Devoret [214], describes the standard procedure for quantizing a circuit. We would describe briefly here. It involves identifying a Hamiltonian description for the circuit (there are many Hamiltonians depending on the representation chosen), by first choosing a spanning tree [7] and associating with each node n a voltage V_n and a current I_n which relate to the node flux Φ_n and charge Q_n by:

$$\Phi_n = \int_{-\infty}^{t} V_n(t)dt \tag{3.3.1}$$

$$Q_n = \int_{-\infty}^{t} I_n(t)dt \tag{3.3.2}$$

The relations between the different V's (or the I's) are given by the Kirchoff equations, that correspond to a certain Lagrangian. From there we can obtain the full Hamiltonian of

[7] A spanning tree is a tree containing all vertices of the circuit network and some or all of its edges. A tree is an undirected graph in which any two vertices are connected by exactly one path, so basically a connected undirected graph with no simple cycles.

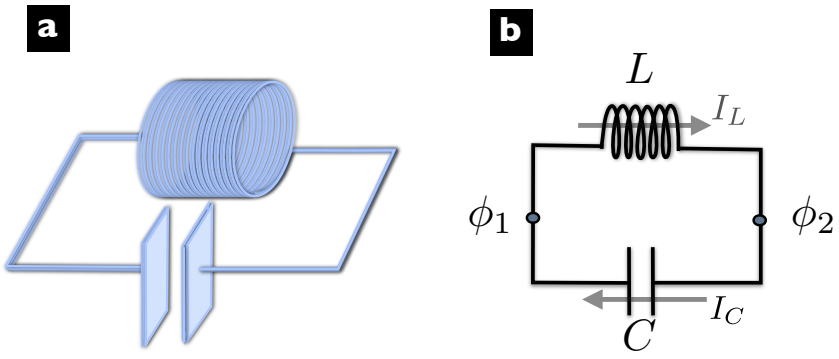

Figure 3.3: a) Simple physical realization. b) Lumped circuit scheme

the system expressed in terms of the Φ's and Q's, which result to be conjugate pairs, and canonical quantization can be finally carried on.

3.3.2 The LC resonator

A very simple example for quantization is the LC resonator as seen in Fig. 3.3.

The Kirchoff equation for this case is basically $I_L = I_C$. By fixing $\Phi_2 = 0$, $\Phi_1 = \Phi$, we can cast the equation as:

$$\frac{\Phi}{L} + C\ddot{\Phi} = 0 \tag{3.3.3}$$

Which can be naturally obtained from the following Lagrangian and Hamiltonian, connected through a Legendre transformation:

$$\mathcal{L}_{LC} = \frac{C\Phi^2}{2} - \frac{\Phi^2}{2L} \rightarrow H = \frac{Q^2}{2C} + \frac{\Phi^2}{2L} \tag{3.3.4}$$

From the equation of motion we can check that $Q = C\Phi$ and Φ verify that the Poisson bracket $\{Q, \Phi\} = 1$ and therefore we can promote them to the operators $\hat{Q}, \hat{\Phi}$. With them we can define the corresponding annihilation and creation operators as:

$$a = \frac{1}{\sqrt{2\hbar L\omega_{\text{LC}}}}\hat{\Phi} + \mathrm{i}\frac{1}{\sqrt{2\hbar C\omega_{\text{LC}}}}\hat{Q} \tag{3.3.5}$$

$$a^\dagger = \frac{1}{\sqrt{2\hbar L\omega_{\text{LC}}}}\hat{\Phi} - \mathrm{i}\frac{1}{\sqrt{2\hbar C\omega_{\text{LC}}}}\hat{Q} \tag{3.3.6}$$

with $\omega_{\text{LC}} = 1/\sqrt{LC}$.

And the Hamiltonian takes the form:

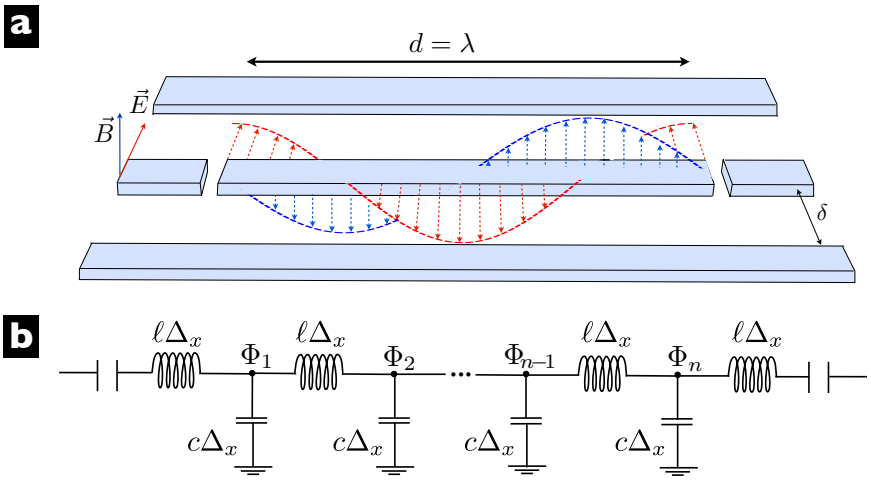

Figure 3.4: Transmission line. a) Simple physical realization. b) Lumped circuit scheme. Image taken from [209]

$$H = \hbar\omega_{\text{LC}}\left(a^\dagger a + \frac{1}{2}\right) \tag{3.3.7}$$

3.3.3 The transmission line

A transmission line, in general, is a structure based on two conductors normally used to guide electromagnetic signals, and capable of supporting a TEM mode. A coaxial cable is a particular kind of transmission line. Other geometries include the two-wire line, the three wire the parallel plate line, the stripline or the microstrip. We will consider a uniform three-wire line, with two ground lines and one central conductor. The line will be interrupted at $x = 0$ and $x = d$, resulting in two capacitors at the edges that act as mirrors and close the resonator cavity.

For the typical situation, the wavelength corresponding to the waves propagating on the line is much smaller than its length and we cannot consider the intensity or voltage to be constant all along, so a treatment using lumped elements is not convenient. Instead we use a distributed treatment where the line is abstractly divided into small segments of size Δx with characteristic impedance and capacitance per unit length, ℓ and c respectively.

In that situation the Kirchoff laws equations are:

$$c\Delta x\ddot{\Phi}_n + \frac{\Phi_{n+1} - 2\Phi_n + \Phi_{n-1}}{\ell\Delta x} = 0 \tag{3.3.8}$$

In the continuum limit we have:

$$v^2\partial_x^2\Phi(x,t) - \partial_t^2\Phi(x,t) = 0 \tag{3.3.9}$$

with a Lagrangian:

$$\mathcal{L}_{\text{line}} = \frac{1}{2}\int_0^d \mathrm{d}x[\dot{\Phi}^2(x,t) + \frac{1}{\ell}(\partial_x\Phi(x,t))^2] \tag{3.3.10}$$

Where $v = 1/\sqrt{\ell c}$ and we note that the line extends from 0 to d. By performing a Fourier expansion of $\Phi(x,t)$ we obtain a Lagrangian of independent harmonic oscillators and defining corresponding $a_n, a_n^\dagger$ operators we get to a final Hamiltonian:

$$H_{\text{line}} = \sum_{n=1}^{\infty} \hbar\omega_n \left(a_n^\dagger a_n + \frac{1}{2}\right) \tag{3.3.11}$$

with $\omega_n = n\omega_r = n/d\sqrt{\ell c}$.

For most cases in this thesis however, we will consider an open transmission line with propagating modes. For that case we can use the regularized Hamiltonian:

$$H_{\text{line}} = \int_{-\infty}^{\infty} \hbar\omega a_\omega^\dagger a_\omega \mathrm{d}\omega \tag{3.3.12}$$

3.3.4 Introducing non-linearity: The Josephson Junction

Considering just linear elements like impedances and capacitances we arrive to equally-spaced energy levels, but in order to create useful qubits, we must isolate the transitions, to properly address them, by achieving a certain degree of unharmonicity. In order to get it we need some sort of nonlinearity. In the atomic case, this nonlinearity is provided by the atomic Coulomb force, which is an inverse square law (and therefore non-linear), in the superconducting case, the nonlinearity is created by using a special element, the Josephson junction.

In 1962, Brian Josephson proved [215] that when two superconductors are separated by a thin insulating layer, their macroscopic wavefunctions overlap, giving rise to a flowing current through the junction depending on the wavefunctions phase difference:

$$I_{1\to 2} = I_0 \sin(\theta_1 - \theta_2) = I_0 \sin(\phi_J) \tag{3.3.13}$$

where $\phi_J = \theta_1 - \theta_2$ is the gauge-invariant phase, and I_0 is the critical current, the maximum supercurrent the union can sustain, which depends on the actual microscopic characteristics of the junction. This relationship represents what is known as the *DC-Josephson effect*, which takes place in absence of an applied voltage. In the case that a voltage $V = V_1 - V_2$ is applied to the junction the phase difference evolves in time as :

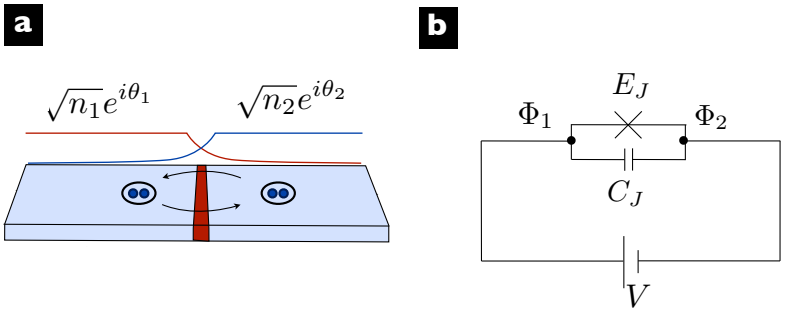

Figure 3.5: a) Physical representation of a Josephson Junction: two superconducting electrodes separated by a thin isolating (oxide) layer (red). The overlap of the superconducting wavefunctions Ψ_1 and Ψ_2 leads to the tunneling of Cooper pairs. b) Circuit version of the Josephson junction subject to an external voltage V. Image taken from [209]

$$\frac{\mathrm{d}\phi_J}{\mathrm{d}t} = \frac{2e}{\hbar}V = \frac{2\pi}{\Phi_0}V \tag{3.3.14}$$

$\Phi_0 = h/2e$ being the magnetic flux quantum (the magnetic flux across any closed loop of a superconductor is quantized [8])

Merging both previous equations be get that an alternating current is created

$$I = I_0 \sin\left(\frac{2\pi}{\Phi_0}Vt + \phi_{J0}\right), \tag{3.3.16}$$

which represents the so called *AC-Josephson effect*. Also, by taking the time derivative of the supercurrent and using Eq. 3.3.14 we obtain:

$$\frac{\mathrm{d}I}{\mathrm{d}t} = \frac{2\pi V I_0}{\Phi_0}\cos(\phi_J) \tag{3.3.17}$$

which let us think of a Josephson junction as a non-linear inductor with an inductance:

$$L_J = \frac{\Phi_0}{2\pi I_0 \cos(\phi_J)} \tag{3.3.18}$$

In an equivalent circuit representation, a faithful approach must also consider a shunted capacitance C_J, natural to the junction, which depends on the geometry and the insulator

[8] In particular for a superconductor loop interrupted by n Josephson Junctions we have the following *fluxoid quantization condition*:

$$\frac{\Phi_0}{2\pi}\sum_{k=1} n\phi_{J_k} + \Phi_{\text{ext}} + \Phi_L = n\Phi_0 \tag{3.3.15}$$

where Φ_L is the flux due to the self inductance of the loop ($\Phi_L \to 0$ for small loops). The orientation of the flux taken defines the phase difference labeling $\phi_{J_k} = \theta_{J_{k_1}} - \theta_{J_{k_2}}$ so that the current associated with the flux flows from 1_k to 2_k.

dielectric properties. Of course this capacitance can be modified using capacitances around the junction, usually by creating islands (small isolated sections of superconductor)

Let us also note that flux and the gauge-invariant phase are intimately related. From Eq. (3.3.1) we have that $\dot{\Phi} = V$, while from the AC-Josephson effect condition $\Phi_0\dot{\phi}_J/2\pi = V$, so:

$$\Delta\phi_J = 2\pi\Delta\Phi/\Phi_0 \tag{3.3.19}$$

And we get that for every change in the flux of one *flux quantum* the invariant phase winds 2π.

Also, if we follow the quantization procedure we eventually obtain the following Hamiltonian:

$$H = E_C\frac{\hat{Q}^2}{e^2} - E_L\cos\left(\frac{2\pi}{\Phi_0}\hat{\Phi}\right) \tag{3.3.20}$$

with $E_C = e^2/2C_J$ and $E_L = I_0\Phi_0/2\pi$ being the charging energy and the Josephson energy of the Junction respectively.

3.3.5 Artificial atoms: The flux qubit

There are several ways of implementing effective two-level systems using superconducting loops, lumped capacitances and inductances and Josephson junctions. In general they are classified considering the regimes in which the Josephson junctions operate, which are defined according to the ratio E_J/E_C. The value of that quotient basically establishes the dominance of one term over the other in the Hamiltonian (3.3.20).

For $E_J/E_C \ll 1$ we have the *charge regime*, the number of Cooper pairs is well defined and the phase fluctuates strongly. For $E_J/E_C \gg 1$ we are in the *flux or phase regime*, as the phase is conserved, while the cooper pair density is not.

In the charge regime we have configurations like the *Cooper-pair box* (also known as *charge qubit*), the *quantronium* and the *transmon*. In the flux regime we have the *flux qubit*, the *phase qubit* and the *fluxonium*. The latter mentioned in each category are basically improved versions of the former, designed with the aim of reducing the effects of charge and flux noise on the qubit state. Also, in the intermediate regimes we have other circuits like the *flux-phase* qubit.

We will concentrate here on describing the flux qubit, as it is the model we will be using along the thesis. It basically consists of a superconducting loop interrupted by three Josephson junctions operating in the flux regime, one of which is significantly smaller than the others, a fact encoded in an α factor.

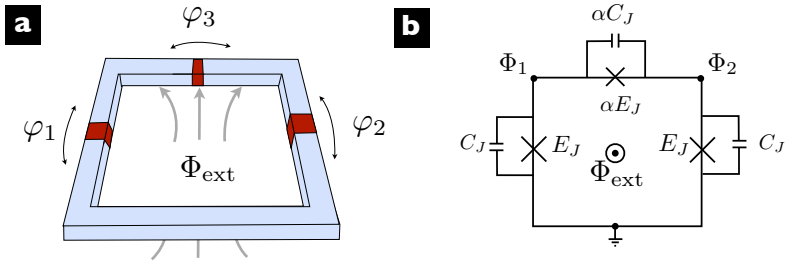

Figure 3.6: a) Physical realization of a flux qubit: a loop interrupted by three josephson junctions. b) Circuit representation. Image taken from [209]

Quantizing the circuit we obtain the Lagrangian:

$$\mathcal{L}_{\text{FQ}} = \frac{1}{2}\sum_{i=1}^{3}\left[C_i\dot{\Phi}_i^2 + E_{J_i}\cos\left(\frac{2\pi}{\Phi_0}\Phi_i\right)\right], \tag{3.3.21}$$

Considering an external magnetic flux being applied Φ_{ext} and using the fluxoid quantization condition 3.3.15 while neglecting the loop's self-inductance we arrive at:

$$\mathcal{L}_{\text{FQ}} = \frac{C_J}{2}\left[(\dot{\Phi}_1^2 + \dot{\Phi}_2^2) + \frac{\alpha}{2}(\dot{\Phi}_1 + \dot{\Phi}_2)^2\right] - U, \tag{3.3.22}$$

where U is the system's potential energy:

$$U(\Phi_1, \Phi_2) = -E_J\left\{\cos\left(\frac{2\pi}{\Phi_1}\Phi_i\right) + \cos\left(\frac{2\pi}{\Phi_0}\Phi_2\right) + \alpha\cos\left[\frac{2\pi(\Phi_{\text{ext}} - \Phi_1 - \Phi_2)}{\Phi_0}\right]\right\}. \tag{3.3.23}$$

With $\Phi_{\text{ext}} = \Phi_0/2$ and $\alpha > 0.5$, U shows a confining profile where the dynamics happens along the diagonal $\Phi_+ = (\Phi_1 + \Phi_2)/2$.

Along that one-dimensional line:

$$U(\Phi_+) = -E_J\left\{2\cos\left(\frac{2\pi}{\Phi_0}\Phi_+\right) + \alpha\cos\left[\frac{2\pi(\Phi_{\text{ext}} - 2\Phi_+)}{\Phi_0}\right]\right\}. \tag{3.3.24}$$

Performing a Legendre transform between the conjugate variables $Q_+ = \partial\mathcal{L}_{\text{FQ}}/\partial\dot{\Phi}_+$ and Φ_+ we finally obtain the Hamiltonian:

$$H = \frac{(1+\alpha)Q_+^2}{2C_J(1+2\alpha)} - E_J\left[2\cos\left(\frac{2\pi}{\Phi_0}\Phi_+\right) + \alpha\cos\left[\frac{2\pi(\Phi_{\text{ext}} - 2\Phi_+)}{\Phi_0}\right]\right\} \tag{3.3.25}$$

This Hamiltonian shows a two-well structure, each well classically corresponding to clockwise and counterclockwise persistent currents in the circuit loop of magnitude I_p :

$$I_p = I_0\sqrt{1 - \frac{1}{4\alpha}} \tag{3.3.26}$$

Diagonalizing the system we distinguish two levels than approach each other as $\Phi_{\text{ext}} = \Phi_0/2$. Around that value we can discard other levels and write the Hamiltonian (3.3.25) in the basis of the persistent currents $\{|\circlearrowleft\rangle, |\circlearrowright\rangle\}$ as:

$$H = \frac{1}{2}(\epsilon\sigma_z + \Delta\sigma_x) \tag{3.3.27}$$

where

$$\epsilon = 2I_p\left(\Phi_{\text{ext}} - \frac{\Phi_0}{2}\right) \tag{3.3.28}$$

is the qubit's magnetic energy due to the existence of a persistent current around the loop, and Δ, proportional to the tunneling rate between the two persistent current states, is the qubit gap:

$$\Delta \simeq \frac{4E_J}{\sqrt{\alpha E_J/E_C}}\mathrm{e}^{-0.15\sqrt{4\alpha(1+2\alpha)E_J/E_C}} \tag{3.3.29}$$

In the qubit eigenbasis:

$$H^{\text{fq}} = \frac{\hbar\omega_q}{2}\sigma_z, \qquad \text{with } \omega_q = \sqrt{\epsilon^2 + \Delta^2} \tag{3.3.30}$$

3.3.6 Qubit - light interaction: Coupling to a transmission line

A transmission line, which the qubits can be coupled to, can be used as a quantum bus to facilitate the exchange of information between qubits or harnessed to perform collective operations. In the context of quantum simulations we may think that it just simulates a 1D electromagnetic environment where our artificial atoms can interact.

In any case, a way had to be envisioned to couple qubits to a transmission line in a setup that is usually referred to as Circuit QED, in contrast to Cavity QED, refering the idea that most situations in the last case can be circuit implemented in this superconductive setting. The way to couple the qubits depends naturally on the type of qubit.

For the flux qubit, the coupling is achieved inductively as in Fig. 3.7. From the circuit we can of course derive the Hamiltonian:

$$H = \hbar\omega\left(a^\dagger a + \frac{1}{2}\right) + \frac{1}{2}(\epsilon\sigma_z + \Delta\sigma_x) \tag{3.3.31}$$

with ϵ is the same as in Eq. (3.3.28), but now the external flux $\Phi_{\text{ext}} = \Phi_{\text{ext}}^{\text{DC}} + \Phi_{\text{ext}}^{\text{AC}}$, impingent on the loop, has two contributions: the flux that we can use as a control variable and the modulation due to the resonator's field, an external AC flux

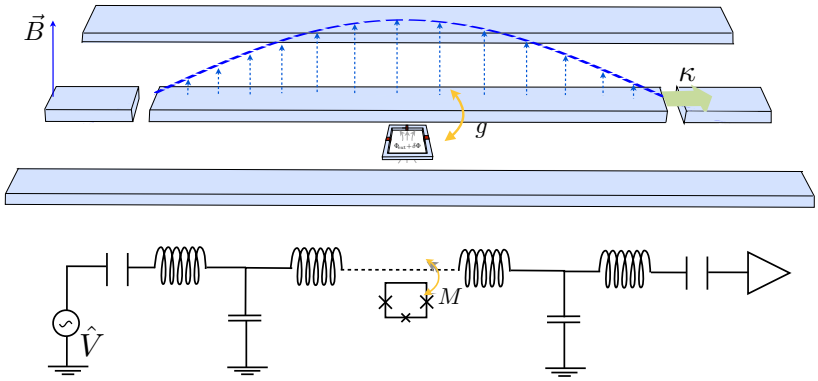

Figure 3.7: a) Physical realization of a flux qubit coupled to a transmission line. b) Circuit representation. Image taken from [209]

$$\Phi_{\text{ext}}^{\text{AC}} = \Phi_{\text{rms}}(a + a^\dagger), \qquad \Phi_{\text{rms}} = MI_{\text{rms}} = M\sqrt{\frac{\hbar\omega_r}{2L_r}} \tag{3.3.32}$$

with $L_r = d\ell$, and M being the mutual impedance which depends on the placement and size of the qubit. Here we have considered only the first resonator mode ω_r to be relevant.

Abusing the notation we will consider $\epsilon = 2I_p\,(\Phi_{\text{ext}}^{\text{DC}} - \Phi_0/2)$, and the new Hamiltonian can be written as:

$$H = \hbar\omega\left(a^\dagger a + \frac{1}{2}\right) + \frac{1}{2}(\epsilon\sigma_z + \Delta\sigma_x) + \hbar g\sigma_z(a + a^\dagger), \qquad \text{with } \hbar g = MI_pI_{rms}. \tag{3.3.33}$$

In the qubit eigenbasis:

$$H^{\text{fq}} = \frac{\hbar\omega_q}{2}\sigma_z + \hbar\omega_r\left(a^\dagger a + \frac{1}{2}\right) + \hbar g(a + a^\dagger)(\cos\vartheta\sigma_z - \sin\vartheta\sigma_x) \tag{3.3.34}$$

where here $\omega_q = \sqrt{\tilde{\epsilon}^2 + \Delta^2}$ and $\tan\vartheta = \Delta/\epsilon$.

If we apply a RWA (which requires that $g \ll \omega_q, \omega_r$) to eliminate the fast rotating terms, we end up with a JC Hamiltonian:

$$H^{\text{fq}} = \frac{\hbar\omega_q}{2}\sigma_z + \hbar\omega_r\left(a^\dagger a + \frac{1}{2}\right) - \hbar g\sin\vartheta\,(a\sigma^+ + a^\dagger\sigma^-) \tag{3.3.35}$$

Again we will consider for most cases an open line instead of a resonator. In that case a sum will have to be performed over a continuum of frequencies for the transmission line modes.

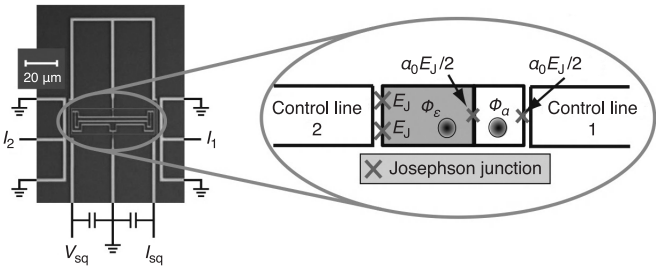

Figure 3.8: Illustration of a gap-tunable qubit with four Josephson junctions placed along two loops: the main loop (shaded in gray), and the α loop, a DC squid replacing what would otherwise have been the α junction of the qubit. The control lines are placed to tune the loop fluxes. Image extracted from [217]

3.3.7 Qubit control

As explained before, the control of the qubit state consists of two different types of rotations. The choice of options is vast both to implement both longitudinal and transversal rotations. As longitudinal rotations can be achieved by just letting the qubit preceed or combining transversal rotations, we could in principle just discuss the implementation of those last ones.

In any case, given Eq. (3.3.27), it should be clear that, if it were possible to modify the values for ϵ and Δ, we would have an easy way to perform 1-qubit operations. As a matter of fact that is a possibility, for ϵ is controlled by the external flux (controlled through a control line ending in a u-turn placed closely enough to the qubit loop), and Δ, which in principle is fixed by geometry, can be made tunable by replacing the unequal junction by a DC-SQUID (check next section) [216]. Fig. 3.8 shows a possible implementation.

Even if the gap is not tunable, the implementation of single rotations can be fully carried on by simply driving the qubit with controlled microwave pulses of frequency ω_d, sent through the control line on top of the DC signal or extra control lines. The consequence is an additional driving term in the Hamiltonian 3.3.27:

$$H_d = \frac{A}{2}\cos(\omega_d t + \phi)\sigma_z \tag{3.3.36}$$

Now, in the eigenbasis of the qubit, this looks as:

$$H_d^{\text{fq}} = \frac{A}{2\hbar\omega_q}\cos(\omega_d t + \phi)\left(\epsilon\sigma_z - \Delta\sigma_x\right) \tag{3.3.37}$$

Now, if we take the full H^{fq}, transform it into a frame rotating with the driving frequency into H' [9] and then perform a RWA (demanding $A \ll \omega_d, \omega_q$) we obtain:

[9] Such a transformation requires a $U = e^{i\omega_d t\sigma_z/2}$. As U is time dependent the transformed hamiltonian can

$$H_{\text{RWA}}^{\text{fq}\ \prime} = \frac{\hbar}{2}(\omega_q - \omega_d)\sigma_z - \frac{A\Delta}{4\hbar\omega_q}[\cos(\phi)\sigma_x - \sin(\phi)\sigma_y] \tag{3.3.38}$$

For the case of resonant driving $\omega_d = \omega_q$, if the pulse is maintained for a certain time t, we can solve the correspondent system of diffential equations and see that the following rotation [10] gets performed :

$$R_t = \begin{pmatrix} \cos(\Omega_R t/2) & [\mathrm{i}\cos(\phi) - \sin(\phi)]\sin(\Omega_R t/2) \\ [\mathrm{i}\cos(\phi) + \sin(\phi)]\sin(\Omega_R t/2) & \cos(\Omega_R t/2) \end{pmatrix} \tag{3.3.39}$$

.

From here we see that, in resonance, Rabi oscillations are generated with a Rabi frequency $\Omega_R = A\Delta/2\hbar^2\omega_q$.

If the qubit had a tunable gap, we could study the same situation but with a σ_x pulse through the second control line.

3.3.8 Qubit readout: DC-SQUID

For flux qubits, several readout methods have been proposed and successfully implemented. They range from the simple switching-DC-SQUID method [28, 120, 121] to more sophisticated techniques such as the inductive readout [122–126] or the bifurcation amplifier [127–130]. The two latter have the potential to achieve quantum non-demolition measurements [131] and very large signal visibility, which are important features for future applications.

Again, several readout methods have been implemented for the flux qubit. Well known are the simple switching-DC-SQUID [218], the inductive readout [219] and the bifurcation amplifier [220]. For most cases the reading is performed by using an additional external readout circuit, mostly a DC-SQUID (Superconducting QUantum Interference Device).

A DC-SQUID is a superconducting loop containing two Josephson junctions. Seen as two JJ placed in parallel, the DC-SQUID is actually equivalent to a single Josephson Junction with effective capacitance $C_{\text{eff}} = 2C_J$ and $E_{\text{eff}}(\Phi_{\text{ext}}) = 2E_J\cos(\pi\Phi_{\text{ext}}/\Phi_0)$ as tunable Josephson energy. The DC-SQUID can be therefore seen as a non-linear inductor, with a value that depends on the magnetic field. As a matter of fact, SQUIDs have been universally used as magnetometers. A theoretically simple measurement procedure that makes use of this fact, the inductive readout, consists in placing the SQUID close to the qubit (or even enclosing it) and therefore coupling both inductively. The two different eigenstates

be calculated as $H' = U^\dagger H U - iU\partial U^\dagger/\partial t$

[10] Always in the rotating frame, eigenstate basis being considered.

have different expectation values for the circulating current that therefore result in different values for the SQUID's non-linear inductance. In order to detect the difference, the DC-SQUID is placed in a resonator. A microwave signal is then applied to the resonator and the outcoming phase depends on the state of the qubit.

For the procedure to be successful, we must demand $\epsilon \gg \Delta$, which means that before the measurement is performed the control flux must be changed to take the qubit far from the degenerate point. We advice the reader to check [219] for further details.

3.3.9 Switchable ultrastrong coupling

We have already devoted a long chapter to the discussion of many important concepts in superconducting circuits and yet there is a particular circuit, considered many times later in this thesis, that we have not analysed so far. That would be the ultrastrong coupling switch [221].

For some of our theoretical proposals we have played with the possibility of switching on an off a quantum field to which "atoms" are coupled strongly. This can be achieved in the context of Circuit QED by recurring to the design depicted in Fig. [3.9]

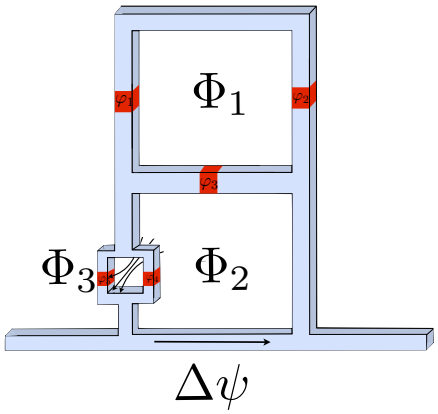

Figure 3.9: Switchable coupling design: a flux qubit (top ring) is coupled to the field $\Delta\psi$ by means of two loops. Varying the magnetic fluxes Φ_2 and Φ_3 we deactivate the qubit-field coupling.

A superconducting flux qubit -upper three-junction loop-, is there galvanically coupled to a quantum field $\Delta\psi$ -transmission line- by means of two additional loops. These extra loops are essential since they allow us to decouple the qubit from the field in an extremely fast way.

As usual in the case of flux qubits, the Josephson energy E_{J_i} of each junction is much greater than its charging energy E_{C_i}, and the Hamiltonian of the three-loop device can be

reduced to a sum of the inductive energy of the junctions,

$$H_J = -\sum_{j=1}^{5} E_{J_j} \cos\varphi_j, \tag{3.3.40}$$

where φ_i is the superconducting phase of the i-th junction.

We can simplify the expression of H_J thanks to the flux quantization around each closed loop, that imposes the following relations to the superconducting phases:

$$\sum_{j} \varphi_j = 2\pi f_i, \quad (i = 1, 2, 3), \tag{3.3.41}$$

where the magnetic frustration parameters $f_i = \Phi_i/\Phi_0$ can be adjusted varying the external magnetic fluxes Φ_i.

Using these conditions in the standard flux qubit configuration, $E_{J1} = E_{J2} = \alpha E_{J3}$, together with $E_{J4} = E_{J5} = \alpha_4 E_{J1}$, the Hamiltonian acquires the following shape:

$$\begin{aligned} H_J = \quad & -E_J \left[\cos(\varphi_1) + \cos(\varphi_2) + \alpha\cos(2\pi f_1 + \varphi_1 + \varphi_2)\right] \\ & - \quad \alpha_{\text{eff}} E_J \cos(2\pi f_{\text{eff}} - \Delta\psi + \varphi_1 + \varphi_2), \end{aligned} \tag{3.3.42}$$

where $\alpha_{\text{eff}} = 2\alpha_4\cos(\pi f_3)$, and $f_{\text{eff}} = f_1 - f_2 + f_3/2$ is an effective magnetic frustration. After including the kinetic terms and quantizing the canonical variables charge and flux, a diagonalisation shows that the first line of (3.3.42) can be identified with the flux qubit Hamiltonian, whereas the second line represents the qubit-field interaction. The shape of this interaction depends on which values the frustrations f_1 and f_2 take, while the interaction strength given by α_{eff}, can be adjusted to ultrastrong values through the control parameter f_3. Note that no RWA has been taken.

In particular, a numerical evaluation of H_J for $(f_1, f_2, f_3) = (0.5, 0.75, 1)$, yields the following effective Hamiltonian in the qubit basis:

$$H = \int dk\omega_k a^\dagger a + \hbar\frac{\Omega}{2}\sigma_z + \alpha_4 E_J \sigma_x \Delta\psi, \tag{3.3.43}$$

where $\Delta\psi$ is given by the expression

$$\Delta\psi(x) = i\int_{-\infty}^{\infty} dk\, \sqrt{N\omega_k}\, e^{ikx} a_k + \text{H.c.}, \tag{3.3.44}$$

and we have included the free Hamiltonian of the field.

On the other hand, if we vary the SQUID magnetic flux up to $f_3 = 0.5$ the interaction is switched off, and the Hamiltonian is

$$H = \int \mathrm{d}k\, \omega_k a^\dagger a + \hbar \frac{\Omega}{2} \sigma_z, \tag{3.3.45}$$

isolating the qubit from the bosonic field.

Therefore, with a fast change of f_3 a switchable interaction can be realized in the laboratory. Current technology with Al qubits [58] allows us to vary the magnetic frustration f_3 in times of less than 0.1 ns, which is much faster than the dynamics of the flux qubit.

Part I

Studies on Quantum Detectors

Modelling How to Probe *Physical* Quantum States and Simulating Acceleration Effects in the Lab

CHAPTER 4

Concepts

We have devoted this part of the thesis to the study of quantum detection processes from both a theoretical and a practical point of view. Detection is actually very relevant to Quantum theory, as it is very close to the measurement process. That might be the reason why defining such a familiar concept with precision is not particularly easy. We will give it a try anyway, but first we want to point out that the word detector is widely used in the community to refer to a general measurement apparatus, and here, on the contrary, we would like to refer only to a particular kind of detectors, those that detect a particle's presence. Why? Because we are very much interested in the particle concept, and taking the empiricist point approach, what a better way to analyze it than focusing on detectors? At the end of the day all the experience we have of particles comes precisely from the measurements that tell us about their trajectories.

We will define a particle presence detector, detector from now on, as a two state meter whose purpose is the detection of particles in a region of spacetime. We may picture it ideally as a box with one or more sides opened and a light attached to it that gets lit on when there is something inside the box, a "particle". Sadly such magical box does not exist but in order to model it we might think how an actual detector works and how the detection process operates.

A normal detection of a field excitation requires it interacting with our detector. Ideally the interaction would happen where both of them coincide in space and time, an then at some point an external observer will check the detector state to find out whether the particle has been detected or not. Ideally it would be the observer directly looking at the particle, but to be faithful to reality, experimenters never directly measure the system of interest,unless by accident (and in that case they would most probably not have the sensitivity required).

Rather, the particle of interest (a photon for example) interacts with a photodetector, which triggers a current in a circuit coupled to a sort of display, which radiates more photons,

which will eventually interact with the retina of the observer, etc. This chain of systems is called the von Neumann chain, and there is one point in it where one must apply the projection postulate in order to analize the process from the point of view of quantum theory [222]. This point is called the Heisenberg's cut. It usually represents the border between classical and quantum worlds and it is usually assumed to be the point where macroscopic material objects come into play . There, the fast decoherence times ensure that the measurement would proceed rather deterministically for the rest of the chain.

So if for the sake of simplicity we leave aside the studies that deal with decoherence and the frontier of quantum and classical, the practical quantum description of the system comes before the Heisenberg's cut, and this his how particle detectors are usually modelled when studying for example relativistic phenomena.

In the early start of the field of RQI, most studies dealt with global states and studied the point of view of accelerated observers and their observations without actually considering any sort of detection process but rather putting the emphasis in coordinate transformations and tracing away the non-accesible regions of the spacetime.

These early investigations on relativistic entanglement helped in the better understanding of its observer-dependent aspects, but their results where merely academic. The entanglement between global modes could never be observed by local observers and let alone properly controlled: Alice could never perform a unitary or a two qubit gate on a global state. However, global mode entanglement, and also entangled localized states, can be accessed by local observers who employ detectors. As a matter of fact, the more one comes closer to more physical scenarios, the more natural becomes the use of detector models.

The Unruh DeWitt detector has enabled the study of many interesting scenarios, starting of course with the seminal work by Unruh [54]. More recently, using an exactly solvable model (where the detector is assumed to be a harmonic oscillator) Lin and Hu [118] have reconsidered the problem of a uniformly accelerated detector in a quantum field but taking special care to analyze it in terms of the information flow and making connections with the information paradox. There are plenty of other analyses considering alternative scenarios. In [223], for example, two detectors are studied, one inertial and one in uniform acceleration, both coupled to the same field. It is then verified that any initial entanglement shared between them two disappears in a finite time, shorter for higher accelerations, as expected. In that particular work, the case of non-uniform acceleration is also explored, concluding that disentanglement slows down, and that uniform acceleration is somehow optimal in that respect. The different case of circular motion, has been considered independently [224]. Also interesting are the possibilities for vacuum entanglement extraction. The case of two

static detectors was studied in [225], and much more recently in a full analysis carried on with two accelerated detectors in [47]. The study of extracting vacuum correlations with detectors has also been explored in [46]. From the cosmological point of view, the use of the UDW detector is also interesting. It has proved for example that the evolution of the entanglement between two point-like detectors can also been used to distinguish between flat and expanding deSitter spacetime [70]

Here we will study the Unruh DeWitt model by deriving it from first principles, but also we would show how to modify it to better model the detection of wavepacket states. Besides this, we will present a different study on non-monotonic entanglement with realistic states carried on with another type of detector, called projective, an original model [139] that was precisely developed to include the Heisenberg's cut in it and so it cannot introduce particles in the field that were not present before. Some claim that this difference makes the latter a more realistic model of particle detector, while the former would be better characterized as a fluctuation detector. We will see later what is meant by that.

For a detailed study on some more detector models and their use in the study of non-local correlations we refer the interested reader to [131].

4.1 The Unruh-DeWitt detector

The Unruh-DeWitt (UDW) detector model describes phenomenologically a monopole detector coupled to a massless scalar field, moving in the four-dimensional Minkowski space. Since its inception, as mentioned above, it has been used to study the response of detectors experiencing acceleration, to provide a proof for the Unruh effect, and particularly as one of the main tools to probe dynamics of entanglement in the context of Relativistic Quantum Information (RQI).

Usually, the detector considered is a quantum system with two internal states, ground state $|g\rangle$ and excited state $|e\rangle$, with Ω (taking $\hbar = 1$) being the energy gap between the two levels. A harmonic oscillator might also be used, although there Ω would be the energy difference between consecutive levels. The detector is then coupled to ϕ according to the following interaction Hamiltonian:

$$H_{\text{int}} = \lambda\, \xi(\tau)\mu(\tau)\phi(\boldsymbol{x}(\tau)) \tag{4.1.1}$$

where λ is the coupling strength, ξ is a switching function which activates during the interaction time , $\mu(\tau)$ the monopole momentum operator and $x(\tau)$ the worldline of the atom.

In spite of the differences between this monopole-scalar field interaction and QED (for instance in the behaviour at very extreme frequencies which may quantitatively differ), it

characterises adequately the matter-radiation interaction in some specific settings [226] (see section 5.2 for further details), while it very accurately models the interaction of internal degrees of freedom of atoms with phonon fields (for example the spin-phonon interaction of ions in a Coulomb crystal, collective excitations of Bose-Einstein condensates [227] and other solid state and analog systems). This model and certain variations of it have been extensively used in the literature for many purposes [164], including thermalization dynamics and decoherence ([228, 229] and references therein), although it is more known for what regards the studies of the Unruh effect and Hawking radiation [54, 230, 231].

As a detector model, it performs commonly under the pointlike approximation, i.e. it has no extension and interacts with the field only in the exact geometric point of the space-time where it is placed.

4.2 Other detector models: projective detector

The other detector model that we use briefly in this thesis was first developed in [139]. We will mention its convenience to study some problems later on in chapter 6, so here we will merely describe its operation.

The model is the idealization of a physical setting of a simple device where a lens is attached to a single-mode fiber ending in a detector. In the ideal version, the state of the single mode is projected in the Fock basis and all the other modes orthogonal to the it are not be affected by the detection. We assume therefore that the detector's response is neither affected by the state of the orthogonal modes nor does it affect their state. The scheme could be generalised to allow the detection of arbitrary modes by placing optical elements in front of the lens, which would transform the given input mode into the single mode transmitted by the fiber.

We will refer to the mode the detector is tuned to as $\psi_D(\boldsymbol{q},\tau)$, which can be decomposed in positive frequency modes as:

$$\psi_D(\boldsymbol{q},\tau) = \sum_i f_i^D u_i(\boldsymbol{q},\tau). \tag{4.2.1}$$

With $f_i^D = (\psi_D, u_i)$. We have used generic coordinate names $(\boldsymbol{q},\tau)$ to represent the co-moving coordinates of the detector in which the mode is defined. In this fashion we fix the mode independently of the detector's state of motion (inertial or uniformely accelerated). We will also assume that $\psi_D(\boldsymbol{q},\tau)$ consists only of positive frequency modes with respect to the detector's proper time τ. The real mode actually would be the combination $\psi_D(\boldsymbol{q},\tau) + \psi_D^*(\boldsymbol{q},\tau)$ which must be a real field solution that describes the wave which couples to the

detector. The $\{u_i(\boldsymbol{q},\tau)\}$ represent the positive frequency modes associated with the detector trajectory expressed in co-moving coordinates.

Until here we were working in classical terms. Now that we enter the quantization realm we will make the hats explicit to avoid confussion. Assume we have the operator $\hat{d} = (\psi_D, \hat{\phi})$ where

$$\hat{\phi} = \sum_i \hat{a}_i u_i(\boldsymbol{q},\tau) + \hat{a}_i^\dagger u_i^*(\boldsymbol{q},\tau), \tag{4.2.2}$$

then:

$$\hat{d} = (\psi_D, \hat{\phi}) = \sum_i \hat{a}_i(\psi_D, u_i) + \hat{a}_i^\dagger(\psi_D, u^*) = \sum_i \hat{a}_i(\psi_D, u_i) = \sum_i f_i^D \hat{a}_i, \tag{4.2.3}$$

and as we see this operator annihilates the co-moving vacuum. It is also verified that $[\hat{d}, \hat{d}^\dagger] = 1$. We can therefore interpret it as a creator of an excitation in the detector mode and assume that the basis $\mathcal{B} = \left\{\frac{\hat{d}^{\dagger n}}{\sqrt{n!}}\right\}$ spans all possible detector states (in the mode ψ_D). $\hat{d}^\dagger\hat{d}$ will be the number operator for particles detected by the detector.

These excitations, which are not eigenstates of the Hamiltonian, are the only subspace accesible from the detector when it comes to observing the whole Hilbert space. When the detector is probing a particular a field state $|\Psi\rangle$ it will only see $\mathrm{Tr}_{\perp\psi_D}|\Psi\rangle\langle\Psi|$, where the trace is taken over the orthogonal complement of the space spanned by $\mathcal{B}$ in the whole Fock space.

The validity of the use of such a detector has been satisfactory verified in the sense that it satisfactory predicts the existence of the well-known Unruh temperature for the case of a uniformly accelerated detector in the presence of the Minkowski vacuum.

The interest of using it as compared to the typical UDW detector for the study of accelerated scenarios is that under this framework a fixed state of the field defined in an inertial frame can be probed for any acceleration, avoiding having to use a different initial state for each acceleration and a non-local initial mode as in the other case (we will understand this better later on). Another alternative for working with localised modes from the beginning is the modification of the UDW model that we propose in the next chapter.

4.3 Simulations: Accelerated detectors

Most of the existing calculations that involve the Unruh DeWitt model have predictions that have never been tested experimentally due to the extreme accelerations needed for the corresponding effects to become observable. In this thesis we will try to make our contribution trying to bridge this gap. At the end of this part, in chapter 7 we will study an analogy

between static quantum emitters coupled to a single mode of a quantum field and accelerated Unruh-DeWitt detectors. We will make an experimental proposal to simulate a variety of relativistic quantum field settings beyond the reach of current computational power, such as high number of qubits coupled to a quantum field following arbitrary non-inertial trajectories. Moreover, we will propose a connection to nonequilibrium physics by showing how a simple rule as the Landau Zener (LZ) probability formula can be used to estimate the probability of excitation and deexcitation of an accelerated atom. We will describe how our scheme can be implemented in trapped ions and circuit QED set-ups.

CHAPTER 5

Wavepacket Detection with the Unruh-DeWitt Model

In this chapter we deal with several issues regarding the localisation properties of the Unruh-DeWitt (UdW) detector model. Since its original formulation as a pointlike detector, the UdW model has been used to study extensively the physics of quantum fields in presence of accelerations or curved backgrounds. Natural extensions of it have tried to take into account the spatial profile of such detectors, but all of them have met a series of problems in their spectral response which render them useless to study some of the most interesting physical scenarios. We provide a derivation of the smeared UdW interaction from QED first principles, then we analyze the spectral response of spatially smeared UdW detectors, and discuss the kind of spatial profiles which are useful for the study of relevant cases.

5.1 Introduction

While this assumption –which will always be an approximation since any physical detector has a finite size– seems to be valid in many scenarios, it is not valid in general even for physically interesting scenarios, and is particularly problematic in some specific settings that we will discuss below. Also, it presents UV divergences as any pointlike interaction and cannot be guaranteed to hold for any context where we consider several detectors undergoing relativistic motion where the pointlike approximation may be violated from some reference frames. Moreover, additional problems with the pointlike nature of the detector arise. For instance, there are various regularisation schemes which yield different transition probabilities [232].

For all these reasons, and keeping in mind that any realistic particle detector has a finite size, it is important to model and understand particle detectors that present a spatial

smearing. However, previous localisation models present a series of issues when it comes to analysing non-vacuum field states. In this work we will show to what extent an Unruh DeWitt detector is a reliable model of electromagnetic atomic transitions, by explicitly analysing the relationship between the atomic wavefunctions and the spatial smearing. We also intend to provide a pedagogical description of the use of a spatially smeared UdW model and we will discuss how to overcome the problems when analysing signals by means of a small but essential modification of the spatial profiles employed in the past. Besides, we will focus on the particular case of spatially smeared uniformly accelerated detectors.

This chapter is organised as follows: In section 5.2 we show from first principles how to relate the spatial profile of the UdW model to the wavefunctions of physical systems under standard QED interactions. In section 5.3 we present the localisation issues of the canonical UdW detector employed in the literature when the size of the detector is comparable to the wavelength they are tuned to. In section 5.4 we propose a way around these difficulties by modifying the spatial profile of the smeared UdW detector. In section 5.5 we discuss how to use these detectors to analyze arbitrary signals in accelerated settings. Finally, section 5.6 contains our conclusions.

5.2 Modelling atomic physics with the Unruh DeWitt detector

An UdW detector is an ad-hoc phenomenological model commonly used to study idealised situations in field theory and non-inertial settings. The model is built specifically for its useful properties and simplicity. While desirable traits are good guidelines for model building, one should always keep the physics in mind. This section is concerned with the build up of a smeared UdW detector out from first principles and standard QED interactions.

First, note that the simple scalar field model (4.1.1) cannot be directly used to relate the UdW model to electromagnetic phenomena due to the vector character of the photon field. The vector version of an UdW interaction with a smeared field operator would be

$$H_{\mathrm{I}} = \sum_{\lambda=+,-} \int d\boldsymbol{x}\, \lambda[\boldsymbol{F}(\boldsymbol{x})\sigma^{+} + \boldsymbol{F}^{*}(\boldsymbol{x})\sigma^{-}] \cdot \boldsymbol{A}(\boldsymbol{x}) \tag{5.2.1}$$

where we have omitted any switching function, as the electromagnetic interaction cannot be switched, and where σ^{-} is the two-level system lowering operator, as is common in the literature. We have also allowed for a complex profile function. The detector is assumed to be inertial; we discuss the treatment of an accelerated UdW detector in sec. 5.5.

The physical system the UdW detector tries to emulate is that of a two-level atom coupled to a quantum electromagnetic field. The Hamiltonian for such a system is well-known and

it is simply

$$\begin{aligned} H_{\mathrm{I}}^{\mathrm{QED}} &= e\boldsymbol{p}_{\mathrm{D}} \cdot \boldsymbol{A}(\boldsymbol{x}, 0) \\ &= \boldsymbol{p}_{\mathrm{D}} \cdot \sum_{\lambda=+,-} \int \frac{d\boldsymbol{p}}{\sqrt{2p}} \left[\epsilon_{\boldsymbol{p},\lambda} a^{\dagger}_{\boldsymbol{p},\lambda} e^{-ipx} + \epsilon^{*}_{\boldsymbol{p},\lambda} a_{\boldsymbol{p},\lambda} e^{ipx} \right], \end{aligned} \tag{5.2.2}$$

where $\boldsymbol{p}_{\mathrm{D}}$ is the detector momentum and in the last two equalities we assume a $(1+1)$-dimensional setting. In this setting, $\mathbf{p}_{\mathrm{D}}$ is itself an operator, the momentum operator of the valence electron of the two-level system. There is a simple way to relate (5.2.2) to (5.2.1); we simply write down the operator in (5.2.2) in terms of field operators and atomic Pauli matrices. There are four possible matrix elements for the $\boldsymbol{p}_{\mathrm{D}}\boldsymbol{A}(\boldsymbol{x}, 0)$ operator in terms of the relevant wavefunctions, $\Psi_g(\boldsymbol{x})$ for the ground state and $\Psi_e(\boldsymbol{x})$ for the excited state of the detector, which can be neatly written into matrix form as,

$$\begin{aligned} H_{\mathrm{I}}^{\mathrm{QED}} &= \alpha \mathbf{I} + \beta\sigma_z + \gamma\sigma_x + \delta\sigma_y, \\ \alpha &= e \sum_{\lambda=+,-} \int \frac{d\boldsymbol{p}}{\sqrt{2p}} \left[a^{\dagger}_{p} \frac{G^{\lambda}_{gg}(\boldsymbol{p}) + G^{\lambda}_{ee}(\boldsymbol{p})}{2} + \mathrm{H.c.} \right], \\ \beta &= e \sum_{\lambda=+,-} \int \frac{d\boldsymbol{p}}{\sqrt{2p}} \left[a^{\dagger}_{p} \frac{G^{\lambda}_{gg}(\boldsymbol{p}) - G^{\lambda}_{ee}(\boldsymbol{p})}{2} + \mathrm{H.c.} \right], \\ \gamma &= e \sum_{\lambda=+,-} \int \frac{d\boldsymbol{p}}{\sqrt{2p}} \left[a^{\dagger}_{p} \frac{G^{\lambda}_{ge}(\boldsymbol{p}) + G^{\lambda}_{eg}(\boldsymbol{p})}{2} + \mathrm{H.c.} \right], \\ \delta &= e \sum_{\lambda=+,-} \int \frac{d\boldsymbol{p}}{\sqrt{2p}} \left[a^{\dagger}_{p} \frac{G^{\lambda}_{ge}(\boldsymbol{p}) - G^{\lambda}_{eg}(\boldsymbol{p})}{2i} + \mathrm{H.c.} \right], \end{aligned} \tag{5.2.3}$$

with

$$G^{\lambda}_{ij}(\boldsymbol{p}) = \int d\boldsymbol{x}\; e^{-ipx} \boldsymbol{\epsilon}_{\boldsymbol{p},\lambda} \cdot (\Psi^{*}_{i}(x)[-i\boldsymbol{\nabla}\Psi_j(x)]). \tag{5.2.4}$$

If we performed the same calculation with the interaction (5.2.1), we would obtain

$$G^{\lambda}_{ij}(\boldsymbol{p}) = [\delta_{ig}\delta_{je} + \delta_{ie}\delta_{jg}] \int d\boldsymbol{x}\; e^{-ipx} \boldsymbol{\epsilon}_{\boldsymbol{p},\lambda} \cdot \boldsymbol{F}(\boldsymbol{x}). \tag{5.2.5}$$

We have thus expressed the physical interaction hamiltonian $H_{\mathrm{I}}^{\mathrm{QED}}$ in the language of (5.2.1). If we only consider the σ_x and σ_y terms, we may compare directly to (5.2.1). From (5.2.4) and (5.2.5) we find that the two Hamiltonians are equivalent with a smearing function

$$\boldsymbol{F}(\boldsymbol{x}) = -i\Psi^{*}_{e}(\boldsymbol{x})\boldsymbol{\nabla}\Psi_g(\boldsymbol{x}). \tag{5.2.6}$$

We have thus made a first connection between (5.2.1) and the physics - *the smearing function can be obtained in terms of the atomic wavefunctions of the two-level system.* This means that

the smeared UdW Hamiltonian commonly used in the literature can be related in a direct manner to the physical properties of the underlying system, directly relating the smearing function to the wavefunctions of the excited and ground states of the two-level atom. Note that the terms with $\mathbf{I}$ and σ_z do not vanish and can never do so unless $\Psi_e = \Psi_g = 0$, or in the dipolar approximation, where $e^{-ipx} \simeq 1$.

The α term can be dealt with full generality, as it can be reabsorbed into the free field Hamiltonian H_{F},

$$H_{\mathrm{F}} + \alpha = \int d\boldsymbol{p} \left[(|p| a^\dagger_{\boldsymbol{p}} a_{\boldsymbol{p}} + \frac{1}{\sqrt{2p}} \left(a^\dagger_{\boldsymbol{p}} \frac{G^\lambda_{gg}(\boldsymbol{p}) + G^\lambda_{ee}(\boldsymbol{p})}{2} + a_{\boldsymbol{p}} \frac{G^\lambda_{gg}(\boldsymbol{p})^* + G^\lambda_{ee}(\boldsymbol{p})^*}{2} \right) \right] \tag{5.2.7}$$

and so defining new modes

$$b_{\boldsymbol{p}} = a_{\boldsymbol{p}} + \frac{e}{(2p)^{3/2}} [G^\lambda_{gg}(\boldsymbol{p}) + G^\lambda_{ee}(\boldsymbol{p})] \tag{5.2.8}$$

and neglecting the usual infinite zero-point contribution, we deal with the α term. We only have to substitute the $a_{\boldsymbol{p}}$ in terms of the $b_{\boldsymbol{p}}$ in γ, which amounts to the addition of a constant term to γ,

$$\alpha_\gamma = \frac{e^2}{4} \Re \left\{ \int \frac{d\boldsymbol{p}}{p} [G^\lambda_{gg}(\boldsymbol{p})^* + G^\lambda_{ee}(\boldsymbol{p})^*)(G^\lambda_{ge}(\boldsymbol{p}) + G^\lambda_{eg}(\boldsymbol{p})] \right\}. \tag{5.2.9}$$

This will induce an extra $\alpha_\gamma \sigma_x$ term in the Hamiltonian, which will be relevant or not depending on how α_γ compares with Ω, the detector system gap. As α_γ / e is typically of order 1 or less, this term will not be important if we are in a perturbation theory regime where the coupling e is assumed to be small. The same considerations apply to α_δ. The analogous correction to β,

$$\alpha_\beta = \frac{e^2}{4} \Re \left\{ \int \frac{d\boldsymbol{p}}{p} [G^\lambda_{gg}(\boldsymbol{p})^* + G^\lambda_{ee}(\boldsymbol{p})^*][G^\lambda_{gg}(\boldsymbol{p}) - G^\lambda_{ee}(\boldsymbol{p})] \right\}, \tag{5.2.10}$$

can be reabsorbed into Ω.

Dealing with β is a more challenging matter. We cannot do the same as before because, even though we could make the Hamiltonian look like that of a free field plus an UdW interaction, the detector and field operators would not commute and hence, even without the interaction, the theory would not be a free theory.

There is one special circumstance in which β vanishes: in systems with a strong spin interaction, so that the gap comes from the spin dependence of the energy levels. This could happen, for instance, in states of an atom within a strong magnetic field. In this case the

atomic wavefunctions of the ground and excited states are the same and therefore $\beta = 0$ exactly. The energy gap is $\hbar\Omega = \mu_{\mathrm{B}} B$. The coupling constant to the electric field is $\approx ed$ where d is a typical dimension of the atom, so in order to be in perturbation theory regime we would require electric fields of order $E < \mu_{\mathrm{B}} B/ed$.

As a particular example, consider the smearing function for a hydrogen atom in its $1s$ state subjected to a magnetic field. According to (5.2.6), we would have

$$\boldsymbol{F}(\boldsymbol{x}) = -i\frac{e^{-r/a_0}}{\pi a_0^4}\boldsymbol{u}_r. \tag{5.2.11}$$

5.3 Localisation issues of the UdW detector

The first UdW localization model was introduced by Schlicht [232] to solve the problems with the non-equivalence of regulators derived from the pointlike nature of the detector. In particular, he proposed a localised spatial profile for the detector (which for computational convenience was chosen to be Lorentzian). This localisation model was further studied by Langlois [233] first, and then by Satz and Louko [234, 235], who envisioned a more general scheme which allowed general spatial profiles to be considered undergoing arbitrary movement throughout spacetime. In these works the interaction Hamiltonian is defined as follows:

$$\begin{aligned} H_I = g\int_0^\infty \frac{d\boldsymbol{k}}{\sqrt{2\omega(2\pi)^3}} \int d\boldsymbol{x}\; F(\boldsymbol{x}) \left(\sigma^+ e^{i\Omega t} + \sigma^- e^{-i\Omega t}\right) \\ \times \left(a_{\boldsymbol{k}}^\dagger e^{-i(\boldsymbol{k}\cdot\boldsymbol{x}-\omega t)} + a_{\boldsymbol{k}} e^{i(\boldsymbol{k}\cdot\boldsymbol{x}-\omega t)}\right) \end{aligned} \tag{5.3.1}$$

Where $F(\boldsymbol{x})$ is the spatial smearing of the detector that is supposed, for simplicity and without loss of generality, at rest and centred in $\boldsymbol{x} = 0$, and Ω represents the frequency gap of the two-level system, in other words, the transition energy between the ground and excited state of the detector. The detector is supposed to be tuned to this frequency, i.e. it is more likely that the detector absorbs field quanta of this frequency than anything else, as we will discuss below. In the case that the detector is point-like $F(\boldsymbol{x}) = \delta(\boldsymbol{x})$, this model becomes the standard UdW detector introduced in [178].

The form of the function $F(\boldsymbol{x})$ must be related to the characteristics of the physical system modelled by the Hamiltonian (5.3.1). In the particular case of a two-level atom, $F(\boldsymbol{x})$ should be obtainable from the wave functions of the ground and excited states of the atom and the matter-radiation interaction Hamiltonian. For the case of atomic spin transitions, the form of the Hamiltonian was derived from first principles in section 5.2.

However, it is interesting to be able to consider detectors whose size becomes comparable with the wavelength to which they are tuned. These regimes cover a great range of extremely interesting physical scenarios, e.g. quantum microwave antennae (for example flux or charge qubits in cQED), Rydberg atoms and cavity based detectors [236, 237], where one can no longer use an atomic wave-function to obtain the form of the Hamiltonian. Yet, it is well known that the point-like model is a good effective description of the physics [236, 237]. As we will discuss below, a question arises when studying the compatibility of the standard spatially smeared UdW model with detectors whose characteristic length is comparable to the wavelength detected beyond the atomic scale.

In the following paragraphs we will point out a fundamental issue with the use of the traditional smeared UdW model when considering spatially extended detectors. For these cases, we propose a way to modify the detector model in order to formulate an effective theory reproducing the correct phenomenology.

Previous works dealing with the localised UdW model just considered the behavior of the detector interacting with the Minkowski vacuum, which is known to have equivalent behavior for all frequencies [234, 235]. In that respect, the problems of the model dealt with in this manuscript have not been studied yet. We will discuss below how they can build up when one tries to process physical signals and photon wavepackets with such a detector.

For most recent analyses [232–235] a real symmetric profile function was chosen. In particular, the spatial profile used for most calculations was a Lorentzian. To illustrate here the problem in the most simple way we will consider a Gaussian profile, but all results apply equivalently to the Lorentzian case or to any other spatial profile.

From the Hamiltonian (5.3.1), the integral over $\boldsymbol{x}$ takes the form of a trivial Fourier transform

$$\begin{aligned} H_I = g \int_0^\infty \frac{d\boldsymbol{k}}{\sqrt{2\omega_{\boldsymbol{k}}(2\pi)^3}} \left(\sigma^+ e^{i\Omega t} + \sigma^- e^{-i\Omega t}\right) \\ \times \left(\hat{F}(\boldsymbol{k}) a_{\boldsymbol{k}}^\dagger e^{i\omega_{\boldsymbol{k}} t} + \hat{F}(-\boldsymbol{k}) a_{\boldsymbol{k}} e^{-i\omega_{\boldsymbol{k}} t}\right) \end{aligned} \tag{5.3.2}$$

where we have made the dispersion relation explicit $\omega_{\boldsymbol{k}} = c|\boldsymbol{k}|$ and

$$\hat{F}(\boldsymbol{k}) = \int d\boldsymbol{x}\; F(\boldsymbol{x}) e^{-i\boldsymbol{k}\cdot\boldsymbol{x}} \tag{5.3.3}$$

is the Fourier transform of the spatial profile.

We can rewrite the Hamiltonian in a way in which the resonant and anti-resonant terms are made explicit:

$$H_I = g \int \frac{d\boldsymbol{k}}{\sqrt{2\omega_{\boldsymbol{k}}(2\pi)^3}} \left[\hat{F}(\boldsymbol{k}) \left(a_{\boldsymbol{k}}^\dagger \sigma^- e^{i(\omega_{\boldsymbol{k}} - \Omega)t} + \text{H.c.}\right)\right.$$

$$+\hat{F}(-\boldsymbol{k})\left(a^{\dagger}_{\boldsymbol{k}}\sigma^{+}e^{i(\omega_{\boldsymbol{k}}+\Omega)t}+\text{H.c.}\right)\Big] \tag{5.3.4}$$

The time evolution operator is computed as the time ordered exponential of the Hamiltonian. When integrating over times, the exponential factors in the Hamiltonian above are highly oscillating except when $\omega_k = c|\boldsymbol{k}| \approx \pm\Omega$ (stationary phase). This is the mathematical reason why a detector is tuned to the frequency of the energy gap between the ground and the excited state, as it is very well known from the study of the matter-radiation interactions [226, 238]. In plain words, if we want to stimulate the transition between ground and excited state we have to 'beam' the detector with radiation tuned to the natural frequency of the transition (on resonance). Otherwise, the probability of transition quickly decreases with the detuning between this natural frequency and the frequency of the radiation stimulating the transition.

Here is the issue. If we choose $F(x)$ to be a localised smooth function such as a Gaussian or a Lorentzian, which is the case for most realistic atoms , the frequency profile $F(\boldsymbol{k})$ will be a localised function centred in $\boldsymbol{k} = 0$. Being this so, its evaluation at Ω/c will give a negligible value, for Ω sufficiently large.

The reason why this issue does not arise in electronic transitions for atoms at rest is because, for most cases, Ω is small enough. For instance, electronic transitions in the hydrogen atom have an Ω in the visible range of the spectrum, whereas the Fourier transform of the spatial profile has a width of $\sim a_0^{-1}$, which extends up to the X-ray spectrum.

However, when we consider accelerated detectors, the Minkowski frequency for a packet centered in Ω as seen from the detector, varies effectively as a function of time as $\omega_R = \Omega e^{a\tau/c}$ (See derivation on section 5.5 and [6]) and even for very small times it goes out of resonance. Even if we compensate the Doppler shift of the wavepacket tuning the detector in real time for the period while packet and detector overlap, we would easily get the problem of the frequency getting too far from our detector support function. If the spatial profile function does not have information about the energy gap between the ground and excited state of the detector, the response of the detector to the resonance frequency (the frequency which, by far, mostly contributes to the estimated transition from the ground and excited state) will be exponentially dampened by the Gaussian or Lorentzian tails. That implies that an accelerated detector would be, in practical terms, incapable of detecting a wavepacket centred on its natural frequency. If we are to analyse signals with UdW detectors, the model should be accordingly modified to avoid this issue.

To illustrate the problem let us consider the most simple 1-D case, and a detector with a Gaussian spatial profile. We can take $F(x)$ to be a normalised Gaussian profile with charac-

teristic length L:

$$F(x) = \frac{1}{L\sqrt{2\pi}} \exp\left(\frac{-x^2}{2L^2}\right) \tag{5.3.5}$$

And so its Fourier Transform $\hat{F}(k)$ will be a Gaussian localised around $k = 0$

$$\hat{F}(k) = \exp\left(\frac{-k^2L^2}{2}\right) \tag{5.3.6}$$

Any frequencies such that $\omega_k \gg 0$ would be exponentially dampened in the integral over k by the weight $\hat{F}(k)$. In particular, if $\Omega >> 0$, the stationary phase contribution $\omega_k = \pm\Omega$ will be zero due to $F(\pm\Omega/c) \approx 0$, effectively cancelling any non-trivial time evolution.

So, as it is illustrated in fig. 5.1, if $\Omega \gg cL^{-1}$ the detector will not ever detect any signal even if it is a powerful pulse tuned to the transition frequency. Therefore, in order to be able to study relativistic settings, some modifications must be made to the model.

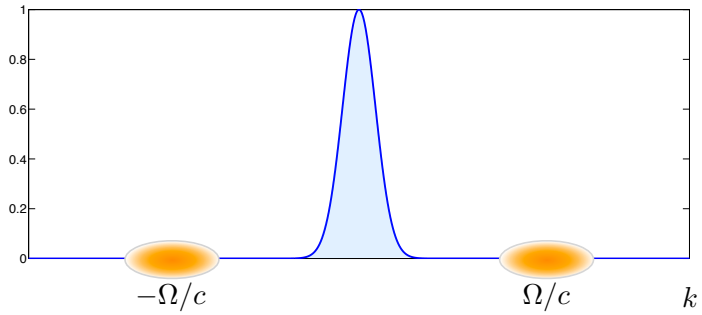

Figure 5.1: A highly localised $\hat{F}(k)$ centred in 0 would practically suppress the possibility of detection for the resonance frequencies to which the detector is most responsive, $k = \pm\Omega/c$. This results in a vanishing transition probability no matter what frequency we use to illuminate the detector.

One could argue that if the detector is very small with respect of the wavelength to which it is tuned (as it is the case of atoms), the Gaussian profile $\hat{F}(k)$ may cover the resonance regions. However, as seen in figure 5.2, if we analyze the probability of transition as a function of the frequency of the radiation with which the detector interacts, its spectral response will be asymmetric in the detuning between the detector natural frequency and the frequency of the radiation stimulating the transition $\Delta = \omega_k - \Omega$.

In other words, if the transition frequency is Ω and the radiation stimulating the transition is detuned from the energy gap of the detector by a small factor δ, the probability of transition will be positively weighted by $\hat{F}(k)$ if $\omega_k = \Omega - \delta$, and dampened if $\omega_k = \Omega + \delta$.

Although a similar asymmetry occurs in realistic atomic transitions (as detailed in section 5.5), the effect is so small that it can be neglected in most circumstances. In practice, no such effects are observed neither in atomic detectors nor in any other settings where quantum systems (like harmonic oscillators) are coupled to quantum fields.

When the size of the detectors increases as to become comparable with the wavelength to which they are tuned, e.g. quantum microwave antennaee (for example flux or charge qubits in cQED), Rydberg atoms and cavity based detectors [236,237], the detector response is also symmetric in frequencies. Therefore the use of the Unruh-DeWitt detector presented above to model those scenarios (where the spatial profile is related to the natural dimension of the detector), can be problematic.

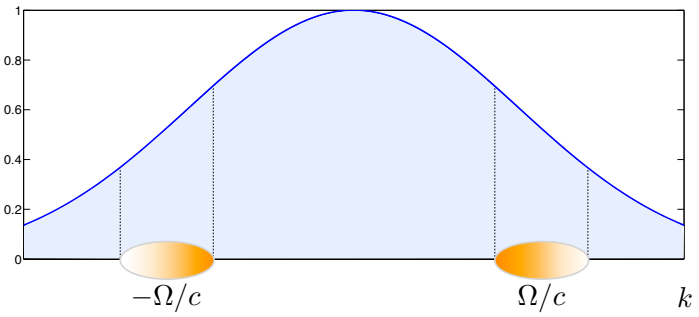

Figure 5.2: A not-so localised $\hat{F}(k)$ centred in 0 would introduce an asymmetry in the detection of frequencies $\omega_k = \Omega \pm \delta\, k = \pm\Omega/c$

5.4 Modulated oscillations in the spatial profile

In most realistic settings, the spectral response function of two level emitters is symmetric with respect to the resonance frequency, thus a small detuning should produce similar effects no matter if it is positive or negative. Also, as we discussed above, if the two level system size is comparable with the wavelength it is tuned to, the localized UdW model employed in the literature will dramatically fail to detect anything, even if it is the case of an intense pulse of radiation centred in the natural frequency of the detector's transition.

Taking these issues into account, we propose a modification of the way in which the UdW detector is spatially smeared. We will do so by feeding the spatial profile with information about the resonance frequency. For that matter, we will introduce a spatial profile which is strongly localized by a function $S(x)$, modulated by internal oscillations associated with the frequency the two level system is tuned to.

If the spatial profile is

$$F(x) = S(x)\cos\left(\frac{\Omega x}{c}\right) \tag{5.4.1}$$

then the spectral profile would be

$$\hat{F}(k) = \frac{1}{2}\left[\hat{S}(k-\Omega/c) + \hat{S}(k-\Omega/c)\right] \tag{5.4.2}$$

which is a localised profile in frequencies around the two resonance regions. If we take $S(x)$ to be the Gaussian profile (5.3.5) then

$$\hat{F}(k) = \frac{1}{2}\left(e^{\frac{1}{2}(k-\Omega/c)^2L^2} + e^{-\frac{1}{2}(k+\Omega/c)^2L^2}\right) \tag{5.4.3}$$

which, as seen in figure 5.3, covers symmetrically the resonance regions.

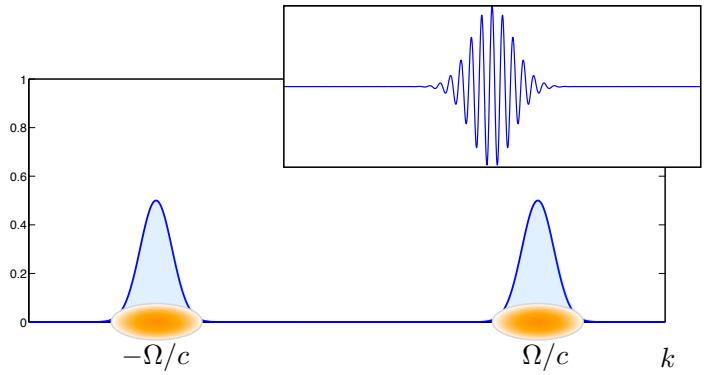

Figure 5.3: A localised $\hat{F}(k)$ can be not centered in 0 by introducing a oscillating term in the spatial profile seen in the inset. The figure shows symmetric detection zones centered in the frequencies $k = \pm\Omega/c$.

By doing this we have the desired spectral response no matter the value of Ω, and the detector is spatially localized around $x = 0$ with a characteristic proper length L. We must stress that the introduction of the cosine factor in (5.4.1) is intended only as a solution to the problem of the unphysical suppression of the transition rates. We do not claim that such a spatial profile is realised, for instance, in inertially moving two-level atoms (where the pointlike approximation is often valid and enough to produce physical results). However, this will not be the case when the UdW detector is used to model more exotic systems where the wavelength of the absorbed and emitted radiation is comparable with the size of the physical system. The problem of considering the physical form of $F(\boldsymbol{x})$ for regular atoms was tackled in section 5.2.

Notice that we are not deriving this effective coupling from first principles. Rather, we are pointing out the limits of applicability of the UdW model to describe extended detectors when the wavelength of the radiation is comparable to their physical extension, and suggesting a way in which the phenomenology of such detectors can be effectively recovered. One can, however, understand this as a process of 'antennization' (classical antennae, that are comparable with the wavelength of the radiation they are tuned to detect, have some periodical structure related to the wavelength they are resonant with). We are providing the extended detector with a spatial periodicity related to the radiation the detector is tuned to.

5.5 Accelerated detectors

In order to provide a complete description of the localised detector model proposed in this note, in this section we will describe how to use this model to analyse arbitrary signals with a spatially smeared uniformly accelerated detector.

There is a well known problem with accelerating rigid bodies: the proper distance between two points of a solid accelerating with the same relativistic acceleration increases with time, eventually destroying the solid when the internal tension it supports is overrun by the relativistic effects.

The reasonable hypothesis for a physical detector is that it has to keep internal coherence. This means that the internal forces that keep the detector together will prevent it from being further smeared due to relativistic effects up to some reasonable acceleration regimes. That means that, effectively, every point of the detector will accelerate with a different acceleration in order to keep up with the rest of its points. The natural formalism to treat this detector is the use of the well-known Fermi-Walker coordinates [232, 239].

Thus, the interaction Hamiltonian of a smeared uniformly accelerated rigid detector is

$$H_{\mathrm{I}}(t) = g\int \frac{dk}{\sqrt{2\omega_k(2\pi)}}\int d\chi\, F(\chi)\left(\sigma^+ e^{i\Omega\tau} + \sigma^- e^{-i\Omega\tau}\right) \left(a_k^\dagger e^{i(\omega_k t(\chi,\tau)-kx(\chi,\tau))} + a_k e^{-i(\omega_k t(\chi,\tau)-kx(\chi,\tau))}\right) \quad (5.5.1)$$

where $\boldsymbol{\chi} = (\chi, 0, 0)$ and τ are the Fermi-Walker coordinates associated with the trajectory of the detector.

These coordinates have the particularity that at every point on the trajectory $x(\tau) = (ct(\tau), x(\tau), 0, 0)$ the hyperplane which is orthogonal to the 4-velocity $u(\tau) = (c\dot{t}(\tau), \dot{x}(\tau), 0, 0)$ is the three-dimensional space which consists of all the events which are simultaneous to $x(\tau)$, where simultaneity is judged from the comoving inertial frame. We assume that we move only in one direction, so that $\chi_1 = \chi, \chi_2 = y = 0, \chi_3 = z = 0$.

If we attach a dreibein to every such hyperplane

$$\begin{aligned} e_{\chi_1} &= (c^{-1}\dot{x}(\tau), \dot{t}(\tau), 0, 0) \\ e_{\chi_2} &= (0, 0, 1, 0), \quad e_{\chi_3} = (0, 0, 0, 1), \end{aligned} \quad (5.5.2)$$

we can characterise every event x_e in a neighborhood of the trajectory with $(\tau_e, \boldsymbol{\chi}_e)$.

These coordinates guarantee a rigid detector (where rigidity means that its 3-geometry as seen from its own momentary rest system is unchanged in the course of proper time). In contrast, in a Rindler frame (standard approach for pointlike detectors) every point of the

detector accelerates with a different proper acceleration, so they cannot account for rigid detectors that have internal coherence. In the F-W frame the detector will accelerate coherently, so this models very well what would happen to an accelerated rigid-body.

The change of coordinates between the inertial system to the Fermi-Walker frame is given by

$$\boldsymbol{x}(\tau,\boldsymbol{\chi}) = \boldsymbol{x}(\tau) + \chi^i \boldsymbol{e}_i(\tau), \quad t(\tau,\boldsymbol{\chi}) = t(\tau) + \frac{\chi^i e_i^0}{c} \tag{5.5.3}$$

For the uniformly accelerated observer, the trajectory (parametrised in terms of comoving time) is

$$x(\tau) = \left[\frac{c^2}{a}\sinh\left(\frac{a\tau}{c}\right), \frac{c^2}{a}\cosh\left(\frac{a\tau}{c}\right), 0, 0\right] \tag{5.5.4}$$

The only relevant component of the dreibein is

$$e_{\chi_1} = \left[\sinh\left(\frac{a\tau}{c}\right), \cosh\left(\frac{a\tau}{c}\right), 0, 0\right] \tag{5.5.5}$$

So, directly from (5.5.3) we read the change of coordinates

$$\begin{aligned} t(\tau,\chi) &= \left(\frac{c}{a} + \frac{\chi_1}{c}\right)\sinh\left(\frac{a\tau}{c}\right) \\ \boldsymbol{x}(\tau,\chi) &= \left[\left(\frac{c^2}{a} + \chi_1\right)\cosh\left(\frac{a\tau}{c}\right), 0, 0\right] \end{aligned} \tag{5.5.6}$$

Within this scheme we compute the probability of excitation of an accelerated detector responding to an arbitrary signal. In first order perturbation theory,

$$P = |g|^2 \int_{\tau_0}^{\tau} d\tau' \int_{\tau_0}^{\tau} d\tau''\, e^{i\Omega(\tau'-\tau'')} \langle y|\, \Psi(\tau'')\Psi(\tau')\, |y\rangle \tag{5.5.7}$$

$$\Psi(\tau) = \int \frac{F(\boldsymbol{\chi})\, dk d\chi}{\sqrt{2c|k|(2\pi)}} \left(a_{\boldsymbol{k}} e^{i(\boldsymbol{k}\cdot\boldsymbol{x}(\boldsymbol{\chi},\tau) - c|\boldsymbol{k}|t(\boldsymbol{\chi},\tau))} + \text{H.c.}\right) \tag{5.5.8}$$

where $|y\rangle$ is a general superposition of plane-wave field modes corresponding to a Minkowskian-shaped wavepacket, prepared in the lab, that we want to analyze with our detector,

$$|y\rangle = \left(\int dk\; y(k) a_k^\dagger\right).|0\rangle \tag{5.5.9}$$

Let us evaluate the time-correlation function $W_y(\tau',\tau'') \equiv \langle y|\, \Psi(\tau'')\Psi(\tau')\, |y\rangle$. The two χ integrals can be rewritten in terms of Fourier transforms greatly simplifying the expression of $W_y(\tau',\tau'')$. To do this we first note that

$$\begin{aligned} kx(\chi,\tau) - ckt(\chi,\tau) &= L(k,\tau)\left(\chi + \frac{c^2}{a}\right) \\ L(k,\tau) &= k e^{a\tau/c} \end{aligned} \tag{5.5.10}$$

Considering that $\omega = ck$, then the complex exponential argument depending on τ as taken directly from the amplitude in (5.5.8) and (5.5.10) goes as

$$\Omega\tau + \frac{c\omega}{a}e^{-a\tau/c}. \tag{5.5.11}$$

So, taking derivatives, the condition for the stationary phase is as follows

$$\Omega - \omega e^{-a\tau/c} = 0. \tag{5.5.12}$$

Now the condition is no longer time independent as in the inertial case [6]. Instead the resonance frequency ω_R will be

$$\omega_R = \Omega e^{a\tau/c}. \tag{5.5.13}$$

which is obviously the inertial resonance frequency but non-trivially Doppler-shifted due to the acceleration.

Now if we define $G^{\pm}(k,\tau) = \hat{F}[\pm L(k,\tau)]$, where $\hat{F}(k)$ is the Fourier transform of $F(\chi)$ as in (5.3.3), we can rewrite $W_x(\tau',\tau'') =$

$$\begin{aligned}
&= \int \frac{\bar{y}(k)y(\kappa)dkd\kappa}{2(2\pi)c\sqrt{|k||\kappa|}} G^{+}(k,\tau'')G^{-}(\kappa,\tau')e^{i\frac{c^2}{a}[L(\kappa,\tau')-L(k,\tau'')]}) \\
&+ \int \frac{|y(\kappa)|^2 dkd\kappa}{2(2\pi)c|k|} G^{+}(k,\tau')G^{-}(k,\tau'')e^{i\frac{c^2}{a}[L(k,\tau'')-L(k,\tau')]} \\
&+ \int \frac{\bar{y}(k)y(\kappa)dkd\kappa}{2(2\pi)c\sqrt{|\kappa||k|}} G^{+}(\kappa,\tau')G^{-}(k,\tau'')e^{i\frac{c^2}{a}[L(k,\tau'')-L(\kappa,\tau')]}
\end{aligned}$$

which can be further simplified if $F(k) = F(-k)$ (true for a Gaussian or Lorentzian profile), then we get $G^{+} = G^{-} = G$ (although in general $G(k) \neq G(-k)$), and if the frequency profile of the signal $y(\omega)$ we want to analyse is chosen to be real, we can rewrite $W_x(\tau',\tau'') =$

$$\begin{aligned}
&= \int \frac{y(k)y(\kappa)dkd\kappa}{(2\pi)c\sqrt{|k||\kappa|}} G(k,\tau'')G(\kappa,\tau')\cos\left[\frac{L(\kappa,\tau')-L(k,\tau'')}{ac^{-2}}\right] \\
&+ \int \frac{[y(\kappa)]^2 dkd\kappa}{2(2\pi)c|k|} G(k,\tau')G(k,\tau'')e^{i\frac{c^2}{a}[L(k,\tau'')-L(k,\tau')]},
\end{aligned} \tag{5.5.14}$$

providing an operative expression for the response of a localized accelerated detector to a given signal.

5.6 Discussion

In this work, we have analysed the problem of wavepacket detection by an UdW model.

By appealing to phenomenological considerations, we have argued that in scenarios where our detector has to respond to a given frequency, the spatial profile considered must

verify certain properties. In particular, we have studied the origin of such a profile function for the case of an atomic detector by takink the task of deriving a UdW equation from first principles, relating the smeared UdW model to the usual $\boldsymbol{p} \cdot \boldsymbol{A}$ form of the QED interaction coupling atoms to the electromagnetic field. We have shown what differences between the models actually result from this calculation. As an outcome, we have shown a way of relating the smearing profile used in the UdW case with the electronic wavefunction of the relevant orbitals of an atom.

Going beyond this atomic example, and especially, when considering the case of detectors comparable with the wavelength to which they are tuned, we show that some information about the spectral response of the detector must be fed in general to the spatial profile. Otherwise the detector will not have the expected behaviour and will dramatically fail to detect radiation on resonance with the two-level system transition.

To solve these problems, we suggest to introduce a spatial oscillation of the profile, which will make the detector tune to the resonance frequency regardless of its size and configuration.

Not all the spatial profiles for the UdW model would be compatible with the experimental response of accelerated particle detectors: the existence of some monopole (or dipolar) momentum that couples the atom to the field with a given characteristic transition frequency requires those oscillations introduced in the spatial profile to reproduce spectra centred in the characteristic transition frequency of the detector . If one thinks of that profile as being something like a charge distribution, then those oscillations would be the responsible for the appearance of the momentum that correctly couples it to the field.

Completing our proposal, we have explained how to use this formalism while calculating the probability of detection of a wavepacket for an accelerated detector.

Finally note that, in parallel with this work, an analysis of the transition rates of smeared UdW detectors coupled to different kinds of physical field modes and undergoing different relativistic motion was carried out by Lee and Fuentes [240].

CHAPTER 6

Non-Monotonic Entanglement of Physical EM Field States in Non-Inertial Frames

We develop a general technique to analyse the quantum effects of acceleration on realistic spatially-localised EM field states entangled in the polarization degree of freedom. We show that for this setting, quantum entanglement may build up as the acceleration increases, providing a clear signature of phenomena related to the Unruh and Hawking effects.

6.1 Introduction

One of the most widely known results in relativistic quantum information is the notion that acceleration may have non-trivial effects on entanglement. A number of works have studied this issue through transformations between inertial and accelerated Fock bases (among many others, [67, 68, 138, 241]). Previous results considered tailored families of states which greatly simplified calculations but whose physical interpretation was not clear. Recently, [139] introduced a projective detector model which constitutes a promising new approach to the issue of field entanglement in non-inertial frames. It was shown in [139] that such detectors present the expected thermal response to the inertial vacuum state of the field (i.e. the Unruh effect [54]) and the model provides a good effective description of particle detection. In this work, we will use this projective model as a practical method to study field entanglement for localised two single-photon bipartite electromagnetic field states.

There are, however, two different approaches to use the projective model introduced in [139]. Here, we will develop a technique to analyse states by working out the Bogoliubov transformations and the change of basis inertial-accelerated modes in some approximate

but physically feasible scenario. A different technique, that allows to obtain exact results for Gaussian states without going through the Bogoliubov coefficients calculation, has been developed in [242].

While the later can be very handy to analyse squeezed states such as those produced in parametric down conversion, it is not clear to what extent it can be used to analyse two single-photon states as those studied in this work. Due to the relevance of non-monotonic entanglement behaviour reported here in the two single-photon regime, it is worth exploring the first approach. Also, the computation of the Bogoliubov transformations between localised inertial and accelerated Fock bases is of much interest in itself for its possible future use.

Let us use the detector model mentioned above [139] to explore bipartite entanglement for two single-photon states entangled in helicities with a Gaussian spread in frequencies. This spatially localised system is observed by two partners: an inertial one, Alice, looking at one of the photons, and an accelerated one, Rob, observing the other photon.

The practical limiting factor of the general formalism presented in this work is computational complexity, which may grow very quickly for some cases of interest. We study for which physical regimes results can be given within current computing power, and suggest how the computational issues of the formalism may be overcome beyond that.

6.2 Setting

We will consider two different observers, Alice and Rob. They are interested in studying field correlations in the electromagnetic field [1]. Alice is an inertial observer, while Rob undergoes a motion with constant proper acceleration $\tilde{a}$ and acceleration frequency $a = \tilde{a}/c$.

Rob's trajectory is best described in terms of Rindler coordinates. We introduce two sets of Rindler coordinates $(\xi_\pm, \tau_\pm)$ whose relation with the Minkowskian coordinates (x, t) is

$$ct = \pm\, \xi_\pm \sinh\left(a\tau_\pm\right), \qquad x = \pm\xi_\pm \cosh\left(a\tau_\pm\right), \tag{6.2.1}$$

with $x > |t|$ for (ξ_+, τ_+) and $x < -|t|$ for (ξ_-, τ_-). These coordinates naturally define two globally hyperbolic and causally disconnected submanifolds in flat spacetime, each being the mirror image of the other, which we call regions I and II following the standard notation of [68, 138]. Any field theory in flat spacetime can be regarded as two independent field theories, one in each of these regions [164]. Without loss of generality we place Rob in Region I.

[1] As usual in the literature, to analyse these effects more clearly we will assume that the acceleration lies in the polarisation quantisation axis so no Thomas precession occurs.

No operations will be carried out involving measurement or communication with region II. Although we make use of some mathematical constructions which mix region I and region II operators, we do so merely as a convenient computational tool. Our results are independent of whatever happens in the causally disconnected region II, thus, the entanglement we find is of a different nature to that present in the Minkowski vacuum state, which displays correlations between regions I and II [54].

At this point, there are two paths to go through: on one hand, we might take a specific model for Alice's and Rob's detectors (such as Unruh-DeWitt), prepare the detectors in a particular state and then let the field-detectors system evolve. After some time the detectors would lose and gain entanglement due to the non-trivial effects of Rob's acceleration. Recent examples of this approach are [49, 243, 244].

Still, this method has the drawback of being dramatically dependent on the details of the detector model assumed and it is very difficult to explore beyond first order perturbation theory or inside small cavities. Besides, depending on the model, the detectors may not inherit all the field correlations and may develop further correlations owing to the specific form of the interaction which do not come directly from field entanglement.

On the other hand, field entanglement has been successfully studied for decades by means of projective measurements on the field state, independently of any detector model. Entanglement between correlated photon pairs is usually accessed this way [245]. This approach also avoids all the complications associated with the detector-dependent settings previously discussed. This is the original approach used (among others) in [67, 68, 138, 241, 246] with completely delocalised Unruh modes [138]. In this line, using the localised projective detector formalism developed in [139] we do not face any problem coming from non-locality and acceleration dependence associated to the Unruh modes.

6.3 Procedure

As common in the literature [68, 247], the Fock space for Alice will be constructed in terms of Minkowski creation operators $a^\dagger_{\omega,\sigma}$ acting on the Minkowski vacuum state $|0\rangle_{\mathcal{M}}$, defined by

$$a_{\omega,\sigma}\,|0\rangle_{\mathcal{M}} = 0. \tag{6.3.1}$$

Here, $\sigma \in \{\uparrow, \downarrow\}$ denotes helicity.

Rob, as an accelerated observer, will build his Fock basis by means of Rindler modes. In this case, the Fock space will be constructed in terms of Rindler creation operators $a^\dagger_{\Omega,\sigma,\mathrm{I}}$

(and their complement $a^\dagger_{\Omega,\sigma,\mathrm{II}}$) acting on the Rindler vacuum state $|0\rangle_{\mathcal{R}}$, defined by

$$a_{\Omega,\sigma,\mathrm{I}}\,|0\rangle_{\mathcal{R}} = a_{\Omega,\sigma,\mathrm{II}}\,|0\rangle_{\mathcal{R}} = 0. \tag{6.3.2}$$

The Rindler modes are labelled by their dimensionless Rindler frequency $\Omega \equiv \Omega'/a$, where Ω' is the Rindler frequency.

Let us consider that Alice and Rob carry detectors able to explore a particular set of modes of the field, but without assuming anything about the particular detector model. Rob's associated field vacuum is not $|0\rangle_{\mathcal{M}}$, but rather, the Rindler vacuum $|0\rangle_{\mathcal{R}}$. This means that Rob will be able to make projective measurements in the subspace spanned by the basis

$$\mathcal{B} = \left\{ \frac{1}{\sqrt{n!}}(d^\dagger_\uparrow)^n\,|0\rangle_{\mathcal{R}}\,, \frac{1}{\sqrt{n!}}(d^\dagger_\downarrow)^n\,|0\rangle_{\mathcal{R}}\,|n\in\mathbb{N}\right\} \tag{6.3.3}$$

with the operators $d^\dagger_\sigma$, which create one 'detector mode' excitation, being a linear combination of Rindler creation operators of definite helicity,

$$d^\dagger_\sigma = \int_0^\infty d\Omega\, g(\Omega) a^\dagger_{\Omega,\sigma,\mathrm{I}}. \tag{6.3.4}$$

We will analyse a very general family of arbitrarily spatially localised entangled states of the form

$$|\Psi\rangle = P\,|a\rangle_{\mathrm{A}}\,|x\rangle_{\mathrm{Rob}} + Q\,|b\rangle_{\mathrm{A}}\,|y\rangle_{\mathrm{Rob}}\,, \qquad |P|^2+|Q|^2 = 1. \tag{6.3.5}$$

Here, the states $|x\rangle_{\mathrm{Rob}}$ and $|y\rangle_{\mathrm{Rob}}$ will be a pair of Minkowskian wavepacket one-particle excitations of opposite helicities, i.e.

$$\begin{aligned} |x\rangle_{\mathrm{Rob}} &= \left(\int d\omega\; x(\omega) a^\dagger_{\omega,\uparrow}\right)|0\rangle_{\mathcal{M}}\,, \\ |y\rangle_{\mathrm{Rob}} &= \left(\int d\omega\; y(\omega) a^\dagger_{\omega,\downarrow}\right)|0\rangle_{\mathcal{M}}\,. \end{aligned} \tag{6.3.6}$$

$|a\rangle_{\mathrm{A}}$ and $|b\rangle_{\mathrm{A}}$ can be assumed to be a pair of Minkowskian wavepackets similar to $|x\rangle_{\mathrm{Rob}}$ and $|y\rangle_{\mathrm{Rob}}$.

As Rob will probe his part of the field state by means of projective measurements on the basis (6.3.3), to compute the effect of these measurements we will have to express first $|x\rangle_{\mathrm{Rob}}$ and $|y\rangle_{\mathrm{Rob}}$ in the Rindler basis.

This change of basis is most easily computed via an intermediate change to the so-called Unruh modes. For bosonic fields, the Unruh modes are defined in terms of the Rindler modes by

$$a_{\mathrm{R},\Omega,\sigma} = \cosh r_\Omega a_{\mathrm{I},\Omega,\sigma} - \sinh r_\Omega a^\dagger_{\mathrm{II},\Omega,-\sigma},$$

$$a_{\mathrm{L},\Omega,\sigma} = \cosh r_\Omega a_{\mathrm{II},\Omega,-\sigma} - \sinh r_\Omega a^\dagger_{\mathrm{I},\Omega,\sigma}, \tag{6.3.7}$$

with $\tanh r_\Omega = e^{-\pi\Omega}$.

The advantage of these modes is that the Minkowski vacuum factorises as [164]

$$|0\rangle_{\mathcal{M}} = \bigotimes_\Omega |0\rangle_{\Omega,\uparrow} |0\rangle_{\Omega,\downarrow} \tag{6.3.8}$$

where $a_{\mathrm{R},\Omega,\sigma} |0\rangle_{\Omega,\sigma} = a_{\mathrm{L},\Omega,\sigma} |0\rangle_{\Omega,\sigma} = 0$. The explicit form of $|0\rangle_{\Omega,\sigma}$ in terms of Rindler modes has been found elsewhere [247]. Eq. (6.3.8) implies that the Unruh and Minkowski modes share the same vacuum state, this meaning that Minkowski-Unruh change of basis preserves the number of particles. Therefore, we may express $|x\rangle_{\mathrm{Rob}}$ and $|y\rangle_{\mathrm{Rob}}$ as

$$\begin{aligned} |x\rangle_{\mathrm{Rob}} &= \int d\Omega \alpha^{\mathrm{R}}_{\omega\Omega} x(\omega) |{\uparrow_{\mathrm{R}\Omega}}\rangle + \int d\Omega \alpha^{\mathrm{L}}_{\omega\Omega} x(\omega) |{\uparrow_{\mathrm{L}\Omega}}\rangle , \\ |y\rangle_{\mathrm{Rob}} &= \int d\Omega \alpha^{\mathrm{R}}_{\omega\Omega} y(\omega) |{\downarrow_{\mathrm{R}\Omega}}\rangle + \int d\Omega \alpha^{\mathrm{L}}_{\omega\Omega} y(\omega) |{\downarrow_{\mathrm{L}\Omega}}\rangle , \\ \text{with } |\sigma_{\mathrm{X}\Omega}\rangle &= a^\dagger_{\mathrm{X},\Omega,\sigma} |0\rangle_{\mathcal{M}} , \ \mathrm{X} = \{\mathrm{L},\mathrm{R}\} \end{aligned} \tag{6.3.9}$$

where the $\alpha^{\mathrm{X}}_{\omega\Omega}$ are the coefficients of the relevant change of basis, which are computed for a scalar field in [138] and adapted for an electromagnetic field in [247].

Substituting (6.3.9) in (6.3.5), we finally express $|\Psi\rangle$ as a linear combination of states entangled between Alice's modes and Unruh modes of the form $|\sigma q_{\mathrm{R}}\rangle_\Omega = (q_{\mathrm{L}} a^\dagger_{\mathrm{L},\Omega,\sigma} + q_{\mathrm{R}} a^\dagger_{\mathrm{R},\Omega,\sigma}) |0\rangle_{\mathcal{M}}$, ($q_{\mathrm{L}}$ being such that $|q_{\mathrm{R}}|^2 + |q_{\mathrm{L}}|^2 = 1$, $q_{\mathrm{R}} \geq q_{\mathrm{L}}$). Namely,

$$|\Psi\rangle = \int d\Omega \ |\Phi\rangle_\Omega , \quad |\Phi\rangle_\Omega = |\phi\rangle_\Omega \bigotimes_{\Omega' \neq \Omega} |0\rangle_\Omega , \tag{6.3.10}$$

$$|\phi\rangle_\Omega = P_\Omega |a\rangle_{\mathrm{A}} |{\uparrow} q_{\mathrm{R}1}\rangle^\Omega_{\mathrm{Rob}} + Q_\Omega |b\rangle_{\mathrm{A}} |{\downarrow} q_{\mathrm{R}2}\rangle^\Omega_{\mathrm{Rob}} . \tag{6.3.11}$$

These states $|\phi\rangle_\Omega$ are precisely those studied in previous works on field entanglement in non-inertial frames [138, 246, 248], and their form in the Rindler basis is well known. We remark that, in contrast to previous works [68, 138, 246, 249], the state (6.3.5) (and consequently (6.3.10)) is the same no matter the acceleration of Rob.

Now, we recall that Rob's detector probes the non-monochromatic modes (6.3.4). To build a complete basis of the Fock space, we need to complete (6.3.4) with their orthogonal complement $D_\perp = \{\alpha^\dagger_1, \alpha^\dagger_2 \ldots\}$ where $\alpha^\dagger_i$ are one-particle creation operators so that $\mathcal{S} = \{d^\dagger_\uparrow, d^\dagger_\downarrow, \alpha^\dagger_1, \alpha^\dagger_2 \ldots\}$ is complete. In this basis, for a state $|n_1\, n_2 \ldots\rangle$ the detector will only be sensitive to the first two entries, which correspond to the detector modes. All we need to do then is tracing out the irrelevant set of modes $\alpha_1, \ldots \alpha_n$. We will end up with a reduced field state containing all the field entanglement accessible to our detector. At this point, we

may quantify this entanglement through any suitable entanglement measure, such as the negativity [250].

Note that the previous results reported in [68, 138, 246, 249] correspond to the choice of $|x\rangle_{\text{Rob}}$ and $|y\rangle_{\text{Rob}}$ to be Unruh excitations of a single fixed frequency Ω_{field}, and imposing a detector profile in adimensional frequencies $g(\Omega) = \delta(\Omega - \Omega_{\text{det}})$. In order to probe the entanglement for those simple modes, these works used a single-frequency detector with fixed Ω'_{det}, which would couple to a dimensionless Rindler frequency $\Omega_{\text{det}} = \Omega'_{\text{det}}/a$. That means that the Ω really probed by the detector depends on its acceleration. For each acceleration a, the field state was chosen peaked around a certain dimensionless Rindler frequency $\Omega_{\text{field}}(a)$, so as to always have $\Omega_{\text{field}} = \Omega'_{\text{det}}/a$. In contrast, using the projective detector model [139] we can probe the same acceleration-independent field state.

Peaked detectors.– With the formalism above, we may consider a physical state and look at the behaviour of entanglement with acceleration on a peaked distribution of Rindler frequencies. Although we will discuss below that our formalism can be extended to arbitrarily spatially smeared detectors, this is a most reasonable first step towards the study of realistic experimental scenarios. Approximately single-frequency detector modes have been constructed in [138] and constitute a nice and simple starting point. Such a detector mode will be spread in space with some finite characteristic length dependent on the frequency spread.

Let us consider the state (6.3.5) with $P = Q = 1/\sqrt{2}$ and Gaussian mode profiles,

$$x(\omega) = y(\omega) = (2\pi\omega)^{-1/4}\, e^{-\frac{(\omega-\omega_0)^2}{4\sigma^2}}. \tag{6.3.12}$$

If we choose $|a\rangle_{\text{A}}$ and $|b\rangle_{\text{A}}$ as another pair of Gaussian modes centered at a frequency far from ω_0, then (6.3.5) represents a normalised version of a two single-photon field state maximally entangled in polarisations.

We now introduce a realistic approximation for a single-mode detector for Rob by caracterising its spectral decomposition in terms of Rindler modes as

$$g_{\text{det}}(\Omega') = \Delta\Omega'^{-1/2}_{\text{det}} \Pi\left(\frac{\Omega' - \Omega'_{\text{det}}}{\Delta\Omega'_{\text{det}}}\right) \tag{6.3.13}$$

where $\Pi(x)$ is the unit step function, the characteristic function of the $[-\frac{1}{2}, \frac{1}{2}]$ interval.

After tracing out the unobserved field frequencies through eqs. (6.3.10) and (6.3.11), we compute the negativity of the relevant reduced state as a function of the acceleration. In order to make this calculation simpler we assume that

$$r_{\Omega_{\text{det}} - \Delta\Omega_{\text{det}}/2} \approx r_{\Omega_{\text{det}}} \approx r_{\Omega_{\text{det}} + \Delta\Omega_{\text{det}}/2}. \tag{6.3.14}$$

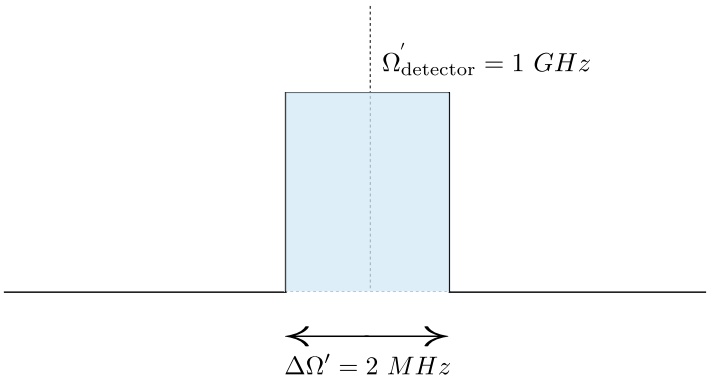

Figure 6.1: (Color online) Frequency profile of the simplified detector mode considered in the text.

From r_Ω definition (6.3.7) we find that for (6.3.14) to hold one must have

$$\frac{\Delta r_{\Omega_{\text{det}}}}{r_{\Omega_{\text{det}}}} \approx \left|\frac{d\ln r_\Omega}{d\Omega}\right|_{\Omega_{\text{det}}} \Delta\Omega_{\text{det}} = \frac{\pi e^{-\pi\Omega_{\text{det}}}\Delta\Omega_{\text{det}}}{\text{atanh}(e^{-\pi\Omega_{\text{det}}})(1+e^{-2\pi\Omega_{\text{det}}})} \ll 0.1 \tag{6.3.15}$$

which assuming a quality factor $Q = \Omega_{\text{det}}/\Delta\Omega_{\text{det}} = 500$ (typical value for microwave filters) happens to be valid for $\Omega_{\text{det}} = \Omega'_{\text{det}}/a \lesssim 10$. Considering $\Omega'_{\text{det}} = 1\,\text{GHz}$, that implies we must have $\tilde{a} = ac \gtrsim 3 \cdot 10^{16} m/s^2$. In this regime, we may assure that the observed effects are the direct consequence of Rob's acceleration, without any other effects playing any important role.

Figure 6.2 shows our results for a reasonable choice of the relevant parameters, along with the Rindler spread of the state (the coefficients of the left and right excitations in (6.3.9)).

Remarkably, the entanglement amplification phenomenon first reported in [246] still survives in this more physical scenario, and in fact it is present in single-photon entangled states.

Note that the amount of entanglement shown in Fig 6.2 is very small. This responds only to the fact that, in this example, we are considering a ultra-narrow-band detector: when looked at from the accelerated frame, the localised Minkowskian states spread over a broad Rindler frequency spectrum. In the simple example presented here we analyse correlations only for a highly peaked frequency spectrum of Rindler frequencies, so a great amount of the entanglement is lost due to the detector not seeing all the relevant frequencies.

In order to see more of the entanglement of the field state, we need a detector whose bandwidth is the most similar to the Rindler frequency distribution corresponding to the initial Minkowski wavepacket. Figures 6.2b and 6.3 show how a Minkowksi Gaussian wave-

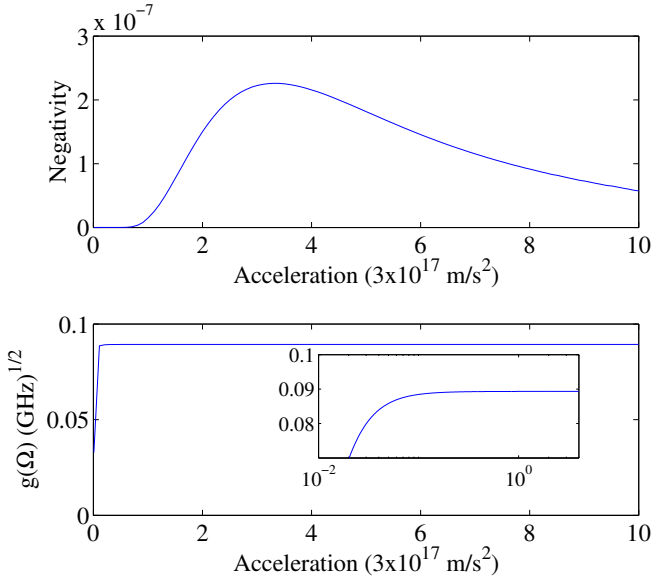

Figure 6.2: (Color online) (a) Negativity as a function of Rob's acceleration for the field state (6.3.5) with Gaussian profiles (6.3.12) with $\sigma = 0.01$ GHz, $\omega_0 = 1$ GHz. The Rindler spread of the detector mode is $\lambda = 2$ MHz. (b) Rindler spread of the field state, defined in (6.3.9), as a function of Rob's acceleration via the map $\Omega = \Omega'_d/a$, with detector Rindler dimensionful frequency $\Omega'_d = 1$ GHz. The inset provides a logarithmic scale of the profile, with the same quantities in both axes.

packet transforms into a well localised state in terms of Rindler modes. If the bandwidth of the detector approaches this localised distribution of Rindler modes, the amount of entanglement detected will be much higher. As we will discuss below, considering wider-band detectors in this formalism is straightforward, but it has a price in terms of computational complexity.

In any case our results mean that protocols of entanglement distillation [251] could be implemented to detect entanglement generation due to acceleration and therefore provide an unmistakable witness of the Unruh effect, easier to detect than the entanglement degradation reported in [68, 138] and others.

6.4 Broadband detectors

Our formalism can be applied to more general detector profiles and multimode detection: once we have determined both the state and the detector mode(s), we may use (6.3.10) to find the relevant reduced state of detector modes. We discuss in this section how computational difficulties appear when considering a more general detector with an arbitrary large mode

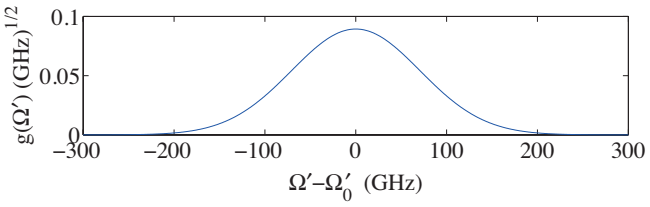

Figure 6.3: (Color online) Localised Rindler frequency spread of the Gaussian-localised Minkowskian state (6.3.12) for $\omega_0 = 1$ Ghz and $\sigma = 0.01$ Ghz, for $\tilde{a} = 3 \cdot 10^{17}\ m/s^2$. A detector mode with this profile in Rindler frequencies would be maximally tuned to the field state being probed and therefore would result in much higher entanglements. Ω_0 comes from an appropriate phase choice of the Minkowskian state.

spread and how to overcome them.

Note that (6.3.10) for the field state prior to tracing out the unobserved degrees of freedom includes a continuous product of frequencies. This means that in order to numerically obtain a reduced state from it, we need to make a sampling in frequencies, and then take a limit of small discretisation step. Let us discretise the frequencies so as to have m sample points within the spread of $g(\Omega)$ and allow up to n excitations per frequency. Then a lower bound in the computational complexity of obtaining the reduced state can be derived just by computing the number of individual operations required to manage the sparse matrices involved in the calculation, giving a complexity growing as

$$\mathcal{O}(a(n)^m). \tag{6.4.1}$$

where $a(n)$ is a monotonously increasing function of n satisfying $a(n) \geq 5$. Such a huge lower bound gives an idea of the intractability of the problem.

Until a way around the computational problems of a big number of frequencies is found, the only procedure to study these regimes is through quantum simulations and condensed matter analog systems (see e.g. [6]) or by considering field states with convenient properties, such as Gaussian states as done in [139] and other families which will be treated elsewhere [242].

6.5 Discussion

We have devised a scheme to analyse field entanglement in non-inertial frames for arbitrary single-photon field states and detector frequency response. To do this we have used the projective detector model introduced in [139]. As a particular case, we dealt with reasonable electromagnetic field states: we have analysed entanglement behaviour of a two-mode

photon state entangled in helicities. We have shown that the quantum effects of relativistic acceleration can actually amplify entanglement and not only destroy it.

Entanglement amplification phenomena have been reported before for some rather unphysical families of states [246], but the present work clearly shows that the effect is a genuine consequence of acceleration in less idealised field states.

This formalism allows us to consider very general and realistic states. In particular, we have thoroughly analysed the case of peaked detectors and studied the rapidly scaling computational costs of considering wide-band detection. These difficulties may be overcome through the use of quantum simulations: Instead of using analog systems to test predictions, we may use them to make predictions. Also, all the conclusions are exportable to a a static black hole scenario by means of the formalism developed in [252].

CHAPTER 7

Accelerated Detectors

7.1 Introduction

The study of accelerated atoms interacting with a quantum field is a fundamental problem, which has attracted a great deal of attention in General Relativity. Even though it has been treated extensively in the literature [168], it still poses intriguing questions, as well as experimental challenges for the detection of quantum effects induced by acceleration. Moreover, the emerging field of relativistic quantum information has recently increased the attention drawn to the topic, and in particular the study of correlations and entanglement in non-inertial scenarios [41].

Acceleration effects in quantum field theory are well understood in the perturbative regime, where, for example, transition rates are obtained for the excitation probability of atoms due to general relativity effects. A physical paradigm in this regime is the detection of the Unruh effect [54], which, roughly, implies that an atom accelerated in the vacuum of the field is excited in the same way as an inertial atom in an effective thermal field state. Going beyond the perturbative regime poses a tough theoretical problem, which gets even harder if one considers a set of emitters, in which case we face a many-body situation, situation particularly relevant from the point of view of relativistic quantum information.

In this chapter we show that a system of accelerated atoms [178] coupled to a bosonic field in the discrete mode approximation [139, 253], shares interesting analogies to time-dependent problems in quantum optics. Our work is motivated by the recent experimental progress that has allowed physicists to develop tools to control the dynamics of single emitters coupled to fields in set-ups such as trapped ions [202] or circuit QED [254] . The application of those systems as analog-simulators of accelerated atoms is particularly relevant to many-body non-perturbative regimes, where numerical calculations are difficult. Furthermore, the insight gained by such analogies motivates the study of physical effects that may

be relevant to the experimental detection of the Unruh effect. For example, collective phenomena such as superradiance [255,256] (which are known to amplify the effective coupling of a set of emitters to the field) could be used to increase detection sensitivity of quantum effects in non-inertial scenarios.

The chapter is structured as follows: We start by presenting the Unruh-DeWitt detector model to characterize an atom coupled to a quantum field. Working in the interaction picture from the comoving atom reference frame, we show how to account for a uniform acceleration in the Hamiltonian. We then proceed to discuss the possible physical implementations in trapped ions and circuit QED. For both cases a model of emitters with controlled time-dependent atom-field couplings is presented, which, after some approximations, yields an identical Hamiltonian. For the sake of simplicity we will refer generically to single quantum emitters as "atoms", and the bosonic mode as "field", being the latter a phonon mode in a Coulomb crystal of trapped ions, or a photon mode confined in cavity in circuit QED. Then, as an illustrative example, we analyze the physics in the case of a single atom to predict the outcome of simple experimental realizations of our ideas. An analogy to a decoupling process is explained in terms of the well-known Landau-Zener formula. Some future research lines on the topic will naturally emerge from our discussion.

7.2 Accelerated Unruh DeWitt detectors

The Unruh-DeWitt detector [168,178,257] is a standard model for a two-level atom coupled to a scalar field. This kind of detectors has been extensively used for multiple purposes such as acknowledging acceleration effects in cavities, measuring quantum correlations between spatially separated regions of spacetime, detecting entanglement degradation due to the Unruh and Hawking effects and proposing set-ups to directly detect such effects. In general, computing time evolution under such a Hamiltonian is a complex problem, and thus, the affordable calculations reduce to very simple scenarios where perturbation theory to the first or second order is adequate.

On the other hand, special interest have the cases where the detectors couple only to a discrete number of modes. Presented in [253] and extended in [139] such settings directly model the interesting case of accelerated atoms going through a cavity. Moreover, they also feature a way to directly measure the Unruh effect considering cavities which are leaky to a finite number of modes [253].

Let us start by presenting the discretized Unruh-DeWitt interaction Hamiltonian consisting in a set of two-level atoms coupled to a scalar field. We assume a set of atoms that are

accelerating with proper acceleration a. From the atoms perspective the Hamiltonian can be rewritten as

$$H_{\mathrm{I}} = \sum_{jm} g_{jm}(\sigma_j^+ e^{i\Omega_j \tau} + \sigma_j^- e^{-i\Omega_j \tau}) \\ (a_m^\dagger e^{i[\omega_m t(\tau,\xi) - k_m x(\tau,\xi)]} + a_m e^{-i[\omega_m t(\tau,\xi) - k_m x(\tau,\xi)]}) \tag{7.2.1}$$

where (τ, ξ) are the proper space-time coordinates of the accelerated detectors, and (t, x) are Minkowskian coordinates. The following relation holds,

$$ct = \xi \sinh(a\tau/c)\,, \qquad x = \xi \cosh(a\tau/c)\,. \tag{7.2.2}$$

Directly from (7.2.2) we see that for constant ξ these coordinates describe hyperbolic trajectories in space-time whose asymptote is the light cone. A uniformly accelerated observer whose proper coordinates are (7.2.2), follows the trajectory of constant Rindler position $\xi = c^2/a$ [239].

If all the detectors follow such a trajectory we can rewrite the Hamiltonian in a form which is suitable to find quantum optical analogs,

$$H_{\mathrm{I}} = \sum_{jm} g_{jm}\left(\sigma_j^+ e^{i\Omega_j \tau} + \mathrm{H.c.}\right)\left(a_m^\dagger e^{i\Phi_m(\tau)} + \mathrm{H.c.}\right), \tag{7.2.3}$$

where τ is the atoms proper time, and

$$\Phi_m(\tau) = -k_m \xi e^{-a\tau/c} = -\frac{k_m c^2}{a} e^{-a\tau/c} = -\frac{\omega_m}{\alpha} e^{-\alpha\tau}, \tag{7.2.4}$$

where we have used the relation $\omega_m = ck_m$, and defined the parameter $\alpha = a/c$. Eq. (7.2.3) defines the Hamiltonian of interest that we aim to simulate. It also reproduces a scenario where an array of detectors are resisting near the event horizon of a Schwarzschild black hole, if we consider in (7.2.3) that $a \approx \kappa/\sqrt{f_0}$, where κ is the surface gravity of the black hole and f_0 is the gravitational redshift factor, following the arguments in [258].

7.3 Physical implementations. Trapped ions

This setup is ideally suited to prepare and measure quantum states by well established experimental techniques [202], which have found an important application in quantum simulation of many-body physics [259], and single particle dynamics in special relativity [196]. Previous proposals also allowed the simulation of quantum fields using trapped ions in general relativistic settings but in different contexts [260], however, paying the price of requiring control on the frequency of the qubit and the coupling strength. In our proposal, only phase

control is needed. Our setting is therefore readily exportable to other experimental set-ups, as shown below.

In our scheme we consider a chain of N ions of mass M. For simplicity, we focus on the single-mode version of (7.2.3), and consider that the bosonic mode is a phonon mode of the chain, namely, the center-of-mass mode which accounts to a homogeneous displacement of all the ions. State-of-the-art techniques may be used to implement phonon sidebands, and to control the atom-field coupling.

The vibrations of a Coulomb chain consists of a set of normal modes described by $H_0 = \sum_n \omega_n a_n^\dagger a_n$, with ω_n the normal mode frequencies, and a_n, $a_n^\dagger$, phonon operators. Levels $|0\rangle$ and $|1\rangle$ are two electronic states of the ions. Two sets of lasers couple those levels by means of Raman transitions, with amplitudes $\Omega_{\mathrm{L},j}$, and two frequencies $\omega_{\mathrm{L}_{1,2}}$, (see [202] for details),

$$H_{\mathrm{L}}(\tau) = \sum_{j,\nu=1,2} \frac{\Omega_{\mathrm{L},j}}{2} \sigma_j^+ e^{ik_{\mathrm{L}} x_j} e^{-i\omega_{\mathrm{L}_\nu}\tau - i\phi_\nu(\tau)} + \mathrm{H.c.}. \tag{7.3.1}$$

This equation represents a standard atom-light interaction term, with the only peculiarity that we consider time dependent phases $\phi_1(\tau)$, $\phi_2(\tau)$. x_j are operators corresponding to the ion displacements, relative to the equilibrium positions along the chain. We express those displacements in terms of phonon operators, $x_j = \sum_n \mathcal{M}_{j,n} \bar{x}_n (a_n + a_n^\dagger)$, where $\mathcal{M}_{j,n}$ are phonon wavefunctions, and $\bar{x}_n = 1/\sqrt{2M\omega_n}$.

We choose laser frequencies close to resonance with the center-of-mass mode, $n = 0$, such that $\omega_{\mathrm{L}_1} = -\omega_0 - \Omega$, $\omega_{\mathrm{L}_2} = \omega_0 - \Omega$, with $\Omega \ll \omega_0$. The coupling (7.3.1) simulates the quantum dynamics of an accelerated Unruh-DeWitt detector if: (i) $k\bar{x}_n \ll 1$ (Lamb-Dicke regime), such that we can expand the exponential in powers of δx_j, and restrict only to linear atom-field couplings. (ii) $\Omega_{\mathrm{L},j}/2 \ll \omega_0$, and $(\Omega_{\mathrm{L},j}/2)k\bar{x}_n \ll \omega_0, |\omega_0 - \omega_n| \neq 0$, so that we can neglect, in a rotating wave approximation (r.w.a.), all couplings to vibrational modes $n \neq 0$. This yields

$$H_{\mathrm{L}}(\tau) = \sum_j g_j \sigma_j^+ e^{i\Omega\tau} \left(a_0 e^{-i\phi_1(\tau)} + a_0^\dagger e^{-i\phi_2(\tau)}\right) + \mathrm{H.c.},$$

where we have used that the center-of-mass vibrational modes fulfills $\mathcal{M}_{j,0} = 1/\sqrt{N}$, such that $g_j = i\Omega_{\mathrm{L}_j} k\bar{x}_0/(2\sqrt{N})$. By choosing phases such that $\phi_1(\tau) = -\phi_2(\tau) = \Phi(\tau)$, we arrive at the single-mode version of Eq. (7.2.3). Including more modes would require additional lasers on resonance with other vibrational modes. Position depending couplings, g_j, and frequencies, Ω_j, may be achieved given a certain intensity profile of the lasers, and by focusing multiple lasers on each ion, respectively.

Typical experimental values are $\omega_0, |\omega_n - \omega_0| \approx 1$ MHz, and $k\bar{x}_0 \approx 0.2$, such that our requirements are fulfilled with values $\Omega_{\mathrm{L}}/2 = 100$ kHz, and $\Omega = 100$ kHz, yielding $g = 20/\sqrt{N}$

kHz. Those values are well above typical decoherence rates in trapped ions. Also, in order to observe analogs to acceleration, $\Phi(\tau)$ has to increase exponentially over a time-scale comparable to the inverse energies involved in the set-up. For example, values $\alpha = 10^{-3}\Omega = 0.1$ kHz, would require to vary the optical phase on times scales of 10 ms. This is technically feasible by using, for example, acousto-optical modulators, and standard experimental techniques from trapped ion quantum computation, which indeed require manipulation on a much shorter time-scale [202]. Our ideas may also be used with spin many-boson models as in [261].

7.4 Physical implementations. Circuit QED

Our second proposed implementation consists of a superconducting qubit coupled to a microwave cavity in the strong-coupling regime [254]. The interest of this kind of setups has been growing in the last years, with very interesting proposals to simulate other relativistic phenomena such as the Dynamical Cassimir effect in [56], or Hawking radiation [262]. In particular, a review on these vacuum amplification processes, and their possible realizations in superconducting circuit setups is to appear soon [263]. The simulation we propose here is different from those in the scenario studied, the kind of effects and the experimental idea behind, which in our case relies on the driving of the qubit frequency only, being particularly well suited [264]. The qubits and field noninteracting Hamiltonian is

$$H_0(\tau) = \omega_0 a^\dagger a + \frac{\epsilon}{2}\sum_j \sigma_{z,j} + H_{\rm d}(\tau), \tag{7.4.1}$$

where ω is the resonant frequency of the mode, and ϵ is the qubit energy. $H_{\rm d}(\tau)$ describes a driving field, for which we assume the following form,

$$H_{\rm d}(\tau) = -\sum_j \sum_{\nu=1,2} \eta_j\, \omega_{{\rm d}_{\nu,j}} \cos(\omega_{{\rm d}_{\nu,j}} t + \phi_\nu(\tau))\sigma_{z,j}. \tag{7.4.2}$$

Note that Eq. (7.4.2) is written as a periodic driving with a phase, $\phi_\nu(\tau)$, which can be considered to evolve slowly in time, in a sense to be quantified below. The qubit-cavity coupling in the Schrödinger picture is given by $H_{\rm I} = g_0\left(\sigma^+ + \sigma^-\right)\left(a + a^\dagger\right)$. We write the coupling in the interaction picture with respect to $H_0(\tau)$,

$$\begin{aligned} H_{\rm I}(\tau) &= g_0 \sum_j (\sigma_j^+ e^{i\epsilon\tau}\mathcal{G}_j(\tau) + {\rm H.c.})(a e^{-i\omega_0\tau} + {\rm H.c.}), \\ \mathcal{G}_j(\tau) &= e^{-2i\sum_\nu \eta \sin(\omega_{d_{\nu,j}}\tau + \phi_\nu(\tau))}, \end{aligned} \tag{7.4.3}$$

where we made the approximation that $\dot\phi(\tau)/\phi(\tau) \ll \omega_{{\rm d}_{\nu,j}}$. Consider now that $\eta \ll 1$, and the choice of frequencies $\omega_{{\rm d}_{1,j}} = \epsilon - \Omega_j - \omega_0$, $\omega_{{\rm d}_{2,j}} = \epsilon - \Omega_j + \omega_0$, and conditions

$\epsilon, \omega_0, |\epsilon - \omega_0| \gg g_0$. We expand $\mathcal{G}(\tau)$ to first order in η_j, and keep only slow-rotating terms in a r.w.a:

$$H_I(\tau) \approx \eta g_0 \sum_j \sigma_j^+ (e^{i\Omega_j \tau - i\phi_1(\tau)} a + e^{i\Omega_j \tau - i\phi_2(\tau)} a^\dagger) + \text{H.c.}.$$

This expression takes the form (7.2.3) by choosing $\phi_1(\tau) = \Phi(\tau)$, $\phi_2(\tau) = -\Phi(\tau)$, and $g_j = g_0 \eta_j$.

In circuit QED, the high energy scales ϵ, ω_0 are in the GHz regime. Low energy scales, such as g_j, Ω_j, may be then in the MHz range. Finally, note that $\dot{\phi}(\tau)/\phi(\tau) = \alpha$. Thus, in order to observe effects from effective acceleration, our scheme requires α on the frequency scale of g_j, Ω_j, such that the driving fields in (7.4.2) have to be controlled with an inverse time in the MHz range. This seems technically feasible, since this rate is slower than typical evolution times in circuit-QED systems. By using different photonic modes in a cavity, as well as local control of qubit couplings, the full multi-mode Hamiltonian (7.2.3) may be implemented.

7.5 Single detector case: non-adiabatic effects induced by acceleration

We will study a simple case with a two-folded purpose in mind: on the one hand it will serve to gain some insight on the parameters required for our experimental proposal while, on the other hand, it will unveil an analogy between non-equilibrium physics and quantum effects induced by acceleration. Let us consider a single atom A, with natural frequency Ω and uniform acceleration frequency $\alpha = a/c = f_a \Omega$, coupled to a single-mode field with proper frequency $\omega > \Omega$.

Let us have A excited at $\tau = 0$ with no excitations in the field. Representing the free eigenstates of atom (A) and field (F) with the notation $|\psi\rangle = |A\, F\rangle$, the initial state would then be $|i\rangle = |e\, 0\rangle$. We let the system evolve naturally and concentrate on the probability for A to decay to its ground state:

$$\mathcal{P}_{A_g}(\tau) = \sum_F |\langle g\, F|U(\tau)|e\, 0\rangle|^2. \tag{7.5.1}$$

It is convenient to analyze the phase in the Hamiltonian (7.2.3). The latter is equivalent to a Hamiltonian in the interaction picture with respect to a time dependent effective frequency

$$\omega_{\text{eff}}(\tau) = \partial_\tau \Phi(\tau) = \omega_0 e^{-\alpha\tau}, \tag{7.5.2}$$

which decreases asymptotically. We can therefore picture this situation as a system starting in a certain low energy state, in this case matching $|e\, 0\rangle$, coupled to a high energy state which

initially happens to be $|g\,1\rangle$. The difference between the two effective energies varies with time as

$$\Delta E_{\text{eff}}(\tau) = \omega_0 e^{-\alpha\tau} - \Omega, \tag{7.5.3}$$

and there will be a level crossing, corresponding to a stationary $\Phi(\tau)$, taking place at $\tau_c = \ln(\omega_0/\Omega)/\alpha$ After a long time (as compared to $1/\alpha$) we can obviously approximate the low

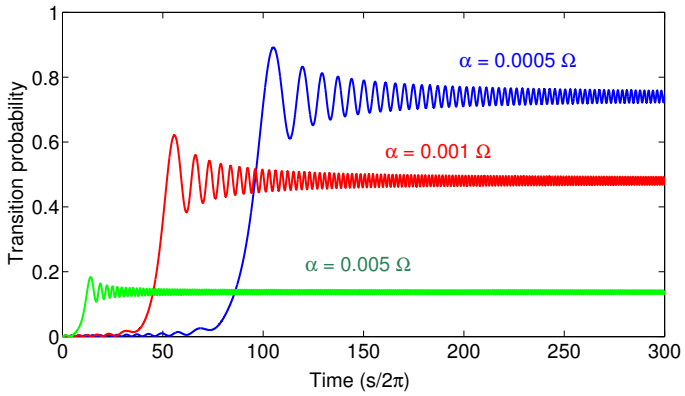

Figure 7.1: (Color online) Time evolution of $\mathcal{P}_{A_g}$ for different accelerations, with the parameter values $g = 0.01\Omega$ and $\omega_0 = 1.33\Omega$. The crossing time and the transition probability fit the Landau-Zener prediction described in (7.5.4).

energy level of the system as $|g\,1\rangle$, and the high as $|e\,0\rangle$ We can therefore establish an analogy between this kind of phenomenon and a typical Landau-Zener transition, making a link between non-equilibrium physics and quantum field theory in curved space-times. If the energy difference happens to vary very slowly (which will be the case if $\alpha \ll g$), we would expect no transition between eigenstates to take place, so the system will stay in the ground state, which means actually decaying into $|g\,1\rangle$. If however, the evolution happens to be diabatic, the probability of transiting into a high excited state (so to say, staying in $|e\,0\rangle$) can be approximated by the Landau-Zener formula:

$$\mathcal{P}_{A_{e(+\infty)}} \simeq e^{-2\pi\Gamma} \Rightarrow \mathcal{P}_{A_{g(+\infty)}} \simeq 1 - e^{-2\pi\Gamma}, \tag{7.5.4}$$

where $\Gamma = g^2/(\partial_\tau \Delta E|_{\tau=\tau_c})$. $\mathcal{P}_{A_g}$ is plotted in Fig. 7.1.

We note several differences with the original Landau-Zener model [265]. Namely, (7.5.3) is not linear but exponential in time; also, in our case, only for small couplings we have a two-level problem (a r.w.a. approximation cannot be performed). Nevertheless, in the regimes considered, L-Z is a very good approximation as shown in Fig. 7.2 The atom stays excited until the phase variation rate slows down at times close to τ_c. Around that moment

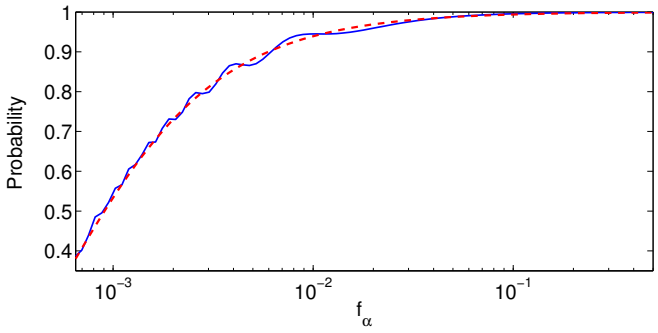

Figure 7.2: (Color online) Comparison between Landau-Zener theoretical prediction (red dashed) and probability for an accelerated detector of remaining in the excited state as a function of the acceleration $a = f_\alpha c\,\Omega$ (blue solid) with parameter values $g = 0.01\Omega$ and $\omega_0 = 1.33\Omega$.

the coupling terms get resonant and the decay probability grows notably. From then on atom and field get progressively decoupled again with the probability stabilizing itself.

7.6 Many emitters case

In this chapter we have given details regarding the single emitter case. However, the setting presented is readily extendible to more general and interesting cases: the Hamiltonian (7.2.1) can be simulated in a system of trapped ions taking into account that the number of qubits in our simulator should be equal or greater than the number simulated emitters.

With these experimental constructions we would be able to explore many-body collective phenomena (such as superradiance) which can amplify the effective coupling of a set of emitters to the field, effectively increasing the detection sensitivity of quantum effects in non-inertial scenarios: we can use these simulators to go beyond the computational limit of classical computers in order to explore collective phenomena that may amplify the relativistic effects imprinted in arrays of many-detectors undergoing relativistic motion, and use what we learn in the simulator to export it to direct detection of the Unruh and Hawking effects in both analog and real general relativistic settings.

To do that we depend on the current technology of quantum control of systems of many qubits and our ability to couple them to the same quantum field. In trapped ions, the required control of systems of more than 10 ions can be achieved with current technology [192]. Considering systems of more than 10 qubits is already way beyond the reach of standard classical computer clusters which have difficulties simulating systems of more than 5 emitters, this exemplifies the convenience of developing this kind of quantum simu-

lators.

7.7 Discussion

We have presented a scheme for simulating a set of accelerated atoms coupled to a single-mode field. First, we have identified the Hamiltonian which yields the evolution as seen by a comoving observer with the atoms. A method has been presented to obtain the same Hamiltonian for circuit QED and trapped ions by inducing time-dependent sidebands in atom-field couplings. Our idea may be extended to many-particle experiments which could simulate results that are not affordable for classical computers such as arbitrary non-inertial trajectories of detectors and many detectors coupled to quantum fields. Finally, by interpreting our results from a Landau-Zener perspective, we have made a new connection between non-equilibrium Physics and quantum effects due to acceleration. This highights an idea that will undoubtedly be exploited in the future, and which has already been explored in recent works [266] a context quite different to this one: general relativistic quantum effects can be studied with tools coming from non-equilibrium Physics.

Part II

Quantum Simulation Proposals

The Fermi problem and short-time detection with implications on how we understand causality

CHAPTER 8

Concepts

Felix, qui potuit rerum cognoscere causas

Publius Vergilius Maro, Virgil, *Georgics, 2-490*

Belief in the causal nexus is superstition.

Ludwig Wittgenstein, *Tractatus Logico-Philosophicus.*

8.1 Causality and Quantum Detection

Causality is a deeply rooted concept in everyone's life. It has, as usually happens to be the case with popular concepts, many more than just one definition. It is also a really important concept for philosophy and physics, and we thought it would be interesting to sketch some of the most important views on it in the following lines.

Commonly, we usually think of causality as the relationship existent between an event or set of events (cause) and a second event or set of events (effect) that happens as a consequence of the first. In that sense, it is also known as causation.

Cause is indeed a very fundamental concept in our mindsets. When we ask "why?" we are asking "what was the cause?". We understand the world in terms of causes and their effects. Causality has therefore been a major subject of study in Philosophy, stretching back out to Aristotle. Centuries later, David Hume made a very influential contribution by changing the focus of the study of causality from the description and classification of the types originally made by Aristotle to an analysis of the process by which we perceive causation. He concluded that the relationship between cause and effect could not perceived,

but rather was part of an inductive process of association. In simple words, we infer that an event B is caused by another event A when A comes before B and whenever A happens, so does B. Rather than real facts, causation nexi would be only stories that we humans tell ourselves to make sense of the world around us. Kuhn elaborated on these ideas and took the uncertainty in the causation inference to formulate his paradigm theory, where new precise observations might give rise to paradigm shifts.

The discussion here has been oversimplified for the sake of pragmatism, as other notions of causation or extended ideas of it also exist (e.g. soft probabilistic causation where an event A leads to an event B with a certain probability).

In any case, and no matter how controversial it can be, it is accepted by many scientists that causation is real and fundamental to the world (causal realism). Whether causation should or not be considered to be fundamental, what cannot be denied is that causal thinking is intrinsically related to our scientific understanding. And this is even more true for social sciences. For natural sciences, the laws of nature connect past and future in mostly deterministic ways [1], while for social sciences it holds on a softer ground. In any case, when a set of initial conditions evolves to a certain outcome, a causal relation is expected to be found. For social sciences, where one has not so much control over the variables of the experiment, it is usually observance of correlations what points out the existence of a causal nexus. But one has to be careful, because there might exist a common cause, therefore the saying "correlation does not imply causation".

The criticism to causal realism has never stopped from the philosophic frontlines. Bertrand Russell himself thought of it as a "relic of a bygone age" [2], an archaic concept that should be relinquished from modern science [267].

That criticism is well posed, as for natural sciences, the basis descriptions are more structural than dispositional, i.e. describe functional relations rather than a cascade of necessary events (e.g. Back-action is a well known feature of some theories and mixes the ideas of cause and effect). It that sense there is a separate approach of scientific realism where the causal relations are not as important as the structure of the theory, which is assumed to be

[1] We are not being rigurous here. For the case of Quantum Mechanics determinism is only the case when observer and system are treated as a whole and therefore no measurement problem appears. Otherwise the description would be probabilistic but even in that case the probabilities would be determined by the state and would not take just random values, and predictions can be made on averages. Chaos theory also has implications. Although chaos does not contradict determinism, it is true that the extreme sensitivity to initial conditions poses, under certain assumptions, difficulties at the time of predicting the outcome of an experiment where chaos takes part.

[2] *The law of causality, I believe, like much that passes muster among philosophers, is a relic of a bygone age, surviving, like the monarchy, only because it is erroneously supposed to do no harm.*

referring to a real underlying structure (ontic structural realism) [268].

Anyhow, after this small digression let us come back to our matter of interest. What physicists understand by causality is seldom interpreted as causation, but rather as what is called "relativistic causality", a concept that relates intimately to the former. As we know from special relativity, given two events A and B, with B laying inside the light cone of A, an absolute time order exists between them, either in all reference systems A came before B (so it is in principle possible for A to have caused B) , or B before A (conversely, B may have caused A).

But that order does not exist if A and B are spacelike separated (B is out of the lightcone of A and viceversa). If that is the case, A and B are said to be causally disconnected. For some reference systems A took place before B, for some others B came before. It is not possible therefore to assume a causal connection between A and B in any typical sense. More precisely, event $A(B)$ cannot have had a causal influence on event $B(A)$, they are "causally shielded" from one another.

In Quantum Field theory that feature is manifest through the microcausality property.

8.1.1 Causality in Quantum Mechanics and Quantum Field Theory

Microcausality

The fact that actions on a spacetime point A cannot have any measurable effect at any other point B out of its lightcone (also known as no-signalling), can be seen as a consequence of the microcausality property, which states that the (anti)commutator of local observable operators $\mathcal{O}_1$ and $\mathcal{O}_2$ acting and evaluated at spacelike separated points, vanishes [269]:

$$[\mathcal{O}_1(x), \mathcal{O}_2(y)]_{(+)} = 0, \text{ if } (x-y)^2 < 0 \tag{8.1.1}$$

Where, of course, x, y, are four-vectors. Microcausality appears "naturally" after canonically quantizing a Lorentz invariant classic field equation [3] but is also an axiom used in the construction of Algebraic Quantum Field Theory [269]. As stated, it is sufficient for no-signaling. Any action at a point x (modelled as the action of local operators), would have no measurable effect in y (nothing that could be detected through measurements recurring to local operators).

We must be careful here. In the paragraph above we have implicitly assumed that having "causal influence" implies having a measurable influence, but what about having a non-measurable influence? As a matter of fact relativity does not prohibit that, on the contrary,

[3] The question is actually quite subtle, for more details check [270]

it allows for the existence of correlations.

In particular, in constructive derivations following canonical quantization techniques, Eq. (8.1.1) is usually obtained for fields as:

$$[\phi(x), \phi(y)]_{(+)} = 0, \text{ if } (x-y)^2 < 0. \tag{8.1.2}$$

Fields at causally-separated points can be used within a single framework for computational purposes. The measurement of one is not intrinsically dependent upon the other but however "correlations" might still exist between measurements, and again, the existence of correlations between space-like separated points does not imply the possibility of producing detectable effects at other points through any sort of pre-determined faster-than-light action. A detailed derivation that faster-than-light communication cannot be established within the framework of QFT can be seen in [29].

Feynman Propagator and Virtual Particles

The existent correlations between spacelike points are encoded in the field propagators. In particular, it is well known that the Feynman propagator D_F [271], which is proportional to the probability amplitude to emit a photon at one location and annihilate it at another location, takes a non-zero value outside of the forward light cone, which seems to collide with causal intuition.

But the truth is that causality arguments cannot be formulated along so simple lines, the actual picture, is much more complicated than such a naïve description. As a matter of fact we must take into account that such a photon, emitted in a point x, is mathematically described as a plane wave of defined momentum, and therefore spreads everywhere in space. In that sense it is not surprising that its absorption anywhere else gives a non-zero contribution. In fact the points x do not correspond to photon positions, they only label the field amplitude in space. For good reasons, position - an operator in NRQM - is demoted to a mere label in QFT. Also, to confort the confused reader a virtual particle view can be called upon. The particles produced and emitted described in the propagator can be virtual and therefore no issue arises.

What has to be clear is that a nonzero time-ordered product for spacelike-separated fields just measures the probability amplitude for the existence of a nonlocal correlation in these quantum vacuum fluctuations, analogous to an EPR correlation. Let us remind also that the propagator is often called two-point correlation function.

This causality issue, first noted by Feynman, has been addresed extensively in the literature starting with Feynman himself [272, 273], Fermi [8] and later Hegerfeldt [274] and

many others [33–35, 275] . Much of this discussion concentrates on the rather well-known Fermi Problem.

8.2 The Fermi Problem

Although we will talk extensively about this problem in much more detail in the following chapter, it is worth discussing it briefly here. Originally proposed by Fermi, it is a thought experiment to check for causality at a microscopic level and has been a constant subject of theoretical debate and discussions during the last few decades.

Fermi [8] considered two two-level neutral atoms A, B, coupled to the electromagnetic field. At $t = 0$, atom A is in its excited state and atom B in its ground state, with no photons present. If A and B are separated by a distance r and v is the speed of light, can A excite B at times $t < r/v$?

The question is quite subtle and we will discuss later how it should be mathematically formulated. Let us here just simply say that it seems natural to expect the probability of excitation for B to be 0 for $t < r/v$. That is in fact what Fermi obtained, although he did so by making an additional assumption, extending the domain of a frequency integration to include negative frequencies as well. Shirokov, however, showed that the result is non-causal, and the causal probability was found by Fermi and others only due to this approximation [31]. Years later, the works of Hegerfeld, Yngvason and others [32–35], clarified that in previous works the final state had not been properly selected and in fact, when the transition probability is properly calculated, it is indeed causal, but only in the sense that it is independent of atom A for $t < R/v$.

Although the problem seems to be pretty simple, its experimental realization has not been achieved yet. In this thesis, we have tried to investigate the causality issue in the context of quantum detection by proposing a feasible experimental test of a 1-D version of the Fermi problem using superconducting qubits. We give an explicit non-perturbative proof of strict causality in this model, showing that the probability of excitation of a two-level artificial atom with a dipolar coupling to a quantum field is completely independent of the other qubit until signals from it may arrive. On top of that we relate this result with previous works which were used to claim apparent causality problems for Fermi's two-atom system and explain in detail why everything is in perfect agreement with the existence of nonlocal correlations.

8.3 Short time behaviour of detectors

While studying the Fermi problem, we devoted quite some time working beyond the Rotating Wave Approximation. Basically, for our Fermi problem proposal, in order to obtain measurable signatures of the expected behavior, we needed to work in an experimental regime where the RWA would no longer be valid. In this case we where working with ultra strong couplings (with an adimensional coupling parameter λ such that $0.1 \lesssim \lambda < 1$)

Following a similar derivation as in [35] we developed a formalism in perturbation theory, that would allow us to work beyond RWA for short times and calculate all the quantities needed for the study of the Fermi problem.

Inspired by those calculations we thought that it would be interesting to use this tool to study the behavior of detectors for short times (as compared to the interaction strength of their coupling to the field) trying to tie it to the event that they intend to detect (in our case, the decay of a photon source). More concretely, we proposed a thought experiment to study the information provided by a detector click about the state of an initially excited two-level system. By computing the time evolution of the corresponding conditioned probability beyond the rotating wave approximation, we showed that a click in the detector is related with the decay of the source only for long times of interaction. For short times, the non-rotating wave approximation effects like self-excitations of the detector forbid a naive interpretation of the detector readings.

CHAPTER 9

The Fermi Problem with Artificial Atoms in Circuit QED

9.1 Introduction

Information cannot travel faster than light. But in quantum theory, correlations may be established between spacelike separated events. These facts are not contradictory, since correlations need to be assisted with classical communication in order to transmit information.

The two physical phenomena above arise in a natural fashion in the following situation, which is the so-called Fermi problem [8], originally proposed by Fermi to check causality at the microscopic level. At $t = 0$ a two-level neutral atom A is in its excited state and a two-level neutral atom B in its ground state, with no photons present. If A and B are separated by a distance r and v is the speed of light, can A excite B at times $t < r/v$? Fermi 's answer was negative but his argument had a mathematical flaw. When a proper analysis is carried on, fundamental quantum theory questions arise due to the interplay between causal signaling and quantum non-local phenomena.

These issues led to a controversy [33,35,274,276] on the causal behavior of the excitation probability of qubit B, whose conclusions were never put to experimental test. A notorious claim on causality problems in Fermi's two-atom system was given in [274]. The reply of [33] was in the abstract language of algebraic field theory and the proof of strict causality of [35] is perturbative, although given to all orders in perturbation theory. The Fermi problem is usually regarded just as a gedanken experiment, and remains untested, essentially because interactions between real atoms cannot be switched on and off.

In this chapter we give a complete description of the problem in a physical framework in which predictions can be verified. This framework will be circuit QED which can be regarded as a 1-D version of Quantum Electrodynamics (QED) with two-level (artificial)

atoms, a testbed which makes it possible to control the interaction and tune the physical parameters. We complete previous descriptions made of the problem and explain how there are no real causality issues for Fermi's two-atom system. We give an explicit non-perturbative proof of strict causality in these setups, showing that the probability of excitation of qubit B is completely independent of qubit A for times $t < r/v$ and for arbitrary initial states. As a matter of fact, this comes as a manifestation of the nonsignaling character of the quantum theory [277]. We also show how this is compatible with the existence of nonlocal correlations at times $0 < t < r/v$, a fact pointed out in various theoretical proposals to entangle qubits at arbitrarily short times [41, 44, 275, 278]. More precisely, we give a non-perturbative proof of the fact that the probability of B being excited and A in the ground state is finite and r-dependent at any time, even for $t < r/v$. We provide also a physical and intuitive explanation of why the conclusions in [274], even if mathematically sound, do not apply to the causality problem. At the end we discuss the time dependence predicted in our model for the various excitation probabilities and suggest a feasible experimental test of causality using superconducting circuits.

9.2 Mathematical Formulation

In what follows we focus on a practical setup of circuit-QED, with two qubits, A and B, interacting via a quantum field. The qubits have two stationary states $|e\rangle$ and $|g\rangle$ separated by an energy $\hbar\Omega$ and interact with a one-dimensional field, $V(x)$, which propagates along a one-dimensional microwave guide that connects them

$$V(x) = i \int_{-\infty}^{\infty} dk \, \sqrt{N\omega_k} \, e^{ikx} a_k + \text{H.c.} \tag{9.2.1}$$

This field has a continuum of Fock operators $[a_k, a_{k'}^\dagger] = \delta(k - k')$, and a linear spectrum, $\omega_k = v|k|$, where v is the propagation velocity of the field. The normalization and the speed of photons, $v = (cl)^{-1/2}$, depend on the microscopic details such as the capacitance and inductance per unit length, c and l. We will assume qubits that are much smaller than the relevant wavelengths, $\lambda = v/\Omega$, and are well separated. Under these conditions the Hamiltonian, $H = H_0 + H_I$, splits into a free part for the qubits and the field

$$H_0 = \frac{1}{2}\hbar\Omega(\sigma_A^z + \sigma_B^z) + \int_{-\infty}^{\infty} dk \, \hbar\omega_k a_k^\dagger a_k \tag{9.2.2}$$

and a point-like interaction between them

$$H_I = \sum_{J=A,B} d_J \, \sigma_J^x \, V(x_J) \tag{9.2.3}$$

Here x_A and x_B are the fixed positions of the atoms, and $d_J\,\sigma_J^x$ is equivalent to the dipole moment in the case of atoms interacting with the electromagnetic field.

The original formulation of the Fermi problem begins with an initial state

$$|in\rangle = |e_A\, g_B\, 0\rangle \tag{9.2.4}$$

in which only qubit A has been excited, while B and the field remain in their ground and vacuum states, respectively. The total probability of excitation of qubit J is the expectation value of the projector onto the excited state $\mathcal{P}_J^e = |e_J\rangle\langle e_J|$. In the Heisenberg picture

$$P_{eJ} = \langle in|\,\mathcal{P}_J^e(t)\,|in\rangle\,, \quad J \in \{A, B\}. \tag{9.2.5}$$

9.3 Proof of Causality

We will prove that for $vt < r$ the probability P_{eB} is *completely independent of the state of qubit A for all initial states.* In the Heisenberg picture this amounts to showing that there appears no observable of A in the projector $\mathcal{P}_B^e(t)$ for $vt < r$. Our proof begins by solving formally the Heisenberg equations for $\mathcal{P}_J^e$

$$\mathcal{P}_J^e(t) - \mathcal{P}_J^e(0) = -\frac{d_J}{\hbar}\int_0^t dt' \sigma_J^y(t') V(x_J, t'). \tag{9.3.1}$$

Integrating the Heisenberg equations of the operators a_k and $a_k^\dagger$ and inserting them in Eq. (9.2.1), the total field evaluated at x in Heisenberg picture is decomposed

$$V(x,t) = V_0(x,t) + V_A(x,t) + V_B(x,t) \tag{9.3.2}$$

into the homogenous part of the field

$$V_0(x,t) = i\int_{-\infty}^{\infty} dk\,\sqrt{N\omega_k}\,e^{i(kx-\omega t)}a_k + \text{H.c.} \tag{9.3.3}$$

and the back-action of A and B onto the field

$$\begin{aligned} V_J(x,t) &= \frac{-id_J\,N}{\hbar}\times \\ &\times\int_0^t \sigma_J^x(t')\int_{-\infty}^{\infty}\omega_k e^{ik(x-x_J)-i\omega_k\,(t-t')}dkdt' + \text{H.c.} \end{aligned} \tag{9.3.4}$$

Eqs. (9.3.1) translates into a similar decomposition for the probabilty $\mathcal{P}_B^e$ with three terms

$$\mathcal{P}_B^e(t) = \mathcal{P}_{B0}^e(t) + \mathcal{P}_{BB}^e(t) + \mathcal{P}_{BA}^e(t) \tag{9.3.5}$$

which are proportional to V_0, V_B and V_A, respectively. The only explicit dependence on A may come from $\mathcal{P}^e_{BA}$ through $V_A(x_B,t)$. Manipulating Eq. (9.3.4) gives

$$V_A(x_B,t) = \frac{-2\pi d_A N}{\hbar}\frac{d}{dr}\left[\sigma^x_A\left(t-\frac{r}{v}\right)\,\theta\left(t-\frac{r}{v}\right)\right] \tag{9.3.6}$$

where the Heaviside function θ shows that strictly $\mathcal{P}^e_{BA}(x_B,t)=0$ for $vt<r$, and no such dependence is possible. We still have to analyze a possible implicit dependence on A through $\mathcal{P}^e_{BB}$, whose expression is

$$\begin{aligned}\mathcal{P}^e_{BB}(t) &= \frac{id_B^2 N}{\hbar^2}\int_0^t dt'\int_0^{t'} dt''\sigma^y_B(t')\sigma^x_B(t'')\\ &\int_{-\infty}^{\infty} dk\,\omega_k e^{-i\,\omega_k(t'-t'')} + \text{H.c.}\end{aligned} \tag{9.3.7}$$

The only implicit dependence could come through the evolution of $\sigma^{x,y}_B(t)$, but again this is not the case. Since $[\sigma^x_B, H_I]=0$, the evolution of σ^x_B does not involve the field in any way, and for $\sigma^y_B(t)$ we have that $\dot{\sigma}^y_B(t) = \Omega\,\sigma^x_B(t)/2 - \frac{d_B}{\hbar}V(x_B,t)\sigma^z_B(t)$ so using again Eq. (9.3.2) and Eq. (9.3.6) we see that the A-dependent part of P^e_{BB} is 0 for $vt<r$. Thus $\mathcal{P}^e_B$ may be finite but is completely independent of qubit A for $vt<r$, as we wanted to show.

So far, we have demonstrated that although $P^e_B(t)$ is non-zero for $vt<r$, the only non-zero contribution is $\mathcal{P}^e_{B0}$, which is not sensitive to the qubit A and thus cannot be used to transmit information between the qubits. Now we will show that this result is compatible with the existence of correlations for $vt<r$. For instance, we consider the probability of finding qubit B excited and qubit A on the ground state $P_{eB,gA}$, which is:

$$P_{eB,gA} = \langle in|\,\mathcal{P}^e_B(t)\mathcal{P}^g_A(t)\,|in\rangle\,, \tag{9.3.8}$$

where $\mathcal{P}^g_A = \mathbb{1}-\mathcal{P}^e_A$. Using Eqs. (9.3.1), (9.3.2) and (9.3.5), we find a term in this probability which is proportional to $\mathcal{P}^e_{BB}\,\mathcal{P}^g_{AA}$ and thus to $V_B(x_B,t)\,V_A(x_A,t)$. From Eq. (9.3.4) we obtain: $V_J(x_J,t)\propto\frac{d}{dt}\{\sigma^x_J(t)\theta(t)\}$. Therefore, we conclude that in (9.3.8) there is an unavoidable dependence on A at any $t>0$, but this is not a causality violation because correlations alone cannot transmit information.

At this point it remains a single question: How can the A-dependent part of P_{eB} be zero while the one of $P_{eB,gA}$ is nonzero for $vt<r$? To better understand it we need less formal results that rely on perturbative expansions, but we would like to remark here that the conclusions above are valid to all orders in perturbation theory.

9.4 Probability of excitation

To obtain the total probability of excitation of qubit B P_{eB} to a given order in perturbation theory, one has to expand to a certain order the operators appearing in Eqs. (9.3.1), (9.3.2),

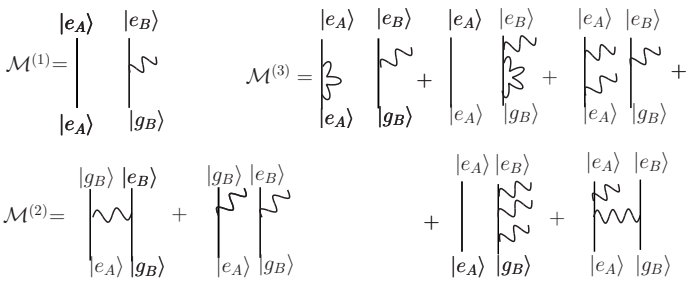

Figure 9.1: The terms of order d_J, d_J^2 and d_J^3 contributing to the amplitude for exciting qubit B.

(9.3.4). The different terms in the expansion can be related to the probabilities of the different physical processes involved. Fig. 9.1 shows the diagrams of the different amplitudes contributing to P_{eB} up to the fourth order in d_J. The lowest order amplitude contributing to a final excited B qubit is of order d_J, which means that terms up to order d_J^3 have to be considered. The only terms leading to this final state will be $\mathcal{M}^{(1)} = v_B$, $\mathcal{M}^{(2)} = x + u_A\, v_B$, $\mathcal{M}^{(3)} = a' v_B + u_A v_A v_B + v_B u_B v_B + \delta\mathcal{M}^{(3)}$ where u_J (v_J) represent the amplitude for single photon emission at qubit J when the qubit is initially in the ground (excited) state, x is the amplitude for photon exchange, a_J are the radiative corrections of qubit J, and finally $\delta\mathcal{M}^{(3)}$ is the amplitude for photon exchange accompanied by a single photon emission at qubit A. Notice that some of these processes are only possible beyond the rotating wave approximation, which breaks down for strongly coupled circuit-QED setups [279] as the ones considered later. Keeping only terms up to fourth order, we have for the probability to get B excited at a time t

$$\begin{aligned} P_{eB}(t) &= |\mathcal{M}^{(1)}|^2 + |\mathcal{M}^{(2)}|^2 + 2\,Re\{\mathcal{M}^{(1)^*}\mathcal{M}^{(2)}\} \\ &+ 2\,Re\{\mathcal{M}^{(1)^*}\mathcal{M}^{(3)}\} + \mathcal{O}(d^5) \end{aligned} \tag{9.4.1}$$

The final states in $\mathcal{M}^{(1)}$ are orthogonal to those in $\mathcal{M}^{(2)}$ and to the three photon terms in $\mathcal{M}^{(3)}$. Hence, their interference vanishes. Besides, we are only interested in the A-dependent part of the probability, so we can remove the r-independent terms left in (9.4.1), marking the remaining contributions with a superscript $^{(r)}$

$$P_{eB}^{(r)}(t) = |\mathcal{M}^{(2)}|^{2^{(r)}} + 2Re\{\mathcal{M}^{(1)^*}\delta\mathcal{M}^{(3)}\} + \mathcal{O}(d^5). \tag{9.4.2}$$

The first term actually gives $P_{eB,gA}$ up to the fourth order, it is positive and A-dependent at all times, as shown in Fig. 9.2a. The second term is not a projector onto any physical state, but an interference term which has the effect of canceling out exactly the first term for $vt < r$ but not for $vt > r$ (cf. Fig. 9.2b). In a nutshell, interference seems to be the physical

mechanism that operates at all orders in perturbation theory to give the causal behavior of the total probability of excitation that we had previously shown.

These perturbative results cast new light on the controversy on the Fermi problem and help us understand *why* our results do not contradict those of Hegerfeldt [274]. Hegerfeldt proved mathematically that the expectation value of an operator consisting of a sum of projectors cannot be zero for all the times $vt < r$, unless it is zero at any time. Indeed, the expectation value of $\mathcal{P}^e_B(t)$ cannot be zero for all $vt < r$, for it always contains the contribution $\mathcal{P}^e_{B0}$ from Eq. (9.3.3). However, as we showed non-perturbatively, the actual relevant question for causality is whether the expectation value of $\mathcal{P}^e_{BA}(t)$ vanishes for $vt < r$ or not, since only this part of the probability is sensitive to qubit A and could be used to transmit information. Besides, according to our above perturbative results to fourth order, the r-dependent part of the probability, that is the expectation value of $\mathcal{P}^e_{BA}(t)$, is not a mere sum of projectors, but also contains interfering terms. Thus, Hegerfeldt's result does not apply and $\mathcal{P}^e_{BA}(t)$ can be zero for $vt < r$ as is actually the case. Both results are in accord with a general fact of Relativistic Quantum Field Theory: two global states can not be distinguished locally with the aid of a local projector annihilating one of the states, since the local observable algebras are Type III von Neumann algebras (See [33, 276] for a discussion).

9.5 Experimental proposal

We will now suggest an experiment to check the causal behavior of P_{eB}. For this we need to control the interaction time at will to access the regions at both sides of $t = r/v$. This, which is highly unrealistic with real atoms, becomes feasible in circuit-QED. While the ideas are valid for both inductive and capacitive couplings, we will focus on using a pair of three-junction flux qubits [280, 281]. Each of the qubits is governed by the Hamiltonian $H_{0J} = \frac{1}{2}\epsilon_J\sigma^z_J + \frac{1}{2}\Delta_J\sigma^x_J$. The energy $\epsilon_J = 2I_p\delta\Phi_{xJ}$, is approximately linear in the external magnetic flux, $\delta\Phi_{xJ}$, measured from the degeneracy point, and we assume that the gap Δ_J is fixed. The result is a qubit energy difference $\Omega_J(\delta\Phi_{xJ}) = \sqrt{(2\,I_p\,\delta\Phi_{xJ})^2 + \Delta_J^2}$.

The coupling between the qubit and the microwave photons is ruled by the dimensionless ratio

$$K_J = \frac{4d_J^2 N}{\hbar^2 v} = 2\,(g/\Omega_J)^2\,. \tag{9.5.1}$$

Here $g = d_J\sqrt{N\Omega}/\hbar$ is the coupling strength between a qubit and the cavity that would be obtained by cutting the transmission line to be perfectly resonant with the qubit transition. These numbers enter the qubit excitation probability computed before (9.4.2) through the product $P^{(r)}_{eB}(t) \propto K_A K_B$. Since $K_J \propto 1/\Omega_J$, we may use the external fluxes to move from

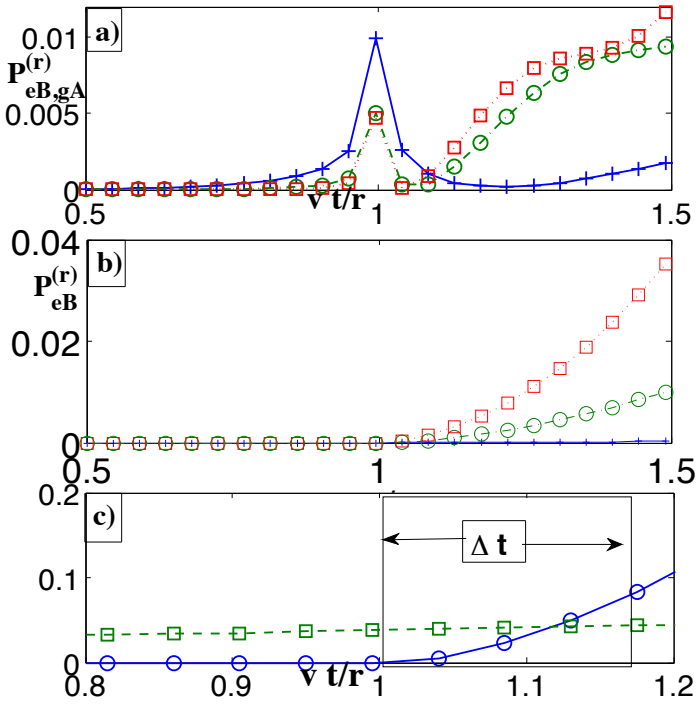

Figure 9.2: (a) $P^{(r)}_{eB,gA}$ and (b) $P^{(r)}_{eB}$ versus vt/r for $\Omega r/v = \frac{\pi}{2}$ (blue, crosses), π (red, squares), and 2π (green, circles) with $K_{A,B} = 0.0225$. For $vt < r$ the qubits are spacelike separated, but there are correlations between them and figure (b) shows the expected causal behavior. (c) $P^{(r)}_{eB}$ (blue, circles) and $|\mathcal{M}^{(1)}|^2$ (green, squares) vs. vt/r for $K_A = 0.20$, $K_B = 0.04$ and a separation of one wavelength $r = 2\pi v/\Omega_{A,B}$. With this data and $\Omega/2\pi \simeq 1$GHz we have $\Delta t \simeq 1$ns. (Color online)

a weakly coupled regime with no qubit excitations, $\Omega_J \ll g$, to the maximum coupling strength, $\Omega_J \simeq \Delta_J$ ($\delta\Phi_{xJ} = 0$).

Let us first discuss how to prepare the initial state (9.2.4) of the Fermi problem. We assume that the system starts in a ground state of the form $|g_A\, g_B\, 0\rangle$. This is achieved cooling with a large negative value of $\delta\Phi_{xJ}$ on both qubits, which ensures a small value of g/Ω_J and K_J. We estimate that couplings $g/\Omega_J < 0.15$ and $\Omega_J \sim 1.5$GHz lower the probability of finding photons in the initial state below 5×10^{-3}, both for vacuum and thermal excitations. Both magnetic fluxes are then raised up linearly in time, $\delta\Phi_{xJ} = \alpha_J t$, to prepare the qubits. Using a Landau-Zener analysis [265] of the process we conclude that an adiabatic ramp $\alpha_B \ll \pi\Delta_B^2/4\hbar I_p$ of qubit B followed by a diabatic ramp [56,57] $\alpha_A \gg \Delta_A^2/\hbar 2I_p$ of qubit A, leads to the desired state $|e_A\, g_B\, 0\rangle$ with a fidelity that can be close to 1, depending only of α_A, α_B as derived from the Landau-Zener formula. Note that the minimum gap Δ_B has to be large enough to ensure that the qubit-line coupling of B remains weak and the qubit does not "dress" the field with photons.

Once we have the initial state, both magnetic fluxes must take a constant value during the desired interaction time. After that, measurements of the probability of excitation of qubit B can be performed with a pulsed DC-SQUID scheme [219, 282]. The timescale of the "jump" of the probability around $t = r/v$ for qubit frequencies in the range of GHz and a separation of one wavelength $r = 2\pi v/\Omega$ is $\Delta t \simeq 1$ns [Fig. 9.2c]. Although the total measurement of the SQUID may take a few μs, the crucial part is the activation pulse (~ 15ns) in which the SQUID approaches its critical current and may switch depending on the qubit state. During this activation period the SQUID and the qubit are very strongly coupled ($g \sim$ GHz), [282] and the qubit is effectively frozen. The time resolution of the measurement is thus determined by the ramp time of the activation pulse, which may be below nanoseconds. Among the sources of noise that are expected, the short duration of the experiment, well below T_1 and T_2 of usual qubits, makes the ambient noise and decoherence pretty much irrelevant. Thermal excitations of the qubits and the line may be strongly suppressed by using larger frequencies (> 1.5GHz). The most challenging aspect is the low accuracy of SQUID measurements, which are stochastic, have moderate visibilities [282] and will demand a large and careful statistics.

On the technical side, it is important to choose carefully the coupling regimes. If we wish to compare with perturbation theory, we need $K_J \ll 1$. However, at the same time the product $K_A K_B$ must take sizable values for $P_{eB} \propto K_A K_B$ to be large. And we need to discriminate the causal signal from the r-independent background of the probability of excitation, whose main contribution is $|\mathcal{M}^{(1)}|^2 \propto K_B$. Thus, a good strategy would be to work with $K_A > K_B$. In Fig. 9.2c we show that it is possible to achieve a regime in which the perturbative approximations are still valid and the r-dependent part of P_{eB} is comparable to $|\mathcal{M}^{(1)}|^2$ in the spacetime region of interest $vt \simeq r$.

9.6 Discussion

To conclude, we have considered a system of two superconducting qubits coupled to a transmission line, which can be suitably described in the framework of 1-D QED with two-level (artificial) atoms. Starting from an initial state with qubit A excited, qubit B in the ground state and no photons, we have illustrated the causal character of the model showing that the probability of excitation of qubit B is completely independent of qubit A when $vt < r$. We have also shown that this is in agreement with the existence of nonlocal correlations and we have used perturbative computations to see the physical mechanism underlying the causal behavior. Finally, we have suggested an experiment feasible with current technology that

would solve the controversy on the Fermi problem.

CHAPTER 10

Short-Time Quantum Detection: Probing Quantum Fluctuations

10.1 Introduction

Quantum detection theory was created to study the behavior of detectors in presence of radiation [283]. Highly satisfactory up to date, it relies on the conspicuous rotating wave approximation (RWA), which neglects the so-called counterrotating terms. These terms give important contributions for strong atom-field couplings and very short times as compared to the system time-scale, meaning that for any effect beyond RWA (bRWA) to be directly acknowledged, our measurements must be very precise and fast. This is problematic for Quantum Optics experiments, due to the very small matter-radiation coupling and the fact that observation times must be at the femtosecond scale for most cases (nanosecond for hyperfine qubits), which is too small for current experiments ($\sim \mu s$ for trapped ions [202]).

However, cQED (cQED) [211] provides a framework in which those phenomena are accessible to study. By using superconducting qubits coupled to a transmission line, the set-up behaves analogously to a 1-D radiation-matter interaction model at the microwave frequency range [210]. Moreover, parameters can be easily tuned, and the qubit-line coupling modulated up to ultrastrong levels [279, 284]. Fast qubit state readout ($\sim ns$) is also possible using a pulsed DC-SQUID scheme [282]. Thus, phenomena bRWA have already been reported [285, 286], Glauber's theory is no longer valid and quantum detectors should be described by a non-RWA model like that of [54].

A direct consequence of the breakdown of the RWA is that a detector in its ground state interacting with the vacuum of the field has a certain probability of getting excited and emitting a photon. There is however not a widespread consensus on the physical reality of this effect. As a matter of fact, there have been attempts of suggesting effective detector models

by imposing this phenomenon to be impossible [287]. We should however recall here that these peculiar effects should not be that discomforting, as the initial state considered is not an eigenstate of the full Hamiltonian bRWA.

To describe those processes we will neither impose any additional constraints nor question their real existence. We will study the following setup: a source S initially excited, a detector D initially in the ground state and both interacting with the electromagnetic field in its vacuum state. If the detector clicks at a given time, does it mean that the source is now in the ground state? This problem amounts to compute the probability of decay for the source, conditioned to the excitation of the detector. We will show that, unlike Glauber's RWA detector, in which this conditioned probability would be equal to 1 at any time, this cQED detector only achieves this value at long times due to the impact of non-RWA effects.

10.2 Mathematical description of the model

We consider a model consisting of two superconducting qubits, S and D, with two levels g and e and separated a distance r. Let us consider that at $t = 0$ S is excited, D is in its ground state and there are no excitations in the transmission line, which will be open, enabling a continuum of modes. Representing the states in terms of qubits and field (F) free eigenstates with the notation $|\psi\rangle = |SDF\rangle$, the initial state would be $|i\rangle_{t=0} = |eg0\rangle$. We intend to study the relevance of bRWA processes by quantifying what information about the state of S can be extracted by knowing qubit D state after a certain time t. For that we will compute the probability $\mathcal{P}_{S_g/D_e}(t)$ of S to have decayed at a certain instant t conditioned we have measured D excited at that moment:

$$\mathcal{P}_{S_g/D_e}(t) = \frac{\mathcal{P}_{[ge*]}}{\mathcal{P}_{[*e*]}} = \frac{\sum_F |\langle geF|e^{-iHt/\hbar}|eg0\rangle|^2}{\sum_{n,F} |\langle neF|e^{-iHt/\hbar}|eg0\rangle|^2}. \tag{10.2.1}$$

$\mathcal{P}_{[ge*]}$ being the probability of having S in the ground state and D excited and $\mathcal{P}_{[*e*]}$ the total probability of excitation of D.

Naively we would expect that $\mathcal{P}_{[*e*]}(t) = 0 \quad \forall t \leq R/c$ and that $\mathcal{P}_{[*e*]}(t) = \mathcal{P}_{[ge*]}(t) \neq 0 \quad \forall t \geq R/c$, so $\mathcal{P}_{S_g/D_e} = 1$. However, in [32] it is shown that $\mathcal{P}_{D_e}(t) \geq 0 \quad \forall t \leq R/c$. As explained in [34, 36], we can split the probability of detector excitation as:

$$\mathcal{P}_{[*e*]}(t) = \mathcal{P}^{(0)}_{[*e*]}(t) + \mathcal{P}^{(R)}_{[*e*]}(t) \tag{10.2.2}$$

The first term, independent of R (and so of S), is the self-excitation term, and so $\mathcal{P}^{(0)}_{[*e*]}(t) \geq 0 \quad \forall t \leq R/c$. The second, dependent on R, refers to excitations due to exchange processes, and behaves causally $\mathcal{P}^{(R)}_{[*e*]}(t) = 0 \quad \forall t \leq R/c$.

One might expect that the effects of $\mathcal{P}^{(0)}_{[*e*]}(t)$ could be accounted by including a sort of "dark current" due to *self-excitations* as compared to the *exchange processes* that would be the only ones to appear if we were thinking naively. In that sense, the analysis here presented might look somehow contrived; however, the very notion of dark current is not valid for short times. The concept itself comes from Fermi's Golden Rule, which predicts a linear dependence of the excitation probability with time. In an analysis bRWA at very short times, akin to that of the Zeno effect or ours, the probability of excitation will result proportional to t^2, and no such thing as a constant stable rate of dark counts can be defined. Since there is no way to experimentally distinguish between the two sort of processes that lead to a detector excitation, the analysis through a conditioned probability seems a reasonable one.

We will consider the following Hamiltonian [213, 288]:

$$\begin{aligned} H &= H_0 + H_I, \\ H_0 &= \sum_{A=\{S,D\}} \frac{\hbar\Omega_A}{2}\sigma_z^A + \int_{-\infty}^{\infty} dk\hbar\omega_k a_k^\dagger a_k, \\ H_I &= -\sum_{A=\{S,D\}} d_A V(x_A)\sigma_x^A. \end{aligned} \tag{10.2.3}$$

Here x_A corresponds to the position of the qubit A, $\hbar\Omega_A$ is the gap between levels for qubit A and V refers to the 1-dimensional field which expands as:

$$V(x) = i\int_{-\infty}^{\infty} dk\sqrt{N\omega_k}e^{ikx}a_k + H.c.. \tag{10.2.4}$$

This field has a continuum of Fock operators $[a_k, a_{k'}^\dagger] = \delta(k-k')$, and a linear spectrum, $\omega_k = v|k|$, where v is the propagation velocity of the field. The normalization and the speed of photons, $v = (cl)^{-1/2}$, depend on the microscopic details such as the capacitance and inductance per unit length, c and l. Note that this model resembles that of an Unruh-DeWitt detector [54]. For our calculations, we will make use of the interaction picture, so we let the initial state $|eg0\rangle$ evolve for a lapse of time t as:

$$\begin{aligned} |\psi(t)\rangle &= U_I(t)\,|eg0\rangle = \mathcal{T}\{e^{-i\int_0^t dt' H_I(t')/\hbar}\}\,|eg0\rangle \\ &= I\,|eg0\rangle + X\,|ge0\rangle + \sum_k A_{1,k}\,|gg1_k\rangle + \sum_k B_{1,k}\,|ee1_k\rangle \\ &\quad + \sum_{kk'} A_{2,kk'}\,|eg2_{kk'}\rangle + \sum_{kk'} B_{2,kk'}\,|ge2_{kk'}\rangle + \ldots \quad . \end{aligned} \tag{10.2.5}$$

Note that all terms but the first three are zero when working in the RWA. For A's coefficients D ends in the ground state, for B's, in the excited one. Here and in the following we will only make explicit the terms that contain contributions for the probabilities up to d_A^4. For

example, terms with 3 or more photons in the amplitude will be excluded, as they give contributions of $\mathcal{O}(d_A^6)$. We will underline the ones relevant in our analysis.

10.3 Probability calculations

Let us define $\mathcal{M}(t;nF) = \langle neF|\psi(t)\rangle$. Thus, the first of the probabilities needed for the computation of $\mathcal{P}_{S_g/D_e}(t)$ (10.2.1) can be written down using (10.2.5) as

$$\mathcal{P}_{[ge*]} = \sum_F |\langle geF|U_I(t)|eg0\rangle|^2 = \sum_F |\mathcal{M}(t;gF)|^2$$
$$= \underline{|X|^2 + \sum |B_2|^2} + \sum |B_4|^2 \dots \quad .$$

The first building block needed is $|X|^2$. Note that

$$\mathcal{P}_{[ge0]} = |\langle ge0|U_I(t)|eg0\rangle|^2 = |\mathcal{M}(t;g0)|^2 = |X|^2. \tag{10.3.1}$$

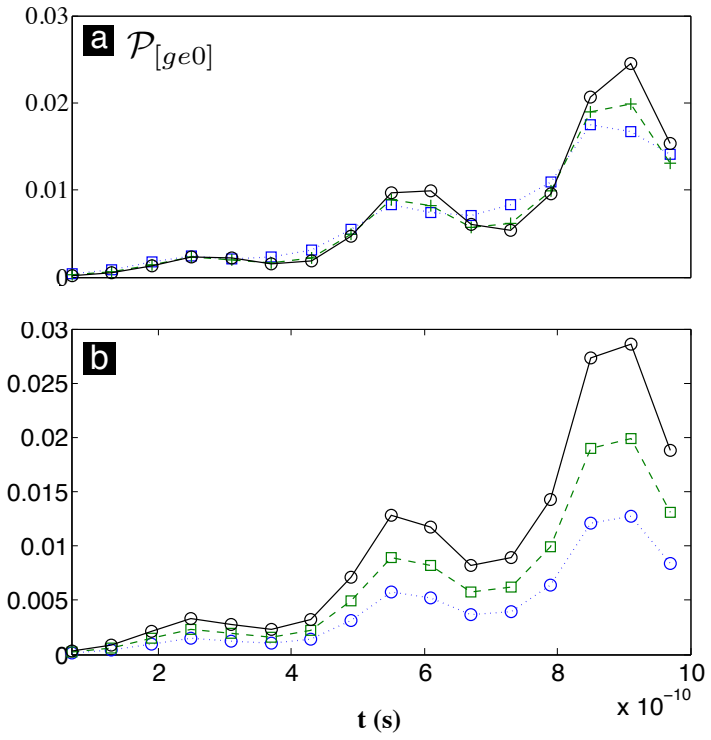

Figure 10.1: a) $P_{[ge0]}$ in front of t for three different values of the distance between qubits $2\pi\frac{r}{\lambda} = 0.1$ (dotted, squares, blue), 0.3 (dashed, crosses, green) and 0.5 (solid, circles, black).For all cases $K_S = K_D = 7.5\cdot 10^{-3}$ and $\Omega/(2\pi) = 1\,Ghz$. b) $P_{[ge0]}$ in front of t for three different values of the coupling strength $K = K_S = K_D = 6\cdot 10^{-3}$ (dotted, squares, blue), $7.5\cdot 10^{-3}$ (dashed, crosses, green) and $9\cdot 10^{-3}$ (solid, circles, black) . For all cases $2\pi\frac{r}{\lambda} = 0.3$ and $\Omega/(2\pi) = 1\,GHz$.

To evaluate $|X|^2$ up to fourth order in perturbation theory, one must consider X has no contributions neither for orders 0 or 1, so the calculation must be performed for orders 2 and above. As a matter of fact, order 2 alone is sufficient. This calculation has been already performed in the appendix of [44], where the perturbative parameter d_A is included in the dimensionless coupling strength $K_A = \frac{4d_A^2 N}{\hbar^2 v} = 2\left(\frac{g_A}{\Omega_A}\right)^2$, with $A = \{S, D\}$, g_A being the qubit-line coupling. We must restrict to times where $K_A \Omega_A t \ll 1$, where our perturbative approach is valid.

In Fig. 10.1 we sketch the evolution of the probability $\mathcal{P}_{[ge0]}$ with time, and its dependence with the coupling and the distance between qubits. Typical values for couplings and distances for a set-up in cQED are considered from here on. At these early stages $\mathcal{P}_{[ge0]}$ is highly oscillatory in time. For a given time, the probability always grows with the coupling strength but depends of the distance in different ways.

To proceed with the calculation of $\mathcal{P}_{[ge*]}$, the terms $B_{2,kk'} = \langle eg0|U_I(t)|ge2_{kk'}\rangle$ must be evaluated. As the final bare state associated has two photons, this implies automatically that orders 0 and 1 are discarded. Once again, order 2 alone fits. The final calculation gives a term symmetric respect to a $k \leftrightarrow k'$ exchange:

$$B_{2,kk'} = f_{kk'} + f_{k'k} = f_{kk'} + \{k \leftrightarrow k'\} \tag{10.3.2}$$

After that, they must be squared and summed as in $\sum |B_2|^2 = \frac{1}{2!}\sum_{kk'} B_{2,kk'} B^*_{2,kk'}$ splitting into two terms: $\sum |B_2|^2 = \sum_{kk'} f_{kk'} f^*_{kk'} + \sum_{kk'} f_{kk'} f^*_{k'k}$, a "direct" one, just the product of the square of the emission amplitudes (explicitly computed in [44]), and a "crossed" one which looks like a photon exchange and is a 1-D version of the crossed term computed in [278]. The summation of the direct terms implies the appearance of expected divergences which can be resolved using a regularization procedure analogous to the one sketched in the appendix of [278]. This procedure requires the times of analysis to be larger than a certain cutoff time t_0, which in this case is related with the typical size of a superconducting qubit $d \simeq 10^{-6}\, m$ [237] and the propagation velocity of the field quanta: $v \simeq 10^8\, m/s$. Thus, $t_0 = d/c \simeq 1 \cdot 10^{-14}\, s$, far below the times considered here.

Notice that B_2 is only non-zero beyond the RWA. In Fig. 10.2 we compare $\mathcal{P}_{[ge*]}$ with $\mathcal{P}_{[ge0]}$. The impact of this non-RWA contribution is seen in the sub-nanosecond regime for a large coupling strength. At larger times, the impact diminishes, $\mathcal{P}_{[ge*]} \simeq \mathcal{P}_{[ge0]}$, and the RWA applies.

The last probability of interest $\mathcal{P}_{[*e*]}$ can be written as

$$\mathcal{P}_{[*e*]} = \sum_{n,F} |\langle neF|U_I(t)|eg0\rangle|^2 = \sum_{n,F} |\mathcal{M}(t; nF)|^2$$

$$= |X|^2 + \sum |B_1|^2 + \sum |B_2|^2 + \sum |B_3|^2 \dots \quad . \quad (10.3.3)$$

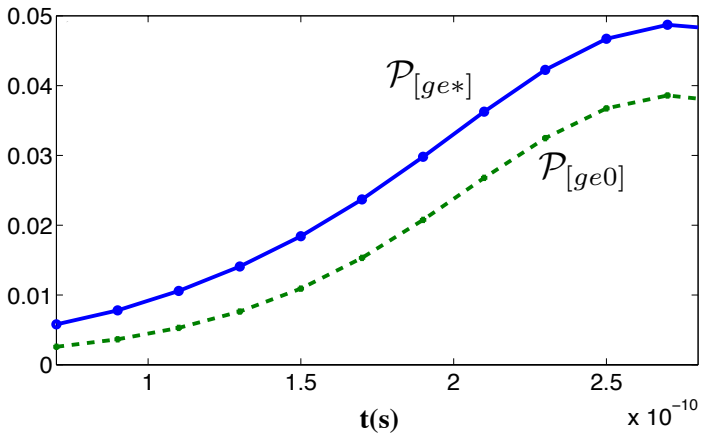

Figure 10.2: $P_{[ge*]}$ (solid, blue, circles) and $P_{[ge0]}$ (dashed, green, crosses) in front of t in s with a distance $2\pi\frac{r}{\lambda} = 0.5$, a coupling strength of $K = K_S = K_D = 3 \cdot 10^{-2}$ and $\Omega/(2\pi) = 1\,GHz$ ($\Omega = \Omega_S = \Omega_D$). The difference between the two graphs is the non-RWA term $\sum |B_2|^2$.

And so we must obtain $\sum |B_1|^2$, which is again a completely non-RWA contribution. For that case the situation gets more complicated, as there are interfering processes of orders 1 and 3 leading to that final state. The four diagrams contributing to $\sum |B_1|^2$ up to fourth order in perturbation theory can be seen in Fig. 10.3. The leading contribution is just the probability of self-excitation of the detector, (first diagram for B_1 in Fig. 10.3) and the other contributions come from the interference of this diagram with the other three. In particular, interference with the third diagram of B_1 is crucial for causality [36]. More details on this computation can be found in [289].

10.4 Conditioned detection probability

With the previous probabilities computed we can finally address the conditioned probability $\mathcal{P}_{S_g/D_e}(t)$, which can be calculated as (10.2.1). Note that in the RWA $\mathcal{P}_{S_g/D_e}(t) = 1$ at any time, since $\mathcal{P}_{[*e*]} = \mathcal{P}_{[ge*]} = \mathcal{P}_{[ge0]}$. The effect of non-RWA contributions to the evolution of $\mathcal{P}_{S_g/D_e}(t)$ can be seen in Figs. 10.4 and 10.5, where the dependence with the coupling and the distance between qubits is considered.

The first thing we notice in Fig. 10.4 is that for short times the information provided by the detector is not very much related to the state of the source, that is, self-excitations and other non-RWA phenomena dominate over the photon exchange between source and detector. For the cases considered, only at interaction times $t \gtrsim 1\,ns \simeq 1/\Omega$ the conditioned

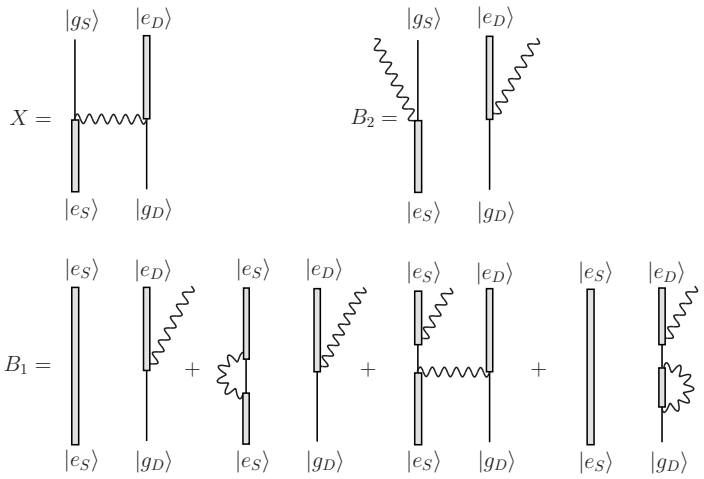

Figure 10.3: The diagrams contributing to X, B_1 and B_2. X represents the amplitude for photon exchange between source and detector, while B_2 is just the amplitude for two single photon emissions, one at each qubit. The leading order contribution to B_1 is the amplitude for a single photon emission at the detector qubit (first diagram), but third-order one-loop corrections (second and fourth) and a photon exchange accompanied by an emission at the source (third) have to be also taken into account. B_1 and B_2 are completely non-RWA diagrams.

probability converges to the RWA prediction and the excitation of the detector is a reliable way to detect the decay of the source. Since the non-RWA contributions are more relevant for large couplings and short distances, the convergence is faster as the distance grows and the couplings diminish, as can be seen in Figs. 10.4 and 10.5. Notice that the ripple frequency we see for instance in Fig. 10.4 comes from higher harmonics of the qubit frequency Ω. It can be thought as a process similar to that of a Rabi oscillation, where the qubits would be absorbing in cycles the photons previously emitted in self-excitations.

10.5 Discussion

These theoretical results could have an impact in real experiments of cQED. In particular, a typical setup to measure the internal state of a flux qubit coupled to a transmission line consists of a SQUID surrounding the qubit. Although the total measurement process could take up to tens of nanoseconds, most of the time the coupling SQUID-qubit is much stronger than K [282] and the dynamics qubit-transmission line is effectively frozen. Thus this dynamics is only important during the activation of the SQUID, a process that may be in the nanosecond regime. For those measurement times, as we have proved, self-excitation effects cannot be disregarded and should manifest themselves.

Besides, it should, in principle, be possible to prepare experiments in the near future

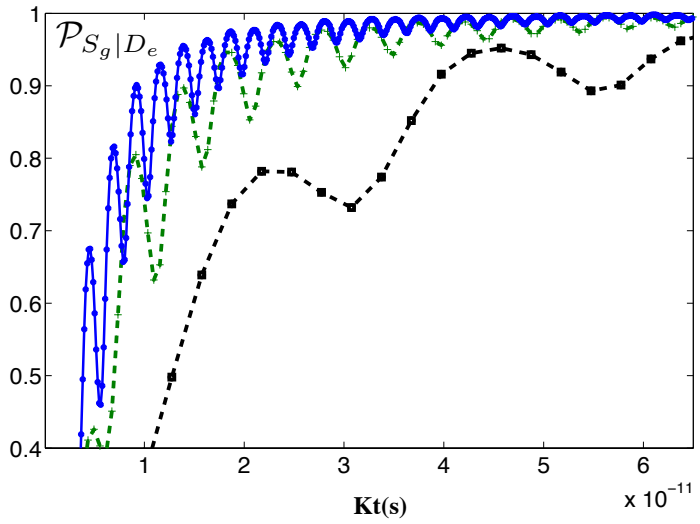

Figure 10.4: $\mathcal{P}_{S_g/D_e}(t)$ (10.2.1) in front of Kt for three different values of $K = K_S = K_D = 7.5 \cdot 10^{-3}$ (solid, blue, circles), $1.5\,10^{-2}$(dashed, green, crosses), $7.5 \cdot 10^{-2}$ (dashed, black, squares). In the three cases $2\pi\frac{r}{\lambda} = 1$ and $\Omega/(2\pi) = 1\,GHz$ ($\Omega = \Omega_S = \Omega_D$).

to test our predictions directly. We do not intend to present here more than just a rough sketch. Such experiments would involve the preparation of the system at $t = 0$ in the initial state $|eg0\rangle$, the switching of the interaction for a certain time t (in the line of previous proposals, as [36, 221, 290, 291]) and then the SQUID-measurement of both qubits S and D. By repeating the experiment several times, the result frequencies should match our theoretical predictions.

To conclude, we have shown that for typical cQED parameters, a significative amount of time is needed to start trusting the state of a detector as informative regarding an initially excited source. This is due to the breakdown of the RWA in cQED. By neglecting the counterrotating terms a total reliability on the information coming out of the detector would be wrongly derived for all time-scales. Our result applies to other setups and quantum detectors, although it is in the case of cQED where it might affect the interpretation of coming experimental results.

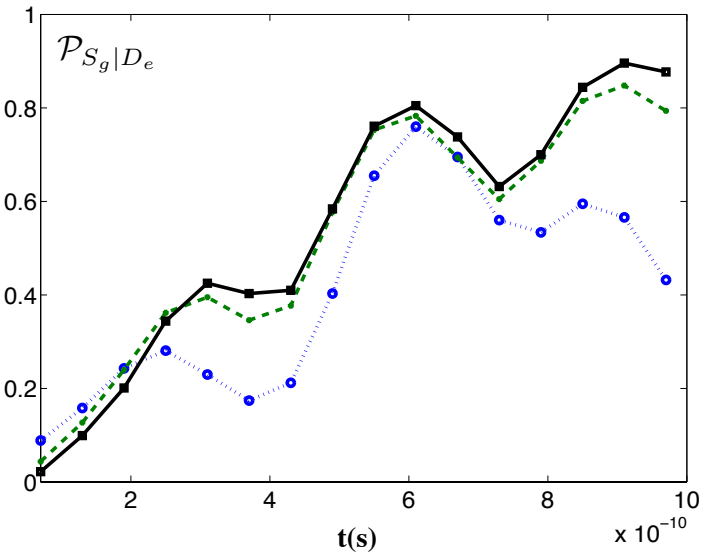

Figure 10.5: $\mathcal{P}_{S_g/D_e}(t)$ (10.2.1) in front of t in s for three different values of the distance $2\pi\frac{r}{\lambda} = 0.5$ (dotted, blue, circles), 0.75 (dashed, green, crosses), 1 (solid, black, squares). In the three cases $K = K_S = K_D = 1.5 \cdot 10^{-2}$ and $\Omega/(2\pi) = 1\,GHz$ ($\Omega = \Omega_S = \Omega_D$).

Part III

Vacuum Correlations and Localization

Alice Lost in The Vacuum,
Timelike and Spacelike Entanglement, Extraction of Correlations,
Local Virtual Particles and Unitary Inequivalence.

CHAPTER 11

Concepts

Después de todo, todo ha sido nada,
a pesar de que un día lo fue todo.
Después de nada, o después de todo
supe que todo no era más que nada.
Grito '¡Todo!', y el eco dice '¡Nada!'.
Grito '¡Nada!', y el eco dice '¡Todo!'.
Ahora sé que la nada lo era todo,
y todo era ceniza de la nada. (...)

José Hierro, *Vida*

The very own existence of such a thing as the *No-Thing* sounds paradoxical and it is precisely, highly problematic. Volumes have been written discussing it. Here however, we do not want to dive into the philosophical historical debates about the *being* and the *not-being*. Quantum mechanically however, as scientists, we have certainly something to say. Under the light of Quantum Field Theory, the nothing has to be reinterpreted as the state with no particles, i.e. the ground state of a quantum field, something quite different from the nothingness. José Hierro, had something to say about it. Although most probably with different implications, he pointed out the secret connection that we will enjoy playing with in the next chapters, namely, that the *No-Thing* has something of the *Every-Thing*. The quantum vacuum, from which mathematically we construct any state, far from being empty and static, it is actuallyfull of action. We will devote this part of the thesis to its analysis, to the study of its local characteristics and its intrinsic correlations.

11.1 The Quantum Vacuum: a Global Entity

The elementary excitations of quantum field theory are countable, a crucial feature for making it able to deal with the physics of elementary particles. These are described by operators which carry information about the energy momentum that these excitations take or give to the field. The ground state of the field, from which no quanta can be removed, thus becomes the vacuum, whose excitations describe the states with one or more particles with well defined momenta. This Fock construction provides simple global operators for the field as a whole. In particular, the total number of particles carried by any specified configuration is easy to address. However, the construction lacks a means to inquire into the local properties of the field. For instance a question as simple as "how are these particles distributed in space?" or more simply, "where is this particle?" are difficult to address if not by indirect means. The root of the problem is that creation and annihilation operators do not belong to the algebra of local operators of the quantum field. This can be understood in physical terms as a consequence of the fact that they describe excitations endowed with sharp momentum and hence expected in principle to be unlocalized in space. The conclusion is that, powerful as it is, the standard Fock space techniques provide only a feeble scaffolding for digging into issues pertaining to the localization of quanta.

In standard Quantum Field Theory, we work constantly with the vacuum state $|0\rangle$, the state annihilated by all particle destruction operators $\hat{a}_k$. Physically, it corresponds to the ground state of the theory and as such, it is defined in all the spacetime region where our theory applies, therefore being a global state. It is also the thermal state with temperature $T = 0K$. Being a global, quantum, non-local state, it should not be that surprising if it shows non-local correlations . This is, as a matter of fact, what happens. As explained in Part II, the Feynman propagator for example does not vanish for spacelike separated points. The existence of spacelike correlations in the quantum vacuum should, at this point, be rather natural to the reader. In this part of the thesis we would like however to link that fact to the problem of particle localizability.

11.2 The Problem of Localizability

In standard non-relativistic quantum mechanics, the concept of a localized particle is mathematically well-defined and straightforward. The theory is described in terms of quantum states that could represent single particles. The self-adjoint position operator X acts on the Hilbert space of states so that an ideal position measurement produces an outcome corresponding to one of its eigenvalues. Using its eigenstates one may build an arbitrarily local-

ized wave-packet in a finite region of position space in such a way that we can assert "The particle is here" with probability 1. Correspondingly, by 'localized' in quantum mechanics we understand wave packets with value different from zero, only on a certain spatial region $\mathcal{R}$. In this sense, if a state $\psi(\mathbf{x})$ verifies

$$\psi(\mathbf{x}) \begin{cases} = 0 \text{ if } \mathbf{x} \notin \mathcal{R} \\ \neq 0 \text{ if } \mathbf{x} \in \mathcal{R} \end{cases}$$

its expectation values for the physical observables trivially vanish outside $\mathcal{R}$. It can be shown [292] that, if the energy spectrum is bounded from below, such a wave packet will spread everywhere instantly, or it will remain confined forever. This fact does not give rise to theoretical problems since the theory is non-relativistic.

It is a well-known fact that the only known consistent relativistic quantum theory is that of *fields* [293]. The basic dynamical variables of the standard model of physics are fields; we have both bosonic fields (the Higgs field, electroweak and strong gauge bosons) and fermionic spinor fields (quarks and leptons) and, perhaps and beyond, the graviton. All of them are subject of relativistic field equations. These theories become consistent with the rules of quantum theory by following quantization procedures, for example that of canonical quantization. The result is a quantum field theory in which the elementary excitations of the various bosonic and fermionic fields come in quanta corresponding to the elementary particles we find in nature, e.g. electrons, muons, neutrinos, photons, etc. These entities are traditionally referred to as 'particles', and commonly thought of as representing, in some appropriate sense, spatially localized quanta of energy. However, several careful studies of quantum field theory [40, 174, 294–296] have proven this picture to be too naive.

One first problem common to all quantum theories is given by Hegerfeldt's theorem [292]:

Theorem 1 *Let the operator H be self-adjoint and bounded from below in a Hilbert space $\mathcal{H}$. Let $\mathcal{O}$ be any positive operator in $\mathcal{H}$ satisfying, and let ψ_0 be any vector in $\mathcal{H}$ so that at $t \in \mathbb{R}$*

$$\psi_t = e^{-iHt}\psi_0$$

Then one of the following two alternative holds:

i) $\langle \psi_t | \mathcal{O}\psi_t \rangle \neq 0$ *for almost all t, or*

ii) $\langle \psi_t | \mathcal{O}\psi_t \rangle = 0$ *for all t.*

Hegerfeldt's theorem can be understood as follows: Suppose that $\mathcal{O}(\mathbf{x})$ is representing some physical observable that gives the probability of finding a particle at $\mathbf{x}$, and let ψ_0 be a localized state in V_0. The theorem asserts that if at time t_0 we perform a measurement of $\mathcal{O}$

outside V_0, then either we have indeed no particles ever (possibility ii)), or immediately after t_0 the probability of finding the particle outside V_0 is non zero (possibility i)), even if $\mathbf{x}$ is arbitrarily far from V_0.

Let us analyze the implications of the theorem for the one-particle sector of quantum field theory. Consider a complex scalar field Φ satisfying the Klein-Gordon equation $\Box\Phi + m^2\Phi = 0$. In the usual formulation in Minkowski spacetime, the Hilbert space of one-particle states $\mathfrak{H}$ of the corresponding quantum field theory is selected by making use of the Poincare invariance of the theory. Then $\mathfrak{H}$ is chosen to be the space of positive frequency solutions to the classical Klein-Gordon equation (*We must remark here that we are dealing with a flat spacetime. A clear separation in positive and negative frequencies in general curved spacetimes is not possible [165], but only on static stationary spacetimes*). Indeed, any positive frequency solution is of the form

$$\phi(\mathbf{x},t) = \int \frac{d^3k}{\sqrt{2\omega_{\mathbf{k}}}} f(\mathbf{k}) e^{-i(\omega_{\mathbf{k}}t - \mathbf{k}\cdot\mathbf{x})} \tag{11.2.1}$$

Hence, one would naively expect that it is possible to define f in such a way that a completely localized wave packet, representing a single localized quantum of energy, could be created, such that $\phi(\mathbf{x},t)$ gives the probability amplitude for finding the particle in $\mathbf{x}$ at time t. Unfortunately, this is not the case. Let us be a bit more precise in the definitions. To this point we have made the reasonable assumption, in analogy with QM, that a positive frequency particle of the form (11.2.1) localized at some instant of time t_0 within some compact region $\mathcal{R} \subset \mathbb{R}^3$ can be mathematically represented by a wave-packet ϕ with support only in $\mathcal{R}$, i.e $\phi(\mathbf{x},t_0) = 0\ \forall \mathbf{x} \notin \mathcal{R}$ for some open set $\mathcal{R}$ of $\mathbb{R}^3$. Conversely, a non-zero ϕ at some point $\mathbf{x}$ would imply a non-zero probability for the particle to be detected there. Then, by virtue of *Hegerfeldt's theorem* or, in more general terms, of the Reeh-Schlieder theorem [40], such a state would violate causality. The basis of Hegerfeldt's argument is the non-local nature of the Hamiltonian when solely acting on positive frequency solutions. It follows from easy analytic arguments that we cannot have compact support for both $\phi(t,\mathbf{x})$ and $\dot{\phi}(t,\mathbf{x})$ using only positive frequencies [297–299]. This fact implies that the N-particle positive frequency solutions do not have compact support and, in order to agree with special relativity, we will need something else for constructing local states.

Summarizing, we can not use positive-frequency one-particle states to construct localized states according to the former 'localization' scheme. Hence, this naive localization prescription does not work. The goal of defining the concept of localization and localized quanta in quantum field theory in an analogous way as done for QM is not trivial, and in fact has generated a large debate in the field [300]. Several localization schemes have been developed and studied, none of them showing general acceptance.

For instance, the Newton-Wigner scheme [301] proposes the following definition for local states: A state ψ representing system (or a particle) at time $t = 0$ in $\mathbf{x} = 0$ satisfies:

1. The set of local states at $t = 0$ in $\mathbf{x} = 0$ form a linear space $\mathcal{S}$ (i.e. superposition of local states are still local).

2. This set of states is invariant under rotations and space and time reflections.

3. (Most important) If ψ is localized as above, then a spatial displacement out of its region of localization makes it orthogonal to $\mathcal{S}$.

Then, by applying the displacement operator $T(\mathbf{a})$ on ψ one can obtain any state localized in $\mathbf{a} = (a_x, a_y, a_z)$. This definition allowed Newton and Wigner to uniquely define position and momentum relativistic operators $\hat{X}_{NW}$ and $\hat{P}$ acting on positive-frequency functions and satisfying the same commutation relations and symmetry properties of the position and momentum operators of standard quantum mechanics. Nevertheless, a detailed study of them shows that: a) these definitions are not Lorentz covariant [302] and b) condition 3, if it holds at $t = 0$, it does not at any $t > 0$: orthogonality of the eigenstates of the Newton-Wigner position operators for spacelike-separeted ones is not preserved in time [292]. In particular this means that a particle prepared in a Newton-Wigner position eigenstate may be found anywhere in physical space infinitesimally after. Therefore, the Newton-Wigner operators are not adequate to model a particle position measurement .

In any case, it must be noted that quantum field theory deals with fields rather than particles, and quantum field states are not one-particle states but rather *Fock states* of the Fock space we have chosen to describe the theory. The $N - particle$ states in quantum field theory (QFT), namely the eigenstates of the particle-number operator, have a well-known non-local character [51, 52]: they are not eigenstates of local operators. However, it seems natural to require that a particle as such should be a local object detected by a local apparatus: a photoelectric detector, a bubble chamber, a calorimeter or a scintillating detector. Such an apparatus would be implemented in the theory via some local operator, and its excitations (i.e. the eigenvalues of the operator), should be interpreted as particles. A state representing such a particle would in principle be expected to satisfy some reasonable localization conditions. How could a Fock state, which spreads over the whole configuration space, be instantaneously absorbed or detected by a local sized apparatus? Both concepts of localization and particle in standard QFT are at loggerheads. In general formulations of QFT the notion of particle depends on the algorithm used to select the one-particle sector of the theory, and there is not a preferred mathematical choice for it [172]. Besides, the former localization conditions for local states (i.e. a *localization scheme*) should be reformulated since

the standard QM approach of vanishing wave-function outside a region of localization $\mathcal{R}$ does not apply in the field domain, as we have seen.

Probably the most elegant and clear concept of localization and localized states in QFT was given by Knight [294]. In his work, Knight carefully defines a state $|\psi_{\mathcal{R}}\rangle$ to be *strictly localized* at some time t_0 within some region $\mathcal{R} \in \mathbb{R}^3$ if it has the same expectation value as the vacuum $|0\rangle$ for any operator $\mathcal{O}(\mathbf{x})$ with $\mathbf{x} \notin \mathcal{R}$, i.e.

$$\langle\psi_{\mathcal{R}}|\mathcal{O}(\mathbf{x})|\psi_{\mathcal{R}}\rangle = \langle 0|\mathcal{O}(\mathbf{x})|0\rangle. \qquad \textit{if } x \notin \mathcal{R} \tag{11.2.2}$$

From there, Knight proves that there are actually *no $N-$particle states with finite N satisfying the property of strict localization*. In other words, it does not matter how much one tries, it is impossible to use Fock states with a finite number of particles to construct such localized states.

It is now clear that the notion of particles in QFT cannot be literally be taken to represent particles, if we understand by these local entities. This aims at the ultimate goal of constructing a notion of particle employable on curved spacetimes backgrounds or for quantum gravity proper. In shorter terms this will lead to the definition of qubits usefull for the tasks of (Relativistic) Quantum Information.

11.3 Extraction of Vacuum Entanglement

We propose a realistic circuit QED experiment to test the extraction of past-future vacuum entanglement to a pair of superconducting qubits. The qubit P interacts with the quantum field along an open transmission line for an interval T_{on} and then, after a time-lapse T_{off}, the qubit F starts interacting for a time T_{on} in a symmetric fashion. After that, past-future quantum correlations of the vacuum will have transferred to the qubits, even if the qubits do not coexist at the same time. We show that this experiment can be realized with current technology and discuss its utility as a possible implementation of a quantum memory.

11.4 Local quanta

In this work we develop a formalism for describing localised quanta for a real-valued Klein-Gordon field in a one-dimensional box $[0, R]$. We quantise the field using *non-stationary local modes* which, at some arbitrarily chosen initial time, are completely localised within the left or the right side of the box. In this concrete set-up we directly face the problems inherent to a notion of local field excitations, usually thought of as elementary particles. Specifically, by

computing the Bogoliubov coefficients relating local and standard (global) quantizations, we show that the local quantisation yields a Fock representation of the Canonical Commutation Relations (CCR) which is *unitarily inequivalent* to the standard one. In spite of this, we find that the local creators and annihilators remain well defined in the global Fock space $\mathfrak{F}^G$, and so do the local number operators associated to the left and right partitions of the box. We end up with a useful mathematical toolbox to analyse and characterise local features of quantum states in $\mathfrak{F}^G$. Specifically, an analysis of the global vacuum state $|0_G\rangle \in \mathfrak{F}^G$ in terms of local number operators shows, as expected, the existence of entanglement between the left and right regions of the box. The local vacuum $|0_L\rangle \in \mathfrak{F}^L$, on the contrary, has a very different character. It is neither cyclic (with respect to any local algebra of operators) nor separating and displays no entanglement between left and right partitions. Further analysis shows that the global vacuum also exhibits a distribution of local excitations reminiscent, in some respects, of a thermal bath. We discuss how the mathematical tools developed herein may open new ways for the analysis of fundamental problems in local quantum field theory.

11.5 Alice and the Slamming Mirror

So we know that the vacuum state of a quantum field is spatially entangled. This is true both in free and confined spaces, for example in an optical cavity. The obvious consequence of this, however, is surprising and intuitively challenging. Namely, that in a mathematical sense half of an empty box is not empty. Formally this is clear, but what does this physically mean in terms of, say, measurements that can actually be made? In this paper we utilize the tools of Gaussian quantum mechanics to easily characterize the reduced state of a subregion in a cavity and expose the spatial profile of its entanglement with the opposite region. We go on an discuss then a thought experiment situation in which a mirror is introduced between the regions. In so doing we expose a simple and physically concrete answer to the above question: the vacuum excitations resulting from entanglement are mathematically equivalent to the real excitations generated by suddenly introducing a mirror. Such an experiment would ideally allow to retain all entanglement present between left and right regions. We conclude by discussing different possibilities for doing a similar experiment in the lab.

CHAPTER 12

Extracting Past-Future Vacuum Correlations Using Circuit QED

12.1 Introduction

The fact that the vacuum of a quantum field presents quantum entanglement was discovered long ago [54,94,95], but it was considered a mere formal result until it was addressed from an applied perspective in [41]. Since then, this intriguing property has attracted a great deal of attention as a possible new resource for Quantum Information tasks [42–45].

As shown in [41], the entanglement contained in the vacuum of a scalar field can be transferred to a pair of two-level spacelike separated detectors interacting with the field at the same time. Unfortunately, this theoretical result seems to be very difficult to translate into an experiment, even in the context of a trapped-ion simulation [42]. Recently, it has also been proven [49] that the vacuum of a massless scalar field contains quantum correlations [1] between the future and the past light cones. A theoretical method of extraction by transfer to detectors interacting with the field at different times has also been proposed [50], but the particular time dependence of the energy gaps seems extremely challenging from the experimental viewpoint. Another ideal proposal involving cavities transparent to a single mode was provided in [243] with a setting that seems even more difficult to tackle experimentally.

On the other hand, circuit QED [211] provides a framework in which the interaction of two-level systems with a quantum field can be naturally considered. The combination of superconducting qubits with transmission lines implement an artificial 1-D matter-radiation

[1] Although in [49] these correlations are referred to as entanglement, such a wording might not be appropriate since quantum states in past and future belong to Hilbert spaces defined in different simultaneity planes. Nevertheless, quantum correlations of this sort can in principle be extracted to physical systems and exploited as a resource for quantum information tasks as in the case of typical entanglement.

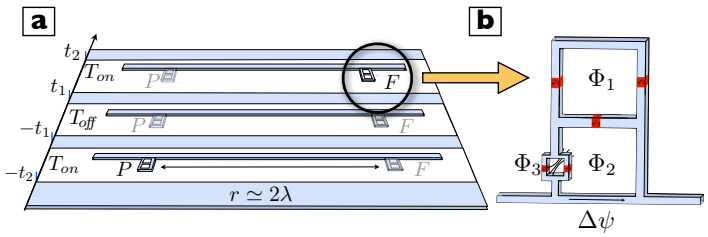

Figure 12.1: Experimental proposal for past-future entanglement extraction. a) Time evolution of our protocol: the qubit P interacts with the vacuum field ($\Delta\psi$) for a time T_{on}. After a certain time T_{off} with no interaction, a second qubit F interacts with the field getting entangled with the qubit P. b) Switchable coupling design: a flux qubit (top ring) is coupled to the field $\Delta\psi$ by ways of two loops. Varying the magnetic fluxes Φ_2 and Φ_3 we deactivate the qubit-field coupling.

interaction, with the advantage of a large experimental accessibility and tunability of the physical parameters. Using these features, fundamental problems in Quantum Field Theory hitherto considered as ideal are now accessible to experiment [58]. In particular, the possibility of achieving an ultrastrong coupling regime [285, 286, 303] has already been exploited to propose a feasible experimental test of the extraction of vacuum entanglement to a pair of spacelike separated qubits [44].

In this chapter we will take advantage of the aforementioned features of circuit QED in the ultrastrong coupling regime in order to propose a realistic experiment for the extraction of past-future correlations [2] contained in the vacuum of a quantum field. We will consider a set-up consisting of a pair of superconducting qubits P and F with constant energy gaps separated by a fixed distance r in a common open transmission line (Fig. 12.1a). First, the interaction of P with the vacuum of the field is on for a time interval T_{on} (we call this interval 'the past'). Then, P is disconnected from the field during a time T_{off}. Finally, the interaction of F is switched on during T_{on} ('the future') while keeping P disconnected. After this procedure, we will show that the qubits can end up in a strongly correlated quantum state, in spite of not having interacted with the field at the same time. We will consider three different spacetime configurations: that the qubits are spacelike or timelike separated, and in the latter case with or without photon exchange allowed. Perhaps the most surprising result is that, even if photon exchange is forbidden, the qubits can get entangled by a transference of vacuum correlations, as we will show. However, this is not the only interesting aspect of our scheme. If there is a certain probability of photon exchange, some classical correlations between the qubits are obviously expected. But is also remarkable that, due to the peculiarities of our circuit QED setup these correlations are quantum and attain a high degree

[2] Note that we will use the term "past-future" correlations to refer to a different and more general notion than "time-like entanglement" or "entanglement between the past and the future light cones".

without the need of a projective measurement of the field. We stress that our proposal is free of idealized requirements such as gaps with unfeasible time dependences. Our switching scheme is fully within reach of current circuit QED technologies, as shown below.

In addition to its interest from the fundamental viewpoint, our protocol has also an important applied counterpart. As suggested in [50], the extraction of past-future quantum correlations enables its use as a quantum channel for quantum teleportation "in time". We will show how this opens the door to a novel kind of quantum memory in which the information of the quantum state of some ancillary qubit P' is codified in the field during T_{off} and then recovered in F using classical information stored in the past - regardless whatever may happen to P after its interaction with the field.

12.2 Theoretical model

From now on we focus on a setup of circuit-QED with two superconducting qubits P and F interacting via a quantum field. The qubits have two stationary states $|e\rangle$ and $|g\rangle$ separated by a constant energy $\hbar\Omega$ and might interact with a 1D field, $\Delta\psi(x)$, which propagates along an open microwave guide or transmission line that connects them

$$\Delta\psi(x) = i\int_{-\infty}^{\infty} dk\,\sqrt{N\omega_k}\,e^{ikx}a_k + \text{H.c.} \tag{12.2.1}$$

This field has a continuum of Fock operators $[a_k, a_{k'}^\dagger] = \delta(k-k')$, and a linear spectrum, $\omega_k = v|k|$, where v is the propagation velocity of the field. The normalization N and the speed of photons, $v = (cl)^{-1/2}$, depend on the microscopic details such as the capacitance and inductance per unit length, c and l. We will assume qubits that are much smaller than the relevant wavelengths, $\lambda = 2\pi\, v/\Omega_J$, ($J = P, F$) and the fixed distance r. Under these conditions the Hamiltonian, $H = H_0 + H_{\text{I}}$, splits into a free part for the qubits and the field $H_0 = \frac{1}{2}\hbar(\Omega_P\sigma_P^z + \Omega_F\sigma_F^z) + \int_{-\infty}^{\infty} dk\,\hbar\omega_k a_k^\dagger a_k$ and a point-like interaction between them

$$H_{\text{I}} = -\sum_{J=P,F} d_J\,\Delta\psi(x_J)\,\sigma_J^x = H_{\text{IP}} + H_{\text{IF}} \tag{12.2.2}$$

Here x_J are the fixed positions of the atoms, and $d_J\,\sigma_J^x$ comes from a dimensional reduction of the matter- radiation interaction hamiltonian with two-level atoms and the electromagnetic field, analogous - but not fully equivalent - to the Unruh-de Witt model. [178].

We choose the following initial state $|\Psi(-t_2)\rangle = |eg0\rangle$, where only qubit P has been excited, in order to analyze the interplay between photon exchange and vacuum correlations effects in the generation of entanglement. According to our past-future scheme (Fig. 12.1a),

the system evolves in the interaction picture into the state

$$|\Psi(t_2)\rangle = \mathcal{T} e^{-i\int_{-t_2}^{t_2} \frac{dt'}{\hbar}[\Theta(-t'-t_1)H_{\rm IP}^{(t')}+\Theta(t'-t_1)H_{\rm IF}^{(t')}]} |eg0\rangle\,, \tag{12.2.3}$$

$\mathcal{T}$ being the time ordering operator.

We use the formalism of perturbation theory up to the second order and beyond Rotating Wave Approximation [44] and trace over the field degrees of freedom to obtain the corresponding two-qubit reduced density matrix ρ_{PF} evaluated at t_2. The degree of entanglement of this X-state can be characterized with the concurrence, which at the considered order is given by: $\mathcal{C}(\rho_{PF}) = 2\Big[|X| - \Big(\sum_k |A_{1,k}|^2 \sum_k |B_{1,k}|^2\Big)^{1/2}\Big]$, X standing for the normalized amplitude of photon - real and virtual - exchange and $\sum_k |A_{1,k}|^2$, $\sum_k |B_{1,k}|^2$ for the total normalized probability of single-photon emission by qubit P and F, respectively. These terms can be computed - following similar techniques as in [44] - as a function of four dimensionless parameters, $\xi_{\rm on}$, $\xi_{\rm off}$, K_P and K_F. The first two, $\xi_{\rm on} = vT_{\rm on}/r$, $\xi_{\rm off} = vT_{\rm off}/r$ allow to discriminate the different spacetime regions. The remaining ones are dimensionless coupling strengths for qubits P and F: $K_J = 4d_J^2 N/(\hbar^2 v) = 2\,(g_J/\Omega_J)^2$. We will restrict to consider times where $2K_J\Omega_J t_2 \ll 1$, needed for our perturbative approach to remain valid.

Three different regions emerge from the parameters above (see Fig.12.2a). If $T_{\rm off} < r/v$, we discriminate between two possibilities. First, if $2T_{\rm on} + T_{\rm off} < r/v$ (region I), there cannot be real photon exchange, but vacuum correlations - or virtual photon exchange - are allowed at any time. If $2T_{\rm on} + T_{\rm off} > r/v$ (region II), F may start to absorb radiation emitted by P in the past somewhen in the future after an interval with no possible absorption (if $T_{\rm on} + T_{\rm off} < r/v$, region IIa) or start to absorb radiation at $t = t_1$ and stop to receive radiation somewhen in the future while the interaction is still on ($T_{\rm on} + T_{\rm off} > r/v$, region IIb). Finally, if $T_{\rm off} > r/v$ (region III) F cannot absorb radiation at all, as in region I. The difference between these two regions is that the qubits are spacelike separated in region I and timelike separated in region III. Only in regions I and III it can be said that we are dealing with a pure effect of transference of the quantum correlations between the past and the future contained in the vacuum. In region II these correlations may be assisted by a certain probability of photon exchange during a given time interval.

In Fig. 12.2b-c we show numerical results for the behavior of the concurrence as a function of $T_{\rm on}$ and $T_{\rm off}$, for coupling strengths $g_J/\Omega_J \simeq 0.1$, such as in cutting-edge experiments of ultrastrong coupling in circuit QED [285,286] and accessible values of the qubit's gaps and distance. We note that qubit-qubit entanglement is sizable in region II. However, the existence or not of entanglement in regions I and III depends much on the distance r between the qubits, as expected. Fig. 12.2b-c show a certain amount of entanglement in regions I and III,

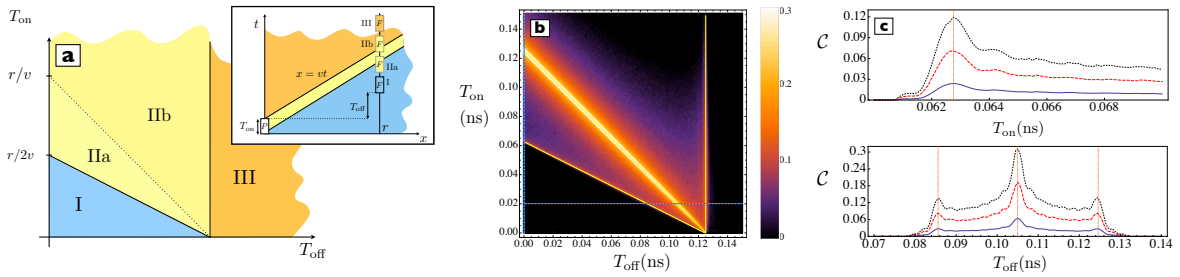

Figure 12.2: a) Diagram of the different spacetime regions. b) Concurrence vs. T_{on} and T_{off} for $g = g_P = g_F$, $\Omega = \Omega_P = \Omega_F = 2\pi \times 1\,\text{GHz}$, $g/\Omega = 0.19$, $r/\lambda = 0.125$. Significant entanglement is generated at both sides of the lines which discriminate between regions. c) Concurrence vs. T_{on} with T_{off} fixed and viceversa along the blue lines shown in b. The peaks match the position of the region edges. Entanglement is generated in region I and III for three different values of the coupling strength $g/\Omega = 0.09$ (blue, solid), 0.15 (red,dashed) and 0.19 (black, dotted) and $T_{\text{off}} = 0$. T_{off} with $T_{\text{on}} = 0.02\,\text{ns}$. Ω and r are the same as in b. The generated entanglement displays a remarkable symmetry for regions I and III.

entailing a pure transference of vacuum correlations. Remarkably, Fig. 12.2c displays also an interesting symmetry between regions I and III: for a given interaction time the entanglement that can be generated only by transference of vacuum correlations is the same regardless whether the qubits are spacelike or timelike separated. This kind of entanglement vanishes as the distance grows (see Fig. 12.3). In general, entanglement is concentrated around $\Omega_J\, T_{\text{on}} \simeq \Omega_J\, T_{\text{off}} \simeq 1$ and $\xi_{\text{on}} \simeq \xi_{\text{off}} \simeq 1$. Thus, for qubit distances of the order of λ as in Fig. 12.3, entanglement shows up in the ns regime, but drifts towards shorter times as the distance diminishes, as can be seen in Fig. 12.2b.

From the experimental viewpoint, our protocol is equally interesting -and probably more amenable- if the qubits are in region II, although the origin of entanglement generation may seem at first glance less theoretically tantalizing in that case. Notice however that even if photon exchange is allowed, our scheme does not include a projective measurement of the field state but a trace over all the field degrees of freedom instead. Under that conditions, the generation of entanglement immediately after the light-cone crossing is not trivial. For instance, this feature does not show up in the standard 3D matter-radiation Hamiltonian where the atoms would only get classical correlations until much longer times [278]. Indeed the relationship of the light cone with entanglement without measurements is a peculiarity of circuit QED in the ultrastrong coupling regime, together with the very high degree of entanglement that can be achieved. Thus, even in region II, what we are introducing here is a novel way of entanglement generation, remarkably different from the standard ones, including quantum buses in superconducting cavities [304].

We note that in our scheme concurrence is 0 for $r = 0$. This could seem at variance

with the results in [50] where extraction of vacuum correlations to pair of timelike separated qubits in the same space point is reported. But notice that in [50] a tailor-made time-dependence for the qubit gap ($\propto 1/t$) is introduced, while in our scheme the gap is constant and we just sharply tune on and off the interaction. As a matter of fact, the proposal in [50] exploits a formal analogy [49]- only fulfilled for massless fields - between the past and the future light cones and the left-right Rindler wedges. However, one must be very careful about the extent to what this analogy is valid: while it is possible to think of the vacuum state as an entangled state of modes observed by causally disconnected observers in the left-right wedges of the space-time [138], it is not clear whether this way of thinking can be transported to the past-future light cones case [3]. This was the reason of the introduction of a singular -and arguably difficult to implement experimentally- energy gap in [50]. However, we have shown that if the qubits are separated by a given distance r and the interaction can be switched on and off fast enough to have finite interaction times, past-future entanglement can be generated between qubits with constant energy gaps.

12.3 Circuit QED realization

We will thus focus on the following setting, aiming to test the results shown in Fig. 12.2. As mentioned in the introduction, it consists of a circuit QED design where two superconducting qubits interact with the vacuum field in such a way that the interaction is on during a finite time [221] and not at the same time for each qubit (see Fig. 12.1a). A first superconducting qubit P (prepared in its excited state by driving it with a microwave pulse) interacts for a time T_{on} with the vacuum field. Subsequently the interaction is switched off. Finally, after a time T_{off}, we switch on the interaction of a second qubit F, generating a certain amount of entanglement between P and F, which can be quantified with quantum state tomography [305]. It must be noted that, even if what we calculate here is a standard entanglement measure (namely the concurrence at time $t = t_2$), we could still use this quantity as a measure of quantum correlations between past and future for the case where qubit P does no longer exist after $t = -t_1$. In this case, the only novelty of the tomography process will be that the local measurements with correlated outcomes would occur at different times.

DISCUSS ULTRASTRONG BRIEFLY

[3] To have a mirror interpretation for a plane-wave-like basis like that provided in [49] we would need observers undergoing forbidden trajectories in the spacetime -horizontal hyperbolas in past and future light cones.

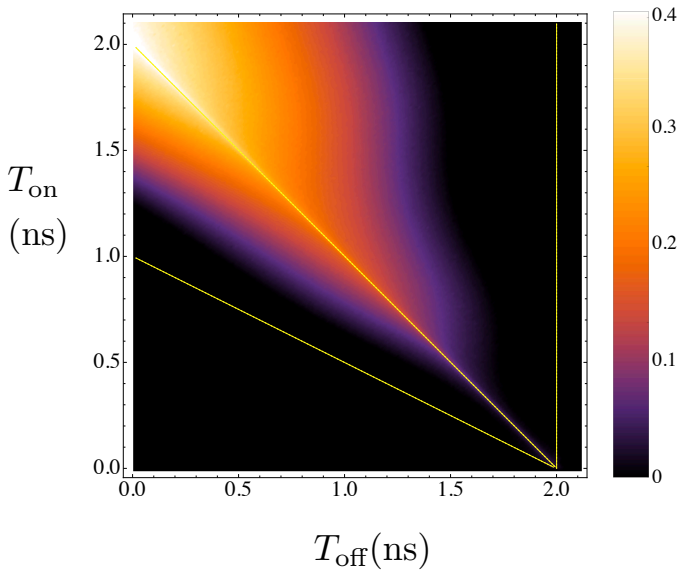

Figure 12.3: Same as in Fig.12.2b except for $r/\lambda = 2$ and $g/\Omega = 0.09$. Entanglement is restricted to region II for long distances.

12.4 Discussion

From the quantum technologies point of view, the ability to extract past-future entanglement from the field using a pair of qubits could be used to implement a device which teleports a quantum state in time - as first suggested in [50] -, or in other words, we could use the field in the transmission line for building up a novel kind of quantum memory. In order to achieve this goal, an observer - say, Paula - in possession of the qubit P and another qubit P' that she wants to teleport, should be able to carry out measurements on her qubits once the interaction had been disconnected at $-t_1$. At some time in the future after t_2, an observer - say, Frank - would use the results of Paula's measurements stored as classical information and locally manipulate the qubit F , in order to transfer the state of P' to F. The fidelity will be a function of the amount of quantum correlations between P and F. Note that during $T_{\rm off}$ the information of the quantum state of P' is codified in the field along the transmission line, regardless whatever happened to P after its interaction and measurement. Then, this information is recovered and embodied in F after its $T_{\rm on}$ and the use of the stored classical bits.

The experimental realization of quantum teleportation has already been achieved in cQED with high fidelity [306], up to the final step of single-shot qubit measurements. The fact that P and F are non-pure states should not prevent us from using them as a resource for teleportation [307, 308]. As shown in figure 12.3, entanglement is strong enough to consider high-fidelity teleportation for quantum states that are separated by times of nanoseconds.

This interval might in principle be even similar to the coherence times of the qubit and the scheme might be used as a quantum memory - provided that the coherence of the field is long enough. In our setting, that time-lapse grows with the qubit spatial separation and the inverse of the qubit gap.

We have proposed a experimentally feasible circuit QED setup to test the extraction of quantum correlations between different times contained in the vacuum of a quantum field. We have shown in particular that sizable past-future vacuum correlations can be transferred to a pair of qubits P and F, which only interact with the field in the past or the future respectively, even if the qubits do not coexist at the same time. Moreover, we discuss the possible technological uses of that entanglement extraction and the potential of our scheme to work as a quantum memory.

CHAPTER 13

Local Quanta

13.1 Introduction

Quantum Field Theory (QFT in short) has proven to be one of the most successful theories in Physics. Its potential to describe the properties of elementary particles has been richly demonstrated within the framework of the Standard Model of Particle Physics. The extraordinary agreement between theoretical and experimental values of the muon $g-2$ anomaly [309], or the recent experimental success vindicating the Higgs mechanism after decades of search [310, 311], are just two examples among many.

Elementary particles in modern physics are commonly thought of as small localized entities moving around in space. A careful examination, however, reveals such an interpretation to be problematic: in QFT a free particle is represented by a superposition of positive-frequency complex-valued modes which satisfy some field equation (e.g. the Klein-Gordon equation). Yet, no superposition of positive-frequency modes can be localized within a region of space, even for an arbitrarily small period of time [292].

This confusing issue is sometimes mistaken as superluminality, see [312] for a clarification. In fact, it can be shown that the time derivative $\dot{\psi}$, for any wave-packet ψ composed exclusively out of positive frequency modes, is non-zero almost everywhere in space.[1] . For that reason, even if ψ propagates in a perfectly causal manner according to the Klein-Gordon equation, it can hardly represent a localized entity. It is problematic to think of the fundamental field excitations of QFT as 'particles' in any common sense of the word.

The problem of localization can be analysed from other angles, for example in terms of

[1] One way of seeing this is by noting that positive frequency solutions also satisfy the square root of the Klein-Gordon equation, i.e. the Schrödinger equation $i\dot{\phi}(\vec{x},t) = \sqrt{-\nabla^2+m^2}\phi(\vec{x},t)$. From there, using the *antilocality* property of the operator $\sqrt{-\nabla^2+m^2}$, it follows that the time derivative $\dot{\phi}$ is necessarily non-zero almost everywhere in space [298]

localization systems. These are defined in terms of a set of projectors E_Δ on bounded spatial regions Δ whose expectation values yield the probability of a position measurement to find the particle within Δ. A theorem by Malament [53] shows that in a Minkowski spacetime, under reasonable assumptions for the projector algebra, no such non-trivial set of projectors exists. There is also a general result (valid for both, relativistic or non-relativistic cases) due to Hegerfeldt [292] proving that, assuming a Hamiltonian with spectrum bounded from below, the expectation value of those projectors is non-zero for almost all times. In particular this applies also to states naively thought to be localized. Also along this line, but in order to describe unsharp localization systems, Busch [313] replaced the use of projectors by more general operators, "effects" (or Positive-Operator Valued Measures – POVM), showing that it is impossible to localize with certainty a particle in any bounded region of space. Furthermore, completing the collection of no-go theorems, Clifton and Halvorson [314] have shown, under a set of natural requirements, that it is not possible to define local number operators associated to any finite region of space. At this point it is also worthwhile mention the well-known problems of other efforts, based on the use of putative observables such as the Newton-Wigner position operator [300, 315, 316].

In addition, there is also a different notion of localization called *strict localizability* [294, 296]. The basic idea is that a state, localized within a region of space at some specific moment in time, should be such that the expectation value of any operator associated to a spacelike separated region should be the same as in the vacuum. In other words, average values of local operators will depend on the state only if the observation is made in the region where the state is localized. However, as shown by Knight, no finite superposition of N-particle states can be strictly localized. Some researchers have adopted the view that the notion of strict localizability is therefore too strong, and suggested that it should be relaxed by allowing for asymptotic localization, implemented by exponential fall-offs out of the localization region. This was called *essential localization* and proposed as a criterion for deciding whether a QFT could describe particles [174].

Although the results and theorems discussed above are well-understood mathematically, they nevertheless remain puzzling from a physical point of view, as they indicate that the quanta of QFT are not, at the fundamental level, particles in any common sense of the word. The situation is further complicated when we consider quantum fields in curved spacetimes, or in the presence of an external field, where there is, in general, no well-defined notion of a particle. This is the well-known *particle number ambiguity*, which have led some researchers to claim that the notion of particle is ultimately not a useful concept. For example, in his book [165], Wald writes:

> *"Indeed, I view the lack of an algorithm for defining a preferred notion of 'particles' in QFT in curved spacetime to be closely analogous to the lack of an algorithm for defining a preferred system of coordinates in classical general relativity. (Readers familiar only with presentations of special relativity based on the use of global coordinates might well find this fact to be alarming.) In both cases, the lack of an algorithm does not, by itself, pose any difficulty for the formulation of the theory."* R. Wald

We shall not be concerned here with the usefulness of the particle concept in QFT. We will rather make practical use of this ambiguity to provide a non-standard quantization procedure yielding a QFT which, by construction, contains strictly localized one-particle states.

Our approach can be viewed as a modification and further elaboration on a previous work by Colosi and Rovelli [317]. Instead of quantizing the field using the standard stationary modes, we employ *non-stationary* modes which are, together with their time-derivatives, completely localized within a region of space at some arbitrary chosen time. These modes then evolve freely and spread out to become completely de-localized. The associated creation and annihilation operators can then be used to construct a local Fock space $\mathfrak{F}^L$ which is distinct from the Fock space $\mathfrak{F}^G$ associated with the standard quantization based on the global (i.e. non-localizable) stationary modes.

The local quantization brings along a notion of *strictly localized particle states* which means that one or more assumptions of the theorems and results discussed above do not hold in our construction. Intriguingly, the local Fock representation of the CCR can be shown to be *unitarily inequivalent* to the global Fock representation. This could be taken as an indication that the local quantization, and the associated localized particle states, are problematic. However, they yield a self-consistent QFT with well-defined state evolution and quanta having a well-defined energy expectation value after the relevant local vacuum energy has been subtracted.

This chapter is organized as follows. Section 13.2 serves to fix notation and conventions as well as to provide the basic background material. In particular, we make explicit the arbitrariness of the choice of a complete set of orthonormal modes for the quantization procedure. In Section 13.3 we briefly discuss the standard quantization based on stationary modes yielding the standard Fock space $\mathfrak{F}^G$. We then discuss the relationship between quantum theories obtained by different choices of modes and provide a sufficient condition for unitary inequivalence. In Section 13.4 a new set of local modes is introduced in order to construct the local Fock space $\mathfrak{F}^L$. Later, in Section 13.5, we prove that the local and the global representations, are unitarily inequivalent. In Section 13.6 we show the local one-particle states are *strictly* localized and evolve causally. We also prove that the Hamiltonian

can be regularized by subtraction of the local vacuum energy. By showing in Section 13.7 that the local creators and annihilators are well-defined operators in the global Fock space $\mathfrak{F}^G$, we end up with a mathematical toolbox enabling us to analyse and characterize states in $\mathfrak{F}^G$. We later check the properties of the vacuum in terms of local number operators. We exhibit the expectation values of the local number operators and quantify their correlations between the two regions. We also introduce a set of quasi-local states on $\mathfrak{F}^G$. In the section 13.8 we study the properties of these quasi-local states, including the positivity of energy and their failure to be strictly localized, while comparing them to local and global states. Then we discuss the possibility of quantum steering using the vacuum and how it relates to the Reeh-Schlieder theorem. We end up with an outline of future extensions of this work and a summary of the conclusions.

13.2 Background material, notation, and conventions

In this section we shall review some background material while fixing notations and conventions used throughout this chapter.

13.2.1 Classical scalar field

Consider a free real scalar field $\phi(x,t)$ in a one dimensional cavity of size R. Varying the Klein-Gordon action

$$S = \frac{1}{2}\int \mathrm{d}x \left(\eta^{\mu\nu}\partial_\mu\phi\partial_\nu\phi - \mu^2\phi^2\right), \tag{13.2.1}$$

and imposing Dirichlet boundary conditions $\phi(0,t) = \phi(R,t) = 0$, we obtain the Klein-Gordon equation

$$\partial_\mu\partial^\mu\phi + \mu^2\phi = (\Box + \mu^2)\phi(x,t) = 0, \tag{13.2.2}$$

where we have put $\hbar = c = 1$ and $\eta_{\mu\nu} = diag(+1,-1)$. The linearity of the equation implies that the space of solutions forms a vector space $\mathfrak{S}$.

13.2.2 Klein-Gordon inner product

The classical field is throughout this chapter taken to be real valued $\phi(x,t) : [0,R]\times\mathbb{R} \to \mathbb{R}$. Nevertheless, at the QFT level, complex valued solutions $\phi : [0,R]\times\mathbb{R} \to \mathbb{C}$ occur naturally and describe one-particle states. The vector space $\mathfrak{S}^{\mathbb{C}}$ of complex valued solutions

of (13.2.2) is equipped with a sesqui-linear (pseudo) inner product called the Klein-Gordon inner product:

$$(\phi_1|\phi_2) = i\int_0^R dx\phi_1^*(x,t)\overset{\leftrightarrow}{\partial}_t\phi_2(x,t) = i\int_0^R dx(\phi_1^*(x,t)\dot{\phi}_2(x,t) - \dot{\phi}_1^*(x,t)\phi_2(x,t)), \quad (13.2.3)$$

with $\dot{} \equiv \partial_t$. The quantity $(\phi_1|\phi_2)$ is conserved in time only if ϕ_1 and ϕ_2 are both solutions and subject to the *same* boundary conditions, i.e. $\phi_1, \phi_2 \in \mathfrak{S}^{\mathbb{C}}$. We note that the Klein-Gordon inner product is not positively definite on $\mathfrak{S}^{\mathbb{C}}$. Thus, although $\mathfrak{S}^{\mathbb{C}}$ is a vector space, it is not a Hilbert space. In fact, the Klein-Gordon product partitions the solutions space $\mathfrak{S}^{\mathbb{C}}$ into three subsets of solutions:

$$\begin{aligned} \phi \in \mathfrak{S}^{\mathbb{C}}_+ \quad &\Rightarrow \quad (\phi|\phi) > 0, \\ \phi \in \mathfrak{S}^{\mathbb{C}}_- \quad &\Rightarrow \quad (\phi|\phi) < 0, \\ \phi \in \mathfrak{S}^{\mathbb{C}}_0 \quad &\Rightarrow \quad (\phi|\phi) = 0, \end{aligned} \quad (13.2.4)$$

corresponding to solutions with positive, negative, and zero Klein-Gordon norm. Real-valued solutions are members of $\mathfrak{S}^{\mathbb{C}}_0$. Moreover, neither of the three subsets $\mathfrak{S}^{\mathbb{C}}_+$, $\mathfrak{S}^{\mathbb{C}}_-$, and $\mathfrak{S}^{\mathbb{C}}_0$ form vector spaces, let alone Hilbert spaces.

13.2.3 Mode bases and the one-particle Hilbert space

We can isolate a one-particle Hilbert space by introducing a complete and orthonormal basis, $\{f_m(x,t), f_m^*(x,t)\}$ with $m \in \mathbb{N}^+$, of the vector space $\mathfrak{S}^{\mathbb{C}}$.[2] We will require all $f_m(x,t)$ to have positive norm, which implies that the complex conjugate ones $f_m^*(x,t)$ have negative norm. The orthonormality conditions read

$$(f_m|f_n) = \delta_{mn}, \quad (f_m^*|f_n^*) = -\delta_{mn}, \quad (f_m^*|f_n) = 0. \quad (13.2.5)$$

A set of modes form a complete set if for any solution $\phi(x,t) \in \mathfrak{S}^{\mathbb{C}}$ we have the following identity

$$\phi(x,t) = \sum_m (f_m|\phi)f_m(x,t) - (f_m^*|\phi)f_m^*(x,t), \quad (13.2.6)$$

up to a zero measure set of points $x \in [0,R]$. Writing out this identity using the definition of the Klein-Gordon inner product (13.2.3) yields

$$\phi(x,t) = i\int dx' \sum_m \left(f_m^*(x',t)f_m(x,t) - f_m(x',t)f_m^*(x,t)\right)\dot{\phi}(x',t)$$

[2] The corresponding *complex structure* takes the form $\mathfrak{J} = i\left(\sum_N |f_m)(f_m| + |f_m^*)(f_m^*|\right)$.

$$- \left(\dot{f}^*_m(x',t) f_m(x,t) - \dot{f}_m(x',t) f^*_m(x,t) \right) \phi(x',t). \tag{13.2.7}$$

Since the Klein-Gordon equation is a second-order partial differential equation, $\phi(x',t)$ and $\dot{\phi}(x',t)$ are independently specifiable. Thus, for the identity to hold for any solution ϕ, and at any time t, we deduce the following completeness relations

$$\begin{aligned} 0 &= \sum_m f^*_m(x',t) f_m(x,t) - f_m(x',t) f^*_m(x,t), \\ \delta(x-x') &= i \sum_m \dot{f}_m(x',t) f^*_m(x,t) - \dot{f}^*_m(x',t) f_m(x,t). \end{aligned} \tag{13.2.8}$$

If we restrict ourselves to real fields, any such a field $\phi(x,t)$ can be expanded as

$$\phi(x,t) = \sum f_m(x,t) a_m + f^*_m(x,t) a^*_m, \tag{13.2.9}$$

where $a_m = (f_m|\phi)$ are complex numbers and $a^*_m = -(f^*_m|\phi)$, the complex conjugates of a_m.

The Hilbert space of one-particle states $\mathfrak{H}$ is then defined to be the vector space spanned by the positive norm modes f_m, i.e.

$$\mathfrak{H} = span(f_m). \tag{13.2.10}$$

The Klein-Gordon product, when restricted to the subspace $\mathfrak{H} \subset \mathfrak{S}^{\mathbb{C}}$, is by construction a positive definite sesqui-linear product. Therefore, $\mathfrak{H}$ is a Hilbert space. In general $\mathfrak{H}$ will depend on the choice of basis $\{f_m, f^*_m\}$ as defined in (13.2.10), leading to the well-known *particle number ambiguity* in QFT [164].

13.2.4 Dirac notation

To keep notation tidy and transparent it will be useful to introduce a Dirac notation to denote the vectors of $\mathfrak{S}^{\mathbb{C}}$. To that end we make the identification $\phi(x,t) \sim |\phi) \in \mathfrak{S}^{\mathbb{C}}$. We will also consider the dual space $\mathfrak{S}^{\mathbb{C}*}$; the vector space of linear maps $\mathfrak{m} : \mathfrak{S}^{\mathbb{C}} \to \mathbb{C}$. The Klein-Gordon product $(\cdot|\cdot) \to \mathbb{C}$ associates any vector $|\phi) \in \mathfrak{S}^{\mathbb{C}}$ to a member of the dual vector space through $(\phi|\cdot) \in \mathfrak{S}^{\mathbb{C}*}$ and so we will write $(\phi| \in \mathfrak{S}^{\mathbb{C}*}$. In this notation the completeness relations (13.2.8) take the succinct form

$$\sum_m |f_m)(f_m| - |f^*_m)(f^*_m| = 1, \tag{13.2.11}$$

where 1 denotes the identity operator on the vector space of solutions $\mathfrak{S}^{\mathbb{C}}$. Note that we use 'round' brackets $|\phi)$ for vectors in $\mathfrak{S}^{\mathbb{C}}$. In contrast we will use the standard brackets $|\psi\rangle$ to denote states of the corresponding QFT to which we now turn.

13.2.5 Quantization

In order to quantize the real-valued classical field $\phi(x,t)$ we first perform the Legendre transformation, which yields the Hamiltonian and canonical momenta

$$H = \int dx \frac{1}{2}\left[\pi^2 + (\nabla\phi)^2 + \mu^2\phi^2\right], \qquad \pi = \dot{\phi}. \tag{13.2.12}$$

Standard Dirac quantization now requires us to turn ϕ and π into operators $\hat{\phi}$ and $\hat{\pi}$, satisfying equal-time canonical commutation relations

$$[\hat{\phi}(x,t), \hat{\pi}(y,t)] = i\delta(x-y), \quad [\hat{\phi}(x,t), \hat{\phi}(y,t)] = 0, \quad [\hat{\pi}(x,t), \hat{\pi}(y,t)] = 0. \tag{13.2.13}$$

For notational convenience and since no confusion arises, we will refer to these operators from now on as ϕ and π, with the hats '$\hat{}$' omitted.

In order to provide a Fock representation of the CCR (13.2.13) we expand the field in some complete and orthonormal basis $\{f_m, f_m^*\}$ and write

$$\begin{aligned}\phi(x,t) &= \sum_m f_m(x,t)a_m + f_m^*(x,t)a_m^\dagger, \\ \pi(x,t) = \dot{\phi}(x,t) &= \sum_m \dot{f}_m(x,t)a_m + \dot{f}_m^*(x,t)a_m^\dagger,\end{aligned} \tag{13.2.14}$$

where $\dot{f}_m \equiv \partial_t f_m$, and a_m and $a_m^\dagger$ have been promoted into operators. If the modes $\{f_m, f_m^*\}$ satisfy the (second of the) completeness relations (13.2.8) then the following standard commutator algebra of creation and annihilation operators

$$[a_m, a_n^\dagger] = \delta_{mn}, \qquad [a_m^\dagger, a_n^\dagger] = 0, \quad [a_m, a_n] = 0, \tag{13.2.15}$$

ensures that we satisfy (13.2.13). As usual, we will define the vacuum state $|0\rangle$ to be the state annihilated by all operators a_m, i.e.

$$a_m|0\rangle = 0 \; \forall m \in \mathbb{N}^+. \tag{13.2.16}$$

A complete and orthonormal set of basis vectors $|n_1, n_2, \dots\rangle$ of the corresponding Fock space $\mathfrak{F}$ is obtained by repeated application of the creation operators on the vacuum state:

$$|n_1, n_2, \dots\rangle = \prod_m \frac{(a_m^\dagger)^{n_m}}{\sqrt{n_m!}}|0\rangle, \tag{13.2.17}$$

where the total number of particles in each basis state is required to be finite, $\sum_k n_k < \infty$, ensuring that $\mathfrak{F}$ is a separable Hilbert space [179].

$\mathfrak{F}$ is, as spanned by this basis, nothing but the symmetrized Fock space associated with the bosonic one-particle Hilbert space $\mathfrak{H}$, i.e.

$$\mathfrak{F}(\mathfrak{H}) = \bigoplus_{n=0}^{\infty} \bigotimes_{S}^{n} \mathfrak{H} = \mathbb{C} \oplus \mathfrak{H} \oplus (\mathfrak{H} \otimes_S \mathfrak{H}) \oplus \dots . \tag{13.2.18}$$

Here we note that the one-particle subspace spanned by the states $|1_m\rangle \equiv a_m^\dagger|0\rangle$ is indeed the same as $\mathfrak{H}$, or explicitly $f_m(x,t) = \langle 0|\phi(x,t)|1_m\rangle$ [318].

13.3 Non-uniqueness of the quantization procedure

In the previous section we described how to quantize a classical real-valued Klein-Gordon field, and deliberately kept the choice of orthonormal modes $\{f_k, f_k^*\}$ unspecified. Although this choice does not affect the classical field theory the situation is different at the QFT level. In fact, different choices of modes may lead to *unitarily inequivalent* Fock representations. A well-known example in this regard is of course the Fulling-Rindler quantization [172]. Examples of a different kind are given in [173]. By the Stone-von-Neumann theorem [319] this is something that can happen only for systems with infinitely many degrees of freedom, which is precisely the case of QFT [320].

13.3.1 Standard (global) quantization

The standard set of complete and orthonormal modes for a quantum field in a cavity is given by the normal modes

$$U_N(x,t) = \mathcal{U}_N(x)e^{-i\Omega_N t} = \frac{1}{\sqrt{R\Omega_N}} \sin\frac{\pi N x}{R} e^{-i\Omega_N t}, \quad U_N^*(x,t) = \mathcal{U}_N(x)e^{+i\Omega_N t}, \tag{13.3.1}$$

with $\Omega_N^2 = \frac{\pi^2 N^2}{R^2} + \mu^2$. We note that $\{U_N, U_N^*\}$ are all stationary solutions with the time dependence confined to a complex phase $e^{\pm i\Omega_N t}$. By computing the Klein-Gordon inner products, e.g. $(U_N|U_M)$, it is easily checked that these modes satisfy the orthogonality conditions (13.2.5). That they form a complete set of modes, and so satisfy the completeness relations (13.2.8), follows from the fact that they are stationary: the first of the completeness relations is identically satisfied, while the second one is satisfied because of the identity of Fourier analysis

$$\sum_N \frac{2}{R} \sin\frac{N\pi x}{R} \sin\frac{N\pi x'}{R} = \delta(x - x'). \tag{13.3.2}$$

Thus we have:

$$\sum_N |U_N)(U_N| - |U_N^*)(U_N^*| = 1. \tag{13.3.3}$$

With this choice of modes, the field operator ϕ and its conjugate momentum π take the form

$$\begin{aligned}\phi(x,t) &= \sum_N U_N(x,t)A_N + U_N^*(x,t)A_N^\dagger,\\ \pi(x,t) &= \sum_N -i\Omega_N \left(U_N(x,t)A_N - U_N^*(x,t)A_N^\dagger\right).\end{aligned} \tag{13.3.4}$$

Now, by making use of the commutation relations (13.2.15), a very simple expression of the (regularized) Hamiltonian operator can be obtained

$$H^G = H - \langle 0_G|H|0_G\rangle = \sum_N \Omega_N A_N^\dagger A_N, \tag{13.3.5}$$

where the infinite vacuum energy $\langle 0_G|H|0_G\rangle = \sum_N \frac{1}{2}\Omega_N$ has been removed. The state $|0_G\rangle$ annihilated by all A_N, will be referred to hereafter as the *global vacuum*. The basis vectors of the corresponding *global* Fock space, denoted by $\mathfrak{F}^G$, are then

$$|n_1, n_2, \dots\rangle = \prod_N \frac{(A_N^\dagger)^{n_N}}{\sqrt{n_N!}}|0\rangle, \tag{13.3.6}$$

and correspond to energy eigenstates of the Hamiltonian H^G. Needless to say, the usefulness of the global modes (13.3.1) stems from the fact that they diagonalize the Hamiltonian operator.

We call the basis (13.3.1) a *global* basis, since no state in the corresponding one-particle Hilbert space $\mathfrak{H}^G = span(U_N)$ can be fully contained within a subregion of $[0, R]$ for any arbitrarily small time interval Δt. As follows from a theorem by Hegerfeldt [292], there is no state such that $\phi(x,\tau) = \dot{\phi}(x,\tau) = 0$ for all $r < x < R$ at any time instant $t = \tau$. Instead, all states in $\mathfrak{H}^G$ have, at almost all time, support in the entire cavity, i.e. they are *global*. As a matter of fact, the non-localizability of one-particle states in Minkowski spacetime is well-known and it has been noted and widely studied in several works, e.g. [294, 296, 312].

13.3.2 Positive norm vs positive frequency

It is important to stress that in the standard global quantization the *positive (negative) norm modes* coincide with *positive (negative) frequency modes*; two conceptually distinct notions, which should not be confused. In fact, what is important for the quantization procedure and the construction of a Fock space is not the partitioning of modes into positive and negative

frequencies, but rather the partitioning into positive and negative norm modes. The latter notion does not require the basic field equations to admit symmetry under time translations but generalizes straightforwardly to non-stationary equations such as a quantum field in a time-dependent spacetime, or in the presence of a varying external field. This is so since the Klein-Gordon inner product, which defines the partitioning into positive and negative norm solutions, remains well defined also in these situations.

We shall exploit this fact in the next section.

13.4 Quantization based on local non-stationary modes

The elementary excitations of the field, defined by the Fock quantization described in Section 13.3.1, consist of global modes which are also stationary. As already mentioned before, using only positive frequencies it is not possible to construct wave packets that are completely localized within a subregion $\mathfrak{R} \subset [0, R]$ of the cavity in the sense that $\phi(x,t) = \dot{\phi}(x,t) = 0$ if $x \notin \mathfrak{R}$. This feature is a consequence of Hegerfeldt's theorem [292]. Forcing $\phi = 0$ outside the region $\mathfrak{R}$ implies a non-zero $\dot{\phi}$ outside the subregion resulting in a wave-packet that at an infinitesimal time later would become non-zero almost everywhere outside the subregion of localization. For such a case, the Hamiltonian density would be non-zero outside the subregion, and in this sense, states in $\mathfrak{H}^G$ cannot be localized.

The standard quantization of a free field relies on global non-localized excitations. Given the freedom in the choice of modes when quantizing a field (see Section 13.2.5) it is suggestive to try, alternatively, to quantize the scalar field using modes representing local excitations. Such an excitation would be, at some instant $t = \tau$, localized and hereafter free to evolve and causally spread out.

These local modes can then be used to find a Fock representation of the CCR as outlined previously, and a 'local' Fock space $\mathfrak{F}^L$ which hopefully admits strictly localized one-particle states. Nevertheless, as will be demonstrated in Section 13.5, the local Fock representation will turn out to be unitarily inequivalent to the global one.

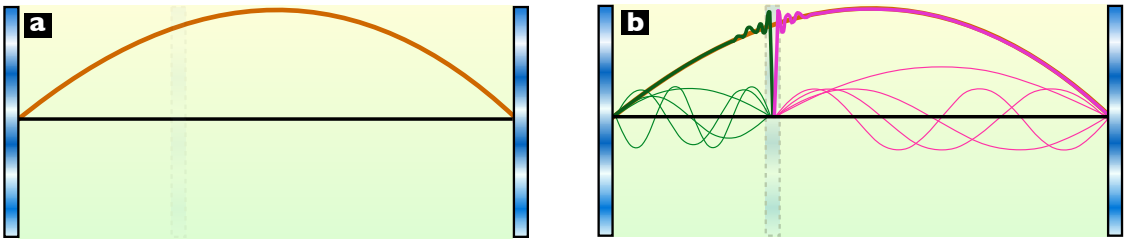

Figure 13.1: a) Simple scheme for quantization in a cavity. Global modes are used to define the one-particle Hilbert space. b) The local modes (defined by imagining an instant partitioning of the cavity), can be used to define a local one-excitation space. They form a complete set of modes, which can expand the global modes almost everywhere. In particular we see in the figure how a decomposition in local modes (up to a cutoff) would look for a global mode $N = 1$ at $t = 0$.

13.4.1 Defining a new set of local modes

In order to motivate the form of the local modes we consider what happens if we place a perfect mirror at $x = r$, imposing a Dirichlet boundary condition at that point, $\phi(x = r, t) = 0$, $\forall t \in \mathbb{R}$. Mathematically speaking we now have two distinct cavities, each with a quantum field. The complete set of orthonormal modes, $\{v_l(x,t), v_l^*(x,t)\}$ and $\{\bar{v}_l(x,t), \bar{v}_l^*(x,t)\}$ for the left and right cavities respectively, are taken to be the usual stationary modes

$$
\begin{aligned}
v_l(x,t) &= \frac{1}{\sqrt{r\omega_l}} \sin\frac{l\pi x}{r} e^{-i\omega_l t}, \qquad v_l^*(x,t) = \frac{1}{\sqrt{r\omega_l}} \sin\frac{l\pi x}{r} e^{+i\omega_l t}, \\
\bar{v}_l(x,t) &= \frac{1}{\sqrt{\bar{r}\bar{\omega}_l}} \sin\frac{l\pi (x-r)}{\bar{r}} e^{-i\bar{\omega}_l t}, \qquad \bar{v}_l^*(x,t) = \frac{1}{\sqrt{r\bar{\omega}_l}} \sin\frac{l\pi (x-r)}{\bar{r}} e^{+i\bar{\omega}_l t},
\end{aligned}
\tag{13.4.1}
$$

where $\omega_l^2 = \frac{\pi^2 l^2}{r^2} + \mu^2$, and $\bar{\omega}_l^2 = \frac{\pi^2 l^2}{\bar{r}^2} + \mu^2$, with $\bar{r} = R - r$. We now quantize the two systems yielding two quantum fields in two distinct cavities. The Fock spaces of the quantum excitations for each cavity are, by construction, localized within $[0, r]$ and $[r, R]$, respectively.

We could now try to analyse the quantum field in the *entire* cavity $[0, R]$ using such local excitations. It is clear that the introduction of a mirror at $x = r$ necessarily changes the physical conditions and we therefore are no longer dealing with the same physical system, i.e. the original cavity in $[0, R]$. At the mathematical level, the introduction of the Dirichlet boundary condition changes the solution space to something different than $\mathfrak{S}^{\mathbb{C}}$. Specifically, the modes $\{v_l(x,t), v_l^*(x,t)\}$ and $\{\bar{v}_l(x,t), \bar{v}_l^*(x,t)\}$ no longer form a basis for $\mathfrak{S}^{\mathbb{C}}$. For this reason, modes of this type are not appropriate for quantizing the field of the full cavity $[0, R]$.

The remedy, however, is simple: instead we will use the local modes (13.4.1) to define the Cauchy *initial conditions*. Although we could take modes well localized at different moments in time, we shall only consider here, for simplicity, modes $\{u_l, u_l^*\}$ and $\{\bar{u}_l, \bar{u}_l^*\}$ localized at time $t = 0$. These modes are then free to spread out over the entire box $[0, R]$ with no

Dirichlet boundary condition imposed at $x = r$. This guarantees that they are still members of the complex solution space, i.e. $u_l, u_l^*, \bar{u}_l, \bar{u}_l^* \in \mathfrak{S}^{\mathbb{C}}$.

In order to mimic the local modes we simply read off the initial conditions from the modes (13.4.1) evaluated at $t = 0$. This yields,

$$u_l(x, t = 0) = \frac{\theta(r - x)}{\sqrt{r\omega_l}} \sin \frac{l\pi x}{r} = \chi_l(x), \qquad \dot{u}_l(x, t = 0) = -i\omega_l \chi_l(x),$$
$$\bar{u}_l(x, t = 0) = \frac{\theta(x - r)}{\sqrt{\bar{r}\bar{\omega}_l}} \sin \frac{l\pi(x - r)}{\bar{r}} = \bar{\chi}_l(x), \qquad \dot{\bar{u}}_l(x, t = 0) = -i\bar{\omega}_l \bar{\chi}_l(x). \tag{13.4.2}$$

Before we determine the form of the local modes $\{u_l(x, t), u_l^*(x, t)\}$ and $\{\bar{u}_l(x, t), \bar{u}_l^*(x, t)\}$ for an arbitrary time t, i.e. solve the Cauchy problem, we should make sure that they do indeed provide a complete and orthonormal basis for the complex solutions space $\mathfrak{S}^{\mathbb{C}}$. Indeed, by explicit calculation (conveniently done at the specific time $t = 0$) we can verify that

$$(u_m|u_l) = \delta_{ml}, \qquad (u_m^*|u_l^*) = -\delta_{ml}, \qquad (\bar{u}_m^*|\bar{u}_l^*) = -\delta_{ml}, \qquad (\bar{u}_m|\bar{u}_) = \delta_{ml}. \tag{13.4.3}$$

That the modes form a complete set of solutions for $\mathfrak{S}^{\mathbb{C}}$ can be seen as follows. First we note that at time $t = 0$ the modes coincide with the Fourier basis on $[0, r]$ and $[r, R]$. By Carleson's theorem of Fourier analysis [321] we have pointwise convergence for almost all points $x \in [0, R]$, i.e. we have convergence in $L^2([0, R], \mathbb{C})$ norm.[3] This means that we can generate any initial conditions at $t = 0$ (up to equivalence in $L^2([0, R], \mathbb{C})$ norm) and thus any solution of $\mathfrak{S}^{\mathbb{C}}$ (Check Figure 13.1 for an illustration). By relating the local modes to the global ones through the Bogoliobov transformations and using the well-known completeness properties for the latter, one can also show that the local modes satisfy (13.2.8) for an arbitrary time t. Hence, in Dirac notation we have

$$\sum_l |u_l)(u_l| + |\bar{u}_l)(\bar{u}_l| - |u_l^*)(u_l^*| - |\bar{u}_l^*)(\bar{u}_l^*| = 1. \tag{13.4.4}$$

13.4.2 Bogoliubov coefficients and evolution

In order to obtain the modes $u_m(x, t)$ and $\bar{u}_m(x, t)$ for any time t we simply make use of the completeness property (13.3.2):

$$|u_m) = \left(\sum_N |U_N)(U_N| - |U_N^*)(U_N^*| \right) |u_m) = \sum_N (U_N|u_m)|U_N) - (U_N^*|u_m)|U_N^*),$$
$$|\bar{u}_m) = \left(\sum_N |U_N)(U_N| - |U_N^*)(U_N^*| \right) |\bar{u}_m) = \sum_N (U_N|\bar{u}_m)|U_N) - (U_N^*|\bar{u}_m)|U_N^*), \tag{13.4.5}$$

[3] We note that if the field ϕ is expanded using the local modes, its value in that mode basis at $x = r$ at time $t = 0$ is identically zero. Thus, we cannot expect to have convergence at $x = r$. Nevertheless, for almost all other points in $[0, R]$ we will have pointwise convergence.

or equivalently

$$u_m(x,t) = \sum_N \alpha_{mN} U_N(x,t) + \beta_{mN} U_N^*(x,t) = \sum_N (U_N|u_m) U_N(x,t) - (U_N^*|u_m) U_N^*(x,t),$$
$$\bar{u}_m(x,t) = \sum_N \bar{\alpha}_{mN} U_N(x,t) + \bar{\beta}_{mN} U_N^*(x,t) = \sum_N (U_N|\bar{u}_m) U_N(x,t) - (U_N^*|\bar{u}_m) U_N^*(x,t). \tag{13.4.6}$$

The Bogoliubov coefficients, $\alpha_{mN} = (U_N|u_m)$, $\beta_{mN} = -(U_N^*|u_m)$, etc., are independent of which time t we calculate them. Indeed, they can be conveniently calculated by easily taking $t = 0$ and using the relations (13.4.6). A straightforward calculation then yields

$$\alpha_{mN} = (U_N|u_m) \quad = (\Omega_N + \omega_m)\mathcal{V}_{mN} \tag{13.4.7a}$$
$$\beta_{mN} = -(U_N^*|u_m) = (\Omega_N - \omega_m)\mathcal{V}_{mN} \tag{13.4.7b}$$
$$\bar{\alpha}_{mN} = (U_N|\bar{u}_m) \quad = (\Omega_N + \omega_m)\bar{\mathcal{V}}_{mN} \tag{13.4.7c}$$
$$\bar{\beta}_{mN} = -(U_N^*|\bar{u}_m) = (\Omega_N - \omega_m)\bar{\mathcal{V}}_{mN} \tag{13.4.7d}$$

where

$$\mathcal{V}_{mN} = \int_0^R dx \mathcal{U}_N(x)\chi_m(x) = \frac{\frac{m\pi}{r}(-1)^m}{\sqrt{Rr\Omega_N\omega_m}(\Omega_N^2 - \omega_m^2)} \sin\frac{N\pi r}{R} \tag{13.4.8}$$
$$\bar{\mathcal{V}}_{mN} = \int_0^R dx \mathcal{U}_N(x)\bar{\chi}_m(x) = \frac{-\frac{m\pi}{\bar{r}}}{\sqrt{R\bar{r}\Omega_N\bar{\omega}_m}(\Omega_N^2 - \bar{\omega}_m^2)} \sin\frac{N\pi r}{R} \tag{13.4.9}$$

Using (13.4.6) we can see that the local modes at any time t are given by:

$$u_m(x,t) = \sum_N \left((\omega_m + \Omega_N)e^{-i\Omega_N t} - (\omega_m - \Omega_N)e^{i\Omega_N t}\right)\mathcal{V}_{mN}\mathcal{U}_N(x),$$
$$\bar{u}_m(x,t) = \sum_N \left((\bar{\omega}_m + \Omega_N)e^{-i\Omega_N t} - (\bar{\omega}_m - \Omega_N)e^{i\Omega_N t}\right)\bar{\mathcal{V}}_{mN}\mathcal{U}_N(x). \tag{13.4.10}$$

Although it is not manifest from the form of the mode expansions (13.4.10), at $t = 0$ the local modes u_m and $\bar{u}_m$ and their time derivatives $\dot{u}_m$ and $\dot{\bar{u}}_m$ are zero outside their respective region of localization. Furthermore, the local modes $u_k(x,t)$ and $\bar{u}_k(x,t)$ and their time-derivatives spread out causally from the initial region . This is illustrated for the first-excited mode $u_{m=1}$ in Figure 13.2.

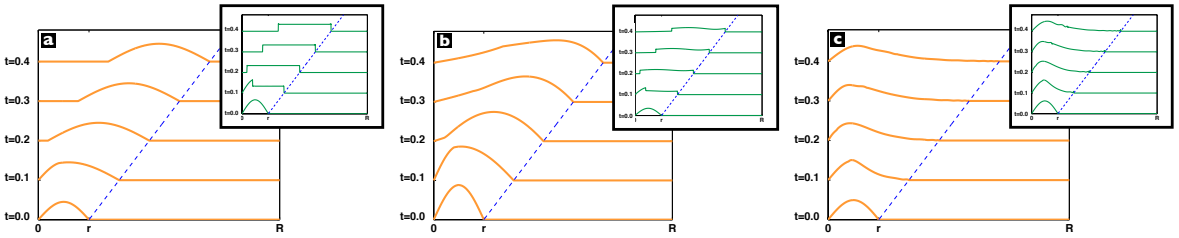

Figure 13.2: Evolution of the first-excited local mode $u_{m=1}(x,t)$ for different times $t = 0, 0.1R \ldots 0.5R$. The mode is localized at t=0 in $\mathfrak{R} = [0, 0.21R]$ within a cavity of size R . The blue dashed line represents the light-cone. a) Massless case. b) Same but with $\mu = 1/r = 1/(0.21R)$. c) Same but with $\mu = 5/r = 5/(0.21R)$. We can verify that, after the localization event in $\mathfrak{R}$ at $t = 0$ the elementary excitation *causally spreads out*, and so does its time derivative $\dot{u}_{k=1}(x,t)$. The mixing of both positive and negative global frequencies has allowed us to build up a localized mode avoiding the non-causal infinite tails that Hegerfeldt's theorem would imply.

13.4.3 Local quantization

We now turn to the quantization using these local modes. First we expand the field operator $\phi(x,t)$ using the local modes

$$\phi(x,t) = \sum_m u_m(x,t)a_m + \bar{u}_m(x,t)\bar{a}_m + u^*_m(x,t)a^\dagger_m + \bar{u}^*_m(x,t)\bar{a}^\dagger_m. \tag{13.4.11}$$

The expressions relating the local and global annihilators are given by

$$\begin{aligned} a_m &= \sum_N (u_m|U_N)A_N + (u_m|U^*_N)A^\dagger_N, \qquad a^\dagger_m = \sum_N (U_N|u_m)A^\dagger_N + (U^*_N|u_m)A_N, \\ \bar{a}_m &= \sum_N (\bar{u}_m|U_N)A_N + (\bar{u}_m|U^*_N)A^\dagger_N, \qquad \bar{a}^\dagger_m = \sum_N (U_N|\bar{u}_m)A^\dagger_N + (U^*_N|\bar{u}_m)A_N. \end{aligned} \tag{13.4.12}$$

The commutation relations

$$[a_m, a_n] = 0, \quad [a_m, a^\dagger_n] = \delta_{mn}, \quad [\bar{a}_m, \bar{a}_n] = 0, \quad [\bar{a}_m, \bar{a}^\dagger_n] = \delta_{mn}, \quad [a_m, \bar{a}_n] = 0, \quad [a_m, \bar{a}^\dagger_n] = 0,$$

and their Hermitian conjugates ensure that the canonical commutation relations (13.2.13) are satisfied. Besides, the local vacuum state $|0_L\rangle$ is defined as the state annihilated by both a_m and $\bar{a}_m$

$$a_m|0_L\rangle = \bar{a}_m|0_L\rangle = 0 \; \forall m \in \mathbb{N}^+. \tag{13.4.13}$$

The orthonormal basis vectors are given, as usual, by the repeated application of the creation operators

$$|n_1, n_2, \ldots\rangle = \prod_m \frac{(a^\dagger_m)^{n_m}}{\sqrt{n_m!}}|0\rangle_L, \qquad |\bar{n}_1, \bar{n}_2, \ldots\rangle = \prod_m \frac{(\bar{a}^\dagger_m)^{\bar{n}_m}}{\sqrt{\bar{n}_m!}}|0\rangle_L, \tag{13.4.14}$$

We note that the creator and annihilation operators corresponding to different subregions necessarily commute. From this we see that the Fock space built from local modes has a tensor product structure

$$\mathfrak{F}^L = \mathfrak{f} \otimes \bar{\mathfrak{f}}, \tag{13.4.15}$$

where $\mathfrak{f}$ and $\bar{\mathfrak{f}}$ are Fock spaces associated with the two regions $[0, r]$ and $[r, R]$. These Fock spaces are defined in the usual fashion by first defining vacuum states $|0\rangle \in \mathfrak{f}$ and $|\bar{0}\rangle \in \bar{\mathfrak{f}}$ and then the basis states by repeated application of the creators $a_m^\dagger$ and $\bar{a}_m^\dagger$. For example, the local vacuum for the whole cavity is then the tensor product $|0_L\rangle = |0\rangle \otimes |\bar{0}\rangle$ and product states can be written as $|\psi, \phi\rangle = |\psi\rangle \otimes |\phi\rangle$.

Notice that $|0_L\rangle$ is not a standard vacuum [179]. Indeed, $|0_L\rangle$ is neither *separating* nor *cyclic* with respect to any local algebra. It is not separating since $a_l|0_L\rangle = 0$ does not imply $a_l = 0$. It is not cyclic since it is a product state.

13.5 Unitary inequivalence

So far we have shown that a quantization based on a different choice of modes, i.e. the local modes, yields a different Fock representation to the one based on stationary global modes. However, as we shall now see, this local Fock representation is not unitarily related to the standard global one.

13.5.1 The unitary inequivalence of global and local representations

By the sufficient condition for unitary inequivalence stated in Section 2.2, all we have to do is to demonstrate that the sum

$$\sum_m \langle 0_G | n_m + \bar{n}_m | 0_G \rangle = \sum_N \langle 0_L | N_N | 0_L \rangle = \sum_{m,N} |(U_N^* | u_m)|^2 + |(U_N^* | \bar{u}_m)|^2 \,, \tag{13.5.1}$$

diverges. To that end it is enough to establish that (13.5.1) diverges for each value of $N \in \mathbb{N}^+$. Explicitly evaluating the sum yields

$$\sum_m |(U_N^* | u_m)|^2 + |(U_N^* | \bar{u}_m)|^2 = \sum_m \left| \frac{\sin \frac{N\pi r}{R}}{\sqrt{Rr\Omega_N \omega_m}} \frac{\frac{m\pi}{r}}{\Omega_N + \omega_m} \right|^2 + \left| \frac{\sin \frac{N\pi r}{R}}{\sqrt{Rr\Omega_N \bar{\omega}_m}} \frac{\frac{m\pi}{\bar{r}}}{\Omega_N + \bar{\omega}_m} \right|^2 . \tag{13.5.2}$$

We now proceed by making use of the integral test for convergence: the sum diverges iff the corresponding integral diverges. The integral is obtained by simply replacing the index m

with a continuous variable x, i.e.

$$\int_1^\infty dx \left(\frac{\sin^2 \frac{N\pi r}{R}}{Rr\Omega_N \sqrt{\frac{\pi^2 x^2}{r^2} + \mu^2}} \frac{\frac{x^2\pi^2}{r^2}}{\left(\Omega_N + \sqrt{\frac{\pi^2 x^2}{r^2} + \mu^2}\right)^2} + \frac{\sin^2 \frac{N\pi r}{R}}{Rr\Omega_N \sqrt{\frac{\pi^2 x^2}{\bar{r}^2} + \mu^2}} \frac{\frac{x^2\pi^2}{\bar{r}^2}}{\left(\Omega_N + \sqrt{\frac{\pi^2 x^2}{\bar{r}^2} + \mu^2}\right)^2} \right).$$

This integrand has the asymptotic behavior $\sim 1/x$ and therefore (13.5.2) diverges, which implies that

$$\sum_N \langle 0_L | N_N | 0_L \rangle = \langle 0_L | N | 0_L \rangle = \infty. \tag{13.5.3}$$

13.5.2 Analysis of the divergences

In order to proceed, it is important to understand why the sum (13.5.1) diverges. As shown in the previous section this behavior comes from summing over m and not N. Specifically, it is easy to show that although summing over m yields an infinite result

$$\langle 0_L | N_N | 0_L \rangle = \sum_m |(U_N^* | u_m)|^2 + |(U_N^* | \bar{u}_m)|^2 = \infty. \tag{13.5.4}$$

The same is not true when summing only over N, i.e. we have

$$\langle 0_G | n_m + \bar{n}_m | 0_G \rangle = \sum_N |(U_N^* | u_m)|^2 + |(U_N^* | \bar{u}_m)|^2 < \infty. \tag{13.5.5}$$

Thus, the global number operators N_N are ill defined in the local Fock space $\mathfrak{F}^L$, which also implies that A_N and $A_N^\dagger$ are not well-defined operators in $\mathfrak{F}^L$. Nevertheless, as we shall see in Section 13.7.1, it will turn out that the local number operators n_m and $\bar{n}_m$ are perfectly well defined in the global Fock space $\mathfrak{F}^G$. This mathematical asymmetry could be taken as a sign that the global Fock space $\mathfrak{F}^G$ is in this respect preferred. However, as we shall see below in Section 13.6.1, the canonical Hamiltonian (13.2.12) can be regularized by subtracting the relevant infinite (local) vacuum energy thus rendering the energy expectation values of all basis states in $\mathfrak{F}^L$ finite and well-defined. Furthermore, we will see in Section 13.6.3 that states in $\mathfrak{F}^L$ can be consistently evolved. In this sense, it seems that the unitarily inequivalent global and local quantum field theories are both possible quantizations of the real Klein-Gordon field in the one-dimensional box.

13.6 Strictly localized one-particle states and their causal evolution

In this section we shall see that the local quantization leads to a mathematically meaningful notion of *local particles*. We show that these states are strictly localized and that the evolution

is causal.

13.6.1 Local quanta and their average energy

The canonical Hamiltonian H defined by equation (13.2.12) contains an infinite vacuum energy, which is regularized by subtraction, i.e.

$$H^G = H - \langle 0_G|H|0_G\rangle. \tag{13.6.1}$$

This regularized Hamiltonian H^G defines a notion of energy of states in the global Fock space $\mathfrak{F}^G$. [4]

We now turn to the question of whether we can define a meaningful notion of energy in the local Fock space $\mathfrak{F}^L$. A good guess is that the regularized Hamiltonian

$$H^L = H - \langle 0_L|H|0_L\rangle, \tag{13.6.2}$$

obtained by subtracting the infinite energy of the local vacuum, is well defined in the local Fock space $\mathfrak{F}^L$. Let us see how this works out. We first define $\mathcal{E}$ as the expectation value of H^G on the local vacuum, i.e.

$$\mathcal{E} \equiv \langle 0_L|H^G|0_L\rangle. \tag{13.6.3}$$

Next we compute the energy expectation value of a local n-particle state $\langle m_l, \bar{0}|H^G|m_l, \bar{0}\rangle$. Substituting the Bogoliobov relations

$$\begin{aligned} A_N &= \sum_l (U_N|u_l)a_l + (U_N|u_l^*)a_l^\dagger + (U_N|\bar{u}_l)\bar{a}_l + (U_N|\bar{u}_l^*)\bar{a}_l^\dagger, \\ A_N^\dagger &= \sum_l (u_l|U_N)a_l^\dagger + (u_l^*|U_N)a_l + (\bar{u}_l|U_N)\bar{a}_l^\dagger + (\bar{u}_l^*|U_N)\bar{a}_l, \end{aligned} \tag{13.6.4}$$

into the definition of H^G we obtain

$$\langle m_l, \bar{0}|H^G|m_l, \bar{0}\rangle = m_l \sum_N \Omega_N \left(|(u_l|U_N)|^2 + |(u_l^*|U_N)|^2\right) + \mathcal{E}.$$

For $m_l = 0$ we would have $\langle 0_L|H^G|0_L\rangle = \mathcal{E}$ and therefore we can write

$$\langle m_l, \bar{0}|H^L|m_l, \bar{0}\rangle = m_l \sum_N \Omega_N \left(|(u_l|U_N)|^2 + |(u_l^*|U_N)|^2\right). \tag{13.6.5}$$

[4] Although the global Hamiltonian H^G is an operator in $\mathfrak{F}^G$, some states in $\mathfrak{F}^G$ may lie outside its domain and thus have an infinite/ill-defined average energy, being for this reason unphysical.

From here we see that the local n-particle state $|m_l, \bar{0}\rangle$ contains m_l units of quanta with the manifestly positive *average* energy

$$\epsilon_l = \sum_N \Omega_N \left(|(u_l|U_N)|^2 + |(u_l^*|U_N)|^2 \right). \tag{13.6.6}$$

A simple integral test of convergence reveals that ϵ is indeed convergent (the corresponding integrand has the asymptotic behavior $\sim \frac{\sin^2 x}{x^2}$). Thus, the regularized Hamiltonian H^L yields finite expectation values for all n-particle particle states $|m_l, \bar{0}\rangle$. Repeating the above calculations we can also see that the n-particle states $|0, \bar{n}_l\rangle$ have finite energy and so do all basis states $|n_l, \bar{n}_m\rangle$. Thus, all basis states of $\mathfrak{F}^L$ and finite superpositions of them will have finite average energy.

13.6.2 Strict localization on the local vacuum

We now proceed to construct *strictly localized* one-particle states in $\mathfrak{F}^L$. As briefly mentioned in the introduction, a state $|\psi\rangle$ is said to be *strictly localized* [294] within a region of space $\mathfrak{R}$ if the expectation value of any local operator $\mathcal{O}(x)$ outside that region (i.e. $x \notin \mathfrak{R}$) is identical to that of the vacuum, i.e.

$$\langle\psi|\mathcal{O}(x)|\psi\rangle = \langle 0|\mathcal{O}(x)|0\rangle \text{ if } x \notin \mathfrak{R}.$$

Since we have based our local quantization on modes u_m and $\bar{u}_m$ which are localized within the regions $[0, r]$ and $[r, R]$ it is reasonable to expect that the one-particle excitation

$$|1_m, \bar{0}\rangle \equiv a_m^\dagger |0_L\rangle = a_m^\dagger |0, \bar{0}\rangle,$$

is strictly localized within $[0, r]$.

Indeed this is the case. The only operators we can build outside the region $[0, r]$, i.e. in $[r, R]$, are expansions in the annihilators and creators $\bar{a}_m$ and $\bar{a}_m^\dagger$, and these all commute with $a_m^\dagger$. Hence, we have

$$\langle\psi|\mathcal{O}(\bar{a}_m, \bar{a}_m^\dagger)|\psi\rangle = \langle 0_L|a_m \mathcal{O}(\bar{a}_m, \bar{a}_m^\dagger) a_m^\dagger|0_L\rangle = \langle 0_L|\mathcal{O}(\bar{a}_m, \bar{a}_m^\dagger) a_m a_m^\dagger|0_L\rangle = \langle 0_L|\mathcal{O}(\bar{a}_m, \bar{a}_m^\dagger)|0_L\rangle,$$

verifying that the state $|1_m, \bar{0}\rangle$ is a strictly localized one-particle state. Clearly, the quantization based on local non-stationary modes provides us with a natural notion of a local particle within the local QFT. Notice however that the notion of strict localization introduced by Knight in [294] made use of the Minkowski vacuum based on stationary solutions of the Klein-Gordon equation. The analogous vacuum state would not be the local vacuum $|0_L\rangle$, but rather the global vacuum $|0_G\rangle$, which is also constructed using stationary modes. As a

matter of fact, the possibility of strictly localized states in $\mathfrak{F}^L$ has to do with the separability of $|0_L\rangle = |0\rangle \otimes |\bar{0}\rangle$, a property not shared by $|0_G\rangle$. Furthermore, local one-particle states do *not* belong to the global Fock space $\mathfrak{F}^G$, which is, as we have shown above, associated with a Fock representation unitarily inequivalent to the local one. We see here that the possibility of local particle states is in our construction intimately related to the existence of unitarily inequivalent representations within QFT.

This construction result should not be considered a mathematical counter-example to the no-go theorems presented in [53, 294, 300]. Indeed, our system does not exhibit translational covariance since we are dealing with a finite box with Dirichlet boundary conditions imposed at the endpoints. It seems nonetheless plausible to us that additional assumptions might be violated in the limit of an infinite unbounded box admitting translation invariance. This possibility should be investigated further.

13.6.3 Causal propagation of local states

The evolution of states in $\mathfrak{F}^L$ is defined by the unitary operator $U^L(t) = \exp(-iH^L t)$ which trivially commutes with H^L, implying that the total energy is conserved. We also note that none of the local n-particle states are eigenstates of H^L, in particular not the local vacuum $|0_L\rangle$. For this reason it will be interesting to study the evolution of these strictly localized states and verify whether they propagate causally, or not.

To do this we shall have to introduce a third region $[\tilde{r}, R]$ with $\tilde{r} > r$ and the local modes associated with it. We define these modes to be completely localized within $[\tilde{r}, R]$ at a *later* moment in time $t = \tau > 0$:

$$\tilde{u}_l(x, t=\tau) = \frac{\theta(x-\tilde{r})}{\sqrt{\tilde{r}\tilde{\omega}_l}} \sin\frac{l\pi(x-\tilde{r})}{R-\tilde{r}} = \bar{\chi}_l(x), \quad \dot{\tilde{u}}_l(x, t=0) = -i\tilde{\omega}_l\tilde{\chi}_l(x) \quad \tilde{\omega}_l^2 = \frac{\pi^2 l^2}{(R-\tilde{r})^2} + \mu^2$$

This defines a new set of creators and annihilators $\tilde{a}_l$ and $\tilde{a}_l^\dagger$ related to the global ones as

$$\begin{aligned} \tilde{a}_l &= \sum_N (\tilde{u}_l|U_N)A_N + (\tilde{u}_l|U_N^*)A_N^\dagger, \\ \tilde{a}_l^\dagger &= \sum_N (U_N|\tilde{u}_l)A_N^\dagger + (U_N^*|\tilde{u}_l|)A_N. \end{aligned} \tag{13.6.7}$$

The local operators $\tilde{\mathcal{O}}(\tau)$ associated with the region $[\tilde{r}, R]$ at time $t = \tau$ will be generated by series expansions in $\tilde{a}_l$ and $\tilde{a}_l^\dagger$.

We can now calculate the commutator $[a_m, \tilde{a}_n^\dagger]$ obtaining

$$[\tilde{a}_n, a_m^\dagger] = \sum_{M,N} \Big[(\tilde{u}_n|U_N)A_N + (\tilde{u}_n|U_N^*)A_N^\dagger, (U_M|u_m)A_M^\dagger + (U_M^*|u_m)A_M\Big]$$

$$= \sum_{M,N} \Big[(\tilde{u}_n|U_N)(U_M|u_m)[A_N, A_M^\dagger] + (\tilde{u}_n|U_N^*)(U_M^*|u_m)[A_N^\dagger, A_M] \Big]$$

$$= (\tilde{u}_n| \left(\sum_N |U_N)(U_N - |U_N^*)(U_N^*| \right) |u_m) = (\tilde{u}_n|u_m).$$

An identical calculation yields $[\tilde{a}_n, a_m] = -(\tilde{u}_n|u_m^*)$.

The fact that the local modes propagate causally (see Section 13.4.2) means that $(\tilde{u}_n|u_m)$ and $(\tilde{u}_n|u_m^*)$ are zero whenever $\tau < |r - \tilde{r}|$, which in turn implies that a_m and $a_m^\dagger$ commute with $\tilde{a}_n$ and $\tilde{a}_n^\dagger$. Thus, any local observable $\tilde{\mathcal{O}}(\tau)$ will commute with $a_m^\dagger$ and a_m whenever $\tau < |r - \tilde{r}|$, that is, whenever the spacetime regions associated with the operators $\tilde{\mathcal{O}}(\tau)$ and the pair $\{a_m, a_n^\dagger\}$ are spacelike. This way, micro-causality is built into the construction.

Besides, we have clearly that

$$\langle 1_m, \bar{0}|\tilde{\mathcal{O}}(\tau)|1_m, \bar{0}\rangle = \langle 0_L|a_m\tilde{\mathcal{O}}(\tau)a_m^\dagger|0_L\rangle = \langle 0_L|\tilde{\mathcal{O}}(\tau)a_m a_m^\dagger|0_L\rangle = \langle 0_L|\tilde{\mathcal{O}}(\tau)|0_L\rangle, \qquad (13.6.8)$$

for $\tau < |r - \tilde{r}|$, which implies that the local one-particle state $|1_m, 0\rangle$ propagates causally as it should. This situation should be contrasted to Knight's strict localization [294] which would state

$$\langle 0_G|a_m\tilde{\mathcal{O}}(\tau)a_m^\dagger|0_G\rangle = \langle 0_G|\tilde{\mathcal{O}}(\tau)|0_G\rangle, \qquad (13.6.9)$$

which in fact does not hold since, as will become clear below, $a_m a_m^\dagger|0_G\rangle \neq |0_G\rangle$.

13.7 Local analysis of the global vacuum

In Section 13.5.2, we pointed to a mathematical asymmetry between the local and global quantum theories. We saw that, while the global number operators are ill defined in $\mathfrak{F}^L$, the case is different for the local number operators as defined in $\mathfrak{F}^G$. In this section we shall demonstrate that the local creators and annihilators are indeed well-defined operators in $\mathfrak{F}^G$, which will allows us to analyse global states using number operators associated with the local quantization. In particular, we will examine the spectrum of local particles and numerically quantify existent space-like correlations of the global vacuum $|0_G\rangle$.

13.7.1 Local operators in $\mathfrak{F}^G$

Let us now show that the local creator and annihilators a_l, $a_l^\dagger$, $\bar{a}_l$, and $\bar{a}_l^\dagger$ are well-defined operators in $\mathfrak{F}^G$. Here we will prove this for a_l. The proof is identical for $a_l^\dagger$, $\bar{a}_l$, and $\bar{a}_l^\dagger$.

It suffices to show that $\langle\psi|a_l^\dagger N a_l|\psi\rangle < \infty$ for any basis state $|\psi\rangle = |n_1, n_2, \dots\rangle$ of $\mathfrak{F}^G$. We first expand the local annihilator

$$a_l = \sum_N (u_l|U_N) A_N + (u_l|U_N^*) A_N^\dagger. \tag{13.7.1}$$

We have that

$$\begin{aligned} a_l|n_1, \dots, n_N, \dots\rangle &= \left(\sum_N (u_l|U_N) A_N + (u_l|U_N^*) A_N^\dagger\right) |n_1, \dots, n_N, \dots\rangle \\ &= \sum_N (u_l|U_N)\sqrt{n_N}|n_1, \dots, n_N - 1, \dots\rangle + (u_l|U_N^*)\sqrt{n_N+1}|n_1, \dots, n_N + 1, \dots\rangle. \end{aligned}$$

Multiplying by the number operator $N = \sum_N N_N$, we obtain

$$\begin{aligned} N a_l|n_1, \dots, n_N, \dots\rangle = \sum_N &(u_l|U_N)\sqrt{n_N}(n-1)|n_1, \dots, n_N - 1, \dots\rangle \\ &+ (u_l|U_N^*)\sqrt{n_N+1}(n+1)|n_1, \dots, n_N + 1, \dots\rangle, \end{aligned} \tag{13.7.2}$$

where n is the number of particles of the basis state, i.e. $N|n_1, n_2, \dots\rangle \equiv n|n_1, n_2, \dots\rangle$. Sandwiching with $\langle n_1, \dots, n_N, \dots|a_l^\dagger$ now gives

$$\langle n_1, \dots, n_N, \dots|a_l^\dagger N a_l|n_1, \dots, n_N, \dots\rangle = \sum_N |(u_l|U_N)|^2 n_N(n-1) + |(u_l|U_N^*)|^2(n_N+1)(n+1).$$

Since

$$\sum_N |(u_l|U_N)|^2 < \infty, \qquad \sum_N |(u_l|U_N^*)|^2 < \infty, \tag{13.7.3}$$

and given that $|n_1, n_2, \dots\rangle$ is a basis state of $\mathfrak{F}^G$ (therefore satisfying $n = \sum_N n_N < \infty$), we see that the action of a_l on any basis state is not pathological . An analogous demonstration with minor changes shows that finite expectation values for the global Hamiltonian are also obtained for these vectors. Thus, since both demonstrations also go through for $a_l^\dagger$, $\bar{a}_l$, and $\bar{a}_l^\dagger$, we have shown that the local creators and annihilators are well-defined linear operators in $\mathfrak{F}^G$ and gi. Nevertheless, as we have stressed above in Section 13.5.2, the situation is not symmetric since A_N and $A_N^\dagger$ are not well defined in $\mathfrak{F}^L$.

13.7.2 Local particle spectrum of the global vacuum

The global vacuum is defined to have zero global particles, i.e $\langle 0_G|N_N|0_G\rangle = 0$. On the other hand, the local quantization developed above yields a natural notion of local particle number $n_l = a_l^\dagger a_l$, $\bar{n}_l = \bar{a}_l^\dagger \bar{a}_l$, corresponding to the number of local excitations we have in the left and right regions of the box, $[0, r]$ and $[r, R]$, respectively. Let us now ask what

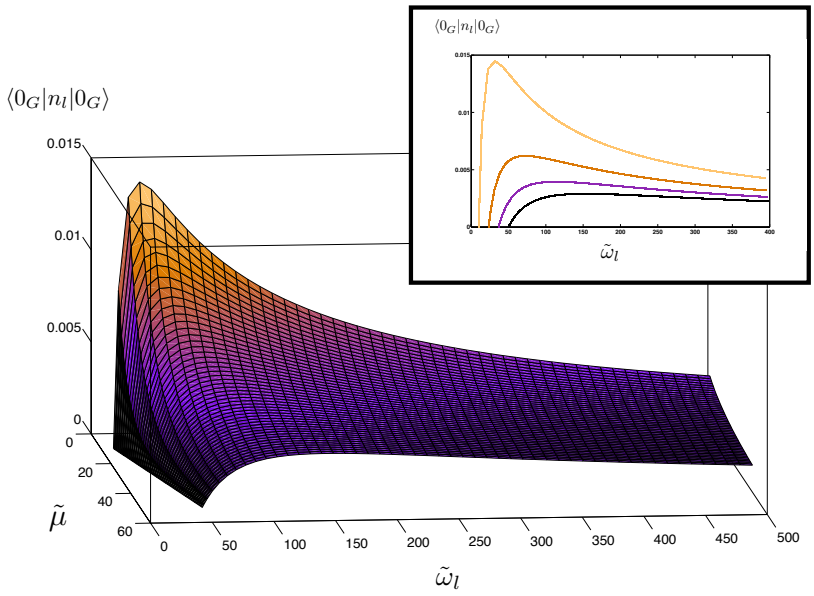

Figure 13.3: Number of local quanta of energy ω_l expected value for the global vacuum for different masses $\mu = \frac{\tilde{\mu}}{R}$ with $\tilde{\mu} \in (10, 50)$. The region of localization is taken to be $\tilde{r}^{-1} = R/r = \pi$. The inset shows discrete values in the same interval for the masses. Higher plots correspond to smaller values. The distribution of local particles in the global vacuum resembles a Planckian spectrum, i.e. a thermal bath of particles.

the distribution of local particles is for the global vacuum. To see this we compute the expectation values

$$\langle 0_G|n_l|0_G\rangle = \langle 0_G|a_l^\dagger a_l|0_G\rangle = \sum_N \frac{l^2\pi^2}{Rr^3\Omega_N\omega_l}\frac{1}{(\Omega_N+\omega_l)^2}\sin^2\frac{\pi N r}{R}. \tag{13.7.4}$$

These depend on three distinct quantities: the size of the cavity R, the size of the region of localization $r < R$, and the mass μ. We could plot the expectation values for different values of these three magnitudes. However, it is more adequate to vary dimensionless quantities, e.g. r/R, $r\mu$, and $R\mu$. We might as well fix $R = 1$, ending up with two independent dimensionless quantities $\tilde{r} = r/R$ and $\tilde{\mu} = R\mu$. Figures 13.3 and 13.4 show the dependence of the expectation values (13.7.4) on these two variables.

In Figure 13.3 we see that when we increase the mass μ we have that

$$\langle 0_G|n_l|0_G\rangle = \sum_N |(u_l|U_N^*)|^2 \to 0.$$

In fact, in the large mass limit the coefficients $(u_l|U_N^*)$ have the asymptotic behavior $\sim \mu^{-2}$ while $(u_l|U_N)$ converge to a non-zero value. Indeed, it is well known that the Compton wavelength $\lambda_C = \mu^{-1}$ determines how well localized a wave-packet, made out of positive frequency modes, can be [315, 322, 323]. Thus, in the limit $\lambda_C \to 0$, or equivalently $\mu \to \infty$, the β-coefficients $(u_l|U_N^*)$ should approach zero.

Another interesting limit is when $r \to R$, case in which local and global modes converge. Intuitively we would expect the local description to approach the global one so that the expectation value of local particles goes to zero (since the global vacuum is defined to have zero global particles). This is illustrated in Figure 13.4. This intuition can be made mathematically precise by studying the convergence of the operators $a_m \to A_m$ as $r \to R$. [5] The relationship between the operators is given by

$$a_l = \sum_N (u_l|U_N)A_N + (u_l|U_N^*)A_N^\dagger, \tag{13.7.5}$$

where

$$\begin{aligned}(u_l|U_N) &= \frac{1}{\sqrt{Rr\Omega_N\omega_l}} \frac{\frac{l\pi}{r}(-1)^l}{\Omega_N - \omega_l} \sin\frac{N\pi r}{R},\\ (u_l|U_N^*) &= -\frac{1}{\sqrt{Rr\Omega_N\omega_l}} \frac{\frac{l\pi}{r}(-1)^l}{\Omega_N + \omega_l} \sin\frac{N\pi r}{R}.\end{aligned} \tag{13.7.6}$$

From here it is easy to show that $(u_l|U_N^*) \to 0$ and $(u_l|U_N) \to \delta_{lN}$ in the limit $r \to R$. It is now clear that we have convergence of a_l and A_l in the *strong* operator topology.

It is important to note that because of unitary inequivalence, the total number of local particles is necessarily infinite, i.e. $\sum_m \langle 0_G|n_m + \bar{n}_m|0_G\rangle = \infty$. In fact, even though Bogoliobov coefficients converge to finite values when $r \to R$, the sum diverges for any r arbitrarily close to R. This is due to the fact that the sum over m and the limit $r \to R$ do not commute, i.e.

$$\lim_{r\to R}\sum_m \langle 0_G|n_m + \bar{n}_m|0_G\rangle \neq \sum_m \lim_{r\to R}\langle 0_G|n_m + \bar{n}_m|0_G\rangle = 0. \tag{13.7.7}$$

[5] We note that for any notion of convergence to make mathematical sense, the operators must act in the same vector space. For example, it is meaningless to claim that a_k converges to A_N as operators defined in the local Fock space $\mathfrak{F}^L$. Indeed, the operators A_N are not even well defined in $\mathfrak{F}^L$. Nonetheless, it is meaningful to study the convergence $a_k \to A_k$ as operators defined in $\mathfrak{F}^G$.

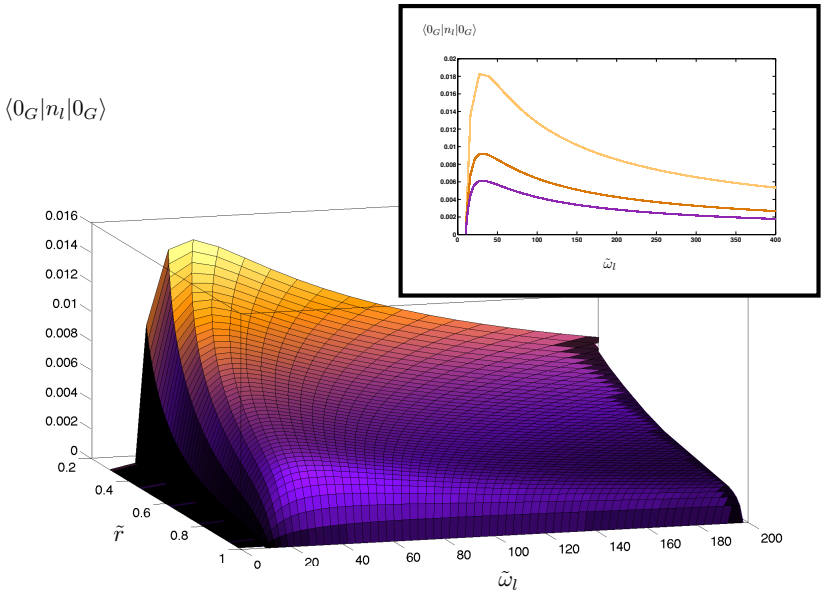

Figure 13.4: Number of particles for the global vacuum for different sizes of the localization region $r \in (0.25R, R)$ with fixed $R = 1$ and $\lambda_c = \frac{R}{10}$. As expected, when $r = R$ the expectation value of the vacuum is zero for all modes, since local and global modes are the same.

Another interesting case is the limit $r \to 0$. Inspecting the coefficients reveal that both $(u_l|U_N)$ and $(u_l|U_N^*)$ have the asymptotic behavior $\sim r$ and thus vanish in the limit. However, the sum $\sum_m \langle 0_G|n_m|0_G\rangle$ approaches a finite non-zero value when $r \to 0$.

13.7.3 Vacuum entanglement

As a second application we will look at vacuum entanglement. We shall study the entanglement between the two regions $[0, r]$ and $[r, R]$ by computing the correlations between local particle numbers as given by $\text{cov}(n_m, \bar{n}_l)$ defined by

$$\text{cov}(n_m, \bar{n}_l) \equiv \langle\psi|n_m\bar{n}_n|\psi\rangle - \langle\psi|n_m|\psi\rangle\langle\psi|\bar{n}_n|\psi\rangle. \tag{13.7.8}$$

We note that if we choose $|\psi\rangle = |0_L\rangle$ then $\text{cov}(n_n, \bar{n}_m)$ is identically zero. However, this is not so for the global vacuum $|\psi\rangle = |0_G\rangle$. The correlations of the global vacuum are more conveniently characterized by the dimensionless values

$$\begin{aligned}\text{corr}(n_m, \bar{n}_n) &= \frac{\langle 0_G|n_m\bar{n}_n|0_G\rangle - \langle 0_G|n_m|0_G\rangle\langle 0_G|\bar{n}_n|0_G\rangle}{\sqrt{\langle 0_G|n_m^2|0_G\rangle - \langle 0_G|n_m|0_G\rangle^2}\sqrt{\langle 0|\bar{n}_n^2|0_G\rangle - \langle 0_G|\bar{n}_n|0_G\rangle^2}} \\ &= \frac{\text{cov}(n_m, \bar{n}_n)}{\sqrt{\text{cov}(n_m, n_m)\text{cov}(\bar{n}_n, \bar{n}_n)}},\end{aligned} \tag{13.7.9}$$

which are known as the correlation coefficients.

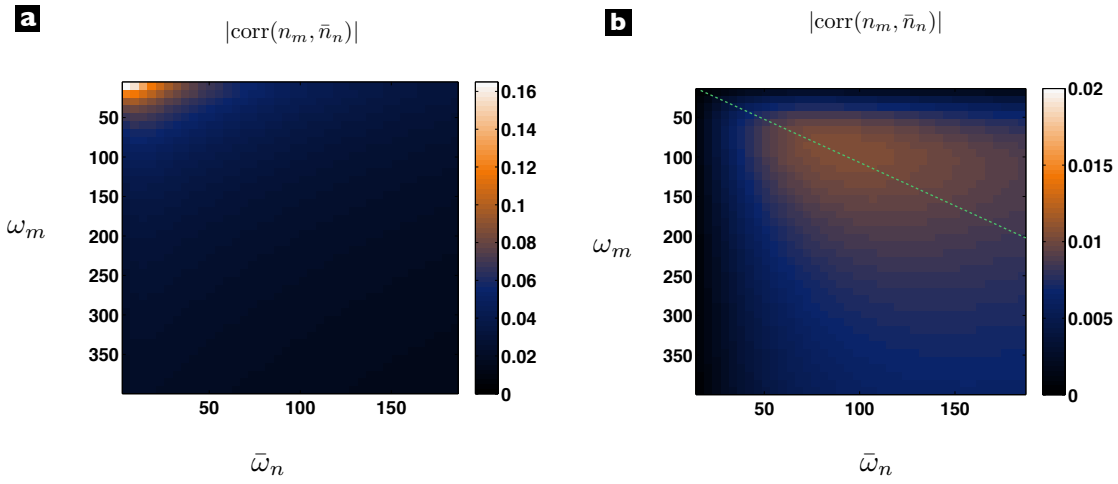

Figure 13.5: Values for the dimensionless correlation coefficients $\mathrm{corr}(n_m, \bar{n}_n)$ for (a) a massless field, and (b) a massive field with $\mu = 5/r$. For both cases the localization region $\mathfrak{R}$ has a size $r = R/\pi$. Notice that instead of plotting with respect to the mode indexes, we are using the mode frequencies. The green line in figure (b) shows the points for which $\omega \simeq \bar{\omega}$

From equation (13.4.12) we have

$$\begin{aligned}\langle 0_G|n_m\bar{n}_n|0_G\rangle &= \langle 0_G|a_m^\dagger a_m \bar{a}_n^\dagger \bar{a}_n|0_G\rangle = \\ &= \sum_{M,N}(U_M^*|u_m)(u_m|U_N)(U_N|\bar{u}_n)(\bar{u}_n|U_M^*) + (U_M^*|u_m)(u_m|U_N)(U_M|\bar{u}_n)(\bar{u}_n|U_N^*) \\ &\quad + (U_M^*|u_m)(u_m|U_M^*)(U_N^*|\bar{u}_n)(\bar{u}_n|U_N^*) \end{aligned} \tag{13.7.10}$$

On the other hand we have that

$$\langle 0_G|n_m|0_G\rangle\langle 0_G|\bar{n}_n|0_G\rangle = \sum_{M,P}(U_M^*|u_m)(u_m|U_M^*)(U_P^*|\bar{u}_n)(\bar{u}_n|U_P^*) \tag{13.7.11}$$

and thus

$$\begin{aligned}&\langle 0_G|n_m\bar{n}_n|0_G\rangle - \langle 0_G|n_m|0_G\rangle\langle 0_G|\bar{n}_n|0_G\rangle = \\ &= \sum_{M,P}(U_M^*|u_m)(u_m|U_P)(U_P|\bar{u}_n)(\bar{u}_n|U_M^*) + (U_M^*|u_m)(u_m|U_P)(U_M|\bar{u}_n)(\bar{u}_n|U_P^*)\end{aligned} \tag{13.7.12}$$

and using the computed inner products (13.4.7) and equation (13.7.4) we obtain

$$\mathrm{corr}(n_m, \bar{n}_n) = \frac{\frac{2\pi^4 m^2 n^2}{R^2 r^3 \bar{r}^3 \omega_m \bar{\omega}_n}\sum_{N,P}\left[\frac{\sin^2\frac{N\pi r}{R}}{\Omega_N\Omega_P(\Omega_N+\omega_m)}\frac{\sin^2\frac{P\pi r}{R}(\Omega_N\Omega_P-\bar{\omega}_n^2)}{(\Omega_P-\omega_m)(\Omega_N^2-\bar{\omega}_n^2)(\Omega_P^2-\bar{\omega}_n^2)}\right]}{\sqrt{\sum_{l,N}\frac{l^2\pi^2}{R r^3\Omega_N\omega_l}\frac{1}{(\Omega_N+\omega_l)^2}\sin^2\frac{\pi N r}{R}}\sqrt{\sum_{l,N}\frac{l^2\pi^2}{R \bar{r}^3\Omega_N\bar{\omega}_l}\frac{1}{(\Omega_N+\bar{\omega}_l)^2}\sin^2\frac{\pi N \bar{r}}{R}}} \tag{13.7.13}$$

an expression that can be numerically evaluated, see Figure 13.5.

A first look to the figures 13.5a and 13.5b reveals that high frequency modes are less correlated than low frequency ones. For small masses ($\mu \ll 1/r$ i.e. $\lambda_C \gg r$) we observe that the maximum of correlations corresponds to the smallest possible frequency value π/r for the localization region (top left corner of figure 13.5a). As the value of the field mass μ increases, the magnitude of the correlations reduces. This is seen by just directly comparing the color scales of 13.5a and 13.5b. Also, as the mass grows, the position of the correlation maximum $(\omega_{\text{max}}, \bar{\omega}_{\text{max}})$ increases linearly, moving along a line of equal frequencies ω and $\bar{\omega}$. For big masses ($\mu \gg 1/R$, i.e. $\lambda_C \ll r$) this is easier to see. For that case $\omega_{\text{max}} \simeq \bar{\omega}_{\text{max}} \propto \mu$, as can be checked in Fig. 13.6a.

Fig. 13.6b, on the other hand, shows the maximum value of the correlations for increasing values of the mass. For the values considered we can see the existence of a power law showing that the correlations decrease as $\text{corr}_{\text{max}} \propto \mu^{-1}$.

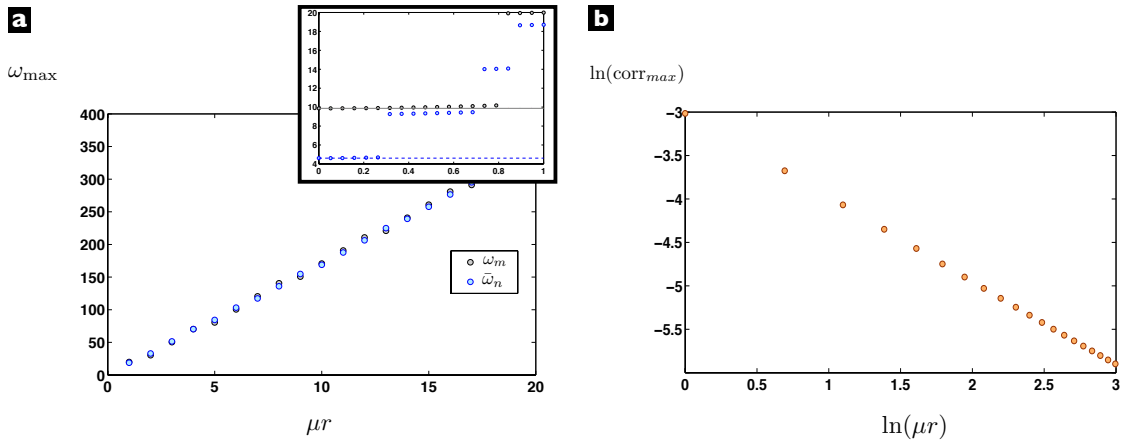

Figure 13.6: a) Frequency plot corresponding to the maximum of correlations for highly massive fields ($\lambda_C < r$). ω_{max} is shown in grey dots, $\bar{\omega}_{\text{max}}$ in blue dots. As we can see both values almost coincide. The inset shows the behavior for small masses. The grey line (solid) corresponds to the minimum frequency value $\omega_{\text{min}} = \pi/r$, while the blue line (dashed) corresponds to the minimum $\bar{\omega}_{\text{min}} = \pi/(R-r)$. b) Value of the logarithm of the maximum correlation coefficient versus the logarithm of the mass μr. The slope takes the value -1. The localization region $\mathfrak{R}$ has a size $r = R/\pi$ for both cases (a) and (b).

13.8 Properties of quasi-local states on the global Fock space

As we have seen in Section 13.6.2, the local quantization based on non-stationary modes yields a natural notion of local one-particle states in $\mathfrak{F}^L$ defined by $a_m^\dagger|0_L\rangle$. On the other hand, since the local creators are well-defined in $\mathfrak{F}^G$, this suggests a natural class of one-

particle states $a_m^\dagger|0_G\rangle$ that we will call *quasi-local states* defined in $\mathfrak{F}^G$. In this section we shall examine the properties of these states. In particular, their failure to be strictly localized states is directly related to the Reeh-Schlieder theorem and vacuum entanglement.

13.8.1 Positivity of energy

For historical reasons - coming from the early attempts of interpreting the solutions of second order Klein-Gordon equation as one-particle wave-functions - it is commonplace to associate the negative frequency states U_N^* with negative energies, and for this reason to regard them as unphysical states. From that point of view it might seem alarming that we have constructed our local modes using both positive and negative frequency energy-eigenstates, i.e. both U_M and U_N^*. Nonetheless, the problem with negative frequencies is a problem in that interpretation and not in relativistic QFT. Indeed, when we adopt the perspective that relativistic QFT arises from the quantization of a relativistic field, no problems associated with negative frequencies appear. Instead the frequencies are related to energy changes associated with the creation or annihilation of individual quanta.

The classical canonical Hamiltonian

$$H = \int dx \frac{1}{2}(\pi^2 + (\partial_x \phi)^2 + \mu^2 \phi^2) \geq 0, \tag{13.8.1}$$

being a sum of squares, is manifestly positive definite and is thus bounded from below by zero. As a quantum operator in the corresponding QFT, it is of course ill-defined due to the infinite vacuum energy. Notwithstanding, the regularized Hamiltonian is a sum of the positive operators N_N, i.e.

$$H^G \equiv H - \langle 0_G|H|0_G\rangle = \sum_N \Omega_N N_N. \tag{13.8.2}$$

It is thus clear that any state in $\mathfrak{F}^G$ has manifestly positive energy and the problem with negative energies is thus avoided by viewing the system, to be quantized, as a classical *field* rather than a classical relativistic particle [324].

One may be worried that acting with the local creators and annihilators (which were constructed using both positive and negative frequencies) on the global vacuum $|0_G\rangle$, one would obtain unphysical states, perhaps with negative energy. However, as we have demonstrated, the action of the local creators and annihilators on any state $|\psi\rangle \in \mathfrak{F}^G$ is well defined. Since all states in $\mathfrak{F}^G$ have manifestly positive energy expectation value it is clear that no problems with negative energy arise.

Nevertheless it is instructive to elaborate on this a bit further. To that end let us investigate whether the state $|\psi_l\rangle = a_l^\dagger|0_G\rangle$ has negative energy. Calculating explicitly the average

energy of a state $|\psi_l\rangle = a_l^\dagger|0_G\rangle$, we get

$$\langle\psi_l|H^G|\psi_l\rangle = \sum_N \Omega_N \langle 0_G|a_l N_N a_l^\dagger|0_G\rangle = \sum_{M,N,P} \Omega_N (u_l|U_M)(U_P|u_l)\langle 0_G|A_M A_N^\dagger A_N A_P^\dagger|0_G\rangle$$
$$= \sum_N \Omega_N (u_l|U_N)(U_N|u_l) = \sum_N \Omega_N |(U_N|u_l)|^2 > 0, \tag{13.8.3}$$

verifying that the energy is manifestly positive. To demonstrate that the energy is finite we first note that $a_l|0_G\rangle$ is not yet normalized:

$$\langle\psi_l|\psi_l\rangle = \langle 0_G|a_l a_l^\dagger|0_G\rangle = 1 + \langle 0_G|n_l|0_G\rangle \neq 1. \tag{13.8.4}$$

The normalized state is therefore given by

$$|\psi_l\rangle = \frac{a_l^\dagger|0_G\rangle}{\sqrt{1+\langle 0_G|n_l|0_G\rangle}}. \tag{13.8.5}$$

By inspecting the Bogoliubov coefficients (13.4.7) and making use of the integral test of convergence we see that $\langle\psi_l|H^G|\psi_l\rangle < \infty$. Hence, we see that the application of the local creation operator $a_k^\dagger$ on the global vacuum $|0_G\rangle$ keeps the state in the global Fock space $\mathfrak{F}^G$, i.e. $|\psi\rangle \in \mathfrak{F}^G$.

We can also consider the state

$$|\phi_l\rangle = \frac{a_l|0_G\rangle}{\sqrt{\langle 0_G|n_l|0_G\rangle}}, \tag{13.8.6}$$

which is not zero since a_l contains both A_N and $A_N^\dagger$, nor does it have less energy than the global vacuum state. A calculation similar to the one above shows that the energy is manifestly positive $\langle\phi|H|\phi\rangle > 0$. Again by the integral test of convergence we could check that the state has, in fact, a finite energy expectation value.

13.8.2 Quantum steering and the Reeh-Schlieder theorem

We are now in a position to address the question of whether the normalized state

$$|\psi_m\rangle = \frac{a_m^\dagger|0_G\rangle}{\sqrt{1+\langle 0_G|n_m|0_G\rangle}}, \tag{13.8.7}$$

can be viewed as a strictly localized one-particle state. The associated wave-packet defined by $\psi_m(x,t) \equiv \langle 0_G|\phi(x,t)|\psi_m\rangle$ is in fact the positive frequency part of u_m, defined in (13.4.10). One might naively suspect that these states should be localized states since they are created by a *local* operation on the vacuum state, i.e. $|0_G\rangle \to a_m^\dagger|0_G\rangle$. The components of this state in the global basis (13.3.6) are given by

$$\frac{a_m^\dagger|0_G\rangle}{\sqrt{1+\langle 0_G|n_m|0_G\rangle}} = \frac{\sum_N (U_N|u_m)A_N^\dagger + (U_N^*|u_m)A_N|0_G\rangle}{\sqrt{1+\langle 0_G|n_m|0_G\rangle}} = \frac{\sum_N (U_N|u_m)|1_N\rangle}{\sqrt{1+\langle 0_G|n_m|0_G\rangle}}, \tag{13.8.8}$$

which we recognize as a superposition of global one-particle excitations. From an analysis by Knight [294] showing that no finite superposition of N-particle states can be strictly localized, we already know that $|\psi_m\rangle$ is not strictly localized. We could stop here, but it is interesting to gain more understanding why this happens.

To investigate this fact, let us see whether the expectation value $\langle\psi_m|\bar{n}_l|\psi_m\rangle$ is different from $\langle 0_G|\bar{n}_l|0_G\rangle$. Computing this difference yields

$$\begin{aligned}\langle\psi_m|\bar{n}_l|\psi_m\rangle - \langle 0_G|\bar{n}_l|0_G\rangle &= \frac{\langle 0_G|a_m\bar{n}_l a_m^\dagger|0_G\rangle}{1+\langle 0_G|n_m|0_G\rangle} - \langle 0_G|\bar{n}_l|0_G\rangle, \\ &= \frac{\langle 0_G|n_m\bar{n}_l|0_G\rangle - \langle 0_G|\bar{n}_l|0_G\rangle\langle 0_G|n_m|0_G\rangle}{1+\langle 0_G|n_m|0_G\rangle} \propto \text{corr}(n_m,\bar{n}_l), \quad (13.8.9)\end{aligned}$$

which not only shows that the one-particle state $|\psi_m\rangle$ is not strictly localized, but also tells us that the reason for it is vacuum entanglement. Indeed, making the replacement $|0_G\rangle \to |0_L\rangle$ and $|\psi_m\rangle \to |1_m,\bar{0}\rangle$ we have $\text{corr}(n_m,\bar{n}_l) = 0$ and the above difference disappears.

It may seem puzzling that we can change the expectation values in the region $[r,R]$ by performing a *local* operation in $[0,r]$. Does this not imply the possibility of superluminal signalling? The answer is no, the reason being that the operation $|0_G\rangle \to |\psi_m\rangle$ is not a unitary operation on the vacuum state since $a_m a_m^\dagger \neq 1$. This local operation does not correspond to something which can be achieved physically by local manipulations solely in $[0,r]$. However, with suitable post-selection, the operation $|0_G\rangle \to |\psi_m\rangle$ could perhaps be implemented, but only by informing the observer in the region $[r,R]$ which states to post-select. This of course would require classical communication, limited by the speed of light [325].

We can view this in the context of the Reeh-Schlieder theorem [40]. This theorem states that by a local *non-unitary* operation in a finite region in space we can obtain, to arbitrary precision, any state at a spatially separated region. The theorem does not go through if we restrict ourselves to local unitary operations.

The situation is different when we replace the global vacuum $|0_G\rangle$ with the local vacuum $|0_L\rangle$. As seen in Section 13.6.2 the key difference is that the local vacuum $|0_L\rangle$ neither cyclic nor separating, or more simply, it is a product state $|0_L\rangle = |0\rangle\otimes|\bar{0}\rangle$ which is therefore not entangled. Thus, no steering whatsoever could take place in this case.

13.8.3 Further properties

In the section 13.8.1 we analysed the positivity of energy of the pseudo-local states

$$|\psi_l\rangle = \frac{1}{\sqrt{1+\langle 0_G|n_l|0_G\rangle}} a_l^\dagger|0_G\rangle \qquad |\phi_l\rangle = \frac{1}{\sqrt{\langle 0_G|n_l|0_G\rangle}} a_l|0_G\rangle, \quad (13.8.10)$$

which are in fact superpositions of global one-particle states $|1_N\rangle = A_N^\dagger|0_G\rangle$, i.e.

$$|\psi_l\rangle = \frac{1}{\sqrt{1+\langle 0_G|n_l|0_G\rangle}}\sum_N (u_l|U_N)|1_N\rangle \qquad |\phi_l\rangle = \frac{1}{\sqrt{\langle 0_G|n_l|0_G\rangle}}\sum_N (u_l|U_N^*)|1_N\rangle \quad (13.8.11)$$

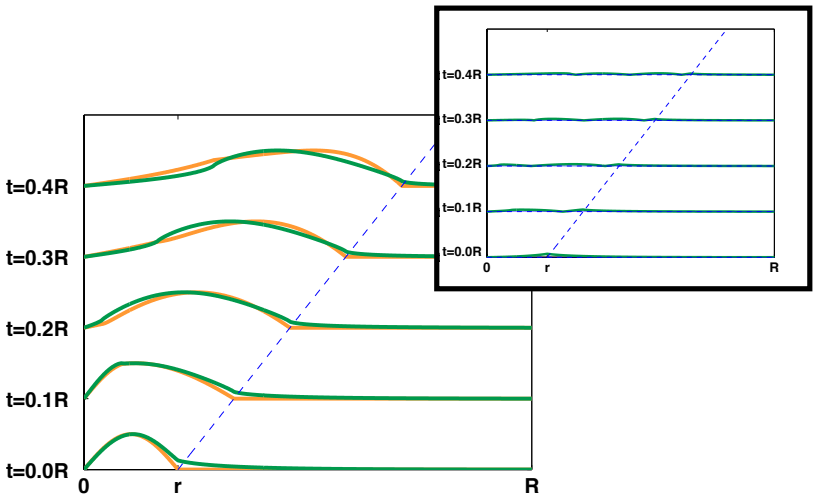

Figure 13.7: Quasi-local modes as compared with local modes. The picture shows the particular case of $r = 0.21R$, $\mu = 1/r$ with mode number $m = 1$. It portraits local modes (zero valued out of the light cone) and quasi-local modes, showing exponential decaying fall-offs around the light cone. The inset shows the difference of both modes at the same scale.

Let us define $|\psi_l^{(r)}\rangle = a_l^{(r)\dagger}|0_G\rangle$, where the (r) superindex refers to the operator corresponding to a localization region of size r. We would expect that state to resemble a one-particle local state, in the sense that the corresponding mode would just be the positive frequency part of the one-particle local mode. That is indeed the case. Figure 13.7 illustrates this case for a particular case of those shown in figure 13.2. We would therefore call these modes, which lie in the global Fock space $\mathfrak{F}^G$, quasi-local modes. For all practical purposes this kind of states could be used as localized and causal to a very good approximation.

Besides that, it is interesting to study how much $|\psi_l^{(r)}\rangle$ states resemble to the one-particle global states, and therefore we will calculate the expectation value :

$$\langle\psi_l^{(r)}|A_N^\dagger A_N|\psi_l^{(r)}\rangle \quad (13.8.12)$$

which happens to be identically equal to

$$|\langle 1_N|\psi_l^{(r)}\rangle|^2 = |\langle 0_G|A_N|\psi_l^{(r)}\rangle|^2 = \frac{|\langle 0_G|A_N a_l^{(r)\dagger}|0_G\rangle|^2}{1+\langle 0_G|n_l|0_G\rangle} = \frac{|(U_N|u_l)|^2}{1+\langle 0_G|n_l|0_G\rangle} \quad (13.8.13)$$

Figure 13.8a shows the expansion of $|\psi_l^{(r)}\rangle$ in terms of global particle states $|1_N\rangle$ for the massless case. We can see that the decomposition is a rather peaked one, and in particular, we can estimate a bandwidth $\Delta\Omega$ for the expansion in global modes. We can define it as the smallest $\Delta\Omega$ for which:

$$\sum_{\Omega_N \in (\omega_l - \Delta\Omega/2, \omega_l + \Delta\Omega/2)} |\langle 1_N | \psi_l^{(r)} \rangle|^2 > 0.95 \tag{13.8.14}$$

In the general case, $\Delta\Omega$ depends on the frequency of the mode ω_l, but tends to an asymptotic value in the limit of big l's, as we can see in the inset of Figure 13.8b, where the dependence with the Klein Gordon mass μ is also plotted. The asymptotic value is independent on the mass, and only dependent on the r/R value. The relationship between these two can be seen in Figure 13.8b. In the limit of small values of r/R, which would correspond to strongly "localized particles", the bandwidth tends to infinity, i.e. we need an infinite amount of global modes to describe the quasi-local particle. For high values of r/R the bandwidth approaches a minimum and we can approximately identify the quasi-local particle states with global states.

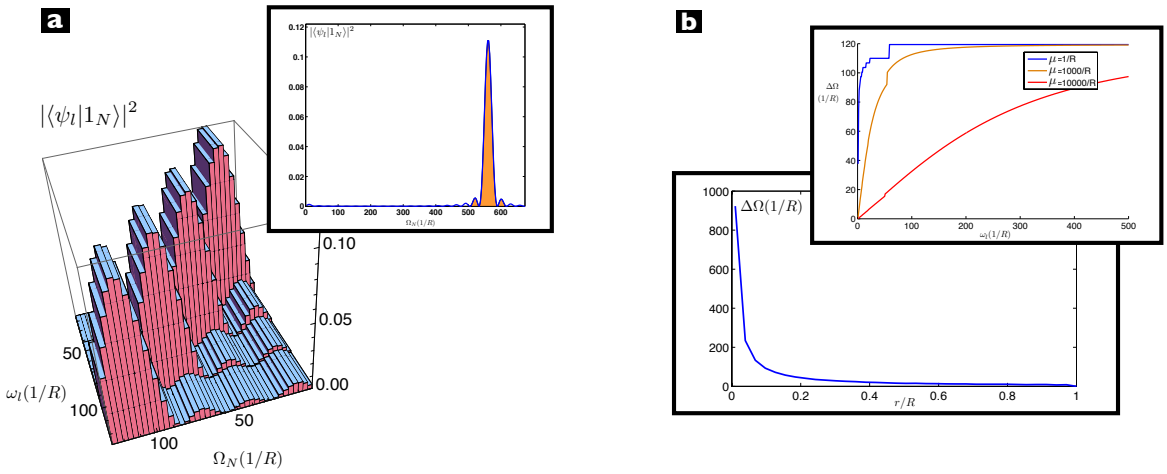

Figure 13.8: Quasi-local state analysis. a) Decomposition of $|\psi_l\rangle$ states in terms of $|1_N\rangle$ global states for a massless case with r=R/9. In the inset, the particular case for $l = 20, \omega_l = \pi l/r \simeq 571/R$. b) The estimated bandwidth $\Delta\Omega$ for quasi-local states is independent of the mode l for big l, but shows a strong dependence with r/R. The inset shows the dependence of $\Delta\Omega$ with l for different masses μ for the case $r = R/9$.

13.9 Discussion

In the extant literature there are several theorems and results that indicate the impossibility of having local particle states, e.g. [53, 292, 294, 300]. We believe that the main obstruction

comes from postulating that the one-particle Hilbert space is spanned by positive frequency modes. In particular, no wave-packet built from these modes can be localized within a finite spatial region, even for an arbitrarily small time interval. However, as pointed out in Wald's exposition of the quantization procedure [165], there is nothing preventing us from making use of a different set of modes. The basic idea of this work was that, basing the quantization procedure on localized modes, we might account for localized one-particle states. Indeed, this turns out to be the case.

These local modes are defined by their initial data. Both the value and time-derivative of the modes are taken to be completely localized within either the right or left partition of the box. This data defines a well-posed Cauchy problem. By Hegerfeldt's theorem, these solutions of the Cauchy problem must contain both positive and negative frequency modes. This marks, at the classical level, a point of departure from the standard quantization procedure.

The creation and annihilation operators associated with these local modes can then be used to build a Fock space $\mathfrak{F}^L$, whose basis states describe local elementary excitations of the quantum field. A set of these basis states, e.g. $|n_k, \bar{0}\rangle$, does in fact represent strictly localized states with respect to the local vacuum $|0_L\rangle \in \mathfrak{F}^L$. This vacuum state, however, does not share the typical properties of a quantum field vacuum. In particular, it is neither cyclic not separating, as it is free from correlations between left and right partitions.

Intriguingly, the local and standard (global) quantum field theories turn out to be *unitarily inequivalent*. Specifically, by computing the Bogoliobov coefficients relating the global and local quantum theories we have found that

$$Tr\ \beta^\dagger\beta \equiv \sum_{k,N} |(u_k|U_N)^*|^2 + |(\bar{u}_k|U_N^*)|^2, \tag{13.9.1}$$

diverges, which is a sufficient condition for establishing unitary inequivalence. Nevertheless, it is important to note that both standard and local quantizations produce self-consistent quantum theories of the field. As a matter of fact, as we have demonstrated, we can evolve states and we also have a well-defined notion of energy after the local vacuum energy has been subtracted from the canonical Hamiltonian.

The existence of unitarily inequivalent representations would seem to confront us with a problem of which Fock representation to choose [326]. The problem of unitary inequivalence disappears, however, when some form of regularization is introduced [327]. Imposing of a wave-number $k = \pi m/r$ cutoff, for example, could solve the issue. Such a cut-off would come naturally, for example, from a quantum theory of gravity requiring a discretization of space(time). A restatement of the theory, which considers the use of measurement apparatuses for a finite time, would also imply the introduction of a frequency cut-off, cir-

cumventing the divergences present in (13.5.2).

Within our approach we nevertheless find that there is a mathematical asymmetry between the two Fock representations. In fact, the divergence of the sum (13.9.1) originates from the summation over the local-mode numbers m. On the other hand, the sum over global-mode numbers N is finite for each specific value of m. A consequence of this fact is that the local creators and annihilators are well-defined operators in the global Fock space, and so are the local number operators. However, the global creators and annihilators turn out to be ill-defined on $\mathfrak{F}^L$. This asymmetry could perhaps be taken as an indication that the global Fock representation is preferred.

In any case, the fact that both local creators and annihilators are well-defined in $\mathfrak{F}^G$ provides us with a useful set of mathematical tools to analyse the properties of the states in $\mathfrak{F}^G$. In particular, by computing the expectation values of the local number operators, we have shown that the global vacuum $|0_G\rangle$ is characterized by a bath of local particles. We also showed, by calculating the correlation coefficients of local number operators, that the local particles associated with the left and right regions are highly entangled in the global vacuum, a feature not shared by the local vacuum $|0_L\rangle$.

Again, the well-defined character of local creators and annihilators in $\mathfrak{F}^G$ also allows us to introduce a new set of quasi-local states defined by applying the local creation operator on the global vacuum, i.e. $|\psi_m\rangle \sim a_k^\dagger|0_G\rangle$. These are natural candidates for *essentially localized* states [174]. We have also shown how these states fail to be strictly localized, a fact related to vacuum entanglement and the Reeh-Schlieder theorem.

Unitary inequivalence seems to be the key problem in the construction of particle localized states, and that could connect with the abstract no-go results by Malament [53] and Clifton *et. al* [300]. However, a proper analysis of this matter would require an adaptation of our setup to incorporate translation covariance, which is an essential assumption in the theorems mentioned.

Clearly there are several topics that deserve further exploration. Here we mention a few of them. For example, it would be nice to express the global vacuum state using the eigenstates $|n_k, \bar{n}_l\rangle$ of the local number operators.[6] Such an expression would allow us to construct the reduced density matrix for the regions $[0, r]$ and $[r, R]$ by partial tracing. From there it would be interesting to see whether the reduced state takes the form of a KMS state. Hopefully we could make contact with existing literature, which examines the entan-

[6] Although the local number operators n_m and $\bar{n}_l$ are well-defined Hermitian operators in $\mathfrak{F}^G$ we note that their eigenstates $|n_m, \bar{n}_l\rangle$ belong to $\mathfrak{F}^L$ and *not* to $\mathfrak{F}^G$. The situation is similar for a non-relativistic quantum particle in a box where the eigenstates of the self-adjoint momentum operator $p = -i\partial_x$ do not belong to the Hilbert space because they do not satisfy the Dirichlet conditions at the boundary.

glement and thermality connected to localized regions of space [328]. In that respect it is perhaps interesting to note that our construction, in contrast to the Minkowski and Rindler quantizations, was not based on standard stationary states. Indeed, while the Minkowski and Rindler quantizations both rely on stationary modes with respect to time translation and boost operators respectively, our construction makes use of manifestly non-stationary states. Whether this provides some advantage remains to be seen. In any case, it would be of interest to analyse in detail the differences and similarities between the Rindler quantization and the one presented here.

CHAPTER 14

Alice and the Slamming Mirror

It is well known that the vacuum state of a quantum field is spatially entangled. This is true both in free and confined spaces, for example in an optical cavity. The obvious consequence of this, however, is surprising and intuitively challenging. Namely, that in a mathematical sense half of an empty box is not empty. Formally this is clear, but what does this physically mean in terms of, say, measurements that can actually be made? In this chapter we utilize the tools of Gaussian quantum mechanics to easily characterize the reduced state of a subregion in a cavity and expose the spatial profile of its entanglement with the opposite region. We go on and discuss a Gedankenexperiment in which a mirror is introduced between the regions. In so doing we expose a simple and physically concrete answer to the above question: the vacuum excitations resulting from entanglement are mathematically equivalent to the real excitations generated by suddenly introducing a mirror. Such an experiment would ideally allow to retain all entanglement present between left and right regions. We conclude by discussing different possibilities for doing a similar experiment in the lab.

14.1 Introduction

It has long been known that the vacuum state of a quantum field displays quantum entanglement between space-like separated regions [329, 330]. Much work has been performed, using a variety of mathematical approaches and models, to understand and characterize the properties of this entanglement [331]. In addition, it has been proposed that this entanglement may be “harvested" (i.e. swapped) to an auxiliary quantum system without the need for causal interaction [41, 70, 278, 332, 333], which may then be used for quantum informational procedures. The existence of spatial entanglement is similarly present in condensed matter and lattice systems [334,335], being a generic property of extended systems with local interactions, of which a quantum field can simply be viewed as a continuum limit. While in

such systems experimental proposals have been put forth for the verification of vacuum entanglement (e.g. a pair of trapped ions) [42], to the authors' knowledge no feasible concrete proposal has yet been suggested for its verification in a true, relativistic, quantum field (e.g. the photon field).

One immediate consequence of vacuum entanglement is that, due to the vacuum being a pure state, the reduced state over any local region in space must necessarily be mixed and thus excited. Relativistic quantum phenomena involving the observer-dependence of particle number, such as the Unruh and Hawking effects, are often attributed to this [164]. Moreover, vacuum entanglement occurs also in enclosed systems, such as an optical cavity or a superconducting circuit. This introduces a conceptually challenging fact: at least formally, *half of an empty box is not empty*. This is a mathematical result which alone gives us little intuition towards actual physical consequences. Under what operational conditions does this phenomenon present itself; what physically sensible measurements (in general) can be made to give this mathematical fact experimental significance?

If an experimentalist has such an empty cavity then what can they do to detect photons in, say, the left half of the cavity (that supposedly contains many)? The answer, as will be explained, is to very quickly introduce a physical boundary (in this case a mirror) between the two sides of the cavity, thus blocking off any influence from the right-hand side while the experimentalist measures the left-hand side. Of course, quickly introducing a boundary (i.e. quickly modifying the Hamiltonian) produces particles similar to what occurs in the dynamical Casimir effect (DCE) [336], which has recently been experimentally observed [58]. The key observation we want to make here, however, is that these real excitations, created by slamming down the mirror, are mathematically equivalent to the vacuum excitations of the reduced state that we attribute to entanglement. That is what it means operationally for half of an empty box to be non-empty. In addition to giving a satisfying interpretation to the problem of local particle content, we will discuss how this realization provides a simple experimental setup that can be used to measure, and perhaps even utilize, local vacuum excitations.

In this chapter we consider both massive and massless scalar fields in a one-dimensional cavity with Dirichlet boundary conditions (i.e. mirrors on the ends). We perform several tasks. To begin, we discuss the difficulties that appear when we intend to measure vacuum excitations and the different alternative scenarios that could allow us to circumvent them. We will present a recently introduced formalism of local quantization [2] that allows us to characterize the reduced state of a sub-region in the cavity and study its local properties formally. At that point we will consider what occurs if a mirror is very quickly introduced

in the middle of the cavity.

We will utilize Gaussian quantum mechanics [337] in order to easily compute and characterize the reduced states of sub-cavity regions and the correlations between them, explaining how this equivalently describes the physics of slamming mirror(s) into the cavity. We will discuss and analyse the spatial structure of entanglement between regions, similar to what has been done in [338] for lattice systems. We will furthermore discuss the time-evolution of the system after slamming a mirror and observe what one would expect: a burst of particles propagating away from it. These excitations, however, are mathematically one and the same with those previously attributed to vacuum entanglement in the local analysis (the only difference is that now they evolve according to a different Hamiltonian). Equivalently, the real excitations produced in the left and right-hand sides are quantum entangled. We also consider the case in which two mirrors are simultaneously introduced, some distance apart. In this case the particles produced in the left and right-hand sides (but ignoring the middle section) can similarly be entangled, despite no common mirror between them. This is possible because, as follows from the main point of our research, the entanglement is simply that which was already present in vacuum prior to the introduction of the mirror.

Lastly, we discuss the experimental feasability of using this scenario to verify vacuum entanglement using current technologies. We note that introducing a mirror in fact represents an very efficient means of harvesting the vacuum entanglement, since afterwards you have two new cavities that contain *all* of the entanglement (up to a UV cut-off determined by how fast the mirror is introduced). This entanglement could then be a resource for quantum computational tasks. This method of harvesting could potentially be much more promising than the usual proposed method of locally interacting a pair of other quantum systems (e.g. artificial atoms) with the field [42, 46, 70], since this is severely limited by the interaction strength.

Throughout this chapter we will work in natural units such that $\hbar = c = k_B = 1$.

14.2 How does one measure the vacuum excitations in a subregion?

To begin, we need to ask ourselves in a general sense what one must do in order to measure localized vacuum fluctuations. What operational procedures can be implemented to do this? Mathematically these fluctuations can arise when tracing out a spatial region of a vacuum field. That is, because there is entanglement between spatial regions, the reduced state of

such a region must necessarily be mixed (and therefore excited). This thus motivates the idea that at least one possible way of measuring these excitations is to isolate oneself to only the subregion of interest. But this means more than simply staying at a fixed location. As we will show later in more detail, a stationary detector interacting with a vacuum field only at a given point or region will still register zero particle detection if it is allowed to measure for a long enough time. Rather, isolating oneself to only a subregion means losing causal contact with the outside; information cannot be allowed to reach our observer from outside the region of interest. Uniform acceleration, for example, is one way of achieving this [54, 164]. Another way is for one to turn their detection device on for only a short time Δt; doing this ensures that the detector is causally isolated from any part of space more than a distance $c\Delta t$ away from it. Indeed switching one's detector on fast enough does cause spurious detection events [7, 136] , however it is questionable if this can be fully attributed to vacuum excitations (i.e. to entanglement) inside a cavity since formally the probability of detection limits to zero only as $\Delta t \to \infty$, which is clearly larger than the cavity length.

Are there any other ways to isolate oneself from outside influence? Indeed, another option that gets the job done is simply to erect a physical boundary. In the cavity scenario this corresponds to placing a perfect mirror at the bipartition boundary. Certainly once such a mirror is installed then an observer in the left-side of the cavity will receive no information from the right-side. Would such an observer then be free to measure local vacuum excitations? How could it be that such a setup suddenly allows the observer to measure what they could not have beforehand? Furthermore, one should be concerned about the fact that quickly placing a mirror in the middle of the cavity is expected to create real particle excitations, similar to what occurs in the dynamical Casimir effect (DCE) [58, 336]. That is, by rapidly changing (in this case, introducing) a boundary condition we are rapidly modifying the Hamiltonian of the system. This will create real excitations in the field that will propagate away from the mirror upon being introduced, and an observer located on one side of this mirror will detect these excitations. Will these particles interfere with the observer's ability of detect the local vacuum excitations that are associated with entanglement between regions?

The answer, as we will elaborate, is that a detection of the mirror-created particles *is* exactly a detection of the local entanglement excitations.

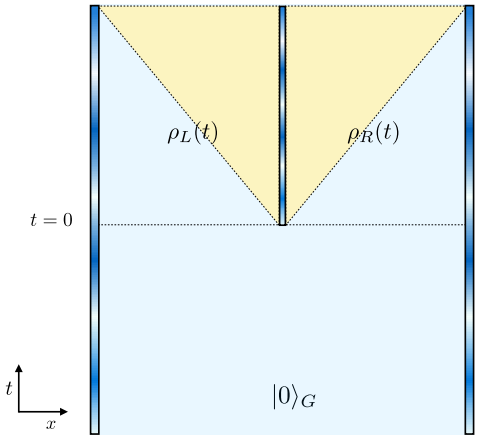

Figure 14.1: Sketch of the one dimensional cavity setting. We start ($t < 0$) considering a cavity in its vacuum state $|0\rangle_G$. At some instant ($t = 0$) we slam a mirror in the cavity separating it into two regions. As explained in the text, the normal modes in these separated subcavities correspond to the localized modes of the cavity without mirror, which we will show suffice to analize states, correlations and particle production when slamming the mirror. The horizontal line corresponds to $t = 0$, the diagonal lines represent the light cone starting at the slamming event.

14.3 Formulation and setting

The first purpose of this section is to present a mathematical framework for the computation and analysis of global cavity states using a local formalism. We will start describing the quantum states in the cavity by introducing a bipartition of it into two subregions, precisely those in which the cavity will eventually be separated by the introduction of a slamming mirror at some instant of time. Later on, in the second part of this section, we will use this formalism to study the physical scenario where a mirror is abruptly introduced in the middle of the cavity.

14.3.1 Local mathematical analysis: local vs. global modes

Here we will briefly introduce the field-theoretic formalism required for our analysis [2,164].

The aim is to spell out what can be ascertained about the physics of a non-localized state spanning the whole cavity, as is the case of the quantum vacuum and generic cavity states, by using localizing mathematical tools. We do not yet introduce a mirror in the middle of the cavity. We will postpone it to the next subsection, once the present goal is achieved.

Let us consider a quantum scalar field $\hat{\phi}(x,t)$ of mass μ within a cavity of length R, such that $x \in [0,R]$. Specifically, we will consider a cavity with Dirichlet (i.e. mirror) boundary conditions, as would be the case in a physical optical cavity, for example. The field is thus constrained to satisfy $\hat{\phi}(0,t) = \hat{\phi}(R,t) = 0$.

Our field can be expanded in the standard form:

$$\hat{\phi}(x,t) = \sum_{m=1}^{\infty} (f_m(x,t)\hat{b}_m + f_m^*(x,t)\hat{b}_m^\dagger). \tag{14.3.1}$$

Here, the set of chosen mode functions $\{f_n\}$ are required to satisfy the Klein-Gordon equation $(\Box + \mu^2)f(x,t) = 0$ as well as the correct boundary conditions. In addition, they must form a complete and orthonormal set with respect to the Klein-Gordon inner product [164]. Aside from these constraints the choice is arbitrary. Making such a choice is equivalent to a choice of Fock basis, for which the operators $\{\hat{b}_n, \hat{b}_n^\dagger\}$ are the corresponding ladder operators.

The standard choice for a Dirichlet cavity, which we will refer to as the *global modes* U_n, are given by

$$U_n(x,t) = \frac{1}{\sqrt{R\Omega_n}} \sin\left(\frac{\pi n x}{R}\right) e^{-\mathrm{i}\Omega_n t} = \mathcal{U}_n(x) e^{-\mathrm{i}\Omega_n t}, \tag{14.3.2}$$

where $\Omega_n^2 = \frac{\pi^2 n^2}{R^2} + \mu^2$ is the frequency of mode n. This choice is convenient because the corresponding Fock states are energy eigenstates of the free-field regularised Hamiltonian (which we will also call the *global Hamiltonian*)

$$\hat{H}_G = \sum_{n=1}^{\infty} \Omega_n \hat{A}_n^\dagger \hat{A}_n, \tag{14.3.3}$$

where here $\{\hat{A}_n, \hat{A}_n^\dagger\}$ are the ladder operators corresponding to the global modes. A state of principal importance for us is the *global vacuum state* $|0_G\rangle$, defined to satisfy $\hat{A}_n |0_G\rangle = 0$ for all n. This is the state of lowest energy with respect to $\hat{H}_G$, and is said to be the state of zero particles, because no A quanta can be removed from it, i.e. a cavity in this state is empty (although not from a local point of view as we discuss later).

While the field decomposition into the global modes is often the most convenient and physically relevant choice, we can also consider a decomposition into a mode basis better suited to study the local physics of a subregion inside the cavity. Say that we decompose our cavity into two regions, one that runs within $x \in [0, r]$ (the left side) and the other within $x \in [r, R]$ (the right side). The lengths of these two sides are thus r and $\bar{r} \equiv R - r$, and we can define a new set of modes $\{u_m(x,t)\}$ and $\{\bar{u}_m(x,t)\}$ for the left and right sides, respectively. The obvious way of doing this is to define these modes to have support at a certain time $t = 0$ only over their corresponding subregions. As pointed out in [2], however, one must be careful that the new basis modes still satisfy the correct boundary conditions of the cavity (and in particular, not extra ones). This requirement immediately implies that if, say the set $\{u_m\}$ are supported only in the left region at $t = 0$, then their support will necessarily exceed this region for later times (u_m satisfies the wave equation and we have not placed an extra

boundary condition between the two regions). This does not turn out to be a hindrance in exploring local physics, however.

Since the global vacuum $|0_G\rangle$ is a stationary state it does not matter at what time we examine its properties; we will choose time $t = 0$. The solution is then to simply define our local modes to be appropriately compactly supported at this instant. To this end, we will define our local modes $u_m(x,t)$ to have initial conditions

$$\begin{aligned} u_m(x,0) &= \frac{\theta(r-x)}{\sqrt{r\omega_m}} \sin\left(\frac{\pi m x}{r}\right), \\ \dot{u}_m(x,0) &= -\mathrm{i}\omega_m u_m(x,0), \\ \bar{u}_m(x,0) &= \frac{\theta(x-r)}{\sqrt{\bar{r}\bar{\omega}_m}} \sin\left(\frac{\pi m (x-r)}{\bar{r}}\right), \\ \dot{\bar{u}}_m(x,0) &= -\mathrm{i}\bar{\omega}_m \bar{u}_m(x,0), \end{aligned} \tag{14.3.4}$$

where $\omega_m^2 = \frac{\pi^2 m^2}{r^2} + \mu^2$ and $\bar{\omega}_m^2 = \frac{\pi^2 m^2}{\bar{r}^2} + \mu^2$. Given the above initial conditions, the local modes will evolve throughout the cavity according to the Klein-Gordon equation. These modes satisfy the proper boundary conditions and constitute a complete and orthonormal basis for the whole cavity [2], and thus form a proper expansion of the field. For our purposes in this section, however, we need only consider the instant $t = 0$ at which they are localized to their respective sides of the cavity. Examining the global vacuum in this basis, at this instant, allows us to fully characterize the reduced state of the subregions and the quantum correlations between them.

Let us denote the local ladder operators associated with the above modes as $\{\hat{a}_m, \hat{a}_m^\dagger\}$ for the left side, and $\{\hat{\bar{a}}_m, \hat{\bar{a}}_m^\dagger\}$ for the right.

Solutions sets to the Klein-Gordon equation are related by a linear *Bogoliubov transformation* [164, 339]. This means that our local modes are related to the global modes via some transformation of the form

$$\begin{aligned} u_m(x,t) &= \sum_{n=1}^{\infty} (\alpha_{mn} U_n(x,t) + \beta_{mn} U_n^*(x,t)), \\ \bar{u}_m(x,t) &= \sum_{n=1}^{\infty} (\bar{\alpha}_{mn} U_n(x,t) + \bar{\beta}_{mn} U_n^*(x,t)). \end{aligned} \tag{14.3.5}$$

Equivalently, in terms of the annihilation operators (from which the creation operators are trivially obtained) we have

$$\begin{aligned} \hat{a}_m &= \sum_{n=1}^{\infty} (\alpha_{mn}^* \hat{A}_n - \beta_{mn}^* \hat{A}_n^\dagger), \\ \hat{\bar{a}}_m &= \sum_{n=1}^{\infty} (\bar{\alpha}_{mn}^* \hat{A}_n - \bar{\beta}_{mn}^* \hat{A}_n^\dagger). \end{aligned} \tag{14.3.6}$$

The *Bogoliubov coefficients*, which are time-independent, are computed via the Klein-Gordon inner products between local and global modes. In our case, they evaluate to [2]

$$\alpha_{mn} = (U_n|u_m) \quad = (\Omega_n + \omega_m)\mathcal{V}_{mn}, \tag{14.3.7}$$

$$\beta_{mn} = -(U_n^*|u_m) = (\Omega_n - \omega_m)\mathcal{V}_{mn}, \tag{14.3.8}$$

$$\bar{\alpha}_{mn} = (U_n|\bar{u}_m) \quad = (\Omega_n + \omega_m)\bar{\mathcal{V}}_{mn}, \tag{14.3.9}$$

$$\bar{\beta}_{mn} = -(U_n^*|\bar{u}_m) = (\Omega_n - \omega_m)\bar{\mathcal{V}}_{mn}, \tag{14.3.10}$$

where

$$\mathcal{V}_{mn} = \int_0^R \mathrm{d}x\, \mathcal{U}_n(x) u_m(x,0) \tag{14.3.11}$$

$$= \frac{\frac{m\pi}{r}(-1)^m}{\sqrt{Rr\Omega_n\omega_m}(\Omega_n^2 - \omega_m^2)} \sin\frac{n\pi r}{R}, \tag{14.3.12}$$

$$\bar{\mathcal{V}}_{mn} = \int_0^R \mathrm{d}x\, \mathcal{U}_n(x) \bar{u}_m(x,0) \tag{14.3.13}$$

$$= \frac{-\frac{m\pi}{\bar{r}}}{\sqrt{R\bar{r}\Omega_n\bar{\omega}_m}(\Omega_n^2 - \bar{\omega}_m^2)} \sin\frac{n\pi r}{R}. \tag{14.3.14}$$

The fact that the β coefficients are non-vanishing implies that the global vacuum $|0_G\rangle$ is, in the local basis, an excited state in the sense that $\hat{a}_m |0_G\rangle \neq 0$ and $\hat{\bar{a}}_m |0_G\rangle \neq 0$, i.e. local quanta can be removed from it, so in this picture the vacuum cannot be considered to be empty. Indeed, the reduced state of, say, the left side of the cavity, is a mixed state. These local excitations, and the local mixedness, are associated with the entanglement present between the two sides of the cavity.

Lastly, as with any Bogoliubov transformation, the above coefficients satisfy the necessary conditions [164]

$$\sum_k (\alpha_{mk}\alpha_{nk}^* - \beta_{mk}\beta_{nk}^*) = \delta_{mn}, \tag{14.3.15}$$

$$\sum_k (\alpha_{mk}\beta_{nk} - \beta_{mk}\alpha_{nk}) = 0, \tag{14.3.16}$$

and similarly for the barred coefficients.

14.3.2 Slamming down a mirror

If we compute the vacuum expectation value of the local number operators $\hat{n}_m = \hat{a}_m^\dagger a_m$ and $\hat{\bar{n}}_m = \hat{\bar{a}}_m^\dagger \hat{\bar{a}}_m$ we find that these are non-zero for the global vacuum state $|0_G\rangle$, indicating

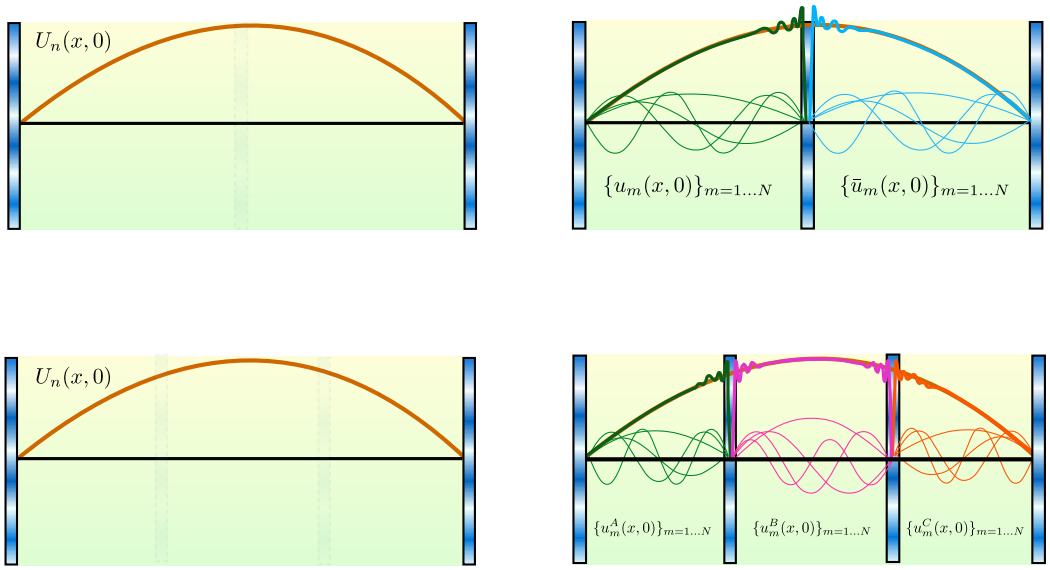

Figure 14.2: The cavity for the cases studied. Top and bottom left figures correspond to the full cavity without mirrors, the light dotted vertical bars indicating the border of the regions chosen in sections IIIA and IIIC to study localization in two or three spatial regions. Top left: Normal modes after slamming a mirror which at $t = 0$ would be equal to the localized modes of the whole cavity in the left and right regions. Bottom left: The same as above for the case when two separated mirrors are slammed simultaneously.

the presence of a bath of 'local particles'. While this observation is mathematically correct we must nevertheless ask ourselves if any operational significance can be attached to this theoretical notion of "local quanta". Can we somehow detect the presence of such local quanta in the lab?

Taking as inspiration the discussion in Sect. 14.2, we claim that a generic (but perhaps not exhaustive) method of achieving this is to informationally block the local region of interest from the rest of the system. In a cavity-field system this can be achieved by introducing a mirror, separating the cavity into two new smaller ones. Indeed, as we will discuss, such an operation *does* allow the detection and characterization of local excitations. This is fundamentally due to the fact that we identify a "real" (i.e. measurable) particle to be an elementary excitation of a *stationary* field mode. By the act of introducing the mirror, what were nonstationary local modes of the full cavity translate into stationary modes of the new small cavity, thus facilitating the measurement of their excitations.

One may be concerned with the unique identification of "a real particle" with "an elementary excitation of a stationary mode". In this work, however, we attempt to be operationally unambiguous and connect as closely as possible with the kinds of measurements that can actually be achieved in the laboratory, necessitating long measurement times as compared to the fundamental time-scale of the cavity. As a detection model let us consider

an idealized, point-like, DeWitt monopole detector that remains at some specific location x_0. The following observation, however, is valid for *any* choice of detector. Let the initial state of the system is taken to be the $|0_G\rangle \otimes |g\rangle$ where $|g\rangle$ is the ground state of the detector. We will present two cases:

First, *without slamming a mirror*, we imagine adiabatically switching on the coupling between field and detector. The adiabatic theorem guarantees that if the system was originally in the ground state of the non-interacting theory, then the system at much later times will be found in the interacting ground state.[1] When we then adiabatically switch off the interaction the combined system will then be found in the non-interacting vacuum and thus will fail to detect the presence of local quanta. This then immediately shows that such a detector will not get excited. Such a procedure does not detect particles when the global system is in its ground state (allowing us to use the adiabatic theorem), which requires the global stationary modes to be in their ground states. It is for this reason that we relate the particle notion with the free stationary modes, which are the ones corresponding to the free eigenstates.

If, on the other hand, *we slam down a mirror* and then follow the same adiabatic detection procedure within one of the sub-cavities then we *will* detect the presence of particles. This is because the local modes, which are stationary after the mirror is introduced, are excited. Critical to our message is that the measurement statistics that will be obtained from this procedure are equivalent to the local virtual particle statistics (i.e. those corresponding to one half of the box) obtained from the transformation presented in Sect. 14.3.1, which simply describes the local physics of the cavity and does not assume the introduction of a mirror.

Concretely, we consider what happens when we instantaneously introduce a mirror at $x = r$ and $t = 0$, i.e. we impose the Dirichlet boundary condition $\phi(r, t) = 0$ for $t \geq 0$. Clearly the instantaneous assumption is not physically realistic, however this turns out not to be a hindrance in elucidating the most realistic, finite-time case. This will be further discussed in Sect. 14.5.2. Given this scenario, it is clear that the set of local modes with initial conditions (14.3.4), which were non-stationary for $t < 0$ prior to the introduction of the mirror, will have a different evolution than before, $u'_m(x, t)$ and $\bar{u}'_m(x, t)$, which for $t \geq 0$ will correspond to *stationary* modes , i.e.

$$u'_m(x,t) = \begin{cases} u_m(x,t) & \text{when } t \leq 0 \\ u_m(x,0)e^{-i\omega_m t} & \text{when } t > 0 \end{cases} \tag{14.3.17}$$

[1] The adiabatic theorem requires a gap between the vacuum energy eigenvalue and other eigenvalues. This is guaranteed since we are dealing with a cavity with a naturally infrared cut-off defined by the size of the cavity R.

$$\bar{u}'_m(x,t) = \begin{cases} \bar{u}_m(x,t) & \text{when } t \leq 0 \\ \bar{u}_m(x,0)e^{-i\bar{\omega}_m t} & \text{when } t > 0 \end{cases} \tag{14.3.18}$$

Please note that after this section we will only need to consider the times $t \geq 0$, and thus will abuse notation by dropping the primes from the mode functions, meaning that for $t > 0$ we will define $u_m(x,t) = u_m(x,0)e^{-\mathrm{i}\omega_m t}$.

Furthermore and analogously, the corresponding global modes $U'_m(x,t)$ would only be stationary modes for $t < 0$; for $t \geq 0$ these modes would be non-stationary.

Equivalently, the sudden introduction of the mirror translates mathematically into a time-dependent Hamiltonian, i.e. we have

$$\hat{H} = \begin{cases} \sum_m \Omega_m \hat{A}^\dagger_m \hat{A}_m & t < 0 \\ \sum_m \omega_m \hat{a}^\dagger_m \hat{a}_m + \bar{\omega}_m \hat{\bar{a}}^\dagger_m \hat{\bar{a}}_m & t \geq 0 \end{cases} . \tag{14.3.19}$$

Physically, the time dependence of the Hamiltonian will cause particle creation similar to the Dynamical Casimir Effect [58, 336].

To determine exactly the amount of particle creation we need to calculate the Bogoliubov coefficients between the modes U'_m and u'_m and $\bar{u}'_m$. These are nothing but the Klein-Gordon inner products $\alpha_{mn} = (u'_m|U'_n)$, $\beta_{mn} = (u'_m|U'^*_n)$, $\bar{\alpha}_{mn} = (\bar{u}'_m|U'_n)$, and $\bar{\beta}_{mn} = (\bar{u}'_m|U'^*_n)$, which we can conveniently evaluate at time $t = 0$. Importantly, due to the specific choice of initial data at $t = 0$ these Bogoliubov coefficients necessarily coincides with those of the previous section, i.e. Eq. (14.3.7). This means that the particle content generated by the mirror is exactly equivalent to the local particle content $(a^\dagger_m a_m, \bar{a}^\dagger_m \bar{a}_m)$ before the mirror is introduced, i.e. the particle content that is associated with entanglement between the two sides of the cavity. Thus, although the sudden introduction of a mirror is usually understood as causing particle creation, it is at the same time an operation that does not change the *local* particle number of the state. The difference now being that these particle contents are associated with stationary modes, meaning that they can be measured using standard techniques of quantum optics.

Moreover, it is not just the particle content, but the state in general that does not change. That is, all particle statistics and correlations (including entanglement) are unchanged by the action of slamming the mirror. Slamming the mirror does of course change the time evolution of the system. For $t < 0$ the system is time-independent, the global vacuum state being stationary with respect to the global Hamiltonian, whereas for $t > 0$ the change of Hamiltonian will cause time evolution (e.g. particles propagating away from the mirror). The key observation, however, is that this difference in evolution is fully encompassed by the difference in spatial evolution of the mode functions themselves and not by any changes in particle content or correlations between them.

14.3.3 Three spatial regions

Before continuing we would also like to describe the case in which the cavity is split into three spatial regions, rather than only two. This will prove useful later when we discuss the operational implications of slamming down mirrors and the possible experimental verification of vacuum entanglement. Note that the extension to any number of regions follows analogously.

Let us proceed by considering a division of our cavity into three sections $\Delta_A = [A_0, B_0], \Delta_B = [B_0, C_0]$, and $\Delta_C = [C_0, R]$ with sizes A, B and C respectively. Let us define:

$$\Pi_Z(x) = \begin{cases} 1 & : x \in \Delta_Z \\ 0 & : x \notin \Delta_Z \end{cases},$$

and set

$$A_0 = 0, \quad B_0 = A, \quad C_0 = A + B, \quad R = A + B + C. \tag{14.3.20}$$

We can build the local modes for these three regions $u_l^Z(x,t)$ by demanding that:

$$u_l^Z(x,0) = \frac{\Pi_Z(x)}{\sqrt{Z\omega_l^Z}} \sin \frac{l\pi(x - Z_0)}{Z}, \tag{14.3.21}$$

$$\dot{u}_l^Z(x,0) = -i\omega_l^Z u_l^Z(x,0). \tag{14.3.22}$$

With:

$$\omega_l^Z = \sqrt{\left(\frac{m\pi}{Z}\right)^2 + \mu^2}, \qquad Z = A, B, C.$$

The new Bogoliubov transformation, analogous to Eq. (14.3.5), is:

$$u_m^Z = \sum_n \alpha_{mn}^Z U_n + \beta_{mn}^Z U_n^*, \qquad Z = A, B, C, \tag{14.3.23}$$

where

$$\alpha_{mn}^Z = (U_n | u_m^Z) \quad = (\Omega_n + \omega_m^Z)\mathcal{V}_{mn}^Z, \tag{14.3.24}$$

$$\beta_{mn}^Z = -(U_n^* | u_m^Z) = (\Omega_n - \omega_m^Z)\mathcal{V}_{mn}^Z, \tag{14.3.25}$$

and

$$\begin{aligned} \mathcal{V}_{mn}^A &= \int_0^A \mathrm{d}x\, \mathcal{U}_n(x) u_m^A(x,0) = \\ &\frac{\frac{m\pi}{A}(-1)^m}{\sqrt{RA\Omega_n\omega_m^A(\Omega_n^2 - \omega_m^{A^2})}} \sin\frac{n\pi A}{R}, \\ \mathcal{V}_{mn}^B &= \int_A^{A+B} \mathrm{d}x\, \mathcal{U}_n(x) u_m^B(x,0) = \end{aligned} \tag{14.3.26}$$

$$\frac{\frac{m\pi}{B}\left[(-1)^m \sin\left(\frac{n\pi(A+B)}{R}\right) - \sin\left(\frac{n\pi A}{R}\right)\right]}{\sqrt{RB\Omega_n\omega_m^B(\Omega_n^2 - \omega_m^{B^2})}}, \tag{14.3.27}$$

$$\mathcal{V}_{mn}^C = \int_{A+B}^{R} \mathrm{d}x\, \mathcal{U}_n(x) u_m^C(x,0) = \frac{-\frac{m\pi}{C}}{\sqrt{RC\Omega_n\omega_m^C(\Omega_n^2 - \omega_m^{C^2})}} \sin\frac{n\pi(A+B)}{R}. \tag{14.3.28}$$

Transforming to this mode basis allows us to describe the local physics of, and the correlations between, these three regions. Similar to the scenario discussed in Sect. 14.3.2, the mode basis described here can be used to describe the process of slamming down two mirrors simultaneously, thereby splitting the cavity into three regions. Exactly the same physics applies in this case, and we will thus not reiterate the material of Sect. 14.3.2.

14.4 Computing the state

In this section we will focus on obtaining a local description of the global vacuum state [2]. This includes the evaluation of the reduced field state of a subregion of a cavity, and a description of the of vacuum entanglement between regions of the cavity. We rely on the formalism of Gaussian quantum mechanics [337] for our exposition. The unfamiliar reader is encouraged to read Appendix. A, which outlines the concepts of Gaussian quantum mechanics that are necessary to understand the main text. A key point to keep in mind, as discussed in the previous section, is that the Bogoliubov transformation (and thus the resulting state) is the same whether we consider this to be with or without the introduction of the mirror. As discussed further in Sect. 14.5.1, the covariance matrix that we compute (i.e. the state) equally well describes both cases.

14.4.1 The state of two regions

We will start by computing the form of the global vacuum upon transforming to the local-mode basis, in the case that we split the cavity into two regions. Let us define the canonically conjugate quadrature operators for the field modes, both global and local. Letting $\{\hat{A}_n, \hat{A}_n^\dagger\}$ be the ladder operators for the global modes, we define the corresponding quadrature operators to be

$$\hat{Q}_n = \frac{1}{\sqrt{2}}(\hat{A}_n + \hat{A}_n^\dagger), \quad \hat{P}_n = \frac{\mathrm{i}}{\sqrt{2}}(\hat{A}_n^\dagger - \hat{A}_n). \tag{14.4.1}$$

[2] It must be pointed out that the mathematical toolbox presented here allow us to work with any Gaussian state, not just the global vacuum. We could, for example, start with with a global thermal state.

Similarly, for the ladder operators $\{\hat{a}_m, \hat{a}_m^\dagger\}$ and $\{\hat{\bar{a}}_m, \hat{\bar{a}}_m^\dagger\}$ of the local modes we have

$$\begin{aligned} \hat{q}_m &= \frac{1}{\sqrt{2}}(\hat{a}_m + \hat{a}_m^\dagger), \quad \hat{p}_m = \frac{\mathrm{i}}{\sqrt{2}}(\hat{a}_m^\dagger - \hat{a}_m), \\ \hat{\bar{q}}_m &= \frac{1}{\sqrt{2}}(\hat{\bar{a}}_m + \hat{\bar{a}}_m^\dagger), \quad \hat{\bar{p}}_m = \frac{\mathrm{i}}{\sqrt{2}}(\hat{\bar{a}}_m^\dagger - \hat{\bar{a}}_m). \end{aligned} \tag{14.4.2}$$

For notational convenience let us define the phase-space vectors $\hat{\mathbf{X}} = (\hat{Q}_1, \hat{P}_1, \hat{Q}_2, \hat{P}_2, \cdots)^T$, $\hat{\mathbf{x}} = (\hat{q}_1, \hat{p}_1, \hat{q}_2, \hat{q}_2, \cdots)^T$, and $\hat{\bar{\mathbf{x}}} = (\hat{\bar{q}}_1, \hat{\bar{p}}_1, \hat{\bar{q}}_2, \hat{\bar{p}}_2, \cdots)^T$.

Within this representation it is straightforward to see that the Bogoliubov transformation from global to local modes, as given in Eq. (14.3.6), is given by the matrix transformations

$$\hat{\mathbf{x}} = \mathbf{S}\hat{\mathbf{X}}, \qquad \hat{\bar{\mathbf{x}}} = \bar{\mathbf{S}}\hat{\mathbf{X}}, \tag{14.4.3}$$

where the matrix $\mathbf{S}$ takes the block form

$$\mathbf{S} = \begin{pmatrix} \mathbf{S}_{11} & \mathbf{S}_{12} & \cdots \\ \mathbf{S}_{21} & \mathbf{S}_{22} & \cdots \\ \vdots & \vdots & \ddots \end{pmatrix}, \tag{14.4.4}$$

with

$$\mathbf{S}_{mn} = \begin{pmatrix} \mathrm{Re}(\alpha_{mn} - \beta_{mn}) & \mathrm{Im}(\alpha_{mn} + \beta_{mn}) \\ -\mathrm{Im}(\alpha_{mn} - \beta_{mn}) & \mathrm{Re}(\alpha_{mn} + \beta_{mn}) \end{pmatrix}, \tag{14.4.5}$$

and similarly for $\bar{\mathbf{S}}$ using the barred Bogoliubov coefficients. It is straightforward to show that such a transformation preserves the canonical commutation relations iff the Bogoliubov conditions Eq. (14.3.15,14.3.16) are satisfied.

Using the specific transformation for our scenario, Eq. (14.3.7), we find the 2×2 blocks of matrices $\mathbf{S}$ and $\bar{\mathbf{S}}$ to be

$$\mathbf{S}_{mn} = 2\mathcal{V}_{mn} \begin{pmatrix} \omega_m & 0 \\ 0 & \Omega_n \end{pmatrix}, \quad \bar{\mathbf{S}}_{mn} = 2\bar{\mathcal{V}}_{mn} \begin{pmatrix} \bar{\omega}_m & 0 \\ 0 & \Omega_n \end{pmatrix} \tag{14.4.6}$$

We note that the off-diagonal entries of these blocks are zero, resulting from the fact that our Bogoliubov coefficients are purely real. This means that the transformation does not mix canonical position and momentum operators, rather the $\hat{q}$ operators of the local basis are combinations of the global $\hat{Q}$'s only, and similarly for the momentum operators.

It is important to keep in mind that individually the matrices $\mathbf{S}$ and $\bar{\mathbf{S}}$ are not symplectic. This is because individually they only map onto a subspace of the total Hilbert space of the

field. [3] This is easily concluded from the fact that the reduced field states of the subregions of the cavity are mixed states, despite the global state being pure (the vacuum). A proper symplectic transformation in phase space can always be associated with a unitary operation acting in the Hilbert space, which will always bring a pure state to another pure state.

Rather, it is the combined transformation

$$\mathbf{S}_{\text{Bogo}} = \begin{pmatrix} \mathbf{S} \\ \bar{\mathbf{S}} \end{pmatrix} \tag{14.4.7}$$

that is formally symplectic (see the discussion in Sect. 14.6.2). This matrix transforms the global mode basis to the local mode basis, including both sides of the cavity:

$$\begin{pmatrix} \hat{\mathbf{x}} \\ \hat{\bar{\mathbf{x}}} \end{pmatrix} = \mathbf{S}_{\text{Bogo}} \hat{\mathbf{X}}. \tag{14.4.8}$$

Given all of this, we are ready to transform the state itself. The global vacuum $|0\rangle_G$ is an example of a Gaussian state, which means that the state is *fully characterized* by its covariance matrix (see Appendix A). We will label $\boldsymbol{\sigma}_G$ the covariance matrix of the global vacuum, represented in the global-mode basis. This is simply given by the identity: $\boldsymbol{\sigma}_G = \mathbf{I}$. To Bogoliubov transform this state to the local basis, $\boldsymbol{\sigma}_{\text{loc}}$, we apply the above symplectic transformation to $\boldsymbol{\sigma}_G$:

$$\begin{aligned} \boldsymbol{\sigma}_{\text{loc}} = \mathbf{S}_{\text{Bogo}} \boldsymbol{\sigma}_G \mathbf{S}_{\text{Bogo}}^T &\equiv \begin{pmatrix} \boldsymbol{\sigma} & \boldsymbol{\gamma} \\ \boldsymbol{\gamma}^T & \bar{\boldsymbol{\sigma}} \end{pmatrix} \\ &= \begin{pmatrix} \mathbf{S}\boldsymbol{\sigma}_G\mathbf{S}^T & \mathbf{S}\boldsymbol{\sigma}_G\bar{\mathbf{S}}^T \\ \bar{\mathbf{S}}\boldsymbol{\sigma}_G\mathbf{S}^T & \bar{\mathbf{S}}\boldsymbol{\sigma}_G\bar{\mathbf{S}}^T \end{pmatrix}. \end{aligned} \tag{14.4.9}$$

Here the covariance matrix $\boldsymbol{\sigma} = \mathbf{S}\boldsymbol{\sigma}_G\mathbf{S}^T = \mathbf{S}\mathbf{S}^T$ represents the reduced field state for the left side of the cavity. Similarly, $\bar{\boldsymbol{\sigma}} = \bar{\mathbf{S}}\bar{\mathbf{S}}^T$ fully characterizes the reduced state of the right side. The off-diagonal matrix $\boldsymbol{\gamma} = \mathbf{S}\bar{\mathbf{S}}^T$, on the other hand, contains the correlation structure between the two sides of the cavity.

These matrices are easily computed. We see that each can be split into 2×2 blocks, for example the reduced state of the left side takes the form

$$\boldsymbol{\sigma} = \begin{pmatrix} \boldsymbol{\sigma}_{11} & \boldsymbol{\sigma}_{12} & \cdots \\ \boldsymbol{\sigma}_{21} & \boldsymbol{\sigma}_{22} & \cdots \\ \vdots & \vdots & \ddots \end{pmatrix}. \tag{14.4.10}$$

[3] The definition of a symplectic matrix $\mathbf{S}$ requires that it be square. However if a linear phase space transformation is not square it is still required to preserve the canonical commutation relations. That is, if we have an $m \times n$ transformation matrix $\mathbf{S}$ on phase space then it must still satisfy $\mathbf{S}\boldsymbol{\Omega}_n\mathbf{S}^T = \boldsymbol{\Omega}_m$, where $\boldsymbol{\Omega}_n$ is the n-mode symplectic form. If $n > m$ then such a transformation corresponds to a symplectic transformation followed by a partial trace, which can of course bring a pure state to a mixed one.

Here the 2×2 block $\boldsymbol{\sigma}_{mm}$ is the covariance matrix (i.e. it *is* the reduced state) of the m'th local (left side) mode. The off-diagonal block $\boldsymbol{\sigma}_{mn}$, where $m \neq n$, contains the correlations between local modes m and n. Using the fact that the $\mathbf{S}_{mn}$ are symmetric we see that these blocks are given by $\boldsymbol{\sigma}_{mn} = \sum_\ell \mathbf{S}_{m\ell}\mathbf{S}_{n\ell}$. Similarly, the state $\bar{\boldsymbol{\sigma}}$ and the correlation matrix $\boldsymbol{\gamma}$ can be split into 2×2 blocks that are given by $\bar{\boldsymbol{\sigma}}_{mn} = \sum_\ell \bar{\mathbf{S}}_{m\ell}\bar{\mathbf{S}}_{n\ell}$ and $\boldsymbol{\gamma}_{mn} = \sum_\ell \mathbf{S}_{m\ell}\bar{\mathbf{S}}_{n\ell}$, respectively.

These are given by

$$\boldsymbol{\sigma}_{mn} = \sum_l 4\mathcal{V}_{ml}\mathcal{V}_{nl} \begin{pmatrix} \omega_m\omega_n & 0 \\ 0 & \Omega_l^2 \end{pmatrix}, \tag{14.4.11}$$

$$\bar{\boldsymbol{\sigma}}_{mn} = \sum_n 4\bar{\mathcal{V}}_{ml}\bar{\mathcal{V}}_{nl} \begin{pmatrix} \bar{\omega}_m\bar{\omega}_n & 0 \\ 0 & \Omega_l^2 \end{pmatrix}, \tag{14.4.12}$$

$$\boldsymbol{\gamma}_{mn} = \sum_l 4\mathcal{V}_{ml}\bar{\mathcal{V}}_{nl} \begin{pmatrix} \omega_m\bar{\omega}_n & 0 \\ 0 & \Omega_l^2 \end{pmatrix}. \tag{14.4.13}$$

Together, these blocks constitute a full characterization of the global vacuum in the local-mode basis, and in particular $\boldsymbol{\sigma}$ fully characterizes the reduced state of the left side of the cavity. Although we have derived the full analytical expressions, it should be noted that in the remainder of the chapter, when we present quantitative results, we have done so by computing the above matrix elements numerically, by performing the sums to convergence.

There are several observations that we can make from this result. The first is that the reduced states $\boldsymbol{\sigma}$ and $\bar{\boldsymbol{\sigma}}$ are clearly excited states, meaning in this language that they are not equal to the identity (the vacuum). Mathematically, this is what is meant by the statement "half of an empty box is non-empty". Equivalently, this is a mathematical description of the particle creation due to instantaneously slamming down a mirror. Another observation is that the correlation structure of the global vacuum in this basis is extremely connected, meaning that every local mode is correlated (if perhaps not entangled) with every other local mode. That is, since the blocks $\boldsymbol{\gamma}_{mn}$ are nonzero this means that every local mode of the left side is correlated with every local mode of the right, and vice versa. Similarly, every local mode is correlated with every other local mode of the same side, as demonstrated by the fact that the blocks $\boldsymbol{\sigma}_{mn}$ and $\bar{\boldsymbol{\sigma}}_{mn}$ are nonzero.

14.4.2 The state of three regions

We will now outline exactly the same procedure for the case of three regions in the cavity (equivalently, the case where two mirrors are simultaneously introduced). This will allow us to consider the entanglement between spatially-separated regions (i.e. the leftmost and

rightmost regions). As we will see, this is crucial for demonstrating that the entanglement obtained by slamming mirrors is derived from the previously existing vacuum entanglement, rather than having been created by the slamming process.

The procedure follows from the Bogoliubov transformation described in Sect. 14.3.3. We will also describe how to obtain the reduced state of two out of the three regions (in fact this is trivial in the language of covariance matrices). In the phase space representation we have equivalent matrix equations as those in Eq. (14.4.3,14.4.4,14.4.5), i. e.:

$$\hat{\mathbf{x}}^Z = \mathbf{S}^Z \hat{\mathbf{X}}, \qquad Z = A, B, C \tag{14.4.14}$$

where $\mathbf{S}^Z$ has the block form as given in Eq. (14.4.4):

$$\mathbf{S}^Z_{mn} = \begin{pmatrix} \mathrm{Re}(\alpha^Z_{mn} - \beta^Z_{mn}) & \mathrm{Im}(\alpha^Z_{mn} + \beta^Z_{mn}) \\ -\mathrm{Im}(\alpha^Z_{mn} - \beta^Z_{mn}) & \mathrm{Re}(\alpha^Z_{mn} + \beta^Z_{mn}) \end{pmatrix} \tag{14.4.15}$$

$$= 2\mathcal{V}^Z_{mn} \begin{pmatrix} \omega^Z_m & 0 \\ 0 & \Omega_n \end{pmatrix}. \tag{14.4.16}$$

The combined transformation, that which is formally symplectic, is given in analogy to Eq. (14.4.7):

$$\mathbf{S}_{\text{Bogo}} = \begin{pmatrix} \mathbf{S}^A \\ \mathbf{S}^B \\ \mathbf{S}^C \end{pmatrix}, \tag{14.4.17}$$

and transforms the global mode basis to the local mode basis of the three regions:

$$\begin{pmatrix} \hat{\mathbf{x}}^A \\ \hat{\mathbf{x}}^B \\ \hat{\mathbf{x}}^C \end{pmatrix} = \mathbf{S}_{\text{Bogo}} \hat{\mathbf{X}}. \tag{14.4.18}$$

Again, to Bogoliubov transform the global state $\boldsymbol{\sigma}_G = \mathbf{I}$ to the local basis we apply this transformation to $\boldsymbol{\sigma}_G$:

$$\boldsymbol{\sigma}_{\text{loc}} = \mathbf{S}_{\text{Bogo}} \boldsymbol{\sigma}_G \mathbf{S}^T_{\text{Bogo}} \equiv \begin{pmatrix} \boldsymbol{\sigma}_A & \boldsymbol{\gamma}_{AB} & \boldsymbol{\gamma}_{AC} \\ \boldsymbol{\gamma}^T_{AB} & \boldsymbol{\sigma}_B & \boldsymbol{\gamma}_{BC} \\ \boldsymbol{\gamma}^T_{AC} & \boldsymbol{\gamma}^T_{BC} & \boldsymbol{\sigma}_C \end{pmatrix}$$

$$= \begin{pmatrix} \mathbf{S}^A \boldsymbol{\sigma}_G \mathbf{S}^{A^T} & \mathbf{S}^A \boldsymbol{\sigma}_G \mathbf{S}^{B^T} & \mathbf{S}^A \boldsymbol{\sigma}_G \mathbf{S}^{C^T} \\ \mathbf{S}^B \boldsymbol{\sigma}_G \mathbf{S}^{A^T} & \mathbf{S}^B \boldsymbol{\sigma}_G \mathbf{S}^{B^T} & \mathbf{S}^B \boldsymbol{\sigma}_G \mathbf{S}^{C^T} \\ \mathbf{S}^C \boldsymbol{\sigma}_G \mathbf{S}^{A^T} & \mathbf{S}^C \boldsymbol{\sigma}_G \mathbf{S}^{B^T} & \mathbf{S}^C \boldsymbol{\sigma}_G \mathbf{S}^{C^T} \end{pmatrix}. \tag{14.4.19}$$

The blocks again represent the reduced state of, and the correlations between, the three regions. For example $\boldsymbol{\sigma}_A$ is the reduced state of the left-most region and $\boldsymbol{\gamma}_{AC}$ contains the correlations between the left-most and right-most regions. As before, each matrix can be further split into 2x2 blocks given by $\boldsymbol{\sigma}^Z_{mn} = \sum_\ell \mathbf{S}^Z_{m\ell}\mathbf{S}^Z_{n\ell}$, $\gamma^{YZ}_{mn} = \sum_\ell \mathbf{S}^Y_{m\ell}\mathbf{S}^Z_{n\ell}$. These are given by

$$\boldsymbol{\sigma}^Z_{mn} = \sum_l 4\mathcal{V}^Z_{ml}\mathcal{V}^Z_{nl}\begin{pmatrix}\omega^Z_m\omega^Z_n & 0\\ 0 & \Omega^2_l\end{pmatrix} \tag{14.4.20}$$

$$\boldsymbol{\gamma}^{YZ}_{mn} = \sum_l 4\mathcal{V}^Y_{ml}\mathcal{V}^Z_{nl}\begin{pmatrix}\omega^Y_m\omega^Z_n & 0\\ 0 & \Omega^2_l\end{pmatrix}. \tag{14.4.21}$$

From here, one may easily study the reduced state of two of the three regions by simply taking the appropriate blocks of Eq. 14.4.19. For example the reduced state of system AC (the left-most and right-most regions) is obtained by tracing out B, which here simply results in the covariance matrix

$$\begin{aligned}\boldsymbol{\sigma}_{\mathrm{AC}} &= \begin{pmatrix}\boldsymbol{\sigma}_A & \boldsymbol{\gamma}_{AC}\\ \boldsymbol{\gamma}^T_{AC} & \boldsymbol{\sigma}_C\end{pmatrix}\\ &= \begin{pmatrix}\mathbf{S}^A\boldsymbol{\sigma}_G\mathbf{S}^{A^T} & \mathbf{S}^A\boldsymbol{\sigma}_G\mathbf{S}^{C^T}\\ \mathbf{S}^C\boldsymbol{\sigma}_G\mathbf{S}^{A^T} & \mathbf{S}^C\boldsymbol{\sigma}_G\mathbf{S}^{C^T}\end{pmatrix}.\end{aligned} \tag{14.4.22}$$

14.5 With vs. without a mirror

Before we proceed to analyse other local features like the entanglement between left and right regions of the cavity, we would like to make a stop to discuss a little bit more conceptually the differences between the analysis of the two possible scenarios, with and without introducing the mirror. Again, what does it mean for half of an empty box to be non-empty? We know that in some sense the reduced state of a subregion of the global vacuum is excited; certainly the state $\boldsymbol{\sigma}$ in Eq. (14.4.11) is an excited state (that is, excited with respect to the local-mode basis, which is the whole point). However, what does this mathematical fact have to do with reality? As discussed earlier, the answer, in fact, is that the real excitations produced by the mirror are mathematically equivalent to the virtual local excitations attributed to vacuum entanglement. Their measurement, therefore, constitutes an achievement of our goal.

14.5.1 Time evolution

Both of the scenarios, with and without a mirror, are equivalent at time $t = 0$. This implies that the Bogoliubov transformation will be exactly the same for both sets (primed and unprimed modes as discussed in the previous sections) as the transformation coefficients are computed using the Klein-Gordon inner product, which contains only the mode functions and their first time-derivatives [164]). Thus, the field state of the left-cavity immediately following the introduction of the mirror will, in fact, be given exactly by the covariance matrix $\boldsymbol{\sigma}$ as given by Eqs. (14.4.10,14.4.11). The only difference now is that the mode-basis that $\boldsymbol{\sigma}$ is associated with is different, in the sense that it evolves differently for $t > 0$. Similarly the reduced state of the right-cavity will be given by $\bar{\boldsymbol{\sigma}}$ and the correlations between the two (separated) cavities will be contained in $\boldsymbol{\gamma}$, the blocks of each being given by Eqs. (14.4.11). Importantly, this means that the entanglement structure contained in the state is exactly the same in both cases . That is, the real particles created in the left-side by slamming down a mirror are entangled with the created particles in the right-side, and this entanglement has exactly the same structure that the original vacuum entanglement present before the mirror was introduced. We will fully discuss this entanglement in Sect. 14.6.

But surely the state of the field has been changed due to the introduction of the mirror. Clearly in some sense it has. We have created real particles. We have added energy to the system by changing the Hamiltonian. The state of the new left-side cavity (for example) is certainly time-dependent. This is not surprising, as we would expect a burst of particles to be propagating away from the newly introduced mirror (shortly we will discuss this further). The reduced state of the left-side of the larger cavity (without a mirror), on the other hand, is by construction time-independent. The global vacuum $|0\rangle_G$ is a stationary state with respect to the global Hamiltonian $\hat{H}_G$, and thus the reduced state will be time-independent as well. In this sense the two states are certainly different.

Nevertheless the state is described by exactly the same covariance matrix. We will now elucidate the nature of time evolution in the case that a mirror has been slammed; indeed we will take advantage of a subtlety in the time evolution that is particularly apparent when working with covariance matrices. First consider, for example, working in the Schrödinger picture. In this case the field in the left-cavity is time-independent: $\hat{\phi}(x,t) = \hat{\phi}(x,t=0) = \sum_m (u_m(x,0)\hat{a}_m + u_m^*(x,0)\hat{a}_m^\dagger)$, where a $u_m(x,0) = \frac{1}{r\omega_m}\sin\frac{\pi m x}{r}$. The state $\hat{\rho}(t)$ is what evolves, and this gives a corresponding time evolution to the covariance matrix elements via $\sigma_{mn}(t) = \text{Tr}(\hat{\rho}(t)(\hat{x}_m\hat{x}_n + \hat{x}_n\hat{x}_m))$. This free evolution can be represented symplectically:

$\boldsymbol{\sigma}(t) = \mathbf{S}_F(t)\boldsymbol{\sigma}\mathbf{S}_F(t)^T$ where [136]

$$\mathbf{S}_F(t) = \bigoplus_m \begin{pmatrix} \cos\omega_m t & \sin\omega_m t \\ -\sin\omega_m t & \cos\omega_m t \end{pmatrix}. \tag{14.5.1}$$

Alternatively we can work in the Heisenberg picture, in which the field is the time-dependent operator

$$\begin{aligned} \hat{\phi}(x,t) &= \sum_m (u_m(x,0)\hat{a}_m e^{-\mathrm{i}\omega_m t} + u_m^*(x,0)\hat{a}_m^\dagger e^{\mathrm{i}\omega_m t}) \\ &= \sum_m (u_m(x,t)\hat{a}_m + u_m^*(x,t)\hat{a}_m^\dagger). \end{aligned} \tag{14.5.2}$$

A subtle issue, however, is that the Heisenberg evolution of the field can be viewed in two ways, as given by the two lines above. In the first line it is the operators themselves that evolve: $\hat{a}_m(t) = \hat{a}_m e^{-\mathrm{i}\omega_m t}$. This corresponds to an evolution of the quadrature operators $\hat{x}_m(t)$ that leads to a symplectic evolution $\mathbf{S}_F(t)$ of the covariance matrix, equivalent to what was obtained in the Schrödinger picture. A key observation is that in both of these pictures it is the *time-independent mode-functions* $u_m(x,0)$ that the *time-dependent covariance matrix* $\boldsymbol{\sigma}(t)$ is associated with. The other way of viewing the evolution, as indicated by the second line in Eq. (14.5.2), is to keep the operators themselves time-independent (thus giving a time-independent $\boldsymbol{\sigma}$) and to rather let the mode-functions $u(x,t)$ contain the time evolution. In this case the covariance matrix does not change, but it is understood that the mode-functions with which it is associated *do* evolve.

This last picture is the one that we will adopt here, in all work below. In this way we do not need to actually consider any evolution in the covariance matrix directly; our state will always be described by the matrix $\boldsymbol{\sigma}$, the same one used to describe the spatial reduced state in the case without a mirror. The time-evolution induced by slamming a mirror is then trivial: it is simply given by the time-dependence already present in the $t > 0$ mode functions defined within the left cavity as $u_m(x,t) = u_m(x,0)e^{-\mathrm{i}\omega_m t}$ and within the right cavity as $\bar{u}_m(x,t) = \bar{u}_m(x,0)e^{-\mathrm{i}\bar{\omega}_m t}$

14.5.2 Finite-time mirror

In the calculations of the next section we will continue to assume an instantaneous introduction of the mirror(s) in the cavity. Before devoting ourselves to this, however, we should briefly discuss how the physics changes if the introduction of the mirror takes place within a finite time window Δt, as of course will always be the case in any physical realization. Let us continue to assume that the introduction happens very fast as compared to the fundamental

time scales of the reduced cavities: $\Delta t \ll 1/\omega_1$ and $\Delta t \ll 1/\bar{\omega}_1$. In this case the low-energy local modes will still see the mirror appear very quickly (i.e. as compared to their free evolution time scale), and so their reduced states and correlations amongst themselves will be well approximated by the covariance matrices of Eqs. (14.4.11). That is, within a low energy sector (the limit of which is determined by how fast the mirror can be introduced) the results that we will present will hold to a good approximation. On the other hand for the very high-energy modes (that see the introduction of the mirror occur very slowly) we can make an adiabatic approximation to conclude that they will evolve to their local ground states. That is, if m is large enough such that $\Delta t \gg 1/\omega_m$ then after the cavity is introduced the reduced state of this mode will approximately be $|0\rangle_m$, defined to satisfy $\hat{a}_m |0\rangle_m = 0$, and will have vanishing correlation with the rest of the system. Clearly there will be a smooth transition between these two regimes, which our work does not capture. Nevertheless by considering only a finite number of modes N, as we will be doing, our description of this set will be accurate as long as $\Delta t \ll 1/\omega_N$.

Note also that, in terms of application, the amount of entanglement that one obtains between cavities after slamming a mirror (which we will discuss in the next section) depends on how fast one's mirror is slammed. The faster it can be achieved, the more entanglement will remain in the two cavities afterwards. This is because the high-energy modes contain entanglement, and thus the more of these modes whose states are not significantly altered by introducing the mirror. the more entanglement we will retained. For modes of too-high energy, $\Delta t \gg 1/\omega_m$, the act of slamming the mirror will destroy the correlations that they have with the opposite side of the cavity.

14.6 Entanglement

We will now enter the results section. We will discuss various aspects of entanglement between the two sides of the cavity (equivalent in both the cases of with and without a cavity, as discussed above). As part of our exposition we will propose a spatial distribution of entanglement between the two sides of the cavity, and see how this naturally leads to the physical picture of bursts of (entangled) particles being produced by slamming down a mirror. We will begin by just discussing a single mirror, and later will move on to the two-mirror case. We will show that with two mirrors, slammed simultaneously some distance apart, there is still entanglement retained between separated regions (i.e. left-most and right-most). We will also discuss how the act of slamming down a mirror can be interpreted as an efficient method of vacuum entanglement harvesting.

Our result are computed numerically from the covariance matrices presented Sect. 14.4. To do so, however, we must restrict to finite matrices. This means taking only a finite number of local modes N, both on the left and right sides. That is, what we actually consider is the reduced state of the first N local modes on each side. This is actually not physically unrealistic since, as discussed in Sect. 14.5.2, our analysis will only be valid for some low-energy regime anyway, depending on how fast the mirror is slammed. Numerically, unless otherwise stated we will take $N = 200$. Note, however, that the reduced state of these first N local modes is exact up to numerically negligible addends. That is, in performing the Bogoliubov transform we made sure to include enough global modes in the sum of Eq. (14.4.11), such that our results converge.

14.6.1 Mode-mode entanglement

With the state of the global vacuum represented in the local-mode basis, as given by Eqs. (14.4.11), we can characterize the entanglement between the two sides of the cavity. We can, for example, consider the two-mode entanglement between each pair of local modes on the left and right side. The correlations between each pair (as given by the two-point correlators of the number operators) have already been computed in [2]. However, for each two-mode pair the fact that they are correlated does not imply that they are entangled because the two-mode state of this pair is mixed. Thus, to extend upon the results of [2] we compute the logarithmic negativity E_N [340] of each pair between the two sides.

To this end, we take the 4×4, two-mode covariance matrix (i.e. the reduced state) of mode m on the left and mode n on the right of the cavity. This is simply

$$\boldsymbol{\sigma}_{\text{two mode}} = \begin{pmatrix} \boldsymbol{\sigma}_{mm} & \boldsymbol{\gamma}_{mn} \\ \boldsymbol{\gamma}_{mn}^T & \bar{\boldsymbol{\sigma}}_{nn} \end{pmatrix}. \tag{14.6.1}$$

From here, we can apply Eq. (A.0.14) to compute E_N between the two modes. The result is displayed in Fig. 14.3, where we consider field masses $\mu = 0$ and $\mu = 15/R$. The cavity is split in two equal regions as $r = 0.5R$. We observe that, perhaps remarkably, nearly every mode is entangled with almost every other. Eventually as m and n become sufficiently different the two-mode entanglement tends to vanish (although they will always have nonzero correlation), but we can see that the decay is very slow. It should be noted that we can similarly compute the entanglement between different local modes from the same side, and in fact doing so produces a qualitatively equivalent plot. A particularly striking feature of the mode-mode entanglement is that the peak entanglement moves to higher mode numbers as the mass of the field is increased. [4] This figure clearly demonstrates that

[4] This behavior is actually expected from the fact that the correlation length in a field goes as the Compton

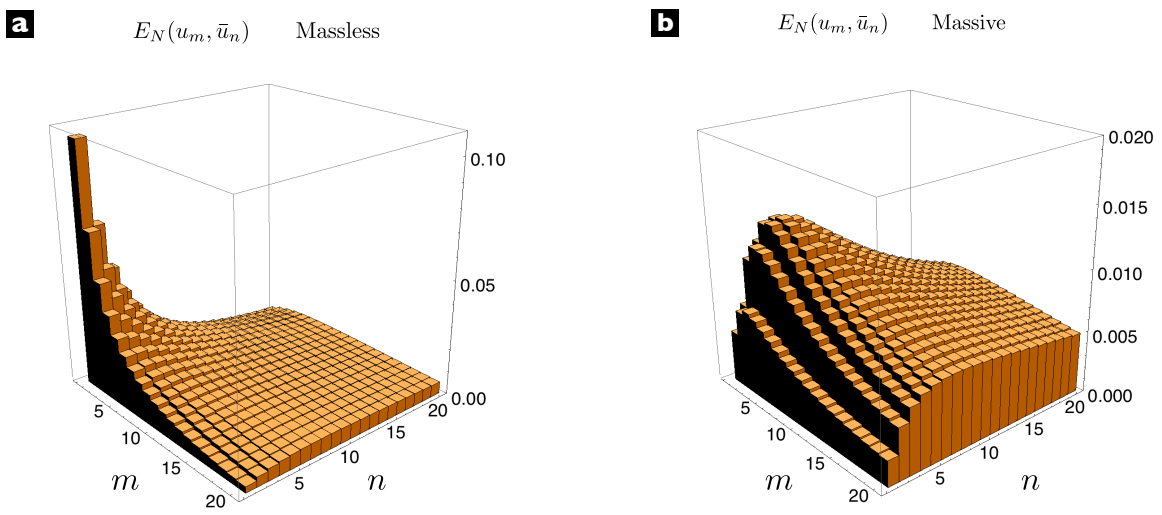

Figure 14.3: (Color online) The logarithmic negativity E_N between local modes u_m and $\bar{u}_n$ on the left and right sides of the cavity, respectively. The cavity is divided in two equal regions $r = 0.5R$. Left: a field mass of $\mu = 0$. Right: a field mass of $\mu = 15/R$.

the two sides of the cavity are entangled. Even a single pair with nonzero entanglement demonstrates this. However even if every pair were separable this would *not* constitute a proof that the two sides as a whole are separable.

This leads to the question of the full, many-mode entanglement between the two sides. We can certainly compute this, given some set of N local modes on either side [337] (specifically we would compute the negativity, not the reduced entropy, as we explain in a moment). This of course gives a non-zero answer, however it is questionable how useful the numerical answer actually is because it will always depend on the number of local modes N considered. The entanglement increases with N, and we expect that it diverges in the $N \to \infty$ limit (check footnote 5), given that the vacuum entanglement is typically known to be UV-divergent. We will thus not concern ourselves with this calculation explicitly. Nevertheless there is a related issue that should be discussed before moving on, which we will now focus on.

14.6.2 The mixedness problem

One would assume that in order to compute the entanglement one should simply compute the reduced entropy (as given by Eq. (A.0.9)) of one side of the cavity, since the global state

wavelength [341], meaning that correlations become more spatially confined with higher mass μ. It follows that what correlations are present between the two sides should be more supported within the modes of smaller wavelength, i.e. those of higher frequency.

is pure. Formally this is true of course, but interestingly the reduced entropy will never be an entanglement measure if one only considers a finite number of local modes N, and in fact this can never be remedied by simply increasing N.

This occurs because, as we have just seen, there is quite a lot of correlation between local modes of different number. This means that the left-side state $\boldsymbol{\sigma}$ (with finite number of modes) will not just be entangled with the opposite side of the cavity but also with the higher-number modes on the same side. That is, the entropy $S(\boldsymbol{\sigma})$ is *not* a measure of entanglement with the other side, but rather with the other side plus all of the higher modes that we have traced away. Put another way: if we compute the full state of both sides $\boldsymbol{\sigma}_{\text{loc}}$, but with the understanding that this corresponds to the reduced state of the first N local modes on the left with the first N on the right (and their correlations), then this state will be mixed despite the fact that the global vacuum is pure. Equivalently, the transformation of Eq.(14.4.7) will never in practice be sympletic. What's more (and rather interestingly) this problem does *not* get better as N is increased [5].

Importantly, such an issue will never arise in any real scenario of a slamming mirror; a finite slamming time Δt fixes this mixedness problem. The introduction of a mirror is just represented by a time-dependent Hamiltonian, and so of course the evolution of the field under this action must be unitary. The system of the two new cavities combined, therefore, must be in a pure state. As discusses in Sect. 14.5.2, a finite Δt will mean that local modes of high enough frequency will not actually be in the state nor share the correlations as predicted

[5] In fact, as we increase the number N of local modes considered (on both sides of the cavity) the global state we obtain becomes *more* mixed, with a higher entropy. We suspect that the entropy diverges in the $N \to \infty$ limit, despite the fact that in a formal sense the result should be a pure state. After a moment of thought this is actually not overly surprising. Consider for a moment the very different system of a spatial volume in free Minkowski space with a field in the Minkowski vacuum. It is well known that the entropy of the reduced state inside the volume scales as its area, meaning that as this region is expanded it becomes more mixed. Thus, despite the field over all of space being in a pure state, one can never approach this by taking the limit of larger and larger regions (the entropy will diverge as the region expands to infinity). In this example the area-law can be physically understood by taking a spatial discretization of the field. A given spatial degree of freedom will largely only be entangled with its nearest neighbors, and thus the area law can be understood considering that the area is proportional to the number of nearest-neighbor connections that the entangling surface crosses. In our scenario we have seen that the global vacuum has a very densely connected entanglement structure in the local-mode basis. Every local mode is entangled with many others, including many others of higher frequency. Thus, by increasing the number of local modes N that we consider we are increasing the number of "entanglement connections" between low and high modes that are separated by the cutoff. Given this intuition it makes sense that the entropy of our global state should increase with increasing N; it arises as a consequence of the system being highly connected. Even so, it is interesting (and perhaps disconcerting) that in the local-mode basis one can never approach purity by considering more and more modes. We suspect that this is deeply connected to the note made in [2] regarding the unitary inequivalence between the global and local mode bases.

from the covariance matrices in Sect. 14.4, which were computed assuming instantaneous slamming. For a real situation, high-frequency local modes will be nearly in their ground states, and importantly have vanishing correlations with anything else, thus remedying the origin of the mixedness problem. The global state in the local basis will indeed be pure beyond a given energy scale, as it must be.

14.6.3 Symplectic diagonalization

Here we will describe the process of symplectically diagonalizing the local states $\boldsymbol{\sigma}$ and $\bar{\boldsymbol{\sigma}}$. This is method by which we can greatly simplify the entanglement structure between the two sides which, given the complexity seen in Fig. 14.3, will be a considerable advantage. We will see in later sections how this process also allows us to make conclusions about the spatial distribution of entanglement as well as see very clearly the propagating "burst" of particles that is produced by slamming down a mirror.

The specifics of local, symplect diagonalization and the method for finding the correct transformations matrices are described in Appendices A and A. We (numerically) find symplectic matrices $\mathbf{S}_D$ and $\bar{\mathbf{S}}_D$ that diagonalize $\boldsymbol{\sigma}$ and $\bar{\boldsymbol{\sigma}}$, respectively: $\mathbf{S}_D\boldsymbol{\sigma}\mathbf{S}_D^T = \mathbf{D}$ and $\bar{\mathbf{S}}_D\bar{\boldsymbol{\sigma}}\bar{\mathbf{S}}_D^T = \bar{\mathbf{D}}$ where

$$\mathbf{D} = \bigoplus_m \begin{pmatrix} \nu_m & 0 \\ 0 & \nu_m \end{pmatrix}, \quad \bar{\mathbf{D}} = \bigoplus_m \begin{pmatrix} \bar{\nu}_m & 0 \\ 0 & \bar{\nu}_m \end{pmatrix}. \tag{14.6.2}$$

Here ν_m and $\bar{\nu}_m$ are the symplectic eigenvalues of $\boldsymbol{\sigma}$ and $\bar{\boldsymbol{\sigma}}$, respectively. Let's just consider the left side for a moment: $\boldsymbol{\sigma} \to \mathbf{D}$. This is simply a change of mode-basis, and we can compute the mode functions associated with this new basis by reading off the Bogoliubov coefficients from $\mathbf{S}_D$ via reversing Eqs. (14.4.4,14.4.5) . Here we will label these coefficients $\zeta_{\ell m}$ and $\eta_{\ell m}$ (in place of the usual α and β notation, respectively). These new mode functions, which we will label $v_\ell(x,t)$, are thus given by

$$\begin{aligned} v_\ell(x,t) &= \sum_m (\zeta_{\ell m} u_m(x,t) + \eta_{\ell m} u_m^*(x,t)) \\ &= \sum_m \frac{1}{\sqrt{r\omega_m}} \sin\left(\frac{\pi m x}{r}\right) (\zeta_{\ell m} e^{-\mathrm{i}\omega_m t} + \eta_{\ell m} e^{\mathrm{i}\omega_m t}). \end{aligned} \tag{14.6.3}$$

We can similarly define a new set of local modes $\bar{v}_\ell(x)$ on the right side of the cavity.

We remind the reader that (as discussed in Sect. 14.5.1) we are working in the "Heisenberg picture", but not such that the $\hat{q}$ and $\hat{p}$ operators evolve (i.e. our covariance matrix is time-independent) but rather such that the mode functions with respect to which we represent the state themselves evolve. In this picture the diagonalizing transformations are of

course time-independent (since the covariance matrix is time-independent). We could, however, arrive at the same set of v-modes working directly in the Schrödinger picture, in which the diagonalizing transformation would be time-dependent [6].

This is a change of mode basis which results in all left-side modes $v_\ell(x,t)$ being in a product state with respect to each other, and similarly with the right-side modes $\bar{v}(x,t)$. I.e. the transformation $\mathbf{S}_D$ removes all correlations between modes on the left side. In this way we are isolating exactly the local spatial modes that contain the entanglement between $\boldsymbol{\sigma}$ and the rest of the system. Furthermore, it turns out that in our system the first mode in this new basis, the one associated with symplectic eigenvalue ν_1 and spatial mode $v_1(x,t)$, is the mode that contains the large majority of the mixedness in $\boldsymbol{\sigma}$. That is, almost all of the symplectic eigenvalues have values very near to unity, meaning that the corresponding modes are very nearly pure. The first value, ν_1, is by far the largest. For example with the parameters $r = 0.5R$, $\mu = 0$, and $N = 200$ (the number of local modes considered) the first several symplectic eigenvalues take the values $\{\nu_\ell\} = (1.840, 1.051, 1.004, 1.000, \cdots)$. Note that as N is increased these values (and thus the entropy of $\boldsymbol{\sigma}$) increase as well. All of this applies equally well to the right-side transformation $\bar{\boldsymbol{\sigma}} \to \bar{\mathbf{D}}$ via $\bar{\mathbf{S}}_D$.

As elaborated on in Appendix A, if the state $\boldsymbol{\sigma}_{\text{loc}}$ of both sides were pure then applying the local transformation $\mathbf{S}_D \oplus \bar{\mathbf{S}}_D$ to $\boldsymbol{\sigma}_{\text{loc}}$ would also diagonalize the off-diagonal (correlation) block $\boldsymbol{\gamma}$. Were this the case then the local mode $v_1(x,t)$ on the left side would be solely correlated with the corresponding mode $\bar{v}_1(x,t)$ on the right side, and similarly for the higher v-modes. Unfortunately, as discussed above, when taking a finite N we necessarily find that $\boldsymbol{\sigma}_{\text{loc}}$ is a mixed state. This means that a local symplectic diagonalization does not produce this one-to-one correspondence between the two sides. Despite this, however, we have found that in fact we very nearly do obtain this correspondence upon local diagonalization. This can be seen in Fig. 14.4 where we plot the logarithmic negativity between modes $v_\ell(x,t)$ and $\bar{v}_\ell(x,t)$ similarly to what is plotted in Fig. 14.3 for the u-modes. Here we have taken $N = 200$ for both the left and right sides. We see that indeed, despite $\boldsymbol{\sigma}_{\text{loc}}$ being mixed, the majority of the entanglement between the two sides is contained in $v_1(x,t)$ and

[6] This can also be done in either of the pictures in which it is the covariance matrix that evolves, $\boldsymbol{\sigma}(t) = \mathbf{S}_F(t)\boldsymbol{\sigma}\mathbf{S}_F(t)^T$, and in which the spatial modes are time independent, $u_m(x,0)$. In this case the diagonalizing transformation will be time-dependent: $\mathbf{S}_D(t)$. However the symplectic spectrum of $\boldsymbol{\sigma}(t)$ will be time-independent, being symplectically invariant. Thus we have $\mathbf{D} = \mathbf{S}_D\boldsymbol{\sigma}\mathbf{S}_D^T = \mathbf{S}_D(t)\boldsymbol{\sigma}(t)\mathbf{S}_D(t)^T = \mathbf{S}_D(t)\mathbf{S}_F(t)\boldsymbol{\sigma}\mathbf{S}_F(t)^T\mathbf{S}_D(t)^T$, from which we can represent the time-dependent diagonalizing transformation as $\mathbf{S}_D(t) = \mathbf{S}_D\mathbf{S}_F(-t)$. We can use this to compute the corresponding time-dependent Bogoliubov coefficients $\gamma_{\ell m}(t)$ and $\eta_{\ell m}(t)$. Using Eq. (14.5.1) and the relation between a symplectic transformation and its corresponding Bogoliubov coefficients, as given by Eqs. (14.4.4,14.4.5), it is straightforward to find that $\gamma_{\ell m}(t) = \gamma_{\ell m}e^{-\mathrm{i}\omega_m t}$ and $\eta_{\ell m}(t) = \eta_{\ell m}e^{\mathrm{i}\omega_m t}$, in agreement with Eq. (14.6.3).

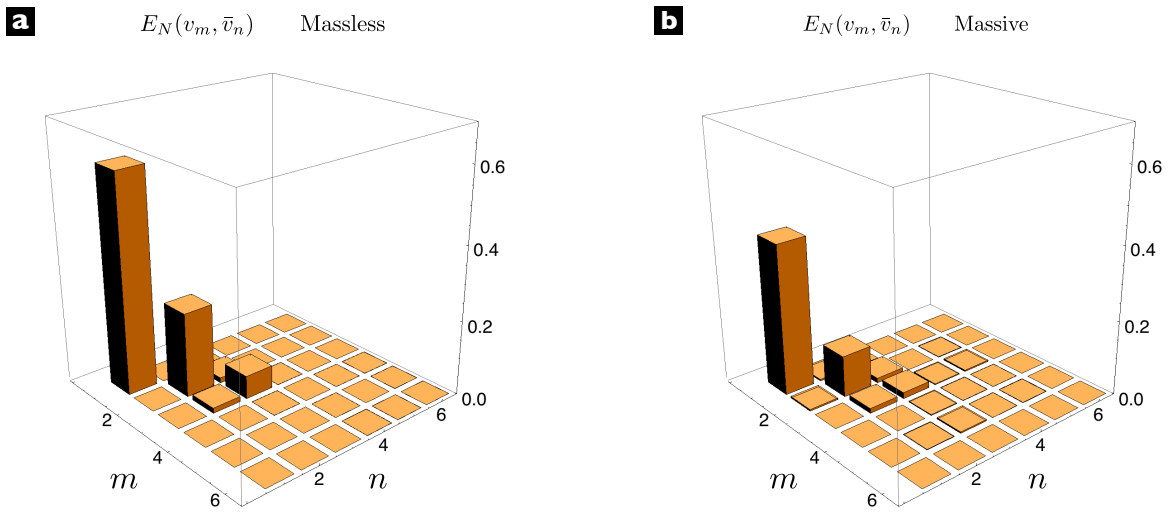

Figure 14.4: (Color online) The logarithmic negativity E_N between local, diagonalizing modes v_m and $\bar{v}_n$ on the left and right sides of the cavity, respectively. The cavity is split into two equal sides, $r = 0.5R$, and $N = 200$ for both the left and right sides. Left: a field mass of $\mu = 0$. Right: a field mass of $\mu = 15/R$.

$\bar{v}_1(x,t)$ (we could also plot the mutual information between modes, in order to get a better idea of the correlations in general, but the result looks nearly identical qualitatively).

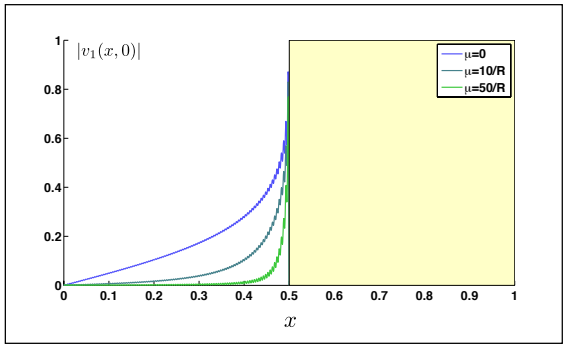

Figure 14.5: (Color online) The function $|v_1(x)|$ in the left-side of the cavity, representing the spatial structure of entanglement with the opposite side. The parameters are given by $r = 0.5R$, and $N = 200$, with different field masses μ considered: 0 (blue), $10/R$ (light blue) and $50/R$ (green). As can be seen: the larger the mass of the field, the closer the entanglement straddles the boundary between the two sides of the cavity, as expected.

14.6.4 Spatial structure of entanglement

One immediate application of finding the locally, symplectically diagonalizing basis is that we are able to discuss and make observations about the spatial structure of entanglement between the two sides of the cavity. For this section we will take $t = 0$, by which we are discussing the local physics of the cavity before the mirror has been introduced. That is,

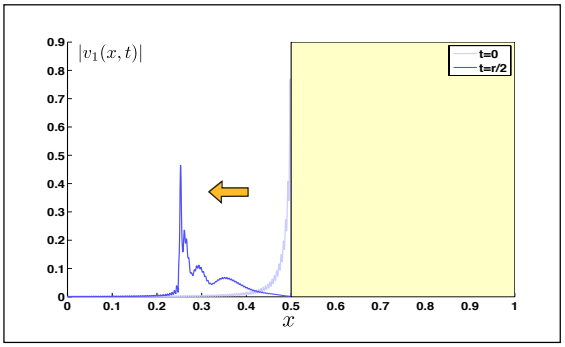

Figure 14.6: (Color online) Evolution of the entanglement spatial structure for the massive case $\mu = 50/R$ after an elapsed time $t = r/2$. We can see a peak for the correlations at exactly the position of the particle-burst front as originated from the slamming. The cavity parameters are the same as in Fig. 14.5

in this section we are simply asking about the local properties of a vacuum field, and not considering yet the time evolution caused by introducing a mirror.

We know that there is spatial vacuum entanglement; the two sides of the cavity are entangled. This fact alone, however, gives no information on how entanglement is spatially distributed. From what is known about vacuum entanglement we expect it to be spatially focused near the boundary between the two regions, since the correlation in a field decays with distance [331, 334, 335]. It is this that leads, for example, to the well-known area-law for the entanglement entropy. There is also evidence that the entanglement characteristic distance goes as the Compton wavelength of the field [341], thus we should also expect the entanglement spatial distribution to hug the boundary more closely as we increase the mass μ of the field.

To obtain information on the spatial structure of entanglement we use a technique very similar to that in [338], which there was used within the context of lattice systems. Since the mode function $v_1(x)$ contains the majority of the entanglement (right now working at $t = 0$), what we propose is that the function $|v_1(x)|$ gives information about the spatial structure of entanglement. The larger $|v_1(x)|$ is at a given x, the more entanglement is localized at that point. Operationally this proposal makes sense; if one were to try to swap this entanglement into an Unruh-deWitt type detector model then it makes sense to place the detector where $|v_1(x)|$ is largest, since this directly translates into the coupling strength between this mode and the detector. Of course there is also entanglement in the higher v-modes, and these would form corrections to our $|v_1|$ estimate. Seen another way, we can consider measuring the entanglement between regions by means of local projective measurements onto a pair of spatial modes [139,342]. Since most of the entanglement is isolated between $v_1(x)$ and $\bar{v}_1(x)$, it is these modes that we would want to measure in order to obtain the greatest amount of

entanglement.

In Fig. 14.5 we plot the function $|v_1(x)|$ at time $t = 0$ using the parameters $r = 0.5R$, $N = 200$, and for three mass values μ of 0, $10/R$, and $50/R$. As can be seen, both of the conditions discussed above are satisfied. Namely, the distribution indeed straddles the boundary between the two sides of the cavity (in this case the boundary is to the right because we are looking at the left side). Furthermore, as the mass μ of the field is increased we see that the distribution becomes more localized at the boundary, representing a decreasing correlation length.

Note that the small vibrations that can be seen in Fig. 14.5 are due solely to taking a finite number N of local modes. As N is increased these vibrations become smaller. However the overall shape of the function does not change upon increasing N; a fact that further indicates that the function $|v_1(x)|$, as plotted, well represents the entanglement structure despite the mixedness problem.

All that we have done here is show the shape of the left-side mode function that contains most of the entanglement with the right side, and how much this can truly be considered a distribution of entanglement is questionable. A more thorough approach to discuss the entanglement spatial structure could be to consider the local reduced states for infinitesimally small regions and see how much these regions are entangled with the right side of the box.

14.6.5 Entangled bursts of particles

In the previous section we have looked at the form of $|v_1(x, t = 0)|$ and claimed it to a good representation of the spatial distribution of entanglement. A next obvious questions is: in the case that we slam down a mirror at $t = 0$, how does $|v_1(x, t)|$ evolve for $t > 0$ and what significance does this have? The time evolution is simply given by Eq. (14.6.3), i.e. $v_1(x, t)$ evolves according to the Klein Gordon equation with initial conditions given by $v_1(x, 0), \dot{v}_1(x, 0)$, as shown in Fig. 14.5. As can be expected, the evolution is that of a wavepacket propagating away from the newly slammed mirror. For example in Fig. 14.6 we plot $|v_1(x, t)|$ at time $t = r/2$ for parameters $r = 0.5R$, $N = 200$, and with a field mass of $\mu = 50/R$.

By construction, however, the state of this evolving mode and the correlations between it and the right-hand cavity are exactly the same as at $t = 0$ (i.e. highly excited and highly entangled with right-hand mode $\bar{v}_1$), when these correlations could be interpreted solely as vacuum entanglement. That is, the state of the propagating wavepacket seen in Fig. 14.6 is highly excited, and is highly entangled with the symmetrically evolving wavepacket in the right-hand cavity. That is, we see exactly the physics we expect, namely that slamming

down a mirror produces bursts of particles that propagate away from it! Similarly in the right-hand cavity the function $\bar{v}_1(x,t)$ represents a burst of particles propagating to the right. A detector placed within one of these cavities will then be able to measure these particles once they hit it. [7] Additionally we see that the bursts on the two sides are entangled, and that they are entangled exactly in the same manner that the vacuum was entangled prior to the introduction of the mirror! In fact, their entanglement directly results from (or rather, it simply *is*) the vacuum entanglement prior to the mirror being slammed.

This emphasizes and illustrates nicely our primary message: that the real excitations created by slamming down a mirror are identical to the "virtual" excitations attributed to the original vacuum entanglement. Furthermore, this perspective motivates an experimental approach to verifying, and perhaps even harvesting and using, vacuum entanglement. That is, if we were able to slam a mirror and measure the real particles, in such a way that we could confirm quantum correlation statistics on the two sides, then this would constitute a verification of vacuum entanglement. We discuss this further in Sect. 14.7.

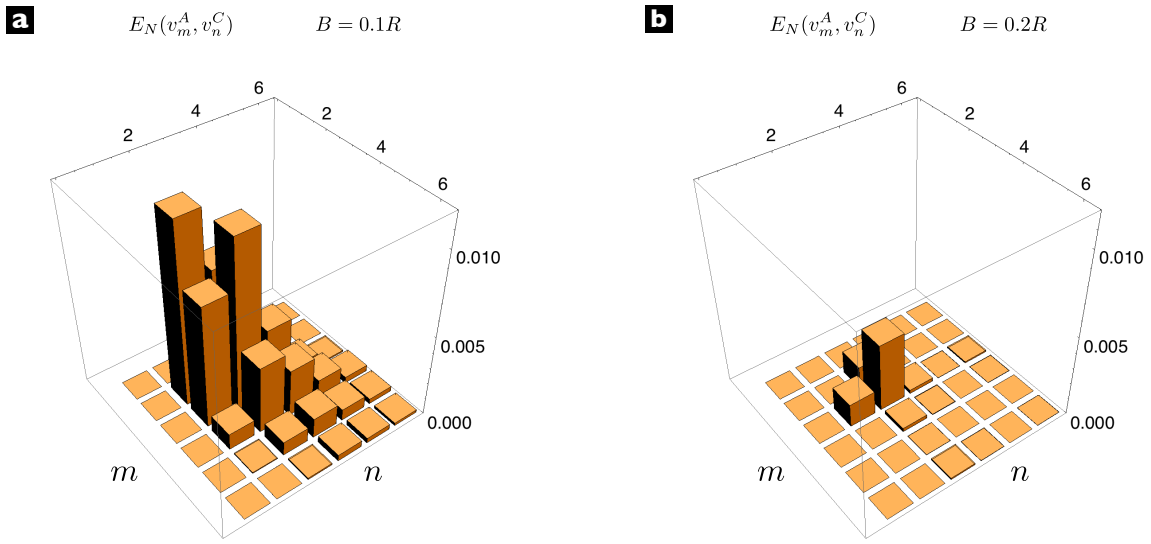

Figure 14.7: (Color online) Two mirror case: logarithmic negativity E_N between local, diagonalizing modes v_m^A and v_n^C on the left and right-most sides of the cavity, respectively. The cavity is in this case split into three regions, $\Delta_A = [0, 0.5R - B/2]$, $\Delta_B = [0.5R - B/2, 0.5R + B/2]$, $\Delta_C = [0.5R + B/2, R]$. We have taken $N = 200$. Left: Size of the middle section B = 0.1R. Right: Size of the middle section B = 0.2R.

The reader should know that this is an approximate picture in regards to visualizing the burst of particles, as we are just using a single delocalized mode $v_1(x,t)$. It is a good approx-

[7] One may be concerned that in Fig. 14.6 there appears to be an amount of acausal signaling. Of course, for a delocalized mode, it makes no sense to strictly talk about causality [136]. In any relevant calculation all modes would be considered and no acausal behavior would be seen.

imate picture, given that this mode contains the majority of excitations. However, in order to gain the full structure of the burst one could instead monitor the change at different times of the expectation values of local number operators attached to small (perhaps infinitesimal) regions. As the burst reaches these small regions we expect these number expectation values to jump, and they will be different from the vacuum expectation values only inside the future light cone of the spacetime point at which we slam the mirror.

14.6.6 Two mirrors

We have just stated that the entanglement between the bursts of particles produced by the slammed mirror, in the left and right-hand sides, comes from the vacuum entanglement that was previously there to begin with. One may, however, be concerned that this is simply one perspective on the situation. One may argue that what really physically occurs is that the act of slamming the mirror locally creates entangled quanta which then propagate away, rather than this entanglement having been previously present.

To debunk this view we need simply consider a slightly different scenario: that of slamming *two* mirrors down simultaneously, some distance apart from each other. It is known (and we will confirm) that there is entanglement between regions of space even when they are separated. This means that when we slam two mirrors the resulting field states in the left-most and right-most cavities will be entangled, as would be measurable from the real particle statistics. In this case one cannot claim that this entanglement was simply created by the mirror, because now there is no common mirror connecting the two regions. In this case it is clear that the entanglement between the two cavities comes directly from the vacuum entanglement that was already present beforehand as no causal signal can connect them.

The mathematics of this scenario is exactly the same as before except that now we must consider splitting the cavity into three regions, as we have already discussed in Sect. 14.4.2. We choose some size for the three regions (here we will take regions A and C to be the same size, and separated by some distance B). We can then take the reduced state of the left-most and right-most regions, as given by Eq. (14.4.22) and perform exactly the same entanglement analysis as we have done above. The result in short is that they are entangled. This validates our above argument since, by construction, this entanglement is present between real, stationary mode excitations after the mirrors have been introduced.

In particular, it is interesting to again perform the local, symplectic diagonalization such that we go to the local mode basis $\{v_m^A, v_n^C\}$. As discussed in Sect. 14.6.3, this procedure fails to produce a nice one-to-one entanglement structure when one's state is mixed. As we saw, the mixedness problem above only causes slight deviations from this structure.

Now, however, the extra mixedness in the AC system caused by tracing out B *really* ruins this structure. We plot in Fig. 14.7 the mode-mode logarithmic negativity between the v^A and v^C-modes for the cases in which the distance B between the two regions is $0.1R$ and $0.2R$, where we have taken $N = 200$ for each region and we use a massless field $\mu = 0$. As we can see, the entanglement rapidly decays with the distance between the regions, as should be expected. We also note that in this case the *higher* v-modes become the dominant entanglement carriers, meaning that to actually measure such entanglement one should try to change the wavepacket form that one is measuring to conform with the shape of $|v_2(x,t)|$ or $|v_3(x,t)|$ or whichever mode carries the most entanglement. It is not overly surprising that $v_1(x,t)$ becomes superseded for a large enough distance B once one realizes that $v_1(x,t)$ largely contains the entanglement localized on the boundary between regions. Once there is no common boundary we therefore rapidly lose this entanglement.

14.7 Experimental motivations and prospects

We would like to devote this section to discuss possible experimental platforms where to observe the phenomena here described. The primary motivation for such an experiment would be the verification of vacuum entanglement and, possibly in the future, an effective method of entanglement harvesting.

We must point out that the description of our model so far has considered an idealized theoretical scenario and has not been adapted to any particular experiment. Moreover, a first analysis shows that such an experiment would be highly challenging and some of the requirements needed (mirror slamming times, high sensitivities...) may require considerable effort before becoming feasible.

First of all, let us focus on the essential elements of the theoretical scheme, which should be imperatively implemented in any experiment of this sort. We require a quantum field in a cavity, which should be taken into its lowest energy state (the vacuum), and a boundary condition (here, a mirror) which will quickly appear somewhere inside the cavity and produce particles similar to the dynamical Casimir effect. For most platforms to be considered the field would be massless, as we will be dealing with electromagnetic fields. In addition, after these particles have been produced they must be detected and, if possible, their entanglement measured.

Before anything else, we should check the amount of particles created. Based on previous results [2], Fig. 14.8 shows the average number of local particles created after slamming the mirror, dividing the cavity in two equal sides. We can see that the maximum amount of

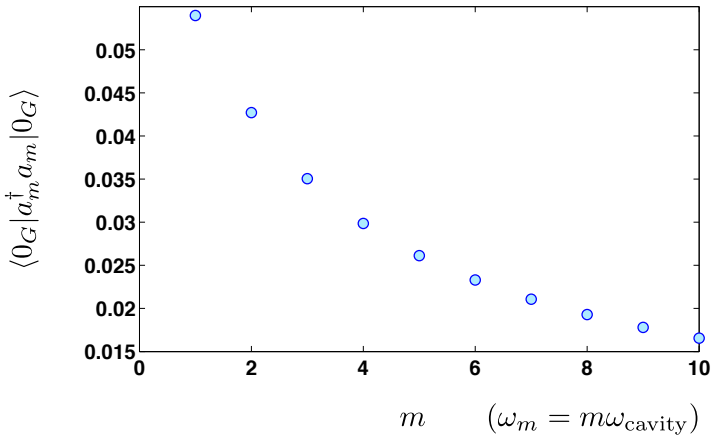

Figure 14.8: The number expectation value of local modes u_m for the case of a massless field $\mu = 0$ and a cavity split in half $r/R = 0.5$.

particles creation is achieved by the first local mode, but that even this is quite small (0.052). The expected value is independent of the cavity size or the speed of the mirror, which sets only the adiabatic UV-cutoff. Any detector that aims to extract those particles would therefore be highly sensitive (and the experiment would need to be ran many times). The relative positioning of the mirror could be modified in order to improve those numbers, but that improvement is only slight and, from our point of view, not relevant enough to be discussed at this point.

The most natural set-up for such an experiment, given the theoretical set-up, would involve the use of an optical cavity [343]. In practice, however, this setup would be almost impossible to implement. In order to obtain reasonable particle production we require a slamming time that satisfies $t_{\text{slam}} \ll 2L/c$. For optical cavity setups this would require a slamming on the order of picoseconds, which is entirely mechanically unattainable with present technology. We conclude that this platform is unsuitable for our needs.

The more promising candidate would be Circuit Quantum Electrodynamics [211, 237]. Several experiments concerned with the peculiar properties of the quantum vacuum (similar to the one here discussed) have been carried on this platform. In particular the first observation of the Dynamical Casimir effect [58]. The kinds of techniques used in that experiment could be very useful in a future proposal. The build up of a mirror inside the cavity, is however, a very different matter, as it implies the "activation" of a boundary that previously was not there. In the case of circuit QED, meandering resonators of lengths ~ 20 mm have been built [254, 344] but longer lengths could be achieved, say of 100 mm. For that size a mirror slamming time of 0.7 ns may be enough to show the effects that we want.

Along these lines, recent work in Circuit QED [345, 346] has shown that a superconduct-

ing qubit coupled to a waveguide can fully reflect single photons, while it being possible to modulate the coupling to the natural mode of the cavity in the ns timescale. That could be the first candidate for the slamming mirror. However for a mirror to reflect all photons the qubit would not be enough; rather the possibility of replacing the qubit with a frequency-tunable cavity which couples to the middle of the cavity could be studied. Very fast tuning of cavities has been proven before ($\sim$ 3 ns) and it is expected to be achievable in the subnanosecond regime [8].

Finally, another experimental platform worthy of consideration would be cold atoms in optical lattices. Although we would be dealing in that case with a discrete quantum field theory (e.g. Bose-Hubbard model), the possibilities for creating "mirror-like" conditions by raising and lowering potential barriers using holographic techniques in the subnanosecond-picosecond regime [347] might very well fit our needs.

14.8 Discussion

We have given an answer to the question of "what does it mean for half of an empty box to be full" by considering a physical scenario in which this statement actually has operational meaning. The procedure that we considered is that of very quickly introducing one or more mirrors into a cavity scalar field prepared in its vacuum state and observing the consequences. Unsurprisingly such an action induced particle creation in the field. The key observation, however, is that these real excitations are mathematically equivalent to the local vacuum excitations related to spatial entanglement in the field. As a result, the real particles that one obtains on either side of the newly introduced mirror are entangled with each other. Furthermore we have proven that this entanglement can not simply have been created by slamming down a mirror, and rather derives directly from the previously present vacuum entanglement. We proved this by also studying the case in which two mirrors, rather than one, are slammed down simultaneously and some distance apart. In this scenario the excitations in the left-most and right-most regions created from this cavity splitting are also entangled with each other, despite there being no common mirror and no possible communication between them. This entanglement is exactly the spatial vacuum entanglement that was already present.

As part of our exposition we utilized Gaussian quantum mechanics to easily derive the reduced states and correlations of the vacuum field in different subregions of the cavity. We have used this technology to discuss the entanglement structure between regions of the cav-

[8] Per Delsing - in a private communication

ity and the time evolution that follows upon slamming down a mirror, including directly relating the entanglement between regions with the burst of particles created by the mirror. This work provides a solid operational interpretation for vacuum entanglement and the local excitations that derive from it; these “virtual" excitations are simply the real excitations that one gets when slamming down a mirror. In addition, this realization motivates a simple experimental proposal for the verification of vacuum entanglement in a cavity system. Indeed we discuss how the act of slamming down a mirror may represent a very effective way of harvesting the vacuum entanglement. We finished by briefly discussing some preliminary experimental prospects for the laboratory realization of this proposal.

In addition to working towards an experimental realization there are many shorter term, theoretical questions in regards to this scenario that can be the subject of future projects. Such projects could include properly taking into account a finite-time introduction of the mirror, computing the response of a detector due to the burst of the particles (and the subsequent entanglement harvesting), and extending the analysis into free space or higher dimensions. Furthermore, the notion of quickly introducing a mirror and the resulting excitations may in fact have strong connections to quantum black hole physics, such as holography [348] and firewalls [349]. An extended study of how our work relates to these areas may be the subject of future research.

Part IV

Conclusions

Conclusions

This thesis has been centered in the study of vacuum correlations in space and time and the use of distinct techniques to probe them: detector models, on the theoretical side, and quantum simulations, on the more practical side. Along this exploration we have obtained results that lie on three different categories, which correspond to the three parts in which the thesis is divided. In the first part, we have studied different detector models when it comes to analyze localized, realistic states. We have also made an experimental proposal to simulate the UDW when accelerated uniformely in the presence of a single-mode field. In the second part of the thesis we have focused on phenomena beyond rotating wave and how they are related to fascinating *a priori* non-expected detector behaviors. In the last part of the thesis, we discuss vacuum correlations starting with an experimental proposal to extract them, followed by a local formalism based on a constructive approach to build local particles. Finally, based on the knowledge and intuitions gathered along the whole thesis, we show how these local particles can actually be produced by slamming a mirror down in a cavity and describe a feasible experiment where a Casimir-like phenomenon is predicted to take place.

Specific outcomes

- **Detector models**

  - We have analyzed the problem of wavepacket detection by an UDW model. We have found that, in order to respond to a given frequency, the spatial profile considered must verify certain properties. We have studied the origin of such a profile function for the case of an atomic detector by deriving an UDW equation from first principles, relating the smeared UDW model to the usual $\boldsymbol{p} \cdot \boldsymbol{A}$ form of the QED interaction coupling atoms to the electromagnetic field. We have discovered a way of relating the smearing profile with the electronic wavefunction of the relevant orbitals of an atom.

- We have also shown that if we want the detector to succeed in detecting resonant radiation, some information about the spectral response of the detector must be fed in general to the spatial profile and we have suggested how to introduce it as spatial oscillations. We have fully described how to use this formalism while calculating the probability of detection of a wavepacket for an accelerated detector.
- Using A projector detector model we have devised a scheme to analyse field entanglement in non-inertial frames for arbitrary single-photon field states and detector frequency response. As a particular case, we have analyzed entanglement behaviour of a two-mode photon state entangled in helicities and shown that the quantum effects of relativistic acceleration can actually amplify entanglement and not only destroy it. We have therefore found that entanglement amplification phenomena, contrary to the extended belief, can exist beyond the rather unphysical families of states where it had been found before. On top of that we have thoroughly analysed the case of peaked detectors and studied the rapidly scaling computational costs of considering wide-band detection. These difficulties may be overcome through the use of quantum simulations. Also all the conclusions are exportable to a a static black hole scenario.
- A method for simulating a set of accelerated Unruh-DeWitt detectors coupled to a single-mode field has been presented in both circuit QED and trapped ions. The idea relies on the induction of time-dependent sidebands in atom-field couplings. We have shown that our idea may be extended to many-particle experiments which could simulate results that are not affordable for classical computers such as arbitrary non-inertial trajectories of detectors or many detectors coupled to quantum fields. Finally, we have made a new connection between non-equilibrium Physics and quantum effects due to acceleration.

- **Quantum Simulations**

  - We have considered a system of two superconducting qubits coupled to a transmission line to study the Fermi problem beyond the rotating wave approximation. In particular we have proposed an experiment feasible with current technology that would solve the controversy on the issue and that, in principle, would show the expected causal behavior. By using a novel approach to switch on an ultrastrong interaction using Landau Zener processes we can effectively connect and disconnect the qubits from the line and perform independent measurements.
  - Inspired by the previous results we have extended the typical regime considered

for cases beyond rotating wave to short times. We have shown that for typical cQED parameters, the information given by a detector from an initially excited source is negligible due to the detector self excitations. It is only after a significative amount of time that we can start start trusting a detector click as informative in that respect. We have seen that this is due to the breakdown of the RWA in cQED. Our result applies to other setups and quantum detectors, although it is in the case of cQED where it might affect the interpretation of coming experimental results.

- **Vacuum Entanglement and Localization**

  - We have analyzed the possibility of extraction of quantum correlations between different times contained in the vacuum of a quantum field. We have proposed a experimentally feasible circuit QED setup to test the sizable past-future vacuum correlations can be transferred to a pair of qubits P and F, which only interact with the field in the past or the future respectively, even if the qubits do not coexist at the same time. We discuss the possible technological uses of that entanglement extraction and the potential of our scheme to work as a quantum memory.
  - Concerned about the theoretical impossibility of having local particle states in QFT, we have explored how these issues would arise in a particular construction. We have identified the main obstruction to be the requirement that the one-particle Hilbert space is spanned by positive frequency modes. In particular, wave-packets built from these modes cannot be localized within a finite spatial region, even for an arbitrarily small time interval. By basing the quantization procedure on localized modes instead, we account for localized one-particle states. We carry on such a task for a KG field in a box. By computing the Bogoliubov coefficients relating local and standard (global) quantizations, we show that both representations are *unitarily inequivalent*. In spite of this, we find that the local creators and annihilators remain well defined in the global Fock space $\mathfrak{F}^G$, and so do the local number operators,ending up with a useful mathematical toolbox to analyse and characterise local features of quantum states in the global Fock space $\mathfrak{F}^G$. Specifically, we analyze the global vacuum state $|0_G\rangle \in \mathfrak{F}^G$ in terms of local number operators and show, as expected, the existence of entanglement between the left and right regions of the box. We study the character of the local vacuum $|0_L\rangle \in \mathfrak{F}^L$, and we find that on the contrary, has no entanglement. When seen under this light we prove that the global vacuum also exhibits a distribution of

local excitations reminiscent, in some respects, of a thermal bath.

– To the question “what does it mean for half of an empty box to be full" we give an answer. By considering a physical scenario where one or more mirrors are very quickly introduced into a cavity, we verify that such an action induces particle creation in the field. By using the local formalism developed earlier we check that these real excitations are mathematically equivalent to the local vacuum excitations related to spatial entanglement in the field. We show that the real particles that one obtains on either side of the newly introduced mirror are entangled with each other. We have proven that this entanglement can not simply have been created by slamming down a mirror, and rather derives directly from the previously present vacuum entanglement. We also show the case in which two mirrors, rather than one, are slammed down simultaneously and some distance apart. In this scenario the excitations in the left-most and right-most regions created from this cavity splitting are also entangled with each other. We use Gaussian quantum mechanics to easily derive the reduced states and correlations of the vacuum field in different subregions of the cavity.

Appendices

APPENDIX A

Appendix: Gaussian Quantum Mechanics

Here we very quickly review the concepts from Gaussian quantum mechanics that are required to understand the material in chapter 14. We do not attempt to justify or derive anything here. Everything that is presented (and much more) can be found in the active literature, for example [337].

Let us deal with a system of N continuous-variable bosonic modes (e.g. harmonic oscillators, or modes of a field). Let the annihilation and creation operators of mode m be $\hat{a}_m$ and $\hat{a}_m^\dagger$, respectively. We can then define the internal position and momentum quadrature operators of this mode to be the canonically conjugate, Hermitian pair

$$\hat{q}_m \equiv \frac{1}{\sqrt{2}}(\hat{a}_m + \hat{a}_m^\dagger), \qquad \hat{p}_m \equiv \frac{\mathrm{i}}{\sqrt{2}}(a_m^\dagger - a_m). \tag{A.0.1}$$

For notational convenience we will arrange these operators into the vector

$$\hat{\mathbf{x}} = (\hat{q}_1, \hat{p}_1, \hat{q}_2, \hat{p}_2, \cdots, \hat{q}_N, \hat{p}_N)^T \tag{A.0.2}$$

, with the m'th entry of this vector labeled $\hat{x}_m$. In this notation the canonical commutation relations take the form

$$[\hat{x}_m, \hat{x}_n] = \mathrm{i}\Omega_{mn}, \tag{A.0.3}$$

where Ω_{mn} are the entries of a matrix called the *symplectic form*, which is given by

$$\mathbf{\Omega} = \bigoplus_{m=1}^{N} \begin{pmatrix} 0 & 1 \\ -1 & 0 \end{pmatrix}. \tag{A.0.4}$$

The state $\hat{\rho}$ of our system is said to be *Gaussian* if its corresponding Wigner function is Gaussian over phase space. Equivalently, the state is fully characterized by the first and

second moments, $\langle \hat{x}_m | = \rangle \mathrm{Tr}(\hat{\rho}\hat{x}_m)$ and $\langle \hat{x}_m \hat{x}_n | = \rangle \mathrm{Tr}(\hat{\rho}\hat{x}_m\hat{x}_n)$. In this work we only need to consider states that have zero-mean (i.e. zero first moments). In this case only the second moments are required. Thus, rather than using the density operator to characterize the state we instead use the $2N \times 2N$ *covariance matrix* $\boldsymbol{\sigma}$, the entries of which are defined to be

$$\sigma_{mn} = \langle \hat{x}_m \hat{x}_n + \hat{x}_n \hat{x}_m | . \rangle \tag{A.0.5}$$

We use this matrix to fully characterize the state.

We can decompose the covariance matrix in 2×2 blocks:

$$\boldsymbol{\sigma} = \begin{pmatrix} \boldsymbol{\sigma}_{11} & \boldsymbol{\sigma}_{12} & \cdots \\ \boldsymbol{\sigma}_{21}^T & \boldsymbol{\sigma}_{22} & \cdots \\ \vdots & \vdots & \ddots \end{pmatrix}. \tag{A.0.6}$$

Here the matrix $\boldsymbol{\sigma}_{mm}$ is in fact the covariance matrix (i.e. reduced state) of mode m. Similarly, $\boldsymbol{\sigma}_{mn}$ contains information about the correlations (e.g. entanglement) between modes m and n, which are completely uncorrelated (i.e. in a product state) iff $\boldsymbol{\sigma}_{mn} = \mathbf{0}$. Taking a partial trace within the covariance matrix formalism is entirely trivial; for example the reduced state of the first two modes is simply the upper-left 4×4 block of $\boldsymbol{\sigma}$.

An important example of a Gaussian state is the ground (vacuum) state of the free Hamiltonian $\hat{H} = \sum_{m=1}^{N} \omega_m \hat{a}_m^\dagger \hat{a}_m$. For this state the covariance matrix is straightforwardly seen to be given by the identity: $\boldsymbol{\sigma}_{\text{vac}} = \mathbf{I}$.

In general, unitary transformations $\hat{U}$ in the Hilbert space that are generated by quadratic Hamiltonians preserve Gaussianity. Such transformations are represented by a *symplectic* transformation $\mathbf{S}$ in the phase space. Namely, such a quadratically generated $\hat{U}$ transforms the elements $\hat{x}_m$ to a new set of quadratures $\hat{\mathbf{x}}' = \hat{U}\hat{\mathbf{x}}\hat{U}^\dagger$ such that the new quadratures are a linear combination of the old: $\hat{\mathbf{x}}' = \mathbf{S}\hat{\mathbf{x}}$, where in order to preserve the canonical commutation relations the matrix $\mathbf{S}$ must be symplectic,

$$\mathbf{S}\boldsymbol{\Omega}\mathbf{S}^T = \mathbf{S}^T\boldsymbol{\Omega}\mathbf{S} = \boldsymbol{\Omega}. \tag{A.0.7}$$

In addition, a matrix must be square in order to be considered symplectic, meaning that it transforms N modes to N modes. It is easily seen that on the level of the covariance matrix this transformation takes the form

$$\boldsymbol{\sigma} \to \boldsymbol{\sigma}' = \mathbf{S}\boldsymbol{\sigma}\mathbf{S}^T. \tag{A.0.8}$$

An important characterization of a given Gaussian state is its *symplectic spectrum*. Every N-mode Gaussian state $\boldsymbol{\sigma}$ has N *symplectic eigenvalues* $\{\nu_m\}$, which are invariant under

symplectic transformations. The covariance matrix is *symplectically diagonalizable*, meaning that there exists a symplectic matrix $\mathbf{S}$ which brings the state to a diagonal form given by $\mathbf{S}\boldsymbol{\sigma}\mathbf{S}^T = \mathbf{D} = \text{diag}(\nu_1, \nu_1, \nu_2, \nu_2, \cdots, \nu_N, \nu_N)$. This diagonalized form is also known as the *Williamson normal form* of the state. We note, for example, that the vacuum state $\boldsymbol{\sigma}_{\text{vac}} = \mathbf{I}$ is already in its Williamson normal form, and that all of its symplectic eigenvalues are equal to unity. Note that the symplectic eigenvalues of $\boldsymbol{\sigma}$ are *not* the same as its regular eigenvalues.

The symplectic eigenvalues of a state must always be larger than or equal to unity: $\nu_m \geq 1 \ \forall \ m$. This is simply a statement of the uncertainty principle, which is saturated iff all symplectic eigenvalues are equal to unity. The symplectic spectrum also specifies the mixedness of a Gaussian state: such a state is pure iff all symplectic eigenvalues are equal to unity. That is, a pure Gaussian state saturates the uncertainty principle. Any uncertainty in the state beyond this must be caused by classical uncertainty, i.e. mixedness. An informationally rigorous measure of mixedness, the von Neumann entropy $S(\boldsymbol{\sigma})$ of the state, can be computed from the symplectic eigenvalues via

$$S(\boldsymbol{\sigma}) = \sum_{m=1}^{N} f(\nu_m), \tag{A.0.9}$$

where

$$f(x) = \frac{x+1}{2}\log\left(\frac{x+1}{2}\right) - \frac{x-1}{2}\log\left(\frac{x-1}{2}\right). \tag{A.0.10}$$

The entropy is zero for a pure state, when $\nu_m = 1$ for all m.

The easiest way to compute the symplectic eigenvalues of a state (if one does not care about the diagonalizing transformation) is to compute the regular eigenvalues of the matrix $i\boldsymbol{\Omega}\boldsymbol{\sigma}$, which come in pairs of $\{\pm\nu_m\}$. There are situations, however, in which one would also like to compute the diagonalizing symplectic transformation itself. The method of doing this is provided in Appendix A. Of particular importance for us is the joint, local diagonalization of a bipartite, pure state. Imagine that we split our set of modes into two groups, A and B. The joint state can then be decomposed as

$$\boldsymbol{\sigma} = \begin{pmatrix} \boldsymbol{\sigma}_A & \boldsymbol{\gamma} \\ \boldsymbol{\gamma}^T & \boldsymbol{\sigma}_B \end{pmatrix}, \tag{A.0.11}$$

where $\boldsymbol{\sigma}_A$ and $\boldsymbol{\sigma}_B$ are the reduced states for groups A and B, respectively, and $\boldsymbol{\gamma}$ contains the correlations between the two groups. Let us assume that the global state is pure. That is, we assume that the symplectic eigenvalues ν_m of $\boldsymbol{\sigma}$ are all equal to unity. This does not mean, however, that the symplectic eigenvalues of $\boldsymbol{\sigma}_A$ and $\boldsymbol{\sigma}_B$ are all equal to unity; indeed they will not be if the bipartitions are entangled. Let us label the "local" symplectic eigenvalues

of these reduced states as $\nu_m^{(A)}$ and $\nu_m^{(B)}$. Because $\boldsymbol{\sigma}$ is pure these two spectrums will in fact be equivalent (with the larger of the two systems having extra symplectic eigenvalues equal to unity); this is equivalent to the fact that the standard local spectrums of reduced density operators in a pure bipartition are equal. Let $\mathbf{S}_A$ be the local symplectic transformation that diagonalizes $\boldsymbol{\sigma}_A$, and similarly we have $\mathbf{S}_B$. Let us then apply these local transformations to our state by acting on $\boldsymbol{\sigma}$ with the joint transformation $\mathbf{S}_A \oplus \mathbf{S}_B$:

$$(\mathbf{S}_A \oplus \mathbf{S}_B)\boldsymbol{\sigma}(\mathbf{S}_A \oplus \mathbf{S}_B)^T = \begin{pmatrix} \mathbf{D}_A & \boldsymbol{\gamma}_D \\ \boldsymbol{\gamma}_D^T & \mathbf{D}_B \end{pmatrix}. \tag{A.0.12}$$

The reduced states have now been put into their Williamson normal forms. Because this is a purely local operation the entanglement between the two sides has not been modified. Importantly, *if* the global state is pure then this transformation produces a correlation matrix $\boldsymbol{\gamma}_D$ that is diagonal as well [337]. This is analogous to the Hilbert space Schmidt decomposition of a pure, bipartite state. In the literature on Gaussian quantum mechanics such a covariance matrix is said to be in *standard form*. The fact that $\boldsymbol{\gamma}_D$ is diagonal means that in this locally transformed basis we obtain a product of pure, two-mode states. That is, each pair is uncorrelated with any others. Generally each such pair of modes will be entangled (in particular, they will be in a two-mode squeezed state). Performing this local symplectic diagonalization is therefore a method of isolating the entanglement between A and B into simple pairs of modes (rather than the entanglement between a given mode in A and the rest of the system being spread across multiple modes in both A and B).

In the case that $\boldsymbol{\sigma}$ is mixed we unfortunately cannot perform the same feat. We can, of course, still locally diagonalize the reduced systems. This removes any mode-mode correlation within A and B themselves. However in this case the resulting correlation matrix $\boldsymbol{\gamma}_D$ will not generally be diagonal, meaning that we can still have a given mode in A being correlated with multiple modes in B, and vice versa.

Lastly, we wish to have a measure of entanglement in Gaussian states. In the case of a globally pure state the entanglement across a bipartition is simply the entropy, Eq. (A.0.9), of either of the two reduced states. In the case in which the state is globally mixed, on the other hand, one can use the logarithmic negativity E_N [337, 340]. For bipartite Gaussian states a non-zero value of E_N is a sufficient condition for non-separability [350] [1]. For a two-mode Gaussian state with covariance matrix

$$\boldsymbol{\sigma}_{\text{two mode}} = \begin{pmatrix} \boldsymbol{\sigma}_{11} & \boldsymbol{\sigma}_{12} \\ \boldsymbol{\sigma}_{21}^T & \boldsymbol{\sigma}_{22} \end{pmatrix} \tag{A.0.13}$$

[1] For (1xN)-mode Gaussian states the condition is also necessary. For 2x2 or larger cases one may find bound entangled states, which are entangled yet their E_N is zero [351].

the logarithmic negativity between the modes is given by

$$E_N = \max(0, -\log z), \tag{A.0.14}$$

where

$$2z^2 = \Delta - \sqrt{\Delta^2 - 4 \det \boldsymbol{\sigma}_{\text{two mode}}}, \tag{A.0.15}$$

and where $\Delta = \det \boldsymbol{\sigma}_{11} + \det \boldsymbol{\sigma}_{22} - 2 \det \boldsymbol{\sigma}_{12}$.

Symplectic diagonalization

Here we describe the method of symplectically diagonalizing a covariance matrix, i.e. putting into its Williamson normal form. To do this it is easier to work in a re-ordered phase space basis in which the q's are packaged together and similarly for the p's:

$$\hat{\mathbf{x}} = (\hat{q}_1, \hat{q}_2, \cdots, \hat{p}_1, \hat{p}_2, \cdots). \tag{A.0.16}$$

In this basis the reduced covariance matrix of Eq. (14.4.10), for example, takes a block form

$$\boldsymbol{\sigma} = \begin{pmatrix} \boldsymbol{\sigma}^{(Q)} & \mathbf{0} \\ \mathbf{0} & \boldsymbol{\sigma}^{(P)} \end{pmatrix}, \tag{A.0.17}$$

where the entries of these blocks, $\sigma^{(Q)}_{mn}$ and $\sigma^{(P)}_{mn}$, are given by the upper left and lower right entries of $\boldsymbol{\sigma}_{mn}$ in Eq. (14.4.11), respectively. The off-diagonal blocks of Eq. (A.0.17) are zero due to the fact that the Bogoliubov transformation to the local basis is purely real. This circumstance in fact makes it considerably easier to symplectically diagonalize $\boldsymbol{\sigma}$, and here we will only cover this case.

Note that in the new basis ordering the symplectic form is given by

$$\boldsymbol{\Omega} = \begin{pmatrix} \mathbf{0} & \mathbf{I} \\ -\mathbf{I} & \mathbf{0} \end{pmatrix}. \tag{A.0.18}$$

Also in this basis the Williamson normal (symplectically diagonalized) form of a covariance matrix is given by $\mathbf{D} = \boldsymbol{\nu} \oplus \boldsymbol{\nu}$, where $\boldsymbol{\nu} = \text{diag}(\nu_1, \nu_2, \cdots)$ contains the symplectic eigenvalues.

We would like to find the symplectic transformation $\tilde{\mathbf{S}}$ that achieves this transformation. Specifically we will let $\tilde{\mathbf{S}}^T(\boldsymbol{\nu} \oplus \boldsymbol{\nu})\tilde{\mathbf{S}} = \boldsymbol{\sigma}$. To this end, we will make an Ansatz and then prove that it is the correct choice. Let us define a matrix $\mathbf{A} \equiv \sqrt{\boldsymbol{\sigma}^{(Q)}}\sqrt{\boldsymbol{\sigma}^{(P)}}$. We claim that the symplectic eigenvalues $\{\nu_m\}$ of $\boldsymbol{\sigma}$ are given by the singular values of $\mathbf{A}$. That is, there are orthogonal matrices $\mathbf{O}_1$ and $\mathbf{O}_2$ such that

$$\mathbf{A} = \mathbf{O}_1^T \boldsymbol{\nu} \mathbf{O}_2. \tag{A.0.19}$$

Let us take these and form another orthogonal matrix given by their direct sum $\mathbf{O} \equiv \mathbf{O}_1 \oplus \mathbf{O}_2$. We now claim that the symplectic matrix $\tilde{\mathbf{S}}$ that diagonalizes $\boldsymbol{\sigma}$ is given by

$$\tilde{\mathbf{S}} = (\boldsymbol{\nu} \oplus \boldsymbol{\nu})^{-1/2} \mathbf{O} \boldsymbol{\sigma}^{1/2}. \tag{A.0.20}$$

Clearly from this definition it is true that $\tilde{\mathbf{S}}^T (\boldsymbol{\nu} \oplus \boldsymbol{\nu}) \tilde{\mathbf{S}} = \boldsymbol{\sigma}$, since $\mathbf{O}$ is orthogonal. However, is it symplectic: $\tilde{\mathbf{S}} \boldsymbol{\Omega} \tilde{\mathbf{S}}^T = \boldsymbol{\Omega}$? By expanding the left-hand side of this equation it is straightforward to see that the transformation will be symplectic iff $\mathbf{O}_1 \mathbf{A} \mathbf{O}_2^T = \boldsymbol{\nu}$, which is equivalent to Eq. (A.0.19).

Thus, finding the symplectic diagonalization is equivalent to finding the singular value decomposition of the matrix $\mathbf{A}$, which is easily done numerically. Note that to go from the matrix $\boldsymbol{\sigma}$ to $\boldsymbol{\nu} \oplus \boldsymbol{\nu}$ in the sense of $\mathbf{S}_D \boldsymbol{\sigma} \mathbf{S}_D^T = \boldsymbol{\nu} \oplus \boldsymbol{\nu}$, the correct transformation will be $\mathbf{S}_D = (\tilde{\mathbf{S}}^T)^{-1} = (\boldsymbol{\nu} \oplus \boldsymbol{\nu})^{1/2} \mathbf{O} \boldsymbol{\sigma}^{-1/2}$.

Bibliography

[1] Eric Brown, Marco del Rey, Hans Westman, and Juan Leon. What does it mean for half of an empty cavity to be full? *arXiv preprint arXiv:1409.4203*, 2014. xix

[2] Matías R. Vázquez, Marco del Rey, Hans Westman, and Juan León. Local quanta, unitary inequivalence, and vacuum entanglement. *Annals of Physics*, 351(0):112 – 137, 2014. xix, 210, 213, 214, 215, 216, 230, 232, 240

[3] Eduardo Martín-Martínez, Miguel Montero, and Marco del Rey. Wavepacket detection with the unruh-dewitt model. *Phys. Rev. D*, 87:064038, Mar 2013. xix, 9, 27

[4] Miguel Montero, Marco del Rey, and Eduardo Martín-Martínez. Nonmonotonic entanglement of physical electromagnetic field states in noninertial frames. *Phys. Rev. A*, 86:012304, Jul 2012. xix, 9, 26, 27

[5] Carlos Sabín, Borja Peropadre, Marco del Rey, and Eduardo Martín-Martínez. Extracting past-future vacuum correlations using circuit qed. *Phys. Rev. Lett.*, 109:033602, Jul 2012. xix, 7, 22

[6] Marco del Rey, Diego Porras, and Eduardo Martín-Martínez. Simulating accelerated atoms coupled to a quantum field. *Phys. Rev. A*, 85:022511, Feb 2012. xix, 7, 22, 26, 27, 101, 107, 117

[7] Marco del Rey, Carlos Sabín, and Juan León. Short-time quantum detection: Probing quantum fluctuations. *Phys. Rev. A*, 85:045802, Apr 2012. xx, 7, 22, 27, 212

[8] Enrico Fermi. Quantum theory of radiation. *Rev. Mod. Phys.*, 4:87–132, Jan 1932. xx, 22, 26, 27, 134, 135, 137

[9] S Braun, M Friesdorf, SS Hodgman, M Schreiber, JP Ronzheimer, A Riera, M del Rey, I Bloch, J Eisert, and U Schneider. Emergence of coherence and the dynamics of quantum phase transitions. *arXiv preprint arXiv:1403.7199*, 2014. xx

[10] Marco del Rey, Alex W Chin, Martin B Plenio, and Susana Huelga. Exploiting structured environments for efficient energy transfer: The phonon antenna mechanism. *J. Phys. Chem. Lett., 2013, 4, pp 903–907*, 2012. xx

[11] Shekhar Borkar and Andrew A. Chien. The future of microprocessors. *Commun. ACM*, 54(5):67–77, May 2011. 3, 16

[12] R. Landauer. Irreversibility and heat generation in the computing process. *IBM J. Res. Dev.*, 5(3):183–191, July 1961. 3, 17

[13] Alexis De Vos. *Reversible computing fundamentals, quantum computing, and applications*. Wiley-VCH John Wiley distributor, Weinheim Chichester, 2010. 3, 17

[14] Norman Margolus and Lev B. Levitin. The maximum speed of dynamical evolution. *Physica D: Nonlinear Phenomena*, 120(1-2):188 – 195, 1998. Proceedings of the Fourth Workshop on Physics and Consumption. 3, 17

[15] Lev B. Levitin and Tommaso Toffoli. Fundamental limit on the rate of quantum dynamics: The unified bound is tight. *Phys. Rev. Lett.*, 103:160502, Oct 2009. 3, 17

[16] A. Einstein, B. Podolsky, and N. Rosen. Can quantum-mechanical description of physical reality be considered complete? *Phys. Rev.*, 47:777–780, May 1935. 4, 18

[17] Charles H. Bennett, Herbert J. Bernstein, Sandu Popescu, and Benjamin Schumacher. Concentrating partial entanglement by local operations. *Phys. Rev. A*, 53:2046–2052, Apr 1996. 5, 20

[18] Charles H. Bennett, Gilles Brassard, Sandu Popescu, Benjamin Schumacher, John A. Smolin, and William K. Wootters. Purification of noisy entanglement and faithful teleportation via noisy channels. *Phys. Rev. Lett.*, 76:722–725, Jan 1996. 5, 20

[19] M. Żukowski, A. Zeilinger, M. A. Horne, and A. K. Ekert. "event-ready-detectors" bell experiment via entanglement swapping. *Phys. Rev. Lett.*, 71:4287–4290, Dec 1993. 5, 20

[20] John S. Bell. On the einstein-podolsky-rosen paradox. *Physics*, 1(3):195–200, 1964. 5, 20

[21] Stuart J. Freedman and John F. Clauser. Experimental test of local hidden-variable theories. *Phys. Rev. Lett.*, 28:938–941, Apr 1972. 5, 20

[22] John F. Clauser. Experimental investigation of a polarization correlation anomaly. *Phys. Rev. Lett.*, 36:1223–1226, May 1976. 5, 20

[23] Edward S. Fry and Randall C. Thompson. Experimental test of local hidden-variable theories. *Phys. Rev. Lett.*, 37:465–468, Aug 1976.

[24] Alain Aspect, Philippe Grangier, and Gérard Roger. Experimental tests of realistic local theories via bell's theorem. *Phys. Rev. Lett.*, 47:460–463, Aug 1981. 5, 20

[25] Alain Aspect, Philippe Grangier, and Gérard Roger. Experimental realization of einstein-podolsky-rosen-bohm gedankenexperiment: A new violation of bell's inequalities. *Phys. Rev. Lett.*, 49:91–94, Jul 1982. 5, 20

[26] Alain Aspect, Jean Dalibard, and Gérard Roger. Experimental test of bell's inequalities using time- varying analyzers. *Phys. Rev. Lett.*, 49:1804–1807, Dec 1982. 5, 20

[27] G.C. Ghirardi, A. Rimini, and T. Weber. A general argument against superluminal transmission through the quantum mechanical measurement process. *Lettere al Nuovo Cimento*, 27(10):293–298, 1980. 6, 22

[28] Ll. Masanes, A. Acin, and N. Gisin. General properties of nonsignaling theories. *Phys. Rev. A*, 73:012112, Jan 2006. 6, 22

[29] Phillippe H. Eberhard and Ronald R. Ross. Quantum field theory cannot provide faster-than-light communication. *Foundations of Physics Letters*, 2(2):127–149, 1989. 6, 22, 134

[30] Charles H. Bennett, Gilles Brassard, Claude Crépeau, Richard Jozsa, Asher Peres, and William K. Wootters. Teleporting an unknown quantum state via dual classical and einstein-podolsky-rosen channels. *Phys. Rev. Lett.*, 70:1895–1899, Mar 1993. 6, 22

[31] M. I. Shirokov. Signal velocity in quantum electrodynamics. *Soviet Physics Uspekhi*, 21(4):345, 1978. 6, 22, 135

[32] Gerhard C. Hegerfeldt. Causality problems for fermi's two-atom system. *Phys. Rev. Lett.*, 72(5):596–599, Jan 1994. 6, 22, 135, 148

[33] Detlev Buchholz and Jakob Yngvason. There Are No Causality Problems for Fermi's Two-Atom System. *Phys. Rev. Lett.*, 73(5):613–616, Aug 1994. 6, 22, 135, 137, 142

[34] P. W. Milonni, D. F. V. James, and H. Fearn. Photodetection and causality in quantum optics. *Phys. Rev. A*, 52(2):1525–1537, Aug 1995. 6, 22, 135, 148

[35] E. A. Power and T. Thirunamachandran. Analysis of the causal behavior in energy transfer between atoms. *Phys. Rev. A*, 56:3395, 1997. 6, 22, 135, 136, 137

[36] Carlos Sabín, Marco del Rey, Juan José García-Ripoll, and Juan León. Fermi problem with artificial atoms in circuit qed. *Phys. Rev. Lett.*, 107:150402, Oct 2011. 6, 148, 152, 154

[37] M. Rédei and S. J. Summers. Quantum probability theory. *Studies in the History and Philosophy of Modern Physics*, 38:390–417, 2007. 7, 23

[38] Dénes Petz. *Quantum information theory and quantum statistics*. Theoretical and Mathematical Physics Series, Springer, 2008. 7, 23

[39] A.S. Holevo. *Statistical Structure of Quantum Theory*. Lecture Notes in Physics Monographs. Springer, 2001. 7, 23

[40] H. Reeh and S. Schlieder. Bemerkungen zur Unitäräquivalenz von lorentzinvarianten feldern. *Nuovo Cim.*, 22:1051, 1961. 7, 23, 161, 162, 203

[41] B. Reznik, A. Retzker, and J. Silman. Violating Bell's inequalities in vacuum. *Phys. Rev. A*, 71:042104, 2005. 7, 23, 119, 138, 167, 209

[42] A. Retzker, J. I. Cirac, and B. Reznik. Detecting Vacuum Entanglement in a Linear Ion Trap. *Phys. Rev. Lett.*, 94:050504, 2005. 7, 23, 167, 210, 211

[43] S. Marcovitch, A. Retzker, M. B. Plenio, and B. Reznik. Critical and noncritical long-range entanglement in Klein-Gordon fields. *Phys. Rev. A*, 80(1):012325, July 2009. 7, 23, 167

[44] C. Sabín, J. J. García-Ripoll, E. Solano, and J. León. Dynamics of entanglement via propagating microwave photons. *Phys. Rev. B*, 81(18):184501, May 2010. 7, 23, 138, 151, 167, 168, 170

[45] M. Cliche and A. Kempf. Relativistic quantum channel of communication through field quanta. *Phys. Rev. A*, 81(1):012330, January 2010. 7, 23, 167

[46] Eduardo Martín-Martínez, Eric G. Brown, William Donnelly, and Achim Kempf. Sustainable entanglement production from a quantum field. *Phys. Rev. A*, 88:052310, Nov 2013. 7, 23, 91, 211

[47] Grant Salton, Robert B. Mann, and Nicolas C. Menicucci. Acceleration-assisted entanglement harvesting and rangefinding. *arXiv preprint arXiv:1408.1395*, 2014. 7, 23, 91

[48] Shih-Yuin Lin and B. L. Hu. Entanglement creation between two causally disconnected objects. *Phys. Rev. D*, 81:045019, Feb 2010. 7, 23

[49] S. Jay Olson and Timothy C. Ralph. Entanglement between the future and the past in the quantum vacuum. *Phys. Rev. Lett.*, 106:110404, 2011. 7, 23, 111, 167, 172

[50] S. J. Olson and T. C. Ralph. Extraction of timelike entanglement from the quantum vacuum. *Phys. Rev. A*, 85(1):012306, January 2012. 7, 23, 167, 169, 172, 173

[51] Michael Redhead. More ado about nothing. *Foundations of Physics*, 25(1):123–137, 1995. 7, 23, 163

[52] Michael Redhead. The vacuum in relativistic quantum field theory. *PSA: Proceedings of the biennial meeting of the Philosophy of Science Association*, 2:77–87, 1995. 7, 23, 163

[53] David Malament. Causal Theories of Time and the Conventionality of Simultaneity. *Nous, Wiley*, 11-3:293–300, 1977. 8, 23, 176, 193, 205, 207

[54] W. G. Unruh. Notes on black-hole evaporation. *Phys. Rev. D*, 14(4):870–892, Aug 1976. 8, 24, 52, 55, 56, 90, 92, 109, 111, 119, 147, 149, 167, 212

[55] S. W. Hawking. Black hole explosions? *Nature*, 248(5443):30–31, 03 1974. 8, 24

[56] J. R. Johansson, G. Johansson, C. M. Wilson, and Franco Nori. Dynamical casimir effect in a superconducting coplanar waveguide. *Phys. Rev. Lett.*, 103:147003, Sep 2009. 8, 24, 61, 123, 143

[57] J. R. Johansson, G. Johansson, C. M. Wilson, and F. Nori. Dynamical Casimir effect in superconducting microwave circuits. *Phys. Rev. A*, 82(5):052509, November 2010. 8, 24, 61, 143

[58] C. M. Wilson, G. Johansson, A. Pourkabirian, J. R. Johansson, T. Duty, F. Nori, and P. Delsing. Observation of the Dynamical Casimir Effect in a Superconducting Circuit. *Nature*, 479:376–379, 2011. 8, 24, 55, 85, 168, 210, 212, 219, 241

[59] Pasi Lähteenmäki, G. S. Paraoanu, Juha Hassel, and Pertti J. Hakonen. Dynamical casimir effect in a josephson metamaterial. *Proceedings of the National Academy of Sciences*, 2013. 8, 24, 61

[60] Marek Czachor. Einstein-podolsky-rosen-bohm experiment with relativistic massive particles. *Phys. Rev. A*, 55:72–77, Jan 1997. 8, 25

[61] Robert M. Gingrich and Christoph Adami. Quantum entanglement of moving bodies. *Phys. Rev. Lett.*, 89:270402, Dec 2002. 9, 26

[62] Jiannis Pachos and Enrique Solano. Generation and degree of entanglement in a relativistic formulation. *Quantum Info. Comput.*, 3(2):115–120, March 2003. 9, 26

[63] Asher Peres, Petra F. Scudo, and Daniel R. Terno. Quantum entropy and special relativity. *Phys. Rev. Lett.*, 88:230402, May 2002. 9, 26

[64] Stephen D. Bartlett and Daniel R. Terno. Relativistically invariant quantum information. *Phys. Rev. A*, 71:012302, Jan 2005. 9, 26

[65] Paul M. Alsing and Gerard J. Milburn. On entanglement and lorentz transformations. *Quantum Info. Comput.*, 2(6):487–512, October 2002. 9, 26

[66] Paul M. Alsing and G. J. Milburn. Teleportation with a uniformly accelerated partner. *Phys. Rev. Lett.*, 91:180404, Oct 2003. 9, 26

[67] P. M. Alsing, I. Fuentes-Schuller, R. B. Mann, and T. E. Tessier. Entanglement of dirac fields in noninertial frames. *Phys. Rev. A*, 74:032326, Sep 2006. 9, 26, 109, 111

[68] I. Fuentes-Schuller and R. B. Mann. Alice falls into a black hole: Entanglement in noninertial frames. *Phys. Rev. Lett.*, 95:120404, Sep 2005. 9, 26, 109, 110, 111, 113, 114, 116

[69] Eduardo Martín-Martínez, Luis J. Garay, and Juan León. Quantum entanglement produced in the formation of a black hole. *Phys. Rev. D*, 82:064028, Sep 2010. 9, 26

[70] Greg Ver Steeg and Nicolas C. Menicucci. Entangling power of an expanding universe. *Phys. Rev. D*, 79:044027, Feb 2009. 9, 26, 91, 209, 211

[71] Eduardo Martín-Martínez and Nicolas C Menicucci. Cosmological quantum entanglement. *Classical and Quantum Gravity*, 29(22):224003, 2012. 9, 26

[72] Luis J. Garay, Mercedes Martín-Benito, and Eduardo Martín-Martínez. Echo of the quantum bounce. *Phys. Rev. D*, 89:043510, Feb 2014. 9, 26

[73] David Edward Bruschi, Jorma Louko, and Daniele Faccio. Entanglement generation in relativistic cavity motion. *Journal of Physics: Conference Series*, 442(1):012024, 2013. 9, 27

[74] Nicolai Friis, Antony R. Lee, and Jorma Louko. Scalar, spinor, and photon fields under relativistic cavity motion. *Phys. Rev. D*, 88:064028, Sep 2013. 9, 27

[75] Aida Ahmadzadegan, Eduardo Martín-Martínez, and Robert B. Mann. Cavities in curved spacetimes: The response of particle detectors. *Phys. Rev. D*, 89:024013, Jan 2014. 9, 27

[76] T. M. Cover. *Elements of information theory*. Wiley-Interscience, Hoboken, N.J, 2006. 15

[77] David Patterson and John L. Hennessy. *Computer organization and design: the hardware/software interface*. Morgan Kaufmann, Oxford Waltham, MA, USA, 2014. 16

[78] Hen-Sum Philip Wong, D.J. Frank, P.M. Solomon, C.H.J. Wann, and J.J. Welser. Nanoscale cmos. *Proceedings of the IEEE*, 87(4):537–570, Apr 1999. 16

[79] Brian Doyle, Reza Arghavani, Doug Barlage, Suman Datta, Mark Doczy, Jack Kavalieros, Anand Murthy, and Robert Chau. Transistor elements for 30nm physical gate length and beyond. *Intel Technology Journal: Semiconductor Technology and Manufacturing*, 06, May 2002. 16

[80] Seth Lloyd. *Programming the universe: a quantum computer scientist takes on the cosmos*. Knopf, New York, 2006. 17

[81] Seth Lloyd. Ultimate physical limits to computation. *Nature*, 406(6799):1047–1054, 08 2000. 17

[82] A. Einstein. On the development of our views concerning the nature and constitution of radiation. *Salzburg Lecture*, 1909. 18

[83] A. Einstein. General discussion of the new ideas presented. *Solvay congress*, 1927. 19

[84] E. Schrödinger. Die gegenwärtige situation in der quantenmechanik. *Naturwissenschaften*, 23(50):844–849, 1935. 19

[85] E. Schrödinger. Discussion of probability relations between separated systems. *Mathematical Proceedings of the Cambridge Philosophical Society*, 31:555–563, 10 1935. 19, 39

[86] John F. Clauser, Michael A. Horne, Abner Shimony, and Richard A. Holt. Proposed experiment to test local hidden-variable theories. *Phys. Rev. Lett.*, 23:880–884, Oct 1969. 20

[87] John F. Clauser and Michael A. Horne. Experimental consequences of objective local theories. *Phys. Rev. D*, 10:526–535, Jul 1974. 20

[88] Noah Linden and Sandu Popescu. Good dynamics versus bad kinematics: Is entanglement needed for quantum computation? *Phys. Rev. Lett.*, 87:047901, Jul 2001. 21

[89] Lars Lydersen, Carlos Wiechers, Christoffer Wittmann, Dominique Elser, Johannes Skaar, and Vadim Makarov. Hacking commercial quantum cryptography systems by tailored bright illumination. *Nat Photon*, 4(10):686–689, 10 2010. 21

[90] Audun Nystad Bugge, Sebastien Sauge, Aina Mardhiyah M. Ghazali, Johannes Skaar, Lars Lydersen, and Vadim Makarov. Laser damage helps the eavesdropper in quantum cryptography. *Phys. Rev. Lett.*, 112:070503, Feb 2014. 21

[91] Patrick Hayden, Debbie W. Leung, and Andreas Winter. Aspects of generic entanglement. *Communications in Mathematical Physics*, 265(1):95–117, 2006. 23

[92] D. Gross, S. T. Flammia, and J. Eisert. Most quantum states are too entangled to be useful as computational resources. *Phys. Rev. Lett.*, 102:190501, May 2009. 23

[93] Michael J. Bremner, Caterina Mora, and Andreas Winter. Are random pure states useful for quantum computation? *Phys. Rev. Lett.*, 102:190502, May 2009. 23

[94] S. J. Summers and R. F. Werner. The vacuum violates Bell's inequalities. *Phys. Lett. A*, 110:257, 1985. 23, 167

[95] S. J. Summers and R. F. Werner. Bell's inequalities and quantum field theory. II. Bell's inequalities are maximally violated in the vacuum. *J. Math. Phys.*, 28:2448, 1987. 23, 167

[96] Asher Peres and Daniel R. Terno. Quantum information and relativity theory. *Rev. Mod. Phys.*, 76:93–123, Jan 2004. 24

[97] Claus Kiefer. *Quantum gravity*. Oxford University Press, Oxford, 2012. 24

[98] D. Dalvit, P. Milonni, D. Roberts, and F. da Rosa. *Casimir Physics*. Lecture Notes in Physics. Springer, 2011. 24

[99] Giulio Chiribella, Giacomo Mauro D'Ariano, and Paolo Perinotti. Informational derivation of quantum theory. *Phys. Rev. A*, 84:012311, Jul 2011. 25

[100] Erik Verlinde. On the origin of gravity and the laws of newton. *Journal of High Energy Physics*, 2011(4):1–27, 2011. 25

[101] Don N. Page and William K. Wootters. Evolution without evolution: Dynamics described by stationary observables. *Phys. Rev. D*, 27:2885–2892, Jun 1983. 25

[102] Rodolfo Gambini, Rafael A. Porto, Jorge Pullin, and Sebastián Torterolo. Conditional probabilities with dirac observables and the problem of time in quantum gravity. *Phys. Rev. D*, 79:041501, Feb 2009. 25

[103] Ekaterina Moreva, Giorgio Brida, Marco Gramegna, Vittorio Giovannetti, Lorenzo Maccone, and Marco Genovese. Time from quantum entanglement: An experimental illustration. *Phys. Rev. A*, 89:052122, May 2014. 25

[104] Asher Peres, Petra F. Scudo, and Daniel R. Terno. Quantum entropy and special relativity. *Phys. Rev. Lett.*, 88:230402, May 2002. 25

[105] Pablo L. Saldanha and Vlatko Vedral. Spin quantum correlations of relativistic particles. *Phys. Rev. A*, 85:062101, Jun 2012. 26

[106] Daniel R. Terno. Two roles of relativistic spin operators. *Phys. Rev. A*, 67:014102, Jan 2003. 26

[107] Matthew C. Palmer, Maki Takahashi, and Hans F. Westman. {WKB} analysis of relativistic stern-gerlach measurements. *Annals of Physics*, 336(0):505 – 516, 2013. 26

[108] Heiko Bauke, Sven Ahrens, Christoph H Keitel, and Rainer Grobe. What is the relativistic spin operator? *New Journal of Physics*, 16(4):043012, 2014. 26

[109] David Edward Bruschi, Ivette Fuentes, and Jorma Louko. Voyage to alpha centauri: Entanglement degradation of cavity modes due to motion. *Phys. Rev. D*, 85:061701, Mar 2012. 26

[110] Eduardo Martín-Martínez and Juan León. Quantum correlations through event horizons: Fermionic versus bosonic entanglement. *Phys. Rev. A*, 81:032320, Mar 2010. 26

[111] Miguel Montero, Juan León, and Eduardo Martín-Martínez. Fermionic entanglement extinction in noninertial frames. *Phys. Rev. A*, 84:042320, Oct 2011. 26

[112] Nicolai Friis, David Edward Bruschi, Jorma Louko, and Ivette Fuentes. Motion generates entanglement. *Phys. Rev. D*, 85:081701, Apr 2012. 26

[113] Miguel Montero and Eduardo Martín-Martínez. The entangling side of the unruh-hawking effect. *Journal of High Energy Physics*, 2011(7), 2011. 26, 29

[114] David Edward Bruschi, Andrzej Dragan, Ivette Fuentes, and Jorma Louko. Particle and antiparticle bosonic entanglement in noninertial frames. *Phys. Rev. D*, 86:025026, Jul 2012. 26

[115] Eduardo Martín-Martínez and Ivette Fuentes. Redistribution of particle and anti-particle entanglement in noninertial frames. *Phys. Rev. A*, 83:052306, May 2011. 26

[116] Paul M Alsing and Ivette Fuentes. Observer-dependent entanglement. *Classical and Quantum Gravity*, 29(22):224001, 2012. 26

[117] Daniel R. Terno. From qubits to black holes: entropy, entanglement and all that. *International Journal of Modern Physics D*, 14(12):2307–2314, 2005. 26

[118] Shih-Yuin Lin and B L Hu. Entanglement, recoherence and information flow in an accelerated detector quantum field system: implications for the black hole information issue. *Classical and Quantum Gravity*, 25(15):154004, 2008. 26, 90

[119] David Edward Bruschi, Carlos Sabín, Angela White, Valentina Baccetti, Daniel K L Oi, and Ivette Fuentes. Testing the effects of gravity and motion on quantum entanglement in space-based experiments. *New Journal of Physics*, 16(5):053041, 2014. 26

[120] David Rideout, Thomas Jennewein, Giovanni Amelino-Camelia, Tommaso F Demarie, Brendon L Higgins, Achim Kempf, Adrian Kent, Raymond Laflamme, Xian Ma, Robert B. Mann, Eduardo Martín-Martínez, Nicolas C. Menicucci, John Moffat, Christoph Simon, Rafael Sorkin, Lee Smolin, and Daniel R. Terno. Fundamental quantum optics experiments conceivable with satellites-reaching relativistic distances and velocities. *Classical and Quantum Gravity*, 29(22):224011, 2012. 26

[121] Tupac Bravo, Carlos Sabín, and Ivette Fuentes. Analog quantum simulation of gravitational waves in a bose-einstein condensate. *arXiv preprint arXiv:1403.7199*, 2014. 26

[122] Joel Lindkvist, Carlos Sabín, Ivette Fuentes, Andrzej Dragan, Ida-Maria Svensson, Per Delsing, and Göran Johansson. The twin paradox with macroscopic clocks in superconducting circuits. *arXiv preprint arXiv:1401.0129*, 2013. 26

[123] N. Friis, A. R. Lee, K. Truong, C. Sabín, E. Solano, G. Johansson, and I. Fuentes. Relativistic quantum teleportation with superconducting circuits. *Phys. Rev. Lett.*, 110:113602, Mar 2013. 26

[124] Jason Doukas, Shih-Yuin Lin, B.L. Hu, and Robert B. Mann. Unruh effect under nonequilibrium conditions: oscillatory motion of an unruh-dewitt detector. *Journal of High Energy Physics*, 2013(11), 2013. 27

[125] Shih-Yuin Lin, Chung-Hsien Chou, and B. L. Hu. Quantum entanglement and entropy in particle creation. *Phys. Rev. D*, 81:084018, Apr 2010. 27

[126] B L Hu, A Roura, and S Shresta. Vacuum fluctuations and moving atoms/detectors: from the casimir-polder to the unruh-davies-dewitt-fulling effect. *Journal of Optics B: Quantum and Semiclassical Optics*, 6(8):S698, 2004. 27

[127] Shih-Yuin Lin and B. L. Hu. Accelerated detector-quantum field correlations: From vacuum fluctuations to radiation flux. *Phys. Rev. D*, 73:124018, Jun 2006. 27

[128] Eduardo Martín-Martínez and Jorma Louko. Particle detectors and the zero mode of a quantum field. *Phys. Rev. D*, 90:024015, Jul 2014. 27

[129] Dionigi M T Benincasa, Leron Borsten, Michel Buck, and Fay Dowker. Quantum information processing and relativistic quantum fields. *Classical and Quantum Gravity*, 31(7):075007, 2014. 27

[130] Lee Hodgkinson. Particle detectors in curved spacetime quantum field theory. *PhD thesis, The University of Nottingham, arXiv preprint:1309.7281*, 2013. 27

[131] Fabrizio Buscemi and Giuseppe Compagno. Nonlocal quantum-field correlations and detection processes in quantum-field theory. *Phys. Rev. A*, 80:022117, Aug 2009. 27, 91

[132] B L Hu, Shih-Yuin Lin, and Jorma Louko. Relativistic quantum information in detectors-field interactions. *Classical and Quantum Gravity*, 29(22):224005, 2012. 27

[133] Jorma Louko and Alejandro Satz. Transition rate of the unruh-dewitt detector in curved spacetime. *Classical and Quantum Gravity*, 25(5):055012, 2008. 27

[134] Luis C. Barbado and Matt Visser. Unruh-dewitt detector event rate for trajectories with time-dependent acceleration. *Phys. Rev. D*, 86:084011, Oct 2012. 27

[135] Jorma Louko and Alejandro Satz. How often does the unruh-dewitt detector click? regularization by a spatial profile. *Classical and Quantum Gravity*, 23(22):6321, 2006. 27

[136] Eric G. Brown, Eduardo Martín-Martínez, Nicolas C. Menicucci, and Robert B. Mann. Detectors for probing relativistic quantum physics beyond perturbation theory. *Phys. Rev. D*, 87:084062, Apr 2013. 27, 212, 228, 238

[137] David Edward Bruschi, Antony R Lee, and Ivette Fuentes. Time evolution techniques for detectors in relativistic quantum information. *Journal of Physics A: Mathematical and Theoretical*, 46(16):165303, 2013. 27

[138] David E. Bruschi, Jorma Louko, Eduardo Martín-Martínez, Andrzej Dragan, and Ivette Fuentes. Unruh effect in quantum information beyond the single-mode approximation. *Phys. Rev. A*, 82:042332, Oct 2010. 27, 109, 110, 111, 113, 114, 116, 172

[139] A. Dragan, Jason Doukas, Eduardo Martín-Martínez, and David Edward Bruschi. Localized projective measurement of a quantum field in non-inertial frames. *Classical and Quantum Gravity*, 30(23):235006, 2013. 27, 91, 92, 109, 110, 111, 114, 117, 119, 120, 236

[140] Mehdi Ahmadi, David Edward Bruschi, and Ivette Fuentes. Quantum metrology for relativistic quantum fields. *Phys. Rev. D*, 89:065028, Mar 2014. 27

[141] Robert B. Mann and Eduardo Martín-Martínez. Quantum thermometry. *Foundations of Physics*, 44(5):492–511, 2014. 27

[142] Eduardo Martín-Martínez, Andrzej Dragan, Robert B. Mann, and Ivette Fuentes. Berry phase quantum thermometer. *New Journal of Physics*, 15(5):053036, 2013. 27

[143] Carlos Sabín, Angela White, Lucia Hackermuller, and Ivette Fuentes. Dynamical phase quantum thermometer for an ultracold bose-einstein condensate. *arXiv preprint arXiv:1303.6208*, 2013. 27

[144] Andrzej Dragan, Ivette Fuentes, and Jorma Louko. Quantum accelerometer: Distinguishing inertial bob from his accelerated twin rob by a local measurement. *Phys. Rev. D*, 83:085020, Apr 2011. 27

[145] Eric G. Brown, William Donnelly, Achim Kempf, Robert B. Mann, Eduardo Martín-Martínez, and Nicolas C. Menicucci. Quantum seismology. *arXiv preprint arXiv:1407.0071*, 2014. 27

[146] Carlos Sabín, David Edward Bruschi, Mehdi Ahmadi, and Ivette Fuentes. Phonon creation by gravitational waves. *arXiv preprint arXiv:1402.7009*, 2014. 27

[147] Mehdi Ahmadi, David Edward Bruschi, Carlos Sabín, Gerardo Adesso, and Ivette Fuentes. Relativistic quantum metrology: Exploiting relativity to improve quantum measurement technologies. *Sci. Rep.*, 4, 05 2014. 27

[148] Martin B. Plenio and Shashank Virmani. An introduction to entanglement measures. *Quantum Info. Comput.*, 7(1):1–51, January 2007. 35

[149] Ryszard Horodecki, Paweł Horodecki, Michał Horodecki, and Karol Horodecki. Quantum entanglement. *Rev. Mod. Phys.*, 81:865–942, Jun 2009. 35, 38, 41

[150] F. Mintert, C. Viviescas, and A. Buchleitner. Basic concepts of entangled states. In Andreas Buchleitner, Carlos Viviescas, and Markus Tiersch, editors, *Entanglement and Decoherence*, volume 768 of *Lecture Notes in Physics*, pages 61–86. Springer Berlin Heidelberg, 2009. 35

[151] Harold Ollivier and Wojciech H. Zurek. Quantum discord: A measure of the quantumness of correlations. *Phys. Rev. Lett.*, 88:017901, Dec 2001. 38

[152] L Henderson and V Vedral. Classical, quantum and total correlations. *Journal of Physics A: Mathematical and General*, 34(35):6899, 2001. 38

[153] M. Lewenstein, B. Kraus, J. I. Cirac, and P. Horodecki. Optimization of entanglement witnesses. *Phys. Rev. A*, 62:052310, Oct 2000. 38

[154] Asher Peres. Separability criterion for density matrices. *Phys. Rev. Lett.*, 77:1413–1415, Aug 1996. 39

[155] Michał Horodecki, Paweł Horodecki, and Ryszard Horodecki. Separability of mixed states: necessary and sufficient conditions. *Physics Letters A*, 223(1):1–8, 1996. 39

[156] Frank Verstraete. A study of entanglement in quantum information theory. *PhD thesis, Katholieke Universiteit Leuven. ftp://ftp.esat.kuleuven.ac.be/pub/SISTA/verstraete/reports/phd.ps.gz*, 2002. 39

[157] Lane P. Hughston, Richard Jozsa, and William K. Wootters. A complete classification of quantum ensembles having a given density matrix. *Physics Letters A*, 183(1):14 – 18, 1993. 39

[158] Guifre Vidal. Entanglement monotones. *Journal of Modern Optics*, 47(2-3):355–376, 2000. 40, 41

[159] V. Vedral, M. B. Plenio, M. A. Rippin, and P. L. Knight. Quantifying entanglement. *Phys. Rev. Lett.*, 78:2275–2279, Mar 1997. 42

[160] K.M.R. Audenaert, M. Nussbaum, A. Szkoła, and F. Verstraete. Asymptotic error rates in quantum hypothesis testing. *Communications in Mathematical Physics*, 279(1):251–283, 2008. 42

[161] William K. Wootters. Entanglement of formation of an arbitrary state of two qubits. *Phys. Rev. Lett.*, 80:2245–2248, Mar 1998. 43

[162] G. Vidal and R. F. Werner. Computable measure of entanglement. *Phys. Rev. A*, 65:032314, Feb 2002. 43

[163] Luis Garay. Qft in curved spacetimes: Lecture notes. *Lecture notes*, 2014. 46, 56, 57

[164] N. D. Birrell and P. C. W. Davies. *Quantum Fields in Curved Space*. Cambridge University Press, February 1984. 46, 57, 92, 110, 113, 180, 210, 212, 213, 214, 215, 216, 227

[165] Robert Wald. *Quantum field theory in curved spacetime and black hole thermodynamics*. University of Chicago Press, Chicago, 1994. 46, 48, 55, 162, 176, 206

[166] Antony Richard Lee. Localised systems in relativistic quantum information. *PhD thesis, University of Nottingham. arXiv preprint: 1309.4419*, 2013. 46

[167] Wolfgang Rindler. *Essential relativity : special, general, and cosmological*. Springer-Verlag, New York, 1977. 50

[168] Luís C. B. Crispino, Atsushi Higuchi, and George E. A. Matsas. The Unruh effect and its applications. *Rev. Mod. Phys.*, 80:787, 2008. 52, 56, 119, 120

[169] Shin Takagi. Vacuum noise and stress induced by uniform acceleration. *Progress of Theoretical Physics Supplement*, 88:1–142, 1986. 52, 55, 56, 57

[170] Pietro Longhi and Roberto Soldati. Unruh effect revisited. *Phys. Rev. D*, 83:107701, May 2011. 54

[171] Pierre-Henry Lambert. Introduction to black hole evaporation. *Proceedings of Science, Modave*, 2013. 54

[172] S. A. Fulling. Nonuniqueness of canonical field quantization in Riemannian spacetime. *Phys. Rev. D*, 7:2850–2862, 1973. 55, 163, 182

[173] Tracy Lupher. How to construct unitarily inequivalent representations in quantum field theory. *University of Texas Library - Report*, 2008. 55, 182

[174] J. A. Swieca E. Haag. When Does a Quantum Field Theory Describe Particles? *Commun. math. Phys.*, 1:308–320, 1965. 55, 161, 176, 207

[175] P C W Davies. Scalar production in schwarzschild and rindler metrics. *Journal of Physics A: Mathematical and General*, 8(4):609, 1975. 55

[176] William G. Unruh and Robert M. Wald. What happens when an accelerating observer detects a rindler particle. *Phys. Rev. D*, 29:1047–1056, Mar 1984. 56, 57

[177] Alessandro Fabbri. *Modeling black hole evaporation*. Imperial College Press World Scientific Pub, London Singapore Hackensack, NJ, 2005. 57

[178] B. DeWitt. *General Relativity; an Einstein Centenary Survey*. Cambridge University Press, Cambridge, UK, 1980. 57, 99, 119, 120, 169

[179] Rudolf Haag. *Local Quantum Physics: Fields, Particles, Algebras (Theoretical and Mathematical Physics)*. Springer, 1996. 57, 181, 189

[180] Robert M. Wald. *Quantum Field Theory in Curved Spacetime and Black Hole Thermodynamics (Chicago Lectures in Physics)*. University of Chicago Press, 1994. 57

[181] Richard P Feynman. Simulating physics with computers. *International journal of theoretical physics*, 21(6):467–488, 1982. 59

[182] Iulia Buluta and Franco Nori. Quantum simulators. *Science*, 326(5949):108–111, 2009. 61

[183] I. M. Georgescu, S. Ashhab, and Franco Nori. Quantum simulation. *Rev. Mod. Phys.*, 86:153–185, Mar 2014. 61

[184] Several authors. Quantum simulation. *Nature Physics Insight, Focus Issue*, 8(4):277–284, 04 2012. 61

[185] ed. ARDA experts panel, R. J. Hughes. A quantum information science and technology roadmap. *US Government Report LA-UR-04-1778*, 2004, http://qist.lanl.gov. 62

[186] David P. DiVincenzo. The physical implementation of quantum computation. *Fortschritte der Physik*, 48(9-11):771–783, 2000. 62

[187] J. I. Cirac and P. Zoller. Quantum computations with cold trapped ions. *Phys. Rev. Lett.*, 74:4091–4094, May 1995. 62, 67

[188] C. Monroe, D. M. Meekhof, B. E. King, W. M. Itano, and D. J. Wineland. Demonstration of a fundamental quantum logic gate. *Phys. Rev. Lett.*, 75:4714–4717, Dec 1995. 62

[189] M. D. Barrett, J. Chiaverini, T. Schaetz, J. Britton, W. M. Itano, J. D. Jost, E. Knill, C. Langer, D. Leibfried, R. Ozeri, and D. J. Wineland. Deterministic quantum teleportation of atomic qubits. *Nature*, 429(6993):737–739, 06 2004. 62

[190] M. Riebe, H. Haffner, C. F. Roos, W. Hansel, J. Benhelm, G. P. T. Lancaster, T. W. Korber, C. Becher, F. Schmidt-Kaler, D. F. V. James, and R. Blatt. Deterministic quantum teleportation with atoms. *Nature*, 429(6993):734–737, 06 2004. 62

[191] H. Haffner, W. Hansel, C. F. Roos, J. Benhelm, D. Chek-al kar, M. Chwalla, T. Korber, U. D. Rapol, M. Riebe, P. O. Schmidt, C. Becher, O. Guhne, W. Dur, and R. Blatt. Scalable multiparticle entanglement of trapped ions. *Nature*, 438(7068):643–646, 12 2005. 62

[192] Thomas Monz, Philipp Schindler, Julio T. Barreiro, Michael Chwalla, Daniel Nigg, William A. Coish, Maximilian Harlander, Wolfgang Hänsel, Markus Hennrich, and Rainer Blatt. 14-qubit entanglement: Creation and coherence. *Phys. Rev. Lett.*, 106:130506, Mar 2011. 62, 126

[193] BB Blinov, DL Moehring, L-M Duan, and Chris Monroe. Observation of entanglement between a single trapped atom and a single photon. *Nature*, 428(6979):153–157, 2004. 62

[194] R. Blatt and C. F. Roos. Quantum simulations with trapped ions. *Nat Phys*, 8(4):277–284, 04 2012. 62

[195] L. Lamata, J. León, T. Schätz, and E. Solano. Dirac equation and quantum relativistic effects in a single trapped ion. *Phys. Rev. Lett.*, 98:253005, Jun 2007. 62

[196] R. Gerritsma, G. Kirchmair, F. Zähringer, E. Solano, R. Blatt, and C. F. Roos. Quantum simulation of the Dirac equation. *Nature*, 463:68–71, January 2010. 62, 121

[197] T. Rosenband, D. B. Hume, P. O. Schmidt, C. W. Chou, A. Brusch, L. Lorini, W. H. Oskay, R. E. Drullinger, T. M. Fortier, J. E. Stalnaker, S. A. Diddams, W. C. Swann, N. R. Newbury, W. M. Itano, D. J. Wineland, and J. C. Bergquist. Frequency ratio of al+ and hg+ single-ion optical clocks; metrology at the 17th decimal place. *Science*, 319(5871):1808–1812, 2008. 62

[198] S. Earnshaw. On the nature of the molecular forces which regulate the constitution of the luminiferous ether. *Trans. Camb. Phil. Soc*, 7:97–112, 1842. 62

[199] Wolfgang Paul and H. Steinwedel. Ein neues Massenspektrometer ohne Magnetfeld. *Zeitschrift für Naturforschung A*, 8(7):448–450, 1953. 62

[200] Pradip Ghosh. *Ion traps*. Clarendon Press, Oxford University Press, Oxford New York, 1995. 63

[201] Guido Wilpers, Patrick See, Patrick Gill, and Alastair G. Sinclair. A monolithic array of three-dimensional ion traps fabricated with conventional semiconductor technology. *Nat Nano*, 7(9):572–576, 09 2012. 64

[202] D. Leibfried, R. Blatt, C. Monroe, and D. Wineland. Quantum dynamics of single trapped ions. *Rev. Mod. Phys.*, 75(1):281–324, Mar 2003. 66, 71, 119, 121, 122, 123, 147

[203] Jürgen Eschner, Giovanna Morigi, Ferdinand Schmidt-Kaler, and Rainer Blatt. Laser cooling of trapped ions. *J. Opt. Soc. Am. B*, 20(5):1003–1015, May 2003. 68

[204] Stig Stenholm. The semiclassical theory of laser cooling. *Rev. Mod. Phys.*, 58:699–739, Jul 1986. 69

[205] Y Castin, H Wallis, and Jean Dalibard. Limit of doppler cooling. *JOSA B*, 6(11):2046–2057, 1989. 69

[206] Seth Lloyd. Universal quantum simulators. *Science*, 273(5278):1073–1078, 1996. 70

[207] B. P. Lanyon, C. Hempel, D. Nigg, M. Müller, R. Gerritsma, F. Zähringer, P. Schindler, J. T. Barreiro, M. Rambach, G. Kirchmair, M. Hennrich, P. Zoller, R. Blatt, and C. F. Roos. Universal digital quantum simulation with trapped ions. *Science*, 334(6052):57–61, 2011. 70

[208] P. Forn. *Superconducting Qubits and Quantum Resonators.* Casimir PhD series, Delft-Leiden 2010-21, www.library.tudelft.nl/dissertations., 2010. 72

[209] Borja Peropadre. *Control of utrastrongly coupled systems in circuit quatum electrodynamics.* PhD thesis. Universidad Complutense de Madrid. Tesis UCM, http://eprints.ucm.es/24127/1/T35060.pdf, 2013. 72, 74, 76, 78, 80

[210] J. Clarke and F. K. Wilhelm. Superconducting quantum bits. *Nature*, 453:1031–1042, June 2008. 72, 147

[211] J. Q. You and F. Nori. Atomic physics and quantum optics using superconducting circuits. *Nature*, 474(7353):589–597, 06 2011. 72, 147, 167, 241

[212] J. Bardeen, L. N. Cooper, and J. R. Schrieffer. Theory of superconductivity. *Phys. Rev.*, 108:1175–1204, Dec 1957. 72

[213] B. Yurke and J. S. Denker. Quantum network theory. *Phys. Rev. A*, 29:1419–1437, March 1984. 72, 149

[214] Michel H. Devoret. Quantum fluctuations in electrical circuits. *S. Reynaud, E. Giacobino and J.Zinn-Justin, eds. Les Houches, Session LXIII*, page 351, 1995. 72

[215] B.D. Josephson. Possible new effects in superconductive tunnelling. *Physics Letters*, 1(7):251 – 253, 1962. 75

[216] F. G. Paauw, A. Fedorov, C. J. P. M Harmans, and J. E. Mooij. Tuning the gap of a superconducting flux qubit. *Phys. Rev. Lett.*, 102:090501, Mar 2009. 81

[217] Xiaobo Zhu, Shiro Saito, Alexander Kemp, Kosuke Kakuyanagi, Shin-ichi Karimoto, Hayato Nakano, William J. Munro, Yasuhiro Tokura, Mark S. Everitt, Kae Nemoto, Makoto Kasu, Norikazu Mizuochi, and Kouichi Semba. Coherent coupling of a superconducting flux qubit to an electron spin ensemble in diamond. *Nature*, 478(7368):221–224, 10. 81

[218] F. K. Wilhelm B, C. J. P. M. Harmans, and J. E. Mooij. Engineering decoherence in josephson persistent-current qubits. measurement apparatus and other electromagnetic environments. *Eur. Phys. J. B*, pages 111–124, 2003. 82

[219] A. Lupascu, S. Saito, T. Picot, P. C. de Groot, C. J. P. M. Harmans, and J. E. Mooij. Quantum non-demolition measurement of a superconducting two-level system. *Nat Phys*, 3(2):119–125, 02 2007. 82, 83, 144

[220] A. Lupaşcu, E. F. C. Driessen, L. Roschier, C. J. P. M. Harmans, and J. E. Mooij. High-contrast dispersive readout of a superconducting flux qubit using a nonlinear resonator. *Phys. Rev. Lett.*, 96:127003, Mar 2006. 82

[221] B. Peropadre, P. Forn-Díaz, E. Solano, and J. J. García-Ripoll. Switchable ultrastrong coupling in circuit QED. *Phys. Rev. Lett.*, 105(2):023601, Jul 2010. 83, 154, 172

[222] H.M. Wiseman and G.J. Milburn. *Quantum Measurement and Control*. Cambridge University Press, 2010. 90

[223] Shih-Yuin Lin, Chung-Hsien Chou, and B. L. Hu. Disentanglement of two harmonic oscillators in relativistic motion. *Phys. Rev. D*, 78:125025, Dec 2008. 90

[224] Jason Doukas and Benedict Carson. Entanglement of two qubits in a relativistic orbit. *Phys. Rev. A*, 81:062320, Jun 2010. 90

[225] Benni Reznik. Entanglement from the vacuum. *Foundations of Physics*, 33(1):167–176, 2003. 91

[226] Marlan O. Scully and M. Suhail Zubairy. *Quantum Optics*. Cambridge University Press, 1997. 92, 101

[227] D. S. Jin, J. R. Ensher, M. R. Matthews, C. E. Wieman, and E. A. Cornell. Collective excitations of a bose-einstein condensate in a dilute gas. *Phys. Rev. Lett.*, 77:420–423, Jul 1996. 92

[228] W. G. Unruh and W. H. Zurek. Reduction of a wave packet in quantum brownian motion. *Phys. Rev. D*, 40:1071–1094, Aug 1989. 92

[229] Serge Massar and Philippe Spindel. Einstein-podolsky-rosen correlations between two uniformly accelerated oscillators. *Phys. Rev. D*, 74:085031, Oct 2006. 92

[230] Roberto Casadio and Giovanni Venturi. The accelerated observer and quantum effects. *Physics Letters A*, 199(1-2):33 – 39, 1995. 92

[231] Roberto Casadio and Giovanni Venturi. The accelerated observer with back-reaction effects. *Physics Letters A*, 252(3-4):109 – 114, 1999. 92

[232] Sebastian Schlicht. Considerations on the unruh effect: causality and regularization. *Classical and Quantum Gravity*, 21(19):4647, 2004. 95, 99, 100, 105

[233] Paul Langlois. Causal particle detectors and topology. *Annals of Physics*, 321(9):2027 – 2070, 2006. 99, 100

[234] Jorma Louko and Alejandro Satz. How often does the unruh–dewitt detector click? regularization by a spatial profile. *Classical and Quantum Gravity*, 23(22):6321, 2006. 99, 100

[235] Jorma Louko and Alejandro Satz. Excited by a quantum field: does shape matter? *Journal of Physics: Conference Series*, 68(1):012014, 2007. 99, 100

[236] M. Brune, J. Bernu, C. Guerlin, S. Deléglise, C. Sayrin, S. Gleyzes, S. Kuhr, I. Dotsenko, J. M. Raimond, and S. Haroche. Process tomography of field damping and measurement of fock state lifetimes by quantum nondemolition photon counting in a cavity. *Phys. Rev. Lett.*, 101:240402, Dec 2008. 100, 103

[237] Alexandre Blais, Ren-Shou Huang, Andreas Wallraff, S. M. Girvin, and R. J. Schoelkopf. Cavity quantum electrodynamics for superconducting electrical circuits: An architecture for quantum computation. *Phys. Rev. A*, 69:062320, Jun 2004. 100, 103, 151, 241

[238] F. W. Cummings. Stimulated emission of radiation in a single mode. *Phys. Rev.*, 140:A1051–A1056, Nov 1965. 101

[239] Charles W. Misner, Kip S. Thorne, and John A. Wheeler. *Gravitation*. W. H. Freeman, September 1973. 105, 121

[240] Antony R. Lee and Ivette Fuentes. Spatially extended unruh-dewitt detectors for relativistic quantum information. *Phys. Rev. D*, 89:085041, Apr 2014. 108

[241] Eduardo Martín-Martínez and Juan León. Quantum correlations through event horizons: Fermionic versus bosonic entanglement. *Phys. Rev. A*, 81(3):032320, 2010. 109, 111

[242] Andrzej Dragan, Jason Doukas, and Eduardo Martín-Martínez. Localized detection of quantum entanglement through the event horizon. *Phys. Rev. A*, 87:052326, May 2013. 110, 117

[243] Andrzej Dragan and Ivette Fuentes. Probing the spacetime structure of vacuum entanglement. *quant-ph/1105.1192*, 2011. 111, 167

[244] Shih-Yuin Lin and B. L. Hu. Backreaction and the unruh effect: New insights from exact solutions of uniformly accelerated detectors. *Phys. Rev. D*, 76:064008, Sep 2007. 111

[245] E. Knill, R. Laflamme, and G.J Milburn. A scheme for efficient quantum computation with linear optics. *Nature*, 409:46–52, 2001. 111

[246] M. Montero and E. Martín-Martínez. The entangling side of the unruh-hawking effect. *JHEP*, 07:006, 2011. 111, 113, 114, 115, 118

[247] Miguel Montero and Eduardo Martín-Martínez. Entanglement of arbitrary spin fields in noninertial frames. *Phys. Rev. A*, 84:012337, 2011. 111, 113

[248] Eduardo Martín-Martínez and Ivette Fuentes. Redistribution of particle and antiparticle entanglement in noninertial frames. *Phys. Rev. A*, 83:052306, 2011. 113

[249] P. M. Alsing, I. Fuentes-Schuller, R. B. Mann, and T. E. Tessier. Entanglement of Dirac fields in noninertial frames. *Phys. Rev. A*, 74:032326, 2006. 113, 114

[250] G. Vidal and R. F. Werner. A computable measure of entanglement. *Phys. Rev. A*, 65:032314, 2002. 114

[251] Charles H. Bennett, Herbert J. Bernstein, Sandu Popescu, and Benjamin Schumacher. Concentrating partial entanglement by local operations. *Phys. Rev. A*, 53:2046, 1996. 116

[252] Eduardo Martín-Martínez, Luis J. Garay, and Juan León. Quantum entanglement produced in the formation of a black hole. *Phys. Rev. D*, 82(6):064028, 2010. 118

[253] Eduardo Martín-Martínez, Ivette Fuentes, and Robert B. Mann. Using berry's phase to detect the unruh effect at lower accelerations. *Phys. Rev. Lett.*, 107:131301, Sep 2011. 119, 120

[254] A. Wallraff, D. I. Schuster, A. Blais, L. Frunzio, R. S. Huang, J. Majer, S. Kumar, S. M. Girvin, and R. J. Schoelkopf. Strong coupling of a single photon to a superconducting qubit using circuit quantum electrodynamics. *Nature*, 431(7005):162–167, 09 2004. 119, 123, 241

[255] M Gross and S Haroche. Superradiance: An essay on the theory of collective spontaneous emission. *Physics Reports*, 1982. 120

[256] Pierre Nataf and Cristiano Ciuti. No-go theorem for superradiant quantum phase transitions in cavity qed and counter-example in circuit qed. *Nat Commun*, 1, 09 2010. 120

[257] Jorma Louko and Kristin Schleich. The exponential law: monopole detectors, bogoliubov transformations, and the thermal nature of the euclidean vacuum in bbbp 3 de sitter spacetime. *Classical and Quantum Gravity*, 16(6):2005, 1999. 120

[258] Eduardo Martín-Martínez, Luis J. Garay, and Juan León. Unveiling quantum entanglement degradation near a Schwarzschild black hole. *Phys. Rev. D*, 82:064006, 2010. 121

[259] C. Schneider, D. Porras, and T. Schaetz. Experimental quantum simulations of many-body physics with trapped ions. *Reports on Progress in Physics*, 75(2):024401, 2012. 121

[260] Paul M. Alsing, Jonathan P. Dowling, and G. J. Milburn. Ion trap simulations of quantum fields in an expanding universe. *Phys. Rev. Lett.*, 94:220401, Jun 2005. 121

[261] D. Porras, F. Marquardt, J. von Delft, and J. I. Cirac. Mesoscopic spin-boson models of trapped ions. *Phys. Rev. A*, 78(1):010101, Jul 2008. 123

[262] P. D. Nation, M. P. Blencowe, A. J. Rimberg, and E. Buks. Analogue hawking radiation in a dc-squid array transmission line. *Phys. Rev. Lett.*, 103:087004, Aug 2009. 123

[263] P. D. Nation, J. R. Johansson, M. P. Blencowe, and Franco Nori. Colloquium, stimulating uncertainty: Amplifying the quantum vacuum with superconducting circuits. *Rev. Mod. Phys.*, 84:1–24, Jan 2012. 123

[264] Diego Porras and Juan José García-Ripoll. Shaping an itinerant quantum field into a multimode squeezed vacuum by dissipation. *Phys. Rev. Lett.*, 108:043602, Jan 2012. 123

[265] C. Zener. Non-Adiabatic Crossing of Energy Levels. *Royal Society of London Proceedings Series A*, 137:696–702, September 1932. 125, 143

[266] P D Nation, M P Blencowe, and Franco Nori. Non-equilibrium landauer transport model for hawking radiation from a black hole. *New Journal of Physics*, 14(3):033013, 2012. 127

[267] B. Russell. *Theory of Knowledge: The 1913 Manuscript (Collected Papers of Bertrand Russell)*. Routledge, 1992 (1913). 132

[268] M. Esfeld. *Causal Realism - Probabilities, Laws, and Structures (The Philosophy of Science in a European Perspective)*. Springer, 2012. 133

[269] N.N. Bogoliubov and etc. *Axiomatic Quantum Field Theory*. Addison Wesley Publishing Company, 1973. 133

[270] Sergei Dubovsky, Alberto Nicolis, Enrico Trincherini, and Giovanni Villadoro. Microcausality in curved space-time. *Phys. Rev. D*, 77:084016, Apr 2008. 133

[271] R. P. Feynman. The theory of positrons. *Phys. Rev.*, 76:749–759, Sep 1949. 134

[272] Richard P. Feynman. *Theory Of Fundamental Processes (Advanced Books Classics)*. Westview Press, 3 1998. 134

[273] Richard Feynman. *Quantum electrodynamics*. Addison-Wesley, Reading, Mass, 1998. 134

[274] Gerhard C. Hegerfeldt. Causality problems for Fermi's two-atom system. *Phys. Rev. Lett.*, 72(5):596–599, Jan 1994. 134, 137, 138, 142

[275] J. D. Franson. Generation of entanglement outside of the light cone. *J. Mod. Opt.*, 55:2117, 2008. 135, 138

[276] J. Yngvason. The role of type III factors in quantum field theory. *Reports on Mathematical Physics*, 55:135–147, February 2005. 137, 142

[277] Ll. Masanes, A. Acín, and N. Gisin. General properties of nonsignaling theories. *Phys. Rev. A*, 73:012112, 2006. 138

[278] J. León and C. Sabín. Generation of atom-atom correlations inside and outside the mutual light cone. *Phys. Rev. A*, 79:012304, 2009. 138, 151, 171, 209

[279] J. Bourassa, J. M. Gambetta, A. A. Abdumalikov, O. Astafiev, Y. Nakamura, and A. Blais. Ultrastrong coupling regime of cavity qed with phase-biased flux qubits. *Phys. Rev. A*, 80(3):032109, Sep 2009. 141, 147

[280] J. E. Mooij, T. P. Orlando, L. Levitov, Lin Tian, Caspar H. van der Wal, and Seth Lloyd. Josephson Persistent-Current Qubit. *Science*, 285(5430):1036–1039, 1999. 142

[281] Yuriy Makhlin, Gerd Schön, and Alexander Shnirman. Quantum-state engineering with Josephson-junction devices. *Rev. Mod. Phys.*, 73(2):357–400, May 2001. 142

[282] T. Picot, R. Schouten, C. J. P. M. Harmans, and J. E. Mooij. Quantum nondemolition measurement of a superconducting qubit in the weakly projective regime. *Phys. Rev. Lett.*, 105(4):040506, Jul 2010. 144, 147, 153

[283] Roy J. Glauber. The quantum theory of optical coherence. *Phys. Rev.*, 130(6):2529–2539, Jun 1963. 147

[284] M. H. Devoret, S. Girvin, and R. Schoelkopf. Circuit-QED: How strong can the coupling between a Josephson junction atom and a transmission line resonator be? *Annalen der Physik*, 519:767–779, October 2007. 147

[285] T. Niemczyk, F. Deppe, H. Huebl, E. P. Menzel, F. Hocke, M. J. Schwarz, J. J. García-Ripoll, D. Zueco, T. Hümmer, E. Solano, A. Marx, and R. Gross. Circuit quantum electrodynamics in the ultrastrong-coupling regime. *Nature Physics*, 6:772–776, October 2010. 147, 168, 170

[286] P. Forn-Díaz, J. Lisenfeld, D. Marcos, J. J. García-Ripoll, E. Solano, C. J. P. M. Harmans, and J. E. Mooij. Observation of the bloch-siegert shift in a qubit-oscillator system in the ultrastrong coupling regime. *Phys. Rev. Lett.*, page 237001, 2010. 147, 168, 170

[287] F. Costa and F. Piazza. Modeling a particle detector in field theory. *New Journal of Physics*, 11(11):113006–+, November 2009. 148

[288] G. Romero, J.J. García-Ripoll, and E. Solano. Photodetection of propagating quantum microwaves in circuit QED. *Physica Scripta Volume T*, 137(1):014004, December 2009. 149

[289] Carlos Sabín. Bipartite entanglement of localized separated system. *PhD thesis, Universidad Complutense de Madrid. arXiv preprint:1112.2084*, 2011. 152

[290] Ying-Dan Wang, A. Kemp, and K. Semba. Coupling superconducting flux qubits at optimal point via dynamic decoupling with the quantum bus. *Phys. Rev. B*, 79:024502, Jan 2009. 154

[291] J. M. Gambetta, A. A. Houck, and Alexandre Blais. Superconducting qubit with purcell protection and tunable coupling. *Phys. Rev. Lett.*, 106:030502, Jan 2011. 154

[292] G. C. Hegerfeldt. Instantaneous Spreading and Einstein Causality in Quantum Theory. *Annalen Phys.*, 7:716–725, 1998. 161, 163, 175, 176, 183, 184, 205

[293] Steven Weinberg. *The Quantum Theory of Fields, Volume 1: Foundations*. Cambridge University Press, 5 2005. 161

[294] James M. Knight. Strict Localization in Quantum Field Theory. *J. Math. Phys.*, 459, 1961. 161, 164, 176, 183, 192, 193, 194, 203, 205

[295] Stephan De Bievre. Where is that quantum? *arXiv: math-ph/0607044v1*, 2006. 161

[296] A. L. Licht. Strict Localization. *J. Math. Phys.*, 4:1443, 1963. 161, 176, 183

[297] Ludger Hannibal. On Hegerfeldt's paradox. *arXiv preprint arXiv:quant-ph/9511006*, 1995. 162

[298] K. Masuda. A Unique Continuation Theorem for Solutions of Wave Equations with Variable Coefficients. *J. Math. Analysis and applications*, 21:369–376, 1968. 162, 175

[299] M. Murata. Anti-locality of certain functions of the Laplace operator. *J. Math. Soc. Japan*, 25, 1973. 162

[300] Hans Halvorson. Reeh- schlieder defeats newton-wigner: On alternative localization schemes in relativistic quantum field theory. *Philosophy of Science*, 68(1):111–133, 2001. 162, 176, 193, 205, 207

[301] T. D. Newton and E. P. Wigner. Localized states for elementary systems. *Rev. Mod. Phys.*, 21:400, 1949. 163

[302] T. O. Philips. Lorentz Invariant Localized states. *Phys. Rev.*, 136:72, 1964. 163

[303] J. Bourassa, J. M. Gambetta, A. A. Abdumalikov, O. Astafiev, and Y. Nakamura. Ultrastrong coupling regime of cavity QED with phase-biased flux qubits. *Phys. Rev. A*, 80:032109, 2009. 168

[304] J. Majer, J. M. Chow, J. M. Gambetta, Jens Koch, B. R. Johnson, J. A. Schreier, L. Frunzio, D. I. Schuster, A. A. Houck, A. Wallraff, A. Blais, M. H. Devoret, S. M. Girvin, and R. J. Schoelkopf. Coupling superconducting qubits via a cavity bus. *Nature*, 449(7161):443–447, 09 2007. 171

[305] M. Steffen, M. Ansmann, R. C. Bialczak, N. Katz, E. Lucero, R. McDermott, M. Neeley, E. M. Weig, A. N. Cleland, and J. M. Martinis. Measurement of the Entanglement of Two Superconducting Qubits via State Tomography. *Science*, 313:1423–1425, September 2006. 172

[306] M. Baur, A. Fedorov, L. Steffen, S. Filipp, M. P. da Silva, and A. Wallraff. Benchmarking a quantum teleportation protocol in superconducting circuits using tomography and an entanglement witness. *Phys. Rev. Lett.*, 108:040502, Jan 2012. 173

[307] Garry Bowen and Sougato Bose. Teleportation as a depolarizing quantum channel, relative entropy, and classical capacity. *Phys. Rev. Lett.*, 87:267901, 2001. 173

[308] S. Albeverio, S. M. Fei, and W.L. Yang. Teleportation with an arbitrary mixed resource as a trace-preserving quantum channel. *Commun. Theor. Phys.*, 38:301–304, 2002. 173

[309] Thomas Blum, Achim Denig, Ivan Logashenko, Eduardo de Rafael, B. Lee Roberts, Thomas Teubner, and Graziano Venanzoni. The Muon (g-2) Theory Value: Present and Future. *US Particle Physics Snowmass Self Study, eprint - arXiv:1311.2198*, 2013. 175

[310] ATLAS collaboration. Evidence for the spin-0 nature of the higgs boson using atlas data. *Physics Letters B*, 726(1-3):120 – 144, 2013. 175

[311] CMS collaboration. Observation of a new boson with mass near 125 GeV in pp collisions at $\sqrt{s} = 7$ and 8 TeV. *Journal of High Energy Physics*, 2013(6):1–127, 2013. 175

[312] E. Karpov, G. Ordonez, T. Petrosky, I. Prigogine, and G. Pronko. Causality, delocalization, and positivity of energy. *Phys. Rev. A*, 62:012103, 2000. 175, 183

[313] Paul Busch. Unsharp localization and causality in relativistic quantum theory. *Journal of Physics A: Mathematical and General*, 32(37):6535, 1999. 176

[314] Hans Halvorson. Locality, localization, and the particle concept: Topics in the foundations of quantum field theory. *PhD thesis, Pittsburg. http://philsci-archive.pitt.edu/346*, April 2001. 176

[315] T. D. Newton and E. P. Wigner. Localized states for elementary systems. *Rev. Mod. Phys.*, 21:400–406, 1949. 176, 196

[316] Gordon N. Fleming. Reeh- schlieder meets newton-wigner. *Philosophy of Science*, 67:pp. S495–S515, 2000. 176

[317] D. Colosi C. Rovelli. What is a particle? *Class.Quant.Grav.*, 26, 2009. 177

[318] Silvan S. Schweber and Physics. *An Introduction to Relativistic Quantum Field Theory (Dover Books on Physics)*. Dover Publications, 2005. 182

[319] J. von Neumann. Die eindeutigkeit der schroedingerschen operatoren. *Mathematische Annalen*, 104(1):570–578, 1931. 182

[320] Laura Ruetsche. *Interpreting Quantum Theories*. Oxford University Press, USA, 2013. 182

[321] Lennart Carleson. On convergence and growth of partial sums of fourier series. *Acta Mathematica*, 116(1):135–157, 1966. 186

[322] Gerhard C. Hegerfeldt. Remark on causality and particle localization. *Phys. Rev. D*, 10:3320–3321, 1974. 196

[323] Iwo Bialynicki-Birula. Exponential localization of photons. *Phys. Rev. Lett.*, 80:5247–5250, 1998. 196

[324] F. Strocchi. Relativistic quantum mechanics and field theory. *Foundations of Physics*, 34(3):501–527, 2004. 201

[325] Stephen J. Summers and Reinhard Werner. The vacuum violates bell's inequalities. *Physics Letters A*, 110(5):257 – 259, 1985. 203

[326] Doreen Fraser. How to take particle physics seriously: A further defence of axiomatic quantum field theory. *Studies in History and Philosophy of Science Part B: Studies in History and Philosophy of Modern Physics*, 42(2):126 – 135, 2011. 206

[327] David Wallace. In defence of naivety: The conceptual status of lagrangian quantum field theory. *Synthese*, 151(1):33–80, 2006. 206

[328] Goffredo Chirco, Hal M. Haggard, and Carlo Rovelli. Coupling and thermal equilibrium in general-covariant systems. *Phys. Rev. D*, 88:084027, 2013. 208

[329] S J. Summers and R Werner. *Commun. Math. Phys*, 110:247, 1987. 209

[330] Mark Srednicki. Entropy and area. *Phys. Rev. Lett*, 71:666, 1993. 209

[331] H. Casini and M. Huerta. Entanglement entropy in free quantum field theory. *J. Phys. A: Math. Theor.*, 42:504007, 2009. 209, 236

[332] Daniel Braun. Entanglement from thermal blackbody radiation. *Phys. Rev. A*, 72:062324, 2005. 209

[333] E. G. Brown. Thermal amplification of field-correlation harvesting. *Phys. Rev. A*, 88:062336, 2013. 209

[334] M. Cramer, J. Eisert, M. B. Plenio, and J. Dreibig. Entanglement-area law for general bosonic harmonic lattice systems. *Phys. Rev. A*, 73:012309, 2006. 209, 236

[335] L. Amico, R. Fazio, A. Osterloh, and V. Vedral. Entanglement in many-body systems. *Rev. Mod. Phys.*, 80:517, 2008. 209, 236

[336] G. Moore. *J. Math. Phys.*, 11:2679, 1970. 210, 212, 219

[337] Gerardo Adesso and Fabrizio Illuminati. Entanglement in continuous-variable systems: recent advances and current perspectives. *J. Phys. A: Math. Theor*, 40:7821, 2007. 211, 221, 231, 253, 256

[338] Alonso Botero and Benni Reznik. Spatial structures and localization of vacuum entanglement in the linear harmonic chain. *Phys. Rev. A*, 70:052329, Nov 2004. 211, 236

[339] N. N. Bogoliubov. On the theory of superfluidity. *J. Phys. (USSR)*, 11:23, 1947. 215

[340] M. B. Plenio. Logarithmic negativity: A full entanglement monotone that is not convex. *Phys. Rev. Lett*, 95:090503, 2005. 230, 256

[341] M. Zych, F. Costa, J. Kofler, and C. Brukner. Entanglement between smeared field operators in the klein-gordon vacuum. *Phys. Rev. D*, 81:125019, 2010. 231, 236

[342] Jason Doukas, Eric G. Brown, Andrzej Dragan, and Robert B. Mann. Entanglement and discord: Accelerated observations of local and global modes. *Phys. Rev. A*, 87:012306, Jan 2013. 236

[343] Paul R. Berman, with contributions from, G. Barton, H.J. Carmichael, J.J. Childs, G. Gabrielse, J. Tan, S. Haroche, J.M. Raimond, E.A. Hinds, H.J. Kimble, P. Meystre, M. Wilkens, T.W. Mossberg, M. Lewenstein, and G. Raithel et al. *Cavity Quantum Electrodynamics (Advances in Atomic, Molecular and Optical Physics)*. Academic Press, 1993. 241

[344] Arjan F. van Loo, Arkady Fedorov, Kevin Lalumière, Barry C. Sanders, Alexandre Blais, and Andreas Wallraff. Photon-mediated interactions between distant artificial atoms. *Science*, 342(6165):1494–1496, 2013. 241

[345] Io-Chun Hoi, C. M. Wilson, Göran Johansson, Tauno Palomaki, Borja Peropadre, and Per Delsing. Demonstration of a single-photon router in the microwave regime. *Phys. Rev. Lett.*, 107:073601, Aug 2011. 241

[346] Io-Chun Hoi, Tauno Palomaki, Joel Lindkvist, Göran Johansson, Per Delsing, and C. M. Wilson. Generation of nonclassical microwave states using an artificial atom in 1d open space. *Phys. Rev. Lett.*, 108:263601, Jun 2012. 241

[347] Philip Zupanzic. *Dynamic Holography and Beamshaping using Digital Micromirror Devices*. LMU Münich, Grainer Lab Harvard, 2013. 242

[348] Steven G. Avery and Borun D. Chowdhury. No holography for eternal ads black holes. *arXiv:1312.3346 [hep-th]*, 2013. 243

[349] Samuel L. Braunstein, Stefano Pirandola, and Karol Zyczkowski. Better late than never: Information retrieval from black holes. *Phys. Rev. Lett*, 110:101301, 2013. 243

[350] R Simon. Peres-horodecki separability criterion for continuous variable systems. *Phys. Rev. Lett*, 84:2726, 2000. 256

[351] R. F. Werner and M. M. Wolf. Bound entangled gaussian states. *Phys. Rev. Lett.*, 86:3658–3661, Apr 2001. 256

Index